A BLOCK-SPRING MODEL FOR JOINTED ROCKS

BAOLIN WANG, B.Sc., M.Sc.

A Thesis

Submitted under the supervision of

Dr. Vinod K. Garga, P.Eng.

in partial fulfillment

of the requirements for the degree of

Doctor of Philosophy

in

Civil Engineering

Department of Civil Engineering
Faculty of Engineering
University of Ottawa
Ottawa, Ontario
Canada, K1N 6N5

ISBN 0-315-85797-8

In memory of my grandfather

ACKNOWLEDGEMENTS

The author of this thesis wishes to express his sincere gratitude to his research supervisor, Dr. Vinod K. Garga, without his support and encouragement this thesis could not have been completed. His guidance and critical review throughout the course of this research work were essential for the completion of this thesis. The author also wishes to thank Messrs. Marc Bétournay, Luc Closset and Yang Yu, Drs. Somchet Vongpaisal and Richard Wan, all of CANMET, and Dr. Luciano Medeiros for their helpful suggestions and encouragement. Mr. Yang Yu provided access to valuable Cassiar Pit Slope data and other materials.

The financial support received from CANMET, Energy,Mines and Resources, Canada, and the Natural Sciences and Engineering Research Council of Canada (NSERC) are gratefully acknowledged.

The work presented in this thesis has benefited greatly from discussions with many colleagues and friends at the University of Ottawa and the National Research Council Canada (NRC). Among them are: Ameir Altaee, Ahmed Derradji-Aout, Kazem Fakharian, David Hansen, Mahbubul Khan, Vince O'shaugnessy, Caizhao Zhan and Ji Zhang.

The author would like to thank his parents for their encouragement and efforts throughout his formal education.

Finally, the author would like to thank his wife, Min, whose understanding, patience and support enabled him to complete this thesis.

ABSTRACT

A numerical method called the Block-Spring Model for analyzing heavily jointed rocks has been developed from first principles. The model simulates the jointed rock mass by an assemblage of rigid blocks interacted through contacts. The contact forces between blocks are determined in terms of the relative displacements between the blocks. By introducing the contact forces and the boundary conditions into the equilibrium equations of the blocks, a set of stiffness equations are obtained in which the unknown variables are the displacements of the blocks. The displacements of the blocks can therefore be determined by solving the stiffness equations. The contact forces between blocks are calculated after the displacements are obtained.

The discontinuities of the jointed rock mass are automatically modelled as the interfaces between the blocks. The deformation behaviour of the joints are governed by a non-tension rule in normal direction. Patton's bi-linear criterion is used to describe the shear failure behaviour of the rock joints. An iteration procedure is applied to describe the progressive failure along the joints. The positions of the blocks are continuously updated based on the displacements obtained after each step of iteration. Therefore, the large scale displacements of the blocks are modelled incrementally with the iteration procedure. During evolution of the block movement, the blocks are allowed to rearrange. The block system may become statically stable or unstable after undergoing large scale displacements. The proposed model therefore identifies unstable blocks by considering the rearrangement of the blocks.

A numerical procedure for simulating the rock bolts has been proposed. The rockbolts are modelled by a series of one dimensional elements interacted with the rock blocks through nodal points. The effect of the rockbolts on the rock masses is evaluated by relating the bolt forces to the displacements of the blocks and by introducing the bolt forces into the equilibrium equations of the blocks. the model can be used to analyze both the end-anchored rock bolts and the fully grouted rock bolts either pre-tensioned or untensioned.

A procedure for modelling the groundwater pressure has also been developed. It has been considered that groundwater may affect the stability of the jointed rock masses by

reducing the effective stresses between the rock blocks. In simulating the groundwater effect on the rock masses, the water pressures imposed on the surfaces of the rock blocks are calculated. These water pressures are introduced into the equilibrium equations of the blocks. The contact forces between blocks determined after solving the equations are the effective forces across the rock joints.

A FORTRAN program, BLOSMER, has been entirely written by the Author based on the procedures of the Block-Spring Model developed during this study. The program can be used to analyze the stability of the surrounding rock masses of either open pits or underground excavations at the shallow depth. It has been applied to several examples to demonstrate the capability of the proposed model. Two case histories have been analyzed in detail with the Block-Spring Model. The numerical results have been compared with the field instrumentation data. Good agreement has been observed between the results from the back analyses with the proposed model and the field measurements in both cases.

The proposed model can be applied for analysis of rock excavations by practicing civil and mining engineers.

TABLE OF CONTENTS

ACKNOWLEDGEMENTS i

ABSTRACT ii

LIST OF TABLES ix

LIST OF FIGURES x

LIST OF SYMBOLS xvi

CHAPTER 1 INTRODUCTION 1

1.1 General 1

1.2 Statement of the Problem 1

1.3 Objectives of the Investigation 2

1.4 Scope of the Investigation 2

1.5 Organization of the Thesis 5

Chapter 2 LITERATURE REVIEW 6

2.1 Introduction 6

2.2 Finite Element Method 6

2.3 Boundary Element Method 8

2.4 Static Rigid Block Models 9

2.4.1 Burman's model 9

2.4.2 Kawai's and Plesha's models 10

2.5 Distinct Element Method 12

2.6 Other Methods 15

2.7 Summary 16

CHAPTER 3 PRINCIPLE OF THE BLOCK-SPRING MODEL 17

3.1 Introduction 17

3.2 Basic Assumptions 18

3.3 Methodology and Formulation 22

3.3.1 Displacements of the blocks 22

3.3.2 Contact forces 28

3.3.3 Contact stiffness 32

3.3.4 Displacement boundary conditions 39

3.3.5 Force boundary conditions and equilibrium equations 42

3.3.6 Stresses within blocks 46

3.3.7 A flowchart for linear analysis 48

3.4 Example 1: Analysis of a Circular Tunnel 50

CHAPTER 4 JOINT FAILURE BEHAVIOUR AND INCREMENTAL PROCEDURE 57

4.1 Introduction 57

4.2 Review of Some Representative Rock Joint Models 57

4.2.1 Patton's joint model 58

4.2.2 Ladanyi and Archambault "LADAR" model 60

4.2.3 Barton-Bandis joint model 61

4.3 Modelling of Joint Strength in the Proposed Model....................62

4.3.1 Joint shear failure criterion....................62

4.3.2 Joint non-tension criterion....................64

4.4 An Iteration Procedure and Large Displacement Problems....................66

4.4.1 Re-setting the contact forces upon failure....................66

4.4.2 An iteration procedure....................68

4.4.3 Determination of unstable blocks....................72

4.4.4 A flowchart of the iteration procedure....................76

4.5 Sequential Excavation Problem....................76

4.5.1 Initial ground stress field....................76

4.5.2 Excavation induced stresses....................83

4.6 Examples 2 and 3: Large Displacement Problems....................87

CHAPTER 5 MODELLING OF ROCKBOLTS....................93

5.1 Introduction....................93

5.2 Modelling of End-Anchored Rockbolt....................94

5.2.1 Numerical representation of the end-anchored rockbolt....................94

5.2.2 Failure criteria....................96

5.3 Modelling of Fully Grouted Rockbolt....................98

5.3.1 Conventional fully grouted rockbolt model....................98

5.3.2 Proposed fully grouted rockbolt model....................100

5.3.3 Determination of the bolt forces....................103

5.3.4 Modification of forces in bolt elements due to bonding failure 107

5.4 Analysis of Rockbolts with the Block-Spring Model 110

5.4.1 Elongation of bolt elements and the block displacements 110

5.4.2 Determination of bolt forces in terms of block displacements 112

5.4.3 Bolt forces in the equilibrium equations 114

5.5 Iteration Procedure, Tensioned and Untensioned Rockbolts 114

5.6 Example 4: Application to a Simple Rock Excavation 118

CHAPTER 6 SIMULATION OF GROUNDWATER PRESSURES 125

6.1 Introduction 125

6.2 Simplifications 125

6.3 Evaluation of the Groundwater Effect 129

6.4 Example 5: Modelling the Effect of Groundwater Pressure 136

CHAPTER 7 COMPUTER PROGRAM FOR THE BLOCK-SPRING MODEL 140

CHAPTER 8 APPLICATION OF BLOSMER TO CASE HISTORIES 145

8.1 Introduction 145

8.2 Application to the Dupont Circle Station Case History 145

8.2.1 Background 145

8.2.2 Analyses of the Dupont Station with BLOSMER 149

8.3 Application to the Cassiar Mine Open Pit Slope 175

8.3.1 Background 175

8.3.2 Analysis with BLOSMER 177

CHAPTER 9 CONCLUSIONS AND RECOMMENDATIONS 185

REFERENCES 188

APPENDIX A REPRESENTATIVE VALUES OF DEFORMATION AND STRENGTH PARAMETER FOR SELECTED ROCKS AND ROCK JOINTS 196

APPENDIX B DERIVATION OF THE AVERAGE STRESS EQUATIONS 200

LIST OF TABLES

Table 4.1 Example 3: Parameters of the rocks and the joints assumed for the simple slope.......90

Table 5.1 Characteristics of the rock and joint filling materials.......118

Table 7.1 Descriptions of major subroutines in the program BLOSMER.......143

Table 8.1 Dupont Station: Basic material properties.......152

Table 8.2 Dupont Station: Rock bolt properties used in BLOSMER analysis.......154

Table 8.3 Cassiar Slope: Material properties used for numerical modelling.......178

Table 8.4 Cassiar Slope: Displacements of the slope obtained from different methods.......184

Table A.1 Typical values of elastic parameters for various rock types.......196

Table A.2 Stiffness factors for the rock joints reported in the literature.......197

Table A.3 Representative values of shear strength parameters for selected rocks and rock joints.......198

LIST OF FIGURES

Fig.2.1 Joint element in FEM (after Goodman, et al., 1968) 7

Fig.2.2 Modelling of discontinuity in BEM 8

Fig.2.3 Burman's rigid block model 10

Fig.2.4 Interaction between blocks in Kawai's model 11

Fig.2.5 Interaction between blocks in DEM 13

Fig.2.6 Comparison of the effects of different damping approaches in the Distinct Element Method (After Cundall, 1987) 15

Fig.3.1 Simulation of jointed rock mass by blocks 19

Fig.3.2 Interactions between blocks 21

Fig.3.3 Modelling of block-to-block contacts by springs 21

Fig.3.4 Displacements of a block 23

Fig.3.5 Determination of displacements of an arbitrary point 24

Fig.3.6 Relative displacements between two blocks 27

Fig.3.7 Normal and shear contact forces 29

Fig.3.8 Horizontal and vertical components of the contact forces 31

Fig.3.9 Typical stress-displacement relations of rock joints 33

Fig.3.10 A hyperbolic relation between normal stress and normal displacement of rock joint (after Goodman, 1976) 34

Fig.3.11 Dimension of the blocks for determination of the stiffness of the intact rock 36

Fig.3.12 A three-spring system in simulating the rock-joint-rock contact 38

Fig.3.13 Application of boundary displacement 40

Fig.3.14 Possible forces on a block 43

Fig.3.15 A flowchart of the Block-Spring Model for linear analysis 49

Fig.3.16 Example 1: An underground circular tunnel 51

Fig.3.17 Example 1: Rock medium considered and discretized blocks 54

Fig.3.18 Example 1: Stress vectors obtained from the proposed model...............55

Fig.3.19 Example 1: Stress distribution on section I-I.....................................56

Fig.4.1 Shear strength envelopes for joints with irregular surface (after Patton, 1966) 59

Fig.4.2 Determination of shear strength of rock joints 63

Fig.4.3 Simulation of contact failure behaviour 65

Fig.4.4 Resetting contact forces after shear failure 67

Fig.4.5 A tangent iteration procedure for stable block system 71

Fig.4.6 A stable block system after large displacement takes place 73

Fig.4.7 An unstable block system resulted after large displacement....................74

Fig.4.8 Iteration procedure for unstable block system.....................................75

Fig.4.9 A flowchart of the iteration cycle performed upon joint failure 77

Fig.4.10 Vertical stress distribution (after Herget, 1986) 78

Fig.4.11 Variation of ratio, $K=\frac{\sigma_h}{\sigma_v}$, with depth (after Herget, 1986) 80

Fig.4.12 Uniformly distributed horizontal load 81

Fig.4.13 Horizontal load with a constant $K=\frac{\sigma_h}{\sigma_v}$ 82

Fig.4.14 Simulation of sequential excavation 84

Fig.4.16 Example 2: A three block system 88

Fig.4.17 Example 2: Final state of the block system from the proposed model 88

Fig.4.18 Example 2: A three block system with block 3 separated from the others 89

Fig.4.19 Example 2: Unstable block system determined by the Block-Spring Model 89

Fig.4.20 Example 3: A simple rock slope with stratified rocks 91

Fig.4.21 Example 3: Intermediate result 91

Fig.4.22 Example 3: Final result 92

Fig.5.1 Simulation of end-anchored rockbolt 95

Fig.5.2 A yield failure criterion for bolt material 97

Fig.5.3 A rigid-plastic criterion for the bolt/rock anchorage 97

Fig.5.4 A typical model of the fully grouted rockbolt 99

Fig.5.5 Representation of rockbolt with elements joined by nodes 101

Fig.5.6 Rockbolt elements bonded to the rock at the nodes 102

Fig.5.7 Bolt forces imposed on rock blocks 104

Fig.5.8 Determination of average shear force between rockbolt and rock block 106

Fig.5.9 Updating the bolt/rock shear force by modifying the rockbolt forces 109

Fig.5.10 Determination of rockbolt elongation and axial force 111

Fig.5.11 A flowchart of the iteration procedure for consideration of rockbolts 117

Fig.5.12 Example 4: An underground excavation in jointed rocks 120

Fig.5.13 Example 4: Unstable block first detected 121

Fig.5.14 Example 4: Another block is detected unstable after the roof is stabilized 122

Fig.5.15 Example 4: All the blocks are stabilized 123

Fig.5.16 Example 4: Displacements of the blocks after three blocks are supported 124

Fig.6.1 Simplification of groundwater problem in rock mass 126

Fig.6.2 Water pressure in rock joint 127

Fig.6.3 A rock element under different water pressures on different faces 128

Fig.6.4 Straight line segments representing the water table and a partially submerged block 130

Fig.6.5 Water pressure on a fully submerged face of a block 131

Fig.6.6 Determination of water pressure on a partially submerged face of a block 133

Fig.6.7 Horizontal and vertical components of the equivalent forces 135

Fig.6.8 Example 5: A hypothetical rock foundation of a concrete dam 137

Fig.6.9 Example 5: Displacement vectors of the dam and the rock blocks 138

Fig.6.10 Example 5: Exaggerated movements of the dam and the rock blocks 139

Fig.7.1 A flowchart of the program BLOSMER 142

Fig.8.1 A cross-section of Dupont Circle Station (After Rodriguez Perez, 1980) 146

Fig.8.2 Dupont Station: A typical geologic cross-section (after Rodriguez Perez, 1980) 148

Fig.8.3 Dupont Station: A Finite Element Mesh and boundary conditions used by Rodriguez Perez (1980) (Also used for BLOSMER analysis) 150

Fig.8.4 Dupont Station: A mesh with rockbolts for BLOSMER 154

Fig.8.5 Dupont Station (Case 1): Displacement vectors of the rock blocks from BLOSMER 156

Fig.8.6 Dupont Station (Case 1): Movements of the rocks obtained from BLOSMER analysis 157

Fig.8.7 Dupont Station: Movements of the rocks obtained from FEM (After Rodriguez Perez, 1980) 158

Fig.8.8 Dupont Station: Settlements at the top of the rock from BLOSMER 159

Fig.8.9 Dupont Station: Settlement trough at top of rock (After Rodriguez Perez, 1980) 160

Fig.8.10 Dupont Station (Case 1 - uniform rockbolt pressure): Comparison of the displacements obtained from the different methods 162

Fig.8.11 Dupont Station (Case 2): Rock displacement vector plot from BLOSMER 167

Fig.8.12 Dupont Station (Case 2 - rockbolts applied in BLOSMER): Comparison of the displacements from different methods 168

Fig.8.13 Dupont Station: Forces along the rock bolts from BLOSMER 171

Fig.8.14 Dupont Station: Rockbolt pressures imposed on the opening walls 174

Fig.8.15 A section of Cassiar Open Pit Slope (after Cassiar Mining Co. & Piteau Associates Engineering Ltd., 1990) 176

Fig.8.16 Cassiar Slope: A mesh of the Block-Spring Model 180

Fig.8.17 Cassiar Slope: Displacement vectors from BLOSMER analysis 181

Fig.8.18 Cassiar Slope: Velocity vector plot from UDEC analysis (after Cassiar Mining Co. & Piteau Associates Engineering Ltd., 1990) 182

Fig.8.19 Cassiar Slope: Comparison of displacements along the slope 183

Fig.B.1 Discretization of boundary S of region A 203

LIST OF SYMBOLS

SINGLE TERMS:

α Angle of the outward normal n of the edge of block from x axis;

A Volume (area) of the block; Area of the cross-section of the rockbolt;

β Angle of the axis of a bar element or of a rock bolt from the x axis;

C Cohesion;

E Elastic modulus;

F Contact force;

ϕ Friction angle;

ϕ_r Residual friction angle;

γ Unit weight;

i Inclination angle of asperities on the surface of the rock joint;

$K=\frac{\sigma_h}{\sigma_v}$ Ratio of horizontal stress to vertical stress;

K_b Stiffness of rockbolt element;

K_d Stiffness of bar element;

K_n Normal contact stiffness;

K_s Shear contact stiffness;

l Length of the edge of the block;

l' Submerged length of the edge of the block;

L Length of the rockbolt element;

ΔL Elongation of the rockbolt element;

M_c	Moment of a force on a block about the centroid of the block;
μ	Poisson's ratio;
n	Outward normal of the edge of block;
P	External load;
P_w	Resultant groundwater pressure transformed to the corners of the block;
q	Groundwater pressure;
R_d	Boundary reactive force;
R_w	Total groundwater pressure on an edge of a block;
S	Shear force along the bolt/rock interface;
σ	Normal stress;
$\bar{\sigma}_{ij}$	Average stress within block;
T	Tension in rockbolt;
τ	Shear stress;
Θ	Rotational component of the displacement of the centroid of a block;
u	Horizontal component of the displacement of an arbitrary point on a block;
U	Horizontal component of the displacement of the centroid of a block;
v	Vertical component of the displacement of an arbitrary point on a block;
V	Vertical component of the displacement of the centroid of a block;
W	Gravity force;
w_0	Prescribed boundary displacement;
x, y	Global Cartesian coordinates;
$\bar{x}$, $\bar{y}$	Local coordinates originated from the centroid of the block.

ARRAYS AND MATRICES:

[B] $[2\times3]$ geometry matrix consisting of local coordinates;

{c} $=\{\cos\alpha, \sin\alpha\}^T$ or $\{\cos\beta, \sin\beta\}^T$, a vector for coordinate transformation:

$[D]_{ij}$ $[2\times6]$ geometry matrix consisting of local coordinates of blocks i & j;

$\{\delta\}$ Relative displacement between blocks in terms of normal and shear components;

{F} Vector of contact forces;

[K] Global stiffness matrix;

$[k]_{ij}$ $[2\times2]$ stiffness matrix relating {F} to $\{\delta\}$ between blocks i and j;

$[K]_{ij}$ $[3\times6]$ stiffness matrix relating {F} to {U} between blocks i and j;

{P} A vector of constants (boundary conditions) in the global stiffness equation:

[T] $[2\times2]$ matrix for coordinate transformation;

$\{\Delta u\}$ Relative displacement between two blocks at the contact point;

{u} Displacement vector of an arbitrary point on a block;

{U} Displacement vector of the centroid of the block.

SUBSCRIPTS:

b Rock bolt;

c Centroid of block;

d Bar element (for displacement boundary condition);

i, j Block numbers (except in $\overline{\sigma}_{ij}$);

i Iteration step;

λ Nodal umber of the rockbolt element;

n Normal direction;

r Residual;

s Shear direction;

w Groundwater;

x Component in x direction;

y Component in y direction.

SUPERSCRIPTS:

T Matrix or vector transposition.

CHAPTER 1
INTRODUCTION

1.1 General

Stability of rock masses is one of the most important concerns in rock excavations in both mining and civil engineering. Evaluation of the state of stress and deformation of the jointed rocks is important from a safety hazard point of view as well as from economical considerations. There is an urgent need in both mining and civil engineering industry for practical yet realistic and reliable analytical techniques for rational design of mine openings, tunnels and underground chambers. In the case of jointed rocks, it becomes essential that the analyses be capable of incorporating the influence of the geological discontinuities. Indeed, one of the most difficult problems in studying the stress and deformation behaviour of the jointed rock masses is the modelling of the discontinuities. The conventional numerical methods, such as the Finite Element Method and the Boundary Element Method, which are popular in analyzing continuous media, may not be suitable for simulating discontinuous rocks. Though some rigid block models have been developed since the 1970's, as will be reviewed in the present thesis, the problem of modelling densely jointed rocks still remains.

The research program outlined in this thesis relates to development of a numerical technique for the analyses of stability of excavations in jointed rocks. In these studies, a new numerical model called the Block-Spring Model has been developed, which is especially suitable for modelling the densely jointed rocks. It is intended to be utilized in the designs of shallow mines or other rock excavations at shallow depth.

1.2 Statement of the Problem

The rocks at shallow depth are often highly jointed or discontinuous. Shallow excavations, such as most road and rail tunnels or the near surface workings in mines, are strongly influenced by the structural discontinuities of the rock mass. The strength of the rock mass often bears little relation to the strength of laboratory specimens of the intact rock between the discontinuities. It is influenced predominantly by the mechanical properties of the discontinuities themselves, and the orientation of the blocks (Fairhurst, 1988). It is therefore essential that any rational method of analysis be capable of modelling the discontinuous nature of the rock.

In practice, the design of near surface workings in mines and other rock excavations, such as surface crown pillars in jointed rock, is generally undertaken on the basis of empirical guidelines. Bétournay (1986) notes: "Extensive CANMET surveys have indicated that so far, most Canadian mines have dimensioned their pillars arbitrarily and conservatively, based on 'personal' experience rather than using an engineering process and methods based on sufficient rock and geotechnical data." Bétournay further notes that "the exact locations of critically oriented/spaced discontinuities, their relationships as well as areas of weakness are essential to maximize the effectiveness of the dimensioning and stability approaches."

The need for rational design methods is also prompted by economical considerations. Often, the rock mass in the surface crown pillars contains valuable veins of mineralized rock. It is therefore of economic interest to be able to design the dimensions and spacing of these pillars without introducing unnecessary conservatism.

1.3 Objectives of the Investigation

The objective of the proposed research is to develop a reliable, yet practical, numerical model for the stability analysis of jointed rocks. The model should be able to simulate the blocky and discontinuous nature of the jointed rocks. The method should permit rational design of either open or shallow underground mines or other rock excavations at shallow depth. It should be able to analyze the effect of rock bolts which have become dominant in the ground support systems in mines. The influence of groundwater must also be investigated as it is often encountered in rock excavations. The ultimate objective, therefore, is to develop a reliable method which is required by the mining and civil engineering industry, and which is applicable in engineering practice.

1.4 Scope of the Investigation

The research was concentrated on the development of a Block-Spring Model for jointed rocks. The model has been developed in its entirety, working from first principles, by the Author. Detailed investigation of the theory and a computation scheme of the model was carried out. The investigations presented herein consisted of the following topics.

(a) Simulation of the discontinuity of the jointed rocks

A dominant feature of the jointed rock mass is the presence of discontinuities. The discontinuities determine the high non-linearity of the jointed rock materials. Modelling of the discontinuities and the non-linearity of the rock masses was one of the major topics in the development of the numerical model.

(b) Explicit modelling of the rock joint strength

The joint conditions may significantly affect the strengths and deformations of the rock masses. The strengths and the deformabilities of the rock joints were explicitly simulated in the numerical model. As the shear strength of the rock joints are usually reduced after local crushing and shearing of the asperities on the joint surfaces, both the peak strengths and the residual strengths of the joints were modelled.

(c) Modelling of large scale sliding of the rock blocks

Rock excavation may disturb the original state of the ground stress and result in deformation of the rock masses. Separation of the rock joints and sliding of the rock blocks may take place. The re-arranged rock blocks may become either stable or unstable depending on the stress and rock structural conditions. It is important that the numerical model be capable of simulating large scale displacement problems in order to serve for rational design of excavations. The capability of modelling large displacements is a special feature of the present study.

(d) Prediction of unstable blocks

Unstable blocks or critical blocks around the excavations are of concern, and the prediction and identification of such blocks is required for safety as well as economy. Such a feature is also useful for the design of ground support of the excavation. Based on the large displacement solution, the design of an underground excavation can be less conservative than that obtained by adopting small displacement assumptions.

(e) Simulation of joint filling materials

The joint filling materials affect the strength of the rock mass to various levels of significance depending on the strengths, deformabilities and thicknesses of the filling materials. Simulation of such effects was also investigated.

(f) Modelling of rockbolts

Rock bolting is probably the most important measure of providing ground support in mines and other rock excavations. The rockbolts are widely used not only to support the rocks directly, but also, most importantly, to help the self support of the rock blocks. The model developed in this research is capable of simulating both the end-anchored rockbolts and the fully grouted rockbolts. Simulations of both pretensioned and untensioned rockbolts have been investigated.

(g) Modelling of groundwater effect

Groundwater is another important factor affecting the stability of the rock masses. The groundwater problems are often encountered in underground engineering. Simulation of the groundwater effect has been incorporated in this research.

(h) Simulation of sequential excavation problems

The designers of underground openings always seek for optimum excavation sequences as both safety and productivity are concerned. Optimizing the sequence of the excavation is required in other rock engineering projects as well. A computational scheme for modelling the stress re-distributions from the original states of stresses was made to solve such problems.

A FORTRAN program was developed based on the investigations of above topics. The computer program was written for general purpose 2-D analyses of a variety of rock excavation problems including open pits or underground mines, tunnels, slopes and foundations. Several examples provide a demonstration of the various features of the proposed model. The model was also verified by application to practical engineering problems, in which the numerical results from the proposed model were compared with those of field observations as well as those from other numerical methods

1.5 Organization of the Thesis

The numerical models available for analyzing the jointed rock masses are reviewed in Chapter 2. The methodology and the basic formulation of the proposed Block-Spring Model are given in Chapter 3. Advanced investigations of the rock joint behaviour, the large displacement and unstable block problems and the analysis of sequential excavation are described in Chapters 4. Other features including simulations of rockbolts and groundwater are discussed in Chapter 5 and 6 respectively. Examples for demonstrating the different features of the proposed Block-Spring Model are given at the end of the particular chapters describing the features. Programming of the proposed model is explained in Chapter 7. The applications of the model to practical engineering problems and case histories are provided in Chapter 8. Chapter 9 concludes the investigations with some recommendations for further research.

Chapter 2
LITERATURE REVIEW

2.1 Introduction

The investigation of numerical modelling of jointed rock masses has been undertaken since late 1960's. At the early stage of the numerical modelling, the Finite Element Method (FEM) was often used to simulate the rock masses with special treatments for the joints (e.g., Zienkiewicz et al., 1968; Goodman et al., 1968; Best, 1970; Ghaboussi et al., 1973; Heuze and Barbour, 1982). Burman (1971) simplified the Finite Element procedure using the rigid blocks instead of the conventional finite elements to simulate the intact rock blocks. Later, Kawai (1977) and Plesha (1983) developed their rigid block models in which modelling of the discontinuities of the media is further simplified. These methods are static approaches which solve the problems by manipulating the stiffness matrices. In 1971, Cundall developed a Distinct Element Method which is especially suitable for analyzing the densely jointed rocks (e.g., Cundall, 1971). The Distinct Element Method simulates the jointed rocks by blocks with a dynamic relaxation procedure. This method is probably better known for its capability of simulating the large scale displacements and collapse of the blocks. The above numerical methods and some other methods are reviewed below.

2.2 Finite Element Method

The Finite Element Method, at its most elementary level, involves replacing a complicated problem of continuously varying functions with an approximate equivalent. Based on this concept, the continuous medium is discretized into a finite number of pieces called elements. The elements interact on each other through their nodal points or nodes. All the elements connected through a node experience the same displacement at that node. The nodal forces and the nodal displacements solved are used to evaluate the stress and deformation of each element.

Investigation for modelling the discontinuous media with the Finite Element Method has been performed by several researchers as mentioned previously. In modelling the jointed rocks, special joint elements were used to simulate the joints, and the conventional finite elements were used to simulate the intact rocks as shown in Fig.2.1 (e.g., Goodman et al., 1968.)

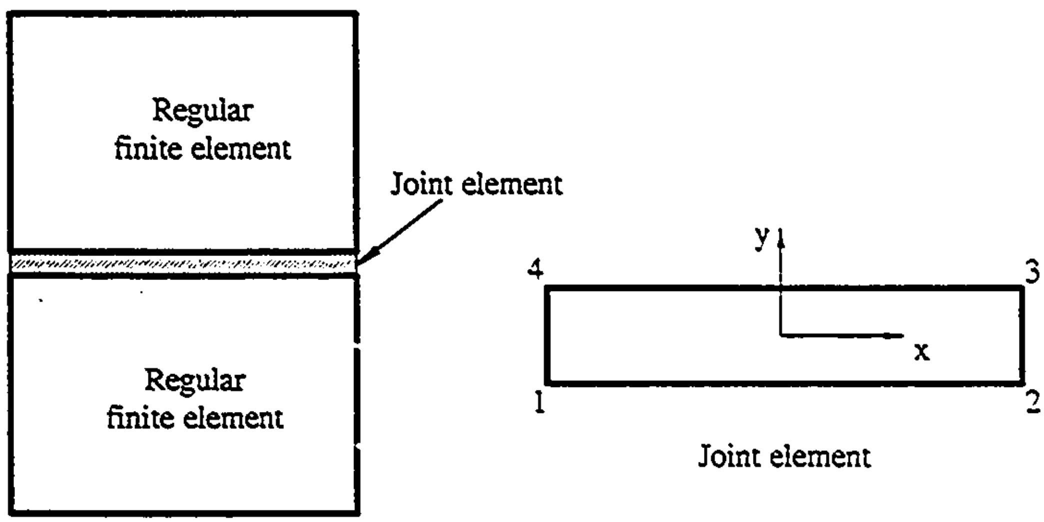

Fig.2.1 Joint element in FEM (after Goodman, et al., 1968)

The joint element is a rectangular element with zero thickness. The stiffness matrix for the joint element is derived in the same way as for the regular finite element. Failure condition of the joint element may be governed by Mohr criterion. If tension occurs in a joint element, the normal and shear stiffnesses, K_n and K_s, are set to zero. If shear failure occurs along a joint, the shear stiffness K_s is set to the residual value $K_{s(residual)}$.

The Finite Element Method has achieved success in the analyses of certain jointed rock problems, particularly in configurations consisting of a few major joints. However, it is difficult to simulate large displacement problems. Also, it is not convenient to simulate heavily jointed rocks, as the number of joint elements is greatly increased and a very large number of degrees of freedom are therefore required.

2.3 Boundary Element Method

Although the Finite Element Method has been used in many practical problems, the Boundary Element Method (BEM) appears as an alternative technique which in many cases can provide more reliable or economical analysis. The Boundary Element Method has evolved rapidly over the past decade or so. The gain in popularity of the method is based on the fact that only the boundary of the continuous medium is discretized into segments (boundary elements). The formulation describes the effects of a load at one segment on the response of the other segments. When the entire set of relations is assembled, a system of simultaneous equations results. By solving these equations, the boundary displacements and tractions can be obtained and then the stresses and strain inside the region can be evaluated.

In modeling the discontinuous media, each discontinuity has to be considered as two parallel boundaries on its two sides and each side has to be divided into segments (elements). Normal and shear springs are used to simulate the interactions between the two boundaries (Fig.2.2) (e.g. Crouch and Starfield, 1983 and Crotty and Wardle, 1985).

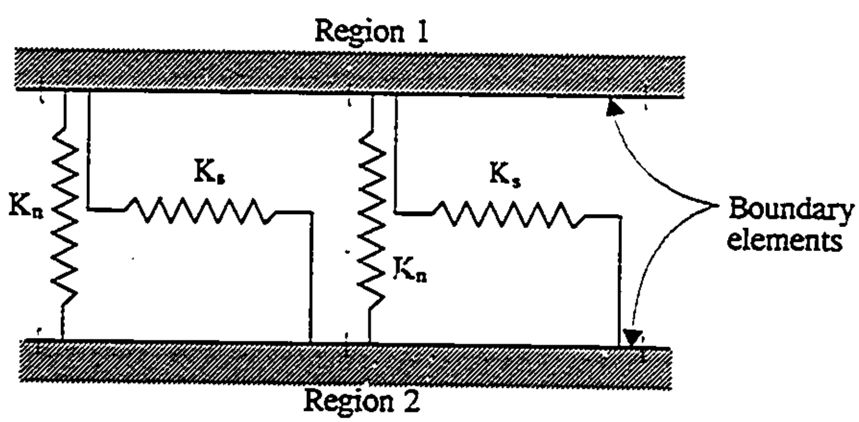

Fig.2.2 Modelling of discontinuity in BEM

Since only the boundaries of the concerned media need to be discretized, the method possesses the following advantages:

a) Smaller amount of data;
b) Reduced set of equations;
c) Proper modelling of infinite domains;
d) No interpolation error inside the domain; and
e) Valuable representation for stress concentration problems.

The disadvantages of the Boundary Element Method are also obvious. The matrices in the system of simultaneous equations are fully populated, and consequently the method requires more computer storage and computer time. For non-homogeneous media, all the boundaries of the different materials must be discretized. This increases the number of the elements and expands the size of the matrices dramatically. Though the Boundary Element Method is efficient in modeling continuous media, it is severely restrictive in modelling densely jointed rocks as discontinuous media because all the discontinuities need to be considered as boundaries.

2.4 Static Rigid Block Models

2.4.1 Burman's model

Similar to the Finite Element approach, Burman (1971, 1974) developed a rigid block model for modelling the discontinua. The rock mass is simulated by an assemblage of rigid blocks which interact through joint elements. In contrast to the Finite Element Method in which the intact rock blocks are simulated by deformable elements (Fig.2.1), Burman's model simulates the intact blocks by rigid blocks (Fig.2.3).

The joint element in Burman's model is a four-node rectangular deformable element, similar to a finite element. The difference of Burman's joint element (Fig.2.3) from the joint element in FEM (Fig.2.1) is that the nodal displacements of Burman's joint element are dependent on the block movements. In contrast, the nodal displacements of the joint element in FEM are variables which need to be determined independently.

In Burman's model, the stiffness matrix for the joint elements is derived based on the principle of the Finite Element Method. The joint stiffness is obtained by an integration over the joint element. As the intact blocks are assumed rigid, the number of degrees of freedom is greatly reduced comparing to Goodman's Finite Element model. However, as the joint elements are used, it is not convenient to re-arrange the interactions between the blocks with development of the block movement. Consequently, it is difficult to simulate large displacement of the blocks.

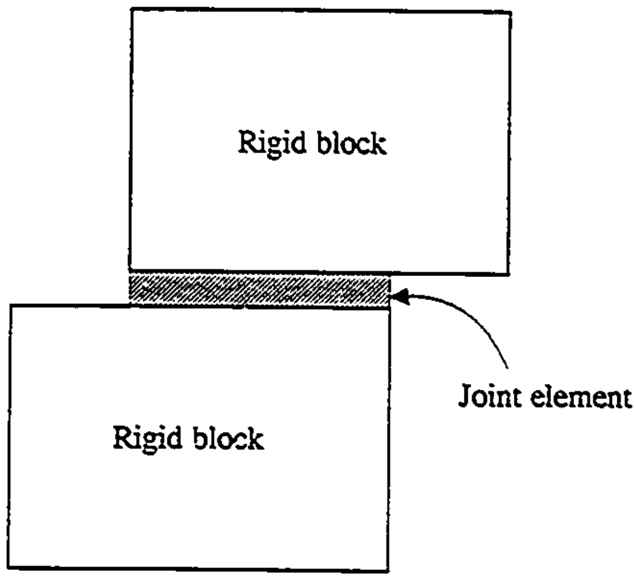

Fig.2.3 Burman's rigid block model

2.4.2 Kawai's and Plesha's models

Kawai (1977) developed a Discrete Element Model originally for continuous media in solid mechanics problems. This model has been introduced to the rock mechanics (see, for example, Kawai, et al., 1981; Niwa, et al., 1984; Hamajima, et al., 1985; and Suzuki, et al., 1985). In the Discrete Element Model, the solid media are discretized into discrete elements. It is assumed that the elements are rigid and are joined face to face through springs which are continuously distributed over the contact area (Fig.2.4). The strain energy is stored in the springs when the media deform. The strain energy is determined by an integral over the contact area between adjacent elements as follows:

$$\Xi = \frac{1}{2}\int_A (k_n\delta_n^2 + k_s\delta_s^2)\, dA$$

where Ξ denotes strain energy in the springs; k_n and k_s are the stiffnesses of normal and shear springs respectively; δ_n and δ_s are deformations of the normal and shear springs respectively and A is the interacting area between the elements.

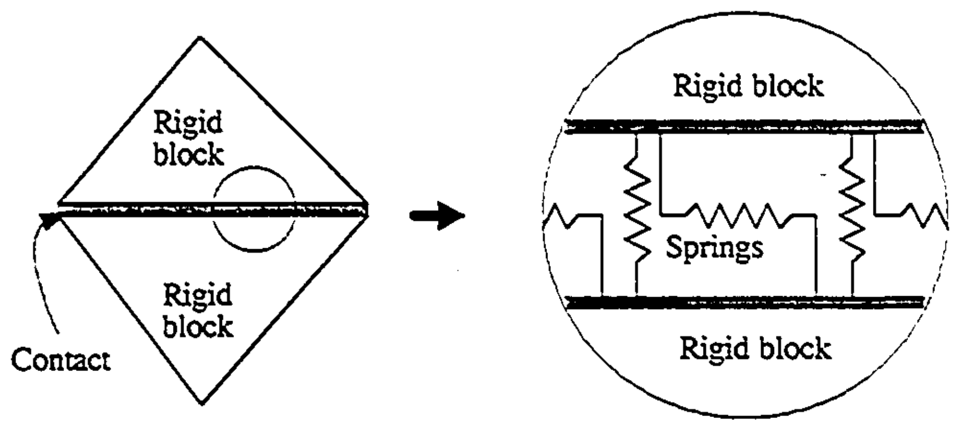

Fig.2.4 Interaction between blocks in Kawai's model

By applying the theorem of minimum potential energy and evaluating the surface integral with a finite difference approach, a set of simultaneous equations are obtained. The deformation of the medium is determined by solving the equations. "The procedures of making overall stiffness matrix and solving simultaneous linear equations are almost the same as FEM." (Suzuki, et al., 1985).

In Kawai's model, the distributed stresses along the boundary surfaces of the elements are evaluated. The development of the model has been concentrated on predicting where the tensile stress develops and where the cracks occur. Cracking occurs between two adjacent elements if the tensile stress exceeds the tensile capacity of the joint (Hamajima, et al., 1985). This method has been successful in predicting tensile zones and development of cracking (Kawai, et al., 1978; Kawai, et al., 1981; Hamajima, et al., 1985; Kawai, et al., 1987). However, the method would be too conservative to determine the stability of the jointed rocks by tensile stresses alone without considering the large displacements of the elements. In fact, as only face to face contact between the elements is allowed, it is difficult to simulate the large displacement and re-arrangement of the elements.

Plesha (1983) also presented a numerical model for jointed media (see also Belytschko, et al., 1984). Plesha's model simulates the jointed media in a manner similar to Kawai's Discrete Element Model. In this model, "the blocks at intersecting joints are assumed always to interact with the same blocks." The block to block contacts are fixed and known. Only edge to edge contacts between blocks are assumed to exist. Hence the model is only valid for small relative displacements of the rock joints. The model, therefore, shares the same limitation as the Discrete Element Model.

2.5 Distinct Element Method

Cundall's Distinct Element Method (DEM) is a discontinues modelling approach for simulating the behavior of jointed rock masses, see, for example, Cundall (1971, 1976, 1987, 1988), Cundall and Strack (1979), Lorig (1984), Lorig, et al., (1986), and Hart, et al., (1988). The method models the rock mass as an assemblage of blocks interacting through edge to edge contacts or corner to edge contacts (Fig.2.5). The use of the corner to edge contact makes the method more flexible in modelling large scale displacement.

The method utilizes an explicit time-stepping (dynamic) algorithm which allows large displacements and rotations. In the dynamic approach, the blocks are assumed to be accelerated by the acting forces including the external forces, the gravity forces and the contact forces between the blocks. Newton's second law of motion is used for each block:

$$F = m\frac{d^2x}{dt^2}$$

where F denotes the resultant force on the block;

m is the mass of the block;

x denotes the dimensional measurement or displacement; and

t denotes time.

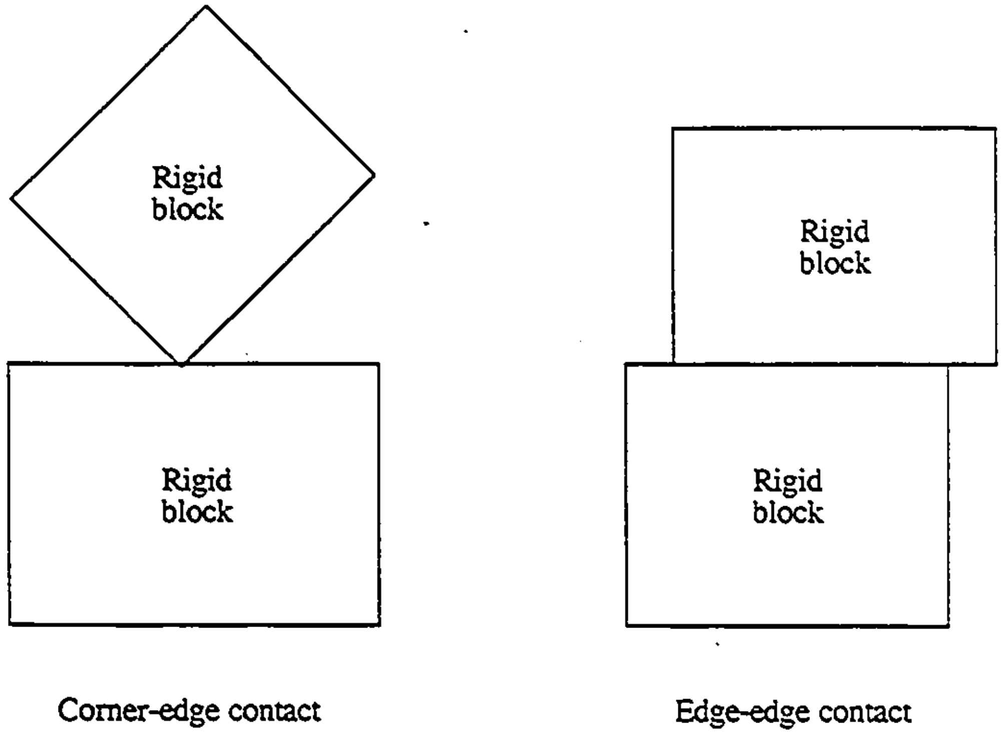

Fig.2.5 Interaction between blocks in DEM

The blocks are relaxed one by one in each time step. The acceleration (d^2x/dt^2), velocity (dx/dt) and the displacement (x) of the relaxed block are determined based on the time interval adopted using the finite difference approximation. The blocks always oscillate due to repeated balance and unbalance of the contact forces. A damping procedure, therefore, has to be used to dissipate the kinematic energy and to make the blocks converge to a statically stable state.

An attractive advantage of the Distinct Element Method is its capability of simulating large scale displacement including the collapse of the rock mass.

While the dynamic scheme is efficient in modelling the large displacements of the blocks, some problems can be introduced by the dynamic procedure in simulating the static behaviour of the rock masses. It should be noted that oscillation of the blocks under static load rarely occurs in the field. The rock blocks usually achieve their static state after corresponding deformation has occurred, rather than by undergoing a large number of cycles of oscillation. Therefore, damping of the blocks should be performed with great care; otherwise, the irrecoverable deformation of the rock mass could be misrepresented. The following difficulties associated with a velocity-proportional damping procedure, as described by Cundall (1987), indicate the possible problems associated with the dynamic approach:

a) The damping introduces body forces, which are erroneous in 'flowing' regions, and may influence the mode of failure in some cases.

b) The optimum proportionality constant depends on the eigenvalues of the matrix, which are unknown unless a complete modal analysis is done. In a linear problem, this analysis needs almost as much computer effort as the dynamic relaxation calculation itself. In a non-linear problem, eigenvalues may be undefined*.

c) In its standard form, velocity-proportional damping is applied equally to all nodes, i.e., a single damping constant is chosen for the whole grid. In many cases a variety of behavior may be observed in different parts of the grid; for example, one region may be failing while another is stable. For such problems, different levels of damping are appropriate for different regions.

Various damping procedures have been proposed to overcome one or more of these difficulties, e.g., Cundall (1987). A simple example was given in Cundall (1987) to compare some of the damping schemes. The comparison is reproduced in Fig.2.6. A column of blocks resting on frictional base was pushed from the left-hand side. The curves in Fig.2.6 show the reaction forces on the left-hand block obtained from different damping procedures. It is indicated that some damping schemes provide better results than the others. Unfortunately, no extensive comparison was reported to show the influences of different damping constants in an individual damping scheme. Also, the response of a complex rock mass to different damping constants, particularly when the deformation of the rock mass is irrecoverable, has not been presented.

---

* Actually, all the large scale displacement problems or the constitutive behavior of the densely jointed rock masses, which the method attempts to solve, are non-linear problems.

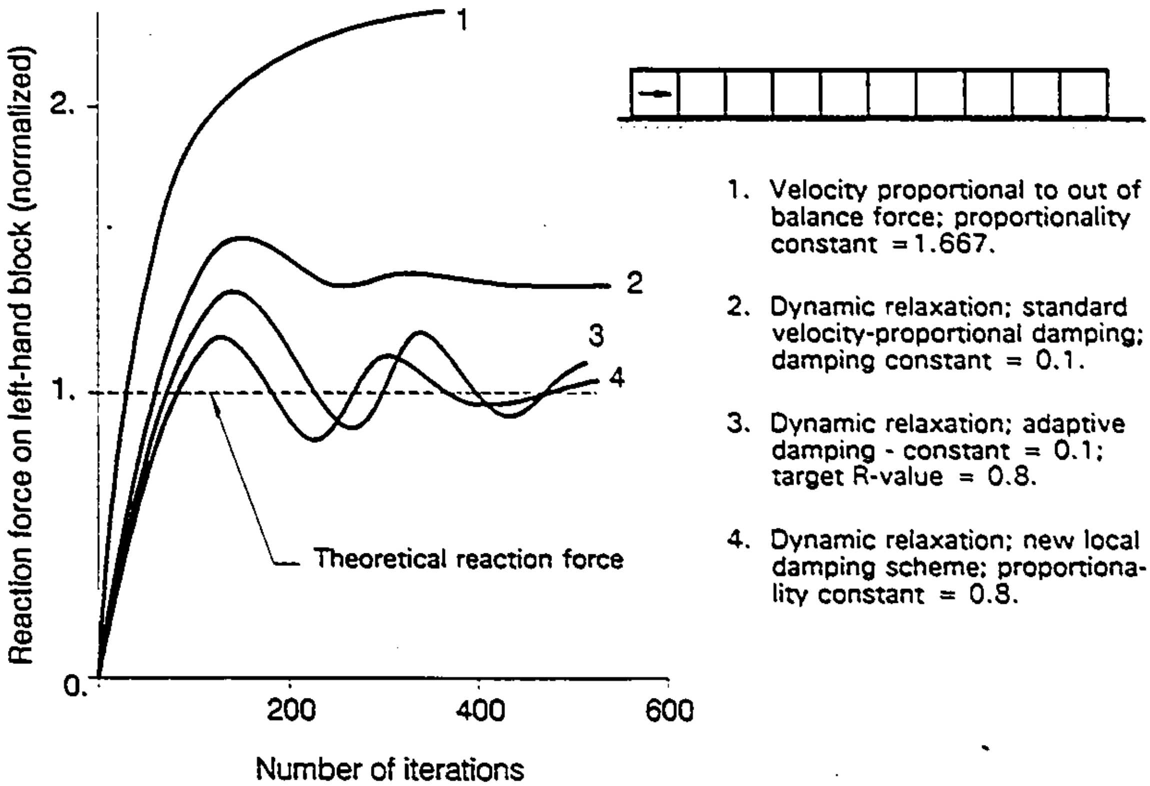

Fig. 2.6 Comparison of the effects of different damping approaches in the Distinct Element Method (After Cundall, 1987)

2.6 Other Methods

Stewart Block Relaxtion Method Stewart (1981) presented a block relaxation precedure which is an extension of the Cundall's dynamic relaxation method (see also, Stewart and Brown, 1984). In Stewart's method, the rock blocks are relaxed one by another. The displacement of the relaxed block is determined using the equilibrium equations. Although the method avoides the damping problem associated with the dynamic procedure, 'the modes of deformation possible in a jointed rock mass may well be dependent on the path taken, i.e., the resulting behaviour is path dependent' (Stewart, 1981).

The Discontinuous Deformation Analysis Shi and Goodman (1988) proposed a Discontinuous Deformation Analysis (DDA) method for jointed rocks. The rock masses were modelled by blocks which were subjected to constant strain and rigid movement. The minimum work theory was used throughout the model to construct the stiffness equations. In order to obtain the compressive normal contact force without overlap between two blocks, a stiff spring is imposed on the contact point and the relative displacement between the two blocks as well as the contact force are adjusted several times. Unfortunately, no further report has been found for the procedures of modelling the different joint conditions, the shear behaviour of the joint and the procedure for nonlinear analysis.

2.7 Summary

From the above review, it can be noted that the available numerical methods for jointed rocks fall into two categories, i.e., static (matrix) procedure and relaxation procedure. The static methods obtain their solutions by assembling the stiffness matrix. The formulations of these static approaches are similar to that of the finite element method. A major limitation of these models is that they are difficult to simulate the real large displacement of the rock blocks, though the discontinuities of the jointed rocks can be well represented.

The Finite Element Method with the joint element incorporated has achieved success in certain applications, see, for example, Rodriguez Perez (1980). However, it is obviously inconvenient for simulating the heavily jointed rock masses.

The other static models assume that the intact rocks are rigid, and the deformation of the rock mass as a whole is resulted from the relative displacements of the blocks. These assumptions are suitable for the densely jointed rock masses in shallow depth where the ground stresses are low and the deformation of the intact rocks can be ignored when compared to the deformation of the joint. In other words, the models are suitable when the stabilities or deformations of the rock masses are governed by the joints. Therefore, upon adopting the rigid block assumptions, the models lose their advantages if the large displacements can not be simulated.

The relaxation procedures are successful in modelling the large displacements of the blocks. However, problems still exist with these methods such as the uncertainty of the damping effect and the path dependent problem.

CHAPTER 3

PRINCIPLE OF THE BLOCK-SPRING MODEL

3.1 Introduction

A numerical method called the Block-Spring Model is proposed here in this thesis as an alternative method for simulating the jointed rock mass. It is aimed at solving the stress and deformation problems of the jointed rock mass in a manner different from the other methods reviewed previously. As Burman (1974) stated, "there can be little doubt that the blocky nature of jointed masses has to be explicitly recognized if meaningful numerical simulation of these masses is to be achieved." Without exception, the proposed Block-Spring Model simulates the jointed rock masses by blocks. However, the proposed model is theoretically and mathematically different from the other models. Also, the procedure has been developed to overcome the major shortcomings of the other methods which can be summarized as follows:

A static approach is used in the proposed model to avoid the difficulties in the dynamic approach, e.g., in choosing an appropriate damping scheme. Therefore the proposed model is fundamentally different from the Distinct Element Model. The Distinct Element Model simulates the static behaviour of the rocks by applying the Newton's Second Law of motion to the rock blocks which causes oscillation of the blocks. The static solution is then obtained by damping the oscillating blocks to a static state. The proposed Block-Spring Model is a static procedure in which the equilibrium conditions of the blocks are used to determine the state of stresses and deformations. In the Distinct Element Model, the rock blocks are relaxed one by another in each time step. In the Block-Spring Model, deformation of the whole rock mass is allowed in the same step. The dynamic relaxation procedure makes the Distinct Element Model capable of simulating the "contact free blocks". Consequently, toppling and collapse of the rock blocks can be modelled. The proposed procedure has not been developed to simulate the "free falling" blocks; however, it has been made capable of modelling the large displacements of the blocks which lead to collapse of the blocks or to a condition of "free falling". As the blocks are allowed to displace at the same time, the proposed model also avoids the path dependent problem, which is associated with the relaxation procedures.

The Block-Spring Model has also been developed to overcome the shortcomings of the other static models. In the static procedures reviewed in the previous chapter, major attention has been paid to studying the discontinuities of the rock media. The Block-Spring Model has been developed not only to simulate the rock discontinuities, but also to model the large displacements of the blocks which are neglected by the other static models. The modelling techniques and formulations in the Block-Spring Model are also different from those in the other static models. The other static models use either deformable joint elements or springs continuously distributed along the contact area to simulate the interactions between blocks. The models are formulated based on the stress-strain relations of the joints. The assumption of the unchanged contacts between blocks restricts the models from simulating the large displacements of the blocks. The proposed Block-Spring Model simulates the interactions between blocks in a simpler manner than the other static models as will be discussed later in this chapter. The model analyses the forces between blocks to allow the direct application of the equilibrium equations of the blocks. The formulation is therefore simpler and more direct. In contrast to other static methods, the acceptance of both edge to edge contact and corner to edge contact between blocks makes the model easier in simulating the re-arrangement of the blocks. As the proposed model has been developed to allow the large displacements to take place, predictions of the unstable blocks can be made in a more realistic manner.

The basic modelling techniques and formulations of the Block-Spring Model are presented in the present chapter. The advanced features of the model are discussed in subsequent chapters.

3.2 Basic Assumptions

In the cases of rock excavations in shallow depth, such as open pits and shallow underground mines, the rock masses around the excavations are usually highly jointed. As in other block models, the Block-Spring Model simulates the jointed rock mass by an assemblage of rock blocks separated by the joints (as shown in Fig.3.1). The ground stresses in these heavily jointed shallow rocks are often low compared to those at greater depth. Deformation of such jointed rock mass is usually governed by the discontinuities rather than the deformation of the intact rock blocks. Therefore, the deformation of the intact blocks is ignored and the blocks are assumed rigid.

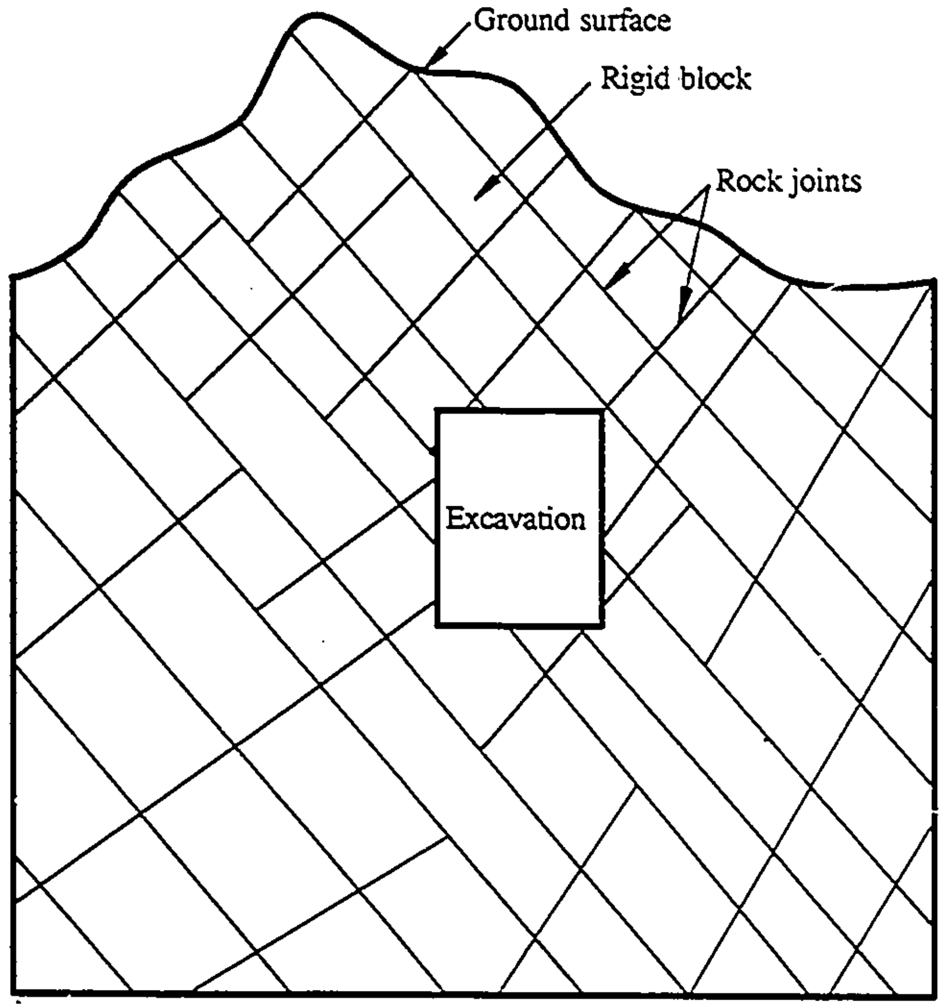

Fig.3.1 Simulation of jointed rock mass by blocks

To simulate the discontinuities of the jointed rock mass, it is assumed that the blocks are in contact along their surfaces. The deformation of the whole rock mass is considered as the result of the relative displacements of the joint surfaces. Similar to Cundall's Distinct Element Model, two types of contacts between blocks are assumed to exist, i.e., corner-to-edge contact and edge-to-edge contact (Fig.3.2). The corner to edge contact is simplified as a point contact. A pair of springs aligned in the normal and shear directions of the contact surface are used to represent the point contact (Fig.3.3.a). The edge-to-edge contact is simplified as two point contacts at the two corners. Similar to the corner-to-edge contact, each point contact in the edge-to-edge contact is simulated by a pair of springs (Fig.3.3.b). The normal and shear contact forces are expressed by the forces in the normal and shear springs respectively. An advantage of using point contact to represent both the corner-to-edge contact and the edge-to-edge contact is that the model can directly deal with forces rather than the distributed stresses along the contact area. The formulation can therefore be simplified. The variation of the contact stresses from one end to the other of the edge-to-edge contact is also reflected by the differences between the forces at the two contact points. The corner-to-edge contact is, in reality, a face-to-face contact rather than a point contact. However, as the contact area is relatively small, the use of a point contact may not introduce significant error. In other words, the stresses distributed on the small contact area may be reasonably well approximated by a concentrated force.

The contact forces result from the relative displacements between the blocks. In the block-spring system, the deformations of the springs can be determined from the relative displacements between blocks. The spring forces, i.e., the contact forces, can therefore be evaluated from the stiffnesses and the deformations of the springs.

The rock block system is considered as initially in equilibrium condition. The application of the external load, including unloading caused by excavation, disturbs the original state of equilibrium of the rock mass. The blocks displace and a set of new contact forces result. If all the forces on the blocks are considered, including gravity forces, contact forces, boundary conditions and any other forces a set of equilibrium equations for all the blocks can be obtained. As the contact forces are determined in terms of the relative displacements of the blocks, the displacements of the blocks can be evaluated by solving the equilibrium equations if the boundary conditions are known.

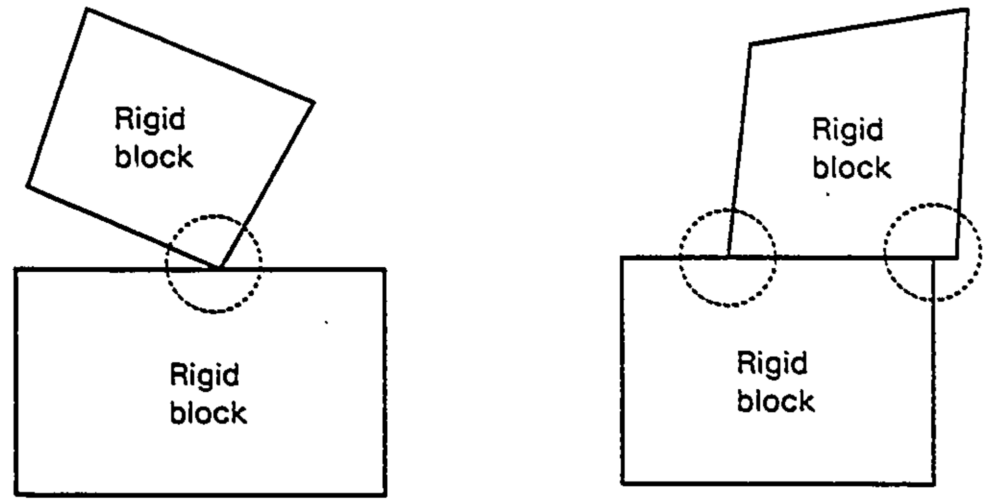

(a) Corner-to-edge contact (b) Edge-to-edge contact

Fig.3.2 Interactions between blocks

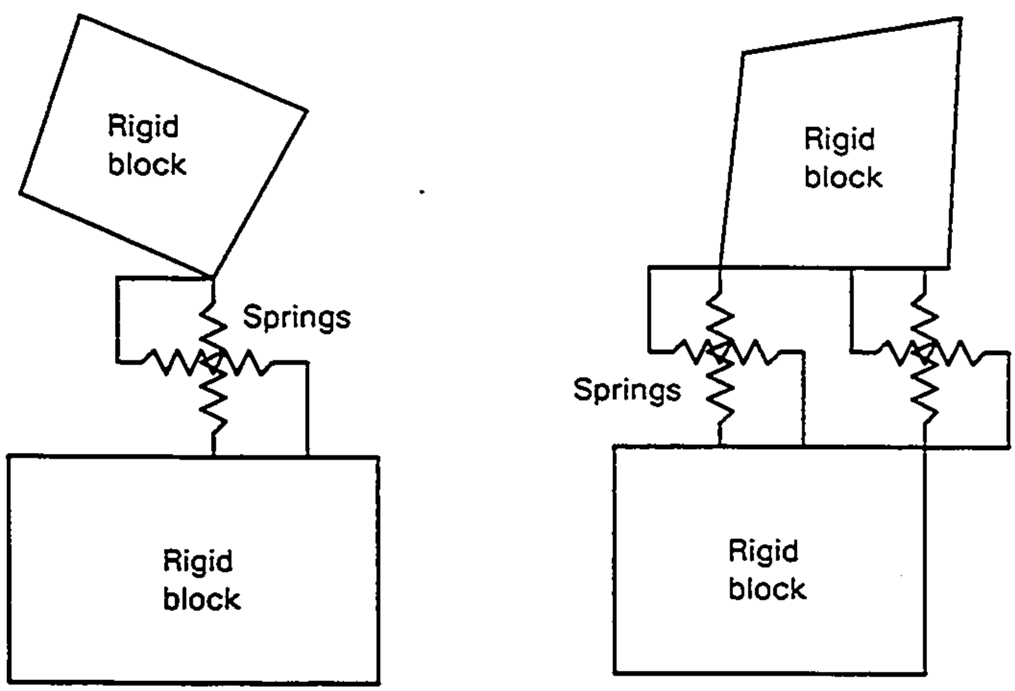

(a) Corner-to-edge contact (b) Edge-to-edge contact

Fig.3.3 Modelling of block-to-block contacts by springs

3.3 Methodology and Formulation

The basic methodology and formulation of the Block-Spring Model are discussed in this section. Detailed procedures for the advanced modelling techniques such as of the failure behaviour of the rock joints and of other features including rock bolt and groundwater, are presented in the following chapters. All the formulations presented in the present thesis are derived for two dimensional cases.

3.3.1 Displacements of the blocks

As the rock blocks are assumed rigid, each block has three degrees of freedom, i.e., two translational displacements and one rotation. The three degrees of freedom of a general block i are represented by the two translations, U_i and V_i, and one rotation Θ_i, of the centroid C_i of the block, as shown in Fig.3.4.

The displacements are defined positive in the directions shown in Fig.3.4. The translations U_i and V_i are positive if they are in the same directions as that of the x and y axes respectively. The rotation Θ_i is positive if the block rotates counterclockwise.

The displacements of any point on block i can be determined in terms of U_i, V_i and Θ_i. The displacements $u_i(Q)$ and $v_i(Q)$ of an arbitrary point Q, for example, on block i in Fig.3.4 may be determined as follows:

Point Q may displace to Q' due to the block translations and from Q' to Q" as a result of the block rotation (Fig.3.5), i.e.,

$$\{u\}_i = \{u'\}_i + \{u''\}_i \tag{3.1}$$

where $\{u\}_i = \begin{Bmatrix} u_i(Q) \\ v_i(Q) \end{Bmatrix}$; $\{u'\}_i = \begin{Bmatrix} u'_i(Q) \\ v'_i(Q) \end{Bmatrix}$; $\{u''\}_i = \begin{Bmatrix} u''_i(Q) \\ v''_i(Q) \end{Bmatrix}$.

$\{u'\}_i$ and $\{u''\}_i$ are the displacements resulted from the block translations and rotation respectively as shown in Fig.3.5.

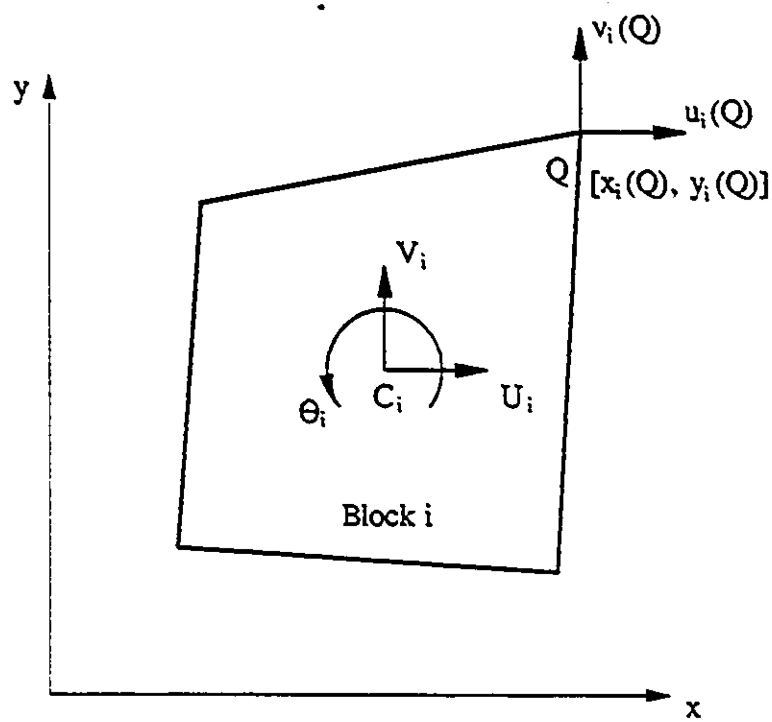

Fig.3.4 Displacements of a block

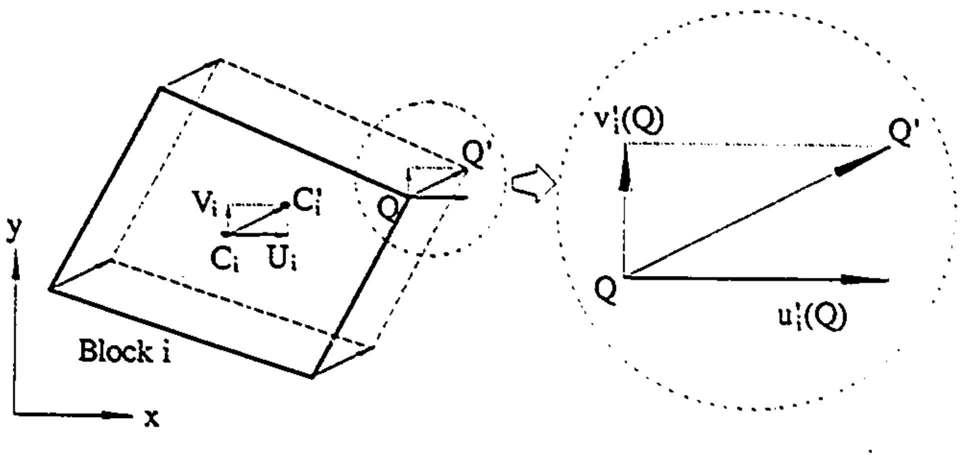

(a) Horizontal and vertical translations

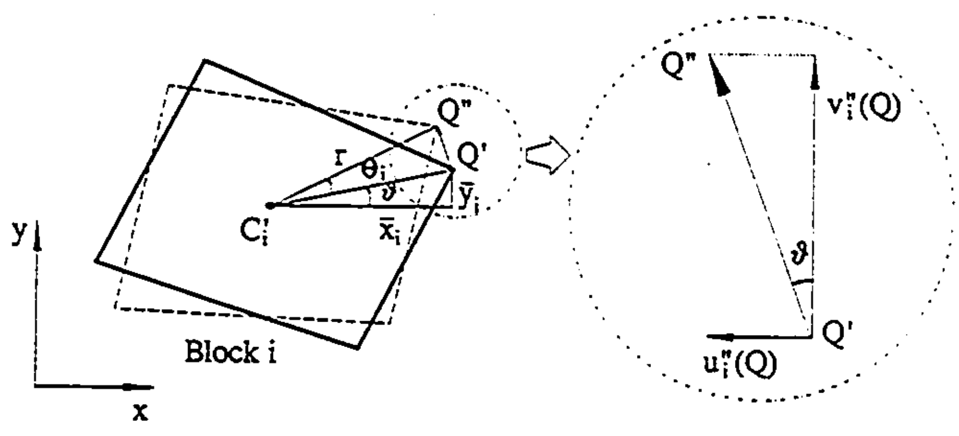

(b) Rotation

Fig.3.5 Determination of displacements of an arbitrary point

The translational component $\{u'\}_i$ is equal to the translation of the centroid of the block, i.e.,

$$\{u'\}_i = \begin{Bmatrix} U_i \\ V_i \end{Bmatrix} \tag{3.2}$$

where U_i and V_i are the horizontal and vertical displacements of the centroid of block i.

If the rotation Θ_i of the block is small in each step of computation, then by considering that $|\overline{Q'Q''}| \approx |r|\,\Theta_i$; $\cos\vartheta = \dfrac{\bar{x}_i}{|r|}$; and $\sin\vartheta = \dfrac{\bar{y}_i}{|r|}$ (as shown in Fig.3.5.b), the displacement $\{u''\}_i$ can be determined by following expression:

$$\{u''\}_i = \Theta_i \begin{Bmatrix} -\bar{y}_i \\ \bar{x}_i \end{Bmatrix} \tag{3.3}$$

where Θ_i is the rotation of block i;

> $\bar{x}_i$, and $\bar{y}_i$ are the local coordinates of point Q relative to the centroid C_i of block i as shown in Fig.3.5.b. The local coordinates can be calculated as follows.

$$\begin{aligned} \bar{x}_i &= x(Q) - x(C_i) \\ \bar{y}_i &= y(Q) - y(C_i) \end{aligned} \tag{3.4}$$

where $x(Q)$, $y(Q)$, $x(C_i)$ and $y(C_i)$ are the coordinates of point Q and the centroid C_i in the global coordinate system.

From Eqs.(3.1), (3.2) and (3.3), the displacement of point Q can be determined in terms of the three degrees of freedom of the block as follows:

$$\{u\}_i = [B]_i \{U\}_i \tag{3.5}$$

where

$$[B]_i = \begin{bmatrix} 1 & 0 & -\bar{y}_i \\ 0 & 1 & \bar{x}_i \end{bmatrix} \tag{3.6}$$

$$\{U\}_i = \begin{Bmatrix} U_i \\ V_i \\ \Theta_i \end{Bmatrix}; \tag{3.7}$$

If there is a common contact point Q between two blocks i and j as shown in Fig.3.6, the relative displacements between the two blocks at point Q may be obtained by applying Eq.(3.5) to both blocks:

$$\{\Delta u\}_{ij} = [D]_{ij} \{U\}_{ij} \tag{3.8}$$

where

$\{\Delta u\}_{ij} = \{u\}_j - \{u\}_i$ is the relative displacement between blocks i and j at point Q;

$$\{U\}_{ij} = \{U_i, V_i, \Theta_i, U_j, V_j, \Theta_j\}^T \tag{3.9}$$

$$[D]_{ij} = [\ -B_i \mid B_j\ ] \tag{3.10}$$

$[D]_{ij}$ is a $[2\times6]$ matrix. Its sub-matrices B_i and B_j are given in Eq.(3.6).

The relative displacements between blocks i and j at point Q may also be transformed to the normal and shear directions of the contact surface:

$$\{\delta\}_{ij} = [T]_i \{\Delta u\}_{ij} \tag{3.11}$$

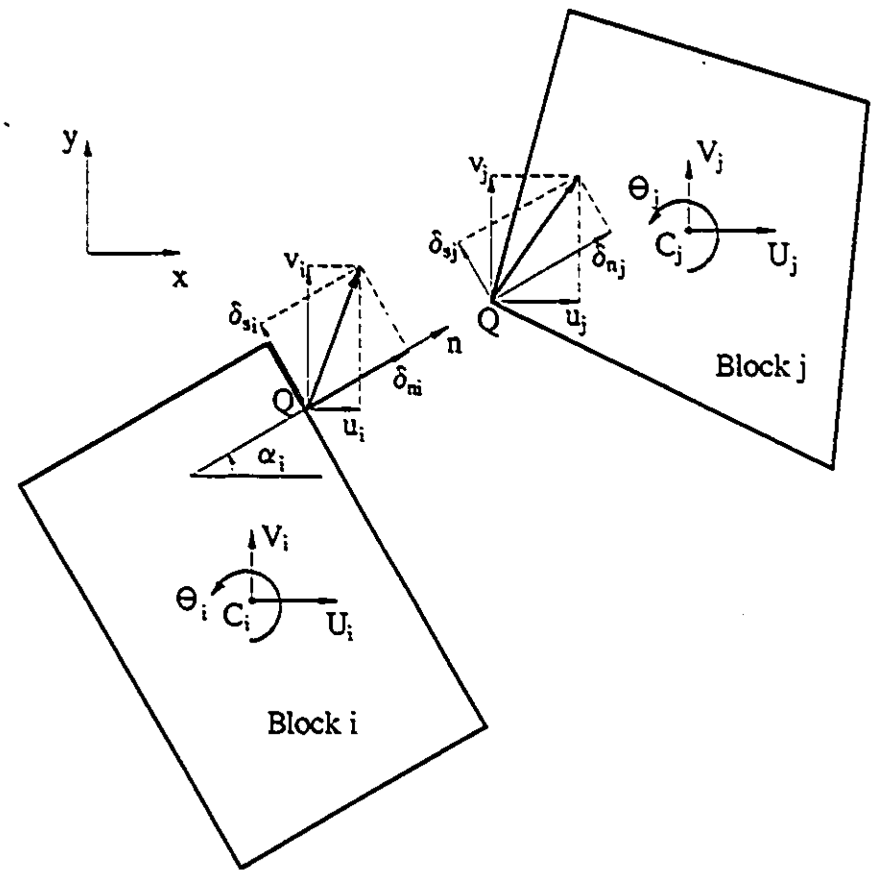

Fig.3.6 Relative displacements between two blocks

where $$\{\delta\}_{ij} = \{\delta\}_j - \{\delta\}_i\,;$$

$$\{\delta\}_i = \begin{Bmatrix} \delta_{ni} \\ \delta_{si} \end{Bmatrix}; \qquad \{\delta\}_j = \begin{Bmatrix} \delta_{nj} \\ \delta_{sj} \end{Bmatrix};$$

δ_{ni}, δ_{si}, δ_{nj} and δ_{sj} are the normal and shear components of the displacements of point Q on blocks i and j (Fig.3.6);

$$[T]_i = \begin{bmatrix} \cos\alpha_i & \sin\alpha_i \\ -\sin\alpha_i & \cos\alpha_i \end{bmatrix} \tag{3.12}$$

α_i is an angle of the outward normal **n** of the contact surface of block i from x axis (Fig.3.6).

3.3.2 Contact forces

The contact forces are represented by the spring forces which can be evaluated from the stiffnesses of the springs (or the contact stiffnesses) and the relative displacements between the blocks. The shear force on the block surface is defined positive if it tends to cause the block to rotate counterclockwise as shown in Fig.3.7. The normal component of the contact forces is defined positive if it is in the same direction as the outward normal of the block surface (Fig.3.7) (i.e., the compressive force is negative). If two blocks i and j are in contact at point Q (Fig.3.7), the normal and shear components of the contact force can be determined by the following expression.

$$\{F_n\}_{ij} = [k]_{ij}\,\{\delta\}_{ij} \tag{3.13}$$

where $$\{F_n\}_{ij} = \begin{Bmatrix} F_n \\ F_s \end{Bmatrix};$$

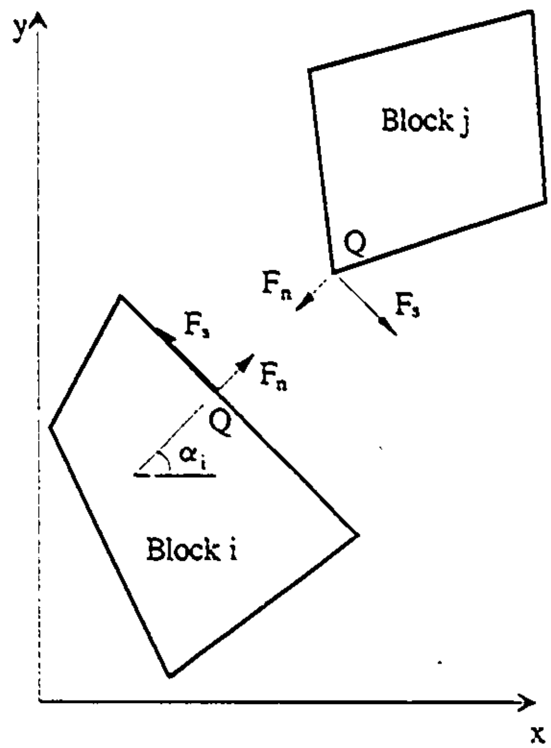

Fig.3.7 Normal and shear contact forces

F_n and F_s are the normal and shear components of the contact force between blocks i and j;

$\{\delta\}_{ij}$ is the relative displacement between the two blocks i and j at the contact point, determined by Eq.(3.11);

$$[k]_{ij} = \begin{bmatrix} K_n & 0 \\ 0 & K_s \end{bmatrix}; \tag{3.14}$$

K_n and K_s are the normal and shear contact stiffnesses between the two blocks.

From Eqs.(3.8), (3.11) and (3.13), the contact forces can be determined in terms of the displacements of the centroids of blocks i and j as follows.

$$\{F_n\}_{ij} = [k]_{ij}\,[T]_i\,[D]_{ij}\,\{U\}_{ij} \tag{3.15}$$

The contact force can be transformed to x and y directions:

$$\{F_x\}_{ij} = [T]_i^T\,\{F_n\}_{ij} \tag{3.16}$$

where $[T]_i$ is defined by Eq.(3.12);

$$\{F_x\}_{ij} = \begin{Bmatrix} F_x \\ F_y \end{Bmatrix};$$

F_x and F_y are the x and y components of the contact force on block i, which are assumed positive if they are in the x and y directions respectively (Fig.3.8).

The same contact force on block j is $\{F_x\}_{ji} = -\{F_x\}_{ij}$.

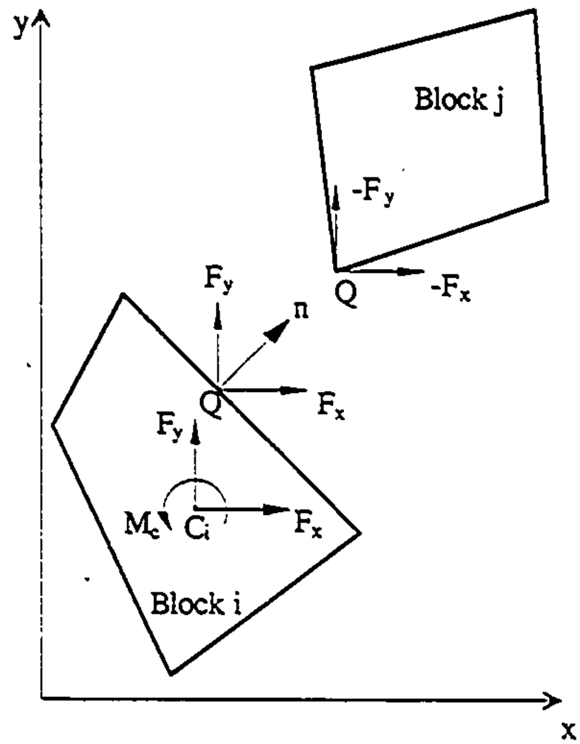

Fig.3.8 Horizontal and vertical components of the contact forces

The contact force $\{F_x\}_{ij}$ may be transformed to the centroid C_i of block i and a set of equivalent forces and moment can be obtained (Fig.3.8):

$$\{F_c\}_{ij} = [B]_i^T \{F_x\}_{ij} \tag{3.17}$$

where
$$\{F_c\}_{ij} = \begin{Bmatrix} F_x \\ F_y \\ M_c \end{Bmatrix}$$

M_c is the moment of $\{F_x\}_{ij}$ on C_i ;
$[B]_i$ is defined in Eq.(3.6).

From Eqs.(3.15), (3.16) and (3.17), $\{F_c\}_{ij}$ can be evaluated from the displacements of the centroids of blocks i and j:

$$\{F_c\}_{ij} = [K]_{ij} \{U\}_{ij} \tag{3.18}$$

where
$$[K]_{ij} = [\ K_i \mid K_j\ ] = [B]_i^T [T]_i^T [k]_{ij} [T]_i [D]_{ij} \tag{3.19}$$

$[K]_{ij}$ is a $[3\times6]$ stiffness matrix for two blocks i and j;

K_i and K_j are $[3\times3]$ sub-matrices of $[K]_{ij}$.

3.3.3 Contact stiffness

The contact stiffnesses K_n and K_s are used in relating the contact forces to the relative displacements between the blocks, as described in the previous section. The contact stiffnesses are usually considered as the deformation parameters of the joints. The normal and shear stiffnesses, K_n and K_s, of the joints can be determined from the slope of the normal stress-normal displacement curve and shear stress-shear displacement curve, respectively (Goodman, et al., 1968). Typical stress-displacement relations of the joints can be described by curves of the type shown in Fig.3.9 (e.g., Goodman, 1976; Schneider, 1976; Patton, 1966; Barton, 1972; and Bandis, et al., 1983).

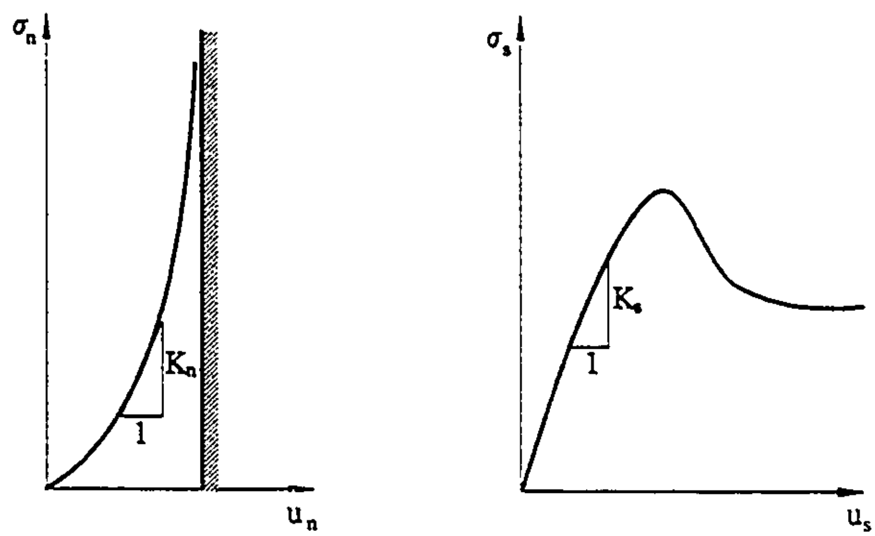

(a) Normal stress-normal displacement relation

(b) Shear stress-shear displacement relation

Fig.3.9 Typical stress-displacement relations of rock joints

According to Brady and Brown (1985), "the normal stress–normal displacement behaviour of discontinuities can be highly non-linear. In many numerical models, this response is assumed to be linear and the normal stiffness, K_n, is assumed to be constant." "The shear stiffness, K_s, calculated as a slope of the shear stress–shear displacement curve, is highly variable and exceedingly difficult to predict. It varies with disturbance of the discontinuity, testing technique, specimen size and normal stress."

Hyperbolic relations between normal stress, σ_n, and normal displacement, u_n, have been used by some investigators to simulate the joint behaviour in normal direction as shown in Fig.3.10 (e.g., Goodman, 1976 and Bandis et al., 1983). The normal stiffness of the rock joint is the slope of the hyperbolic curve, which is highly stress dependent. The joint interlocking behaviour in normal direction could be well represented by the hyperbolic relations.

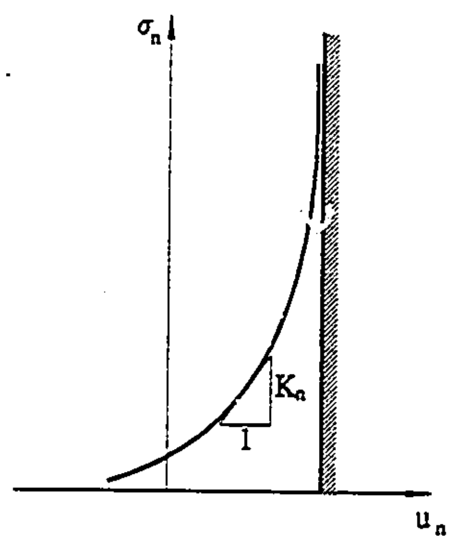

Fig.3.10 A hyperbolic relation between normal stress and normal displacement of rock joint (after Goodman, 1976)

Methods of determining the strength and deformability of the rock mass can be classified into three categories, according to Kulatilake (1984), i.e., (1) the direct testing method; (2) the empirical correlation method; and (3) the analytical decomposition model method. The empirical correlation method relates the deformability and strength to index properties such as RQD (Rock Quality Designation) and JRC (Joint Roughness Coefficient) (e.g., Barton and Choubey, 1977; Hoek and Brown, 1980). The analytical decomposition methods determine the strength and deformability of rock mass from the strength and deformation properties of the discontinuities and of the intact rock.

In Cundall's Distinct Element Model (Cundall, 1987; and Lorig, 1984) and Plesha's rigid block model (Plesha, 1983; Belytschko, et al. 1984), the joint stiffness factors are assumed constant. The joint stiffness constants are determined from the joint tests or by referring to the data available from similar cases. In some numerical models such as Kawai's Discrete Element Model (Hamajima, et al., 1985), the deformabilities of both the intact materials and the joints are considered in determining the contact stiffness constants.

Though the intact rock blocks are assumed rigid in the proposed Block-Spring Model, the deformability of the intact rocks is considered in the contact stiffnesses in addition to that of the joints. The contact stiffness factors (or the stiffnesses of the springs) K_n and K_s represent the deformabilities of both the joints and the intact rock materials. A procedure presented by Kawai, et al. (1978) for evaluating the stiffnesses of the solid materials is used here for intact rocks.

If blocks i and j consisting of the same material are in contact with each other (Fig.3.11), the contact stiffnesses from the intact rock can be determined by considering the stress-strain relations (for plane strain problem; the normal stress σ_n is approximated by ignoring the effect of the normal strain in the other direction):

$$\sigma_n = E' \varepsilon_n; \qquad \tau_s = G \nu_{ns} \tag{3.20}$$

where
$$E' = \frac{(1-\mu)\,E}{(1+\mu)\,(1-2\mu)}, \qquad G = \frac{E}{2\,(1+\mu)} \tag{3.21}$$

E is the elastic modulus and μ is the Poisson's ratio of the rock material.

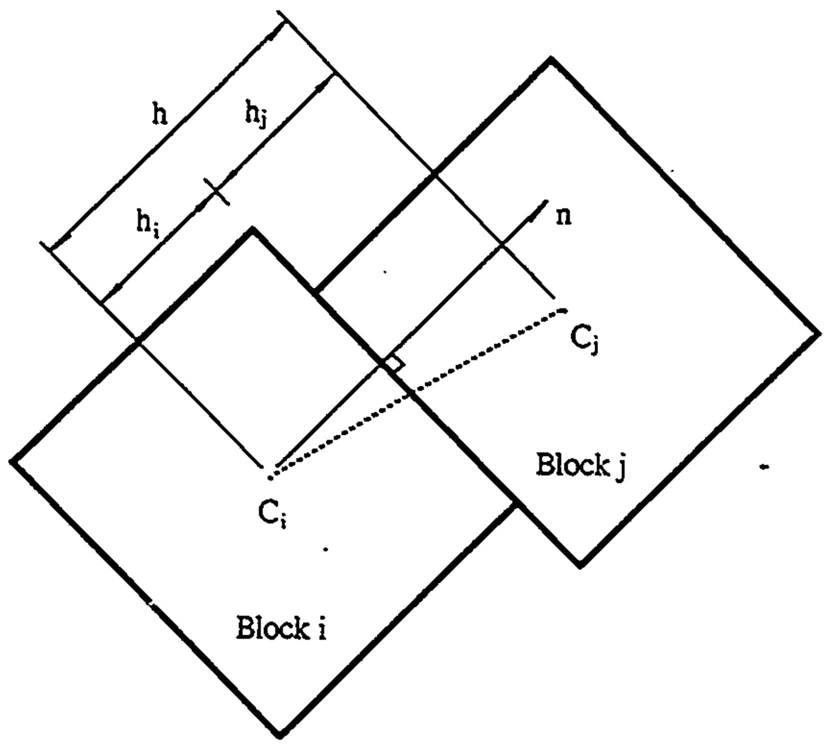

Fig.3.11 Dimension of the blocks for determination of the stiffness of the intact rock

The strain components, ε_n and ν_{ns}, can be approximated by the following finite difference expressions.

$$\varepsilon_n = \frac{\delta_n}{h}; \qquad \nu_{ns} = \frac{\delta_s}{h} \tag{3.22}$$

where h is a projection of $\overline{C_iC_j}$ on normal n of the contact surface (Fig.3.11);

δ_n and δ_s are the normal and shear components of the relative displacement between C_i and C_j, the centroids of blocks i and j.

On the other hand, the stresses can be obtained from the stiffness of the two blocks as follows:

$$\sigma_n = K_n' \delta_n; \qquad \tau_s = K_s' \delta_s \tag{3.23}$$

where K_n' and K_s' may be considered as the normal and shear stiffnesses of the intact rocks.

By introducing Eqs.(3.22) and (3.23) into Eq.(3.20), the stiffnesses of the intact rocks can be obtained as follows:

$$K_n' = \frac{E'}{h}; \qquad K_s' = \frac{G}{h} \tag{3.24}$$

Similarly, if the rock materials of the two blocks are different, K_n' and K_s' can be determined by the following equations.

$$K_n' = \frac{1}{\frac{1}{K_{ni}'} + \frac{1}{K_{nj}'}}; \qquad K_s' = \frac{1}{\frac{1}{K_{si}'} + \frac{1}{K_{sj}'}} \tag{3.25}$$

where $$K_{nk}' = \frac{E_k'}{h_k}; \qquad K_{sk}' = \frac{G_k}{h_k} \quad (k=i, j) \tag{3.26}$$

the subscript k (=i, j) denotes the block number;

h_i and h_j are as shown in Fig.3.11;

To determine E_k' and G_k using Eq.3.21, the elastic modulus E and the Poisson's ratio μ for block k should be used. Typical values of E and μ for selected rocks are listed in Table A.1 in Appendix A.

The contact stiffness may be affected significantly by the joint conditions such as the joint roughness and participation of the soft filling materials. The joint stiffnesses must therefore also be considered. If the joint stiffnesses are K_n'' and K_s'', the equivalent contact stiffnesses K_n and K_s, considering both the intact rocks and the joint, may be determined by the following equations.

$$K_n = \frac{1}{\frac{1}{K_n'} + \frac{1}{K_n''}} ; \qquad K_s = \frac{1}{\frac{1}{K_s'} + \frac{1}{K_s''}} \tag{3.27}$$

The equivalent rock-joint-rock stiffness may be considered as the stiffness of a three component spring as shown in Fig.3.12.

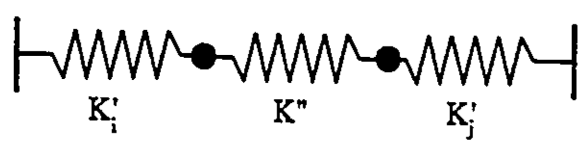

Fig.3.12 A three-spring system in simulating the rock-joint-rock contact

The joint stiffnesses, K_n'' and K_s'', have to be determined based on the joint conditions. Experimental data are often available in the literature (see, for example, Rosso, 1976; Goodman, 1976; Belytschko, et al., 1984). A summary of joint stiffness factors for various rock joints reported in the literature is given in Table A.2 in Appendix A.

The joint stiffness may be calculated using Eq.(3.26) if the joint filling material is so thick that the interference between the asperities on the rock surfaces can be ignored. According to Celestino (1980), to determine if a filling is thick enough to significantly influence the strength and deformability of the joints, it is necessary to consider the geometry of the asperities. The strength of the joint approaches the strength of the filling material as the thickness increases and the interference between asperities disappears. If the thickness of the filling is greater than the height of the asperities, the joint stiffness can be calculated from Eq.(3.26). In these equations, h_k should be replaced by the thickness of the filling and, E_k and G_k by the properties of the filling material.

It should be noted that K_n and K_s determined from Eq.(3.27) are the equivalent contact stiffnesses corresponding to the unit area. As the springs between the blocks represent certain contact area, K_n and K_s should be multiplied by the relevant contact area to obtain the spring stiffnesses.

3.3.4 Displacement boundary conditions

The known boundary displacement may be applied through a special one dimensional bar element. Fig.3.13 shows a general case for applying the boundary displacement.

If the displacement, w_0, of point B on block i is known in a direction deviating an angle β from the x axis, a bar element may be placed at point B in that particular direction as shown in Fig.3.13.(a). It is assumed that the outer end B' of the bar element displaces w_0 along its axial direction. The inner end of the bar element is pinned on point B on block i. If the known displacement w_0 is neither in horizontal direction nor in the vertical direction, a reference point B' should be specified with coordinates [x(B'), y(B')] to determine the direction of the prescribed displacement. The reference point B' can be such that the vector $\overline{B'B}$ indicates the direction of the prescribed boundary displacement w_0 (Fig.3.13.a).

In order that point B displaces w_0 , the bar element should be rigid. A stiffness factor, K_d, of the bar element should therefore be specified as a large number, say 10^{20} (unit [F/L]).

The displacement $\{u\}_i$ of point B may be determined by Eq.3.5. The displacement, w_i, of point B, in the axial direction of the bar element may be transformed from $\{u\}_i$ as follows:

$$w_i = \{c\}_d^T \{u\}_i \tag{3.28}$$

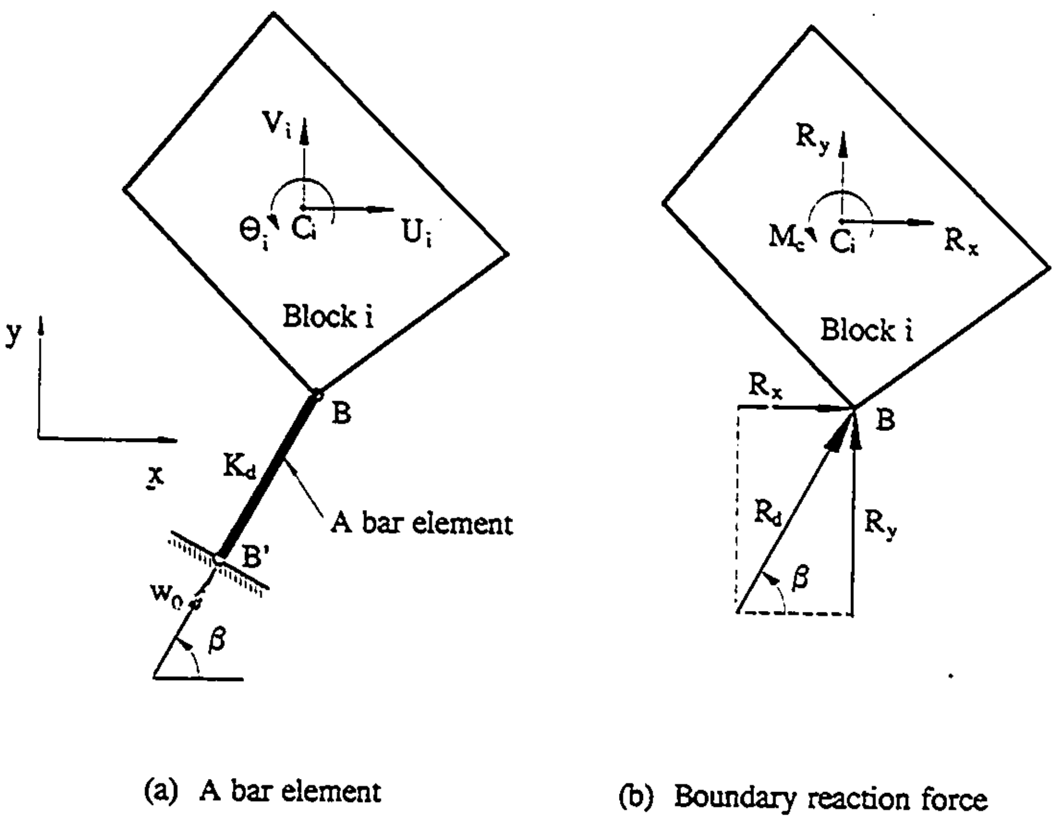

Fig.3.13 Application of boundary displacement

where $$\{c\}_d^T = \{\cos\beta,\ \sin\beta\} \tag{3.29}$$

β is the angle between the axis of the bar element and the x axis.

The reaction force, R_d, on point B (Fig.3.13) from the bar element can be evaluated by

$$R_d = K_d\,(w_0 - w_i) \tag{3.30}$$

where K_d is the stiffness of the bar element (a specified large number).

From Eqs.(3.5), (3.28) and (3.30), the boundary reaction force, R_d, can be determined in terms of $\{U\}_i$, the displacement of the centroid of block i, and the prescribed displacement, w_0, as follows.

$$R_d = K_d\,w_0 - K_d\,\{c\}_d^T\,[B]_i\,\{U\}_i \tag{3.31}$$

Again, the reaction force, R_d, may be transformed to the centroid of block i and a set of equivalent forces and moment can be obtained.

$$\{R_c\}_i = [B]_i^T\,\{c\}_d\,R_d \tag{3.32}$$

where

$\{R_c\}_i = \{R_x, R_y, M_c\}^T$ is the equivalent force obtained from transforming R_d to the centroid C_i of the block;

$[B]_i$ is given in Eq.(3.6);

$\{c\}_d$ is given in Eq.(3.29).

From Eqs.(3.31) and (3.32), an equation similar to Eq.(3.18) can be obtained:

$$\{R_c\}_i = \{R_0\}_i + [K_d]_i \{U\}_i \tag{3.33}$$

where

$$\{R_0\}_i = K_d w_0 [B]_i^T \{c\}_d \tag{3.34}$$

$$[K_d]_i = -K_d [B]_i^T \{c\}_d \{c\}_d^T [B]_i \tag{3.35}$$

$[K_d]_i$ is a $[3 \times 3]$ stiffness matrix.

3.3.5 Force boundary conditions and equilibrium equations

The Block-Spring Model is developed based on the equilibrium condition of all the blocks. It is assumed that the blocks are in static equilibrium state under a system of forces. The force system on the blocks may consist of the gravity forces, W, the external applied forces, P, the boundary reaction forces, R, and the contact forces, F, as shown in Fig.3.14. (Other forces including rockbolt forces and groundwater pressures will be discussed in later chapters.)

The gravity force, on a block i, is represented by a concentrated force, W_i, on the centroid of the block, which can be evaluated by the unit weight and the volume of the block as follows:

$$W_i = \gamma_i A_i \tag{3.36}$$

where γ_i is the unit weight of the rock material;

A_i is the volume of block i.

For consistency, the gravity force is written in a body force vector:

$$\{W\}_i = \begin{Bmatrix} W_x \\ W_y \\ 0 \end{Bmatrix} \tag{3.37}$$

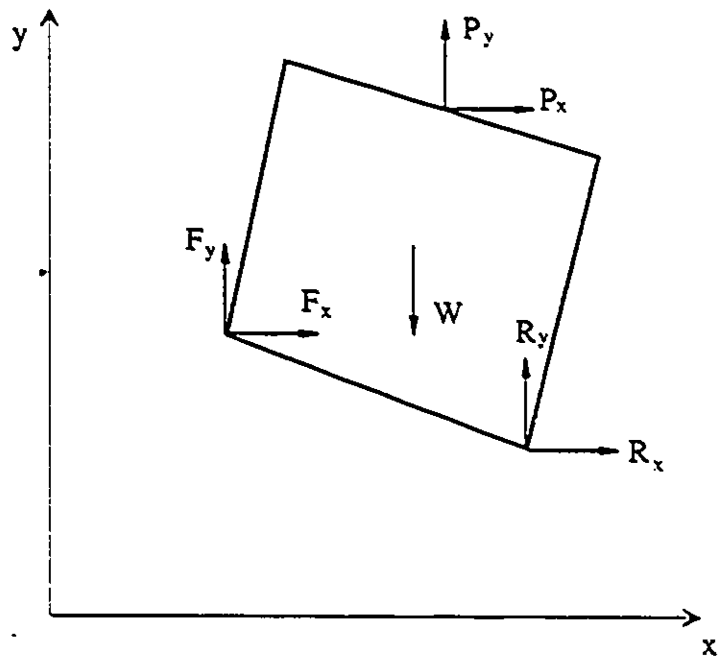

Fig.3.14 Possible forces on a block

If the body force consists of only the gravity force and the y axis is vertical, then $W_x=0$ and $W_y=-W_i$.

If an external load, $\{P\}_i = \{P_x, P_y\}^T$, is applied on block i, it may also be transformed to the centroid of the block as follows:

$$\{P_c\}_i = [B]_i^T \{P\}_i \tag{3.38}$$

where $\{P_c\}_i = \begin{Bmatrix} P_x \\ P_y \\ M_c \end{Bmatrix}$; M_c is a moment of $\{P\}_i$ on the centroid C_i of block i;

$[B]_i$ is defined in Eq.(3.6)

If all the forces on block i are considered, following equilibrium condition should be satisfied:

$$\sum \{X\}_i = 0 \tag{3.39}$$

where $\{X\}_i = \{X, Y, M_c\}^T$ denotes the forces and moments transformed to the centroid of b! ck i.

Eqs.(3.18), (3.33), (3.37) and (3.38) may be introduced into Eq.(3.39) to obtain three equilibrium equations for block i. A set of global stiffness equations may be assembled as follows if all the blocks in the rock mass are considered.

$$[K] \{U\} = \{P\} \tag{3.40}$$

where $[K]$ is a $3N \times 3N$ stiffness matrix if there are N blocks;

$\{U\}$ is a 3N-component column vector consisting of the unknown displacements of the N blocks;

$\{P\}$ is a 3N-component column vector consisting of the boundary conditions.

In a general case, if two blocks, i and j, are in contact to each other the corresponding terms reflecting the effects of the contact may be assembled into the global stiffness equations as follows:

$$
\begin{array}{cc}
 & \begin{array}{ccc} \qquad\quad i \qquad\quad & \qquad\quad j \qquad\quad & \qquad\qquad \end{array} \\
\begin{array}{c} \\ \\ i \\ \\ \\ \\ j \\ \\ \\ \end{array} &
\left[\begin{array}{ccc}
\ddots & \cdots & \cdots \\
\hline
\underset{(3\times3)}{[K_i]_{ij} + [K_d]_i} & \underset{(3\times3)}{[K_j]_{ij}} & \\
\hline
\cdots & \ddots & \cdots \\
\hline
\underset{(3\times3)}{[K_i]_{ji}} & \underset{(3\times3)}{[K_j]_{ji} + [K_d]_j} & \\
\hline
\cdots & \cdots & \ddots
\end{array}\right]
\end{array}
\left\{\begin{array}{c}
\vdots \\ \hline U_i \\ V_i \\ \theta_i \\ \hline \vdots \\ \hline U_j \\ V_j \\ \theta_j \\ \hline \vdots
\end{array}\right\}
=
\left\{\begin{array}{c}
\vdots \\ \hline -\Sigma\{R_0\}_i \\ -\Sigma\{P_c\}_i \\ -\Sigma\{W\}_i \\ \hline \vdots \\ \hline -\Sigma\{R_0\}_j \\ -\Sigma\{P_c\}_j \\ -\Sigma\{W\}_j \\ \hline \vdots
\end{array}\right\}
\tag{3.41}
$$

where $[K_i]_{ij}$ and $[K_j]_{ij}$ are the two sub-matrices of matrix $[K]_{ij}$ in Eq.(3.19);

$[K_d]_i$ is given in Eq.(3.35);

$\{R_0\}_i$ is defined in Eq.(3.34);

$\{P_c\}_i$ is given in Eq.(3.38);

$\{W\}_i$ is defined in Eq.(3.37).

The global stiffness matrix [K] in Eq.(3.40) is symmetric. The nonzero components of the matrix are distributed only in a diagonal band, which can be narrow if the blocks are properly numbered. Therefore, only half-band of the matrix needs to be stored for computation. The half-band-width, NBW, of the matrix can be calculated as follows:

$$NBW = 3\,(\,1 + \Delta I_{max}\,) \tag{3.42}$$

where $$\Delta I_{max} = \max\,(\,|\,i - j\,|\,);$$

i and j are the numbers of any two blocks in contact in the mesh.

By solving the global stiffness equations in Eq.(3.40), the displacements {U} of all the blocks can be obtained. The contact forces and the boundary reaction forces can therefore be evaluated using Eqs.(3.15) and (3.31) respectively.

3.3.6 Stresses within blocks

As mentioned earlier, the stability or the strength of the densely jointed rock masses is usually governed by the discontinuity. The deformation of the block assembly as a whole can often be considered as the result of the movements of the blocks only. In such cases, variation of stress within an individual block is less important. However, the average stresses within the blocks may help to understand the stress distribution in the whole rock mass.

The average stress within each block may be calculated using a procedure presented by Drescher and De Josselin de Jong (1972) which was proposed for determination of average stresses in their photoelastic analysis of granular material. The procedure was also used in the Distinct Element Method for evaluating the average stresses within rigid blocks and simply deformable blocks (e.g., Maini, et al., 1978; Lorig, 1984). The same procedure is used here for determination of the average stresses within the blocks. As no detailed derivation of such formulae was provided and no body forces were considered in the derivations in the above mentioned references, the author of the present thesis performed his own derivation based on the original idea presented by Drescher and De Josselin de Jong (1972). The detailed derivation considering the body forces is given in Appendix B for easy reference for an interested reader. The Einstein summation convention for repeated indices is used in derivation of the equations in this section.

The average stress, $\overline{\sigma_{ij}}$ (i=1, 2 and j=1, 2), in a block with volume A can be determined by the following expression:

$$\overline{\sigma_{ij}} = \frac{1}{A} \int_A \sigma_{ij} \, dA \tag{3.43}$$

where σ_{ij} represents the stress state within the block.

It is assumed that the stress state in the block is in equilibrium, i.e., the general equilibrium equation, $\sigma_{kj,k} + b_j = 0$, applies. The term b_j denotes the j component of the body force on a unit volume. The integral over volume A in Eq.(3.43) can be transformed into an integral along the boundary S of the volume A using Green's theorem and considering the equilibrium condition.

$$\overline{\sigma_{ij}} = \frac{1}{A} \int_S x_i \, f_j \, ds \tag{3.44}$$

where x_i denotes the i local coordinate of the integral point on the boundary S;

f_j denotes the j-component of the traction acting on the integral point on S.

The term of the body force b_j disappears from Eq.(3.44) (see Appendix B for details).

The average stress in Eq.(3.44) may be determined numerically as follows:

$$\overline{\sigma_{ij}} = \frac{1}{A} \sum_Q x_i(Q) \, F_j(Q) \tag{3.45}$$

where $F_j(Q)$ denotes the j component of the force acting on point Q;

$x_i(Q)$ denotes the i local coordinate of point Q.

After the contact forces and the boundary restrictions are obtained, the average stress within each block can be evaluated using Eq.(3.45) by considering all the forces on the boundary of the block.

3.3.7 A flowchart for linear analysis

The procedures discussed so far provide the fundamentals of the Block-Spring Model. The scheme is still a "one way" analysis from discretizing the rock media to calculating the stress distribution, and can be summarized in a flowchart shown in Fig.3.15. This "one way" scheme can be used for one step linear analysis. For analyzing the non-linear behaviour of the jointed rocks, special techniques are still required, which are discussed in later chapters.

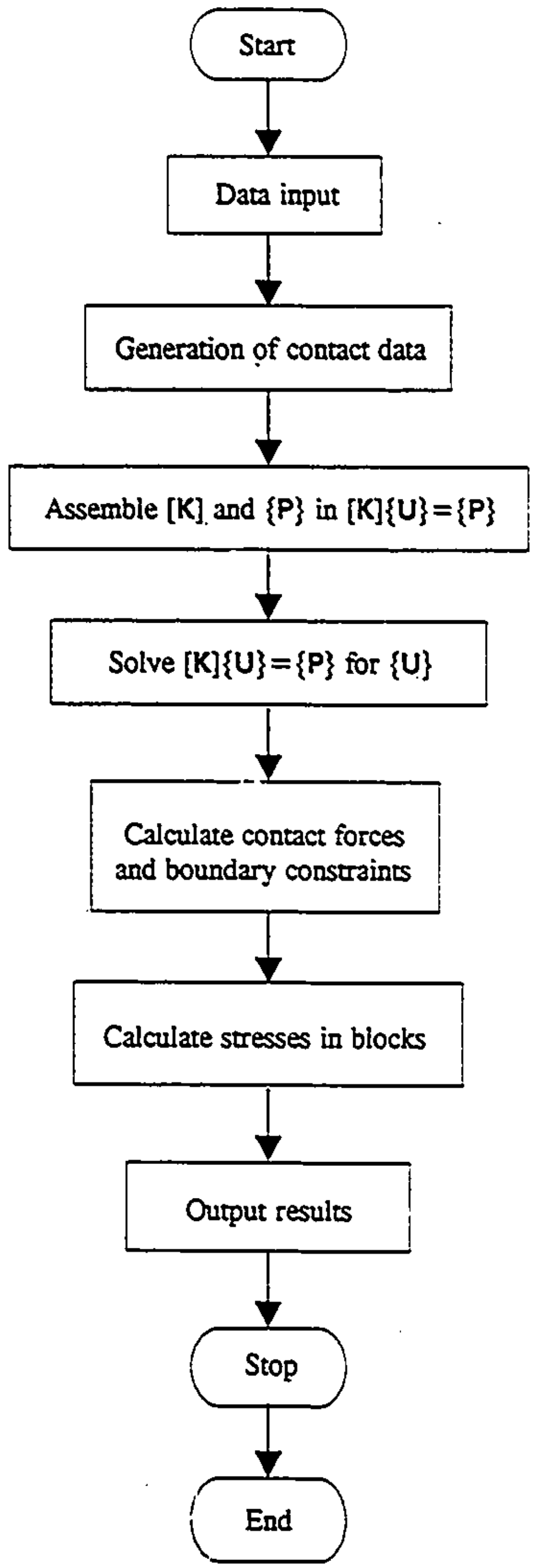

Fig.3.15 A flowchart of the Block-Spring Model for linear analysis

3.4 Example 1: Analysis of a Circular Tunnel

Although the Block-Spring Model has been developed for analyzing the discontinuous rocks, it may also be used to analyze the continuous media by discretizing the media into blocks manually. Before the techniques for non-linear analysis are introduced, an example is presented here for demonstrating the Block-Spring Model in simulating the linear behaviour of the continuous media.

The following is an application of the computation scheme to a circular opening in an elastic continuum. An ideal case is selected here so that the results from the proposed model can be compared with a closed form solution.

Fig.3.16 shows a cross section of an underground circular tunnel with diameter D=4m. The depth of the center tunnel, H, is 11m. The medium is subjected to vertical stress p due to gravity and lateral pressure q (Fig.3.16). The theoretical solution of the radial, tangential and shear stresses are given by the theory of elasticity (Jumikis, 1983) as follows:

$$
\begin{aligned}
\sigma_r &= -\frac{p+q}{2}\left(1-\frac{a^2}{r^2}\right)+\frac{p-q}{2}\left(1+\frac{3\,a^4}{r^4}-\frac{4\,a^2}{r^2}\right)\cos 2\theta \\
\sigma_\theta &= -\frac{p+q}{2}\left(1+\frac{a^2}{r^2}\right)-\frac{p-q}{2}\left(1+\frac{3\,a^4}{r^4}\right)\cos 2\theta \\
\tau_{r\theta} &= -\frac{p-q}{2}\left(1-\frac{3\,a^4}{r^4}+\frac{2\,a^2}{r^2}\right)\sin 2\theta
\end{aligned}
\tag{3.46}
$$

where σ_r, and σ_θ, are normal stresses in radial and tangential directions respectively;

$\tau_{r\theta}$ is the shear stress on a plane normal to r;

r and θ are the polar coordinates of the point under consideration (Fig.3.16);

a is the radius of the opening;

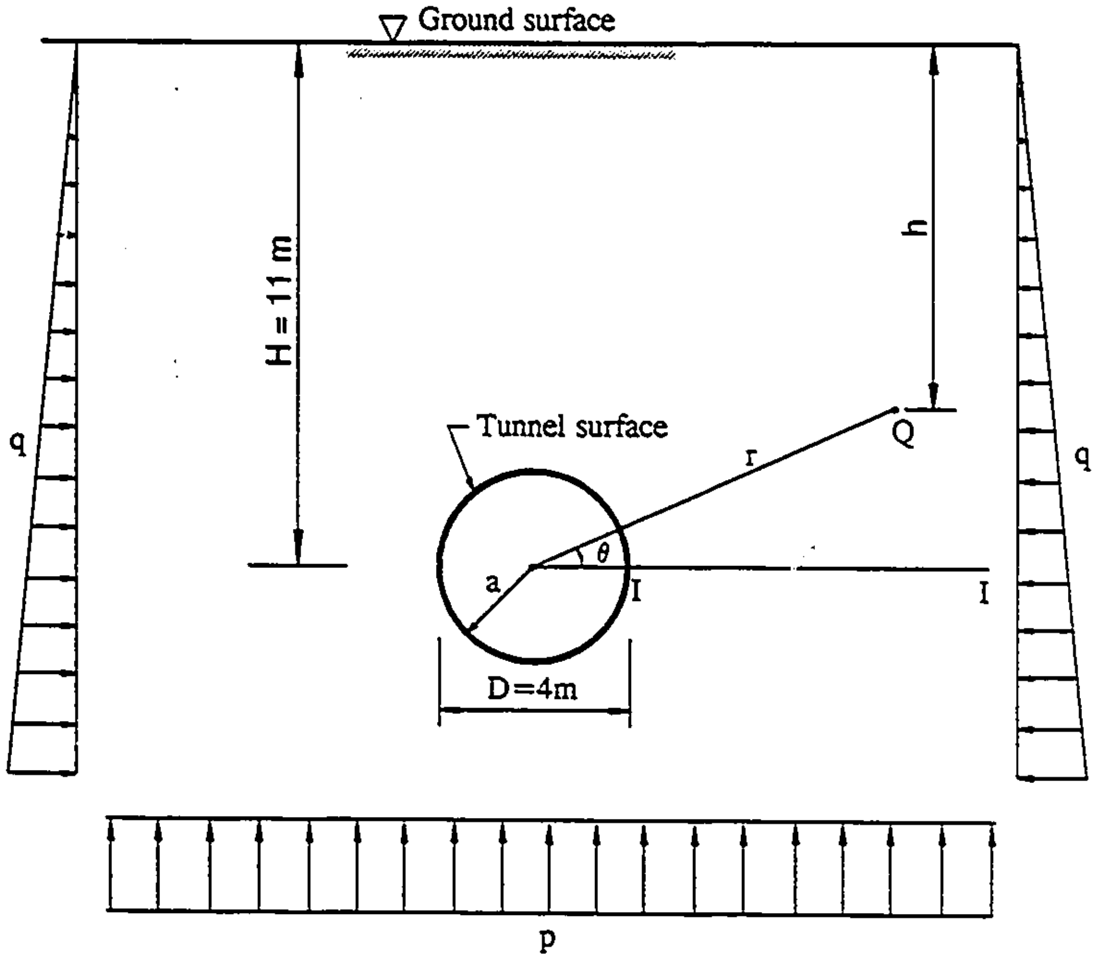

Fig.3.16 Example 1: An underground circular tunnel

$$p = \gamma h$$
$$q = \frac{\mu}{1-\mu}\gamma h \tag{3.47}$$

γ is the unit weight of the rock medium;

μ is the Poisson's ratio of the material;

h is the depth of the point under concern.

In this example, the stresses on section I-I in Fig.3.16 are calculated. The parameters used are as follows.

$a = 2$ m;	$\gamma = 26$ kN/m^3;
$h = 11$ m;	$E = 50$ GPa;
$\theta = 0°$;	$\mu = 0.25$.

The shear stress, $\tau_{r\theta}$, on section I-I is zero. Obviously, σ_r is the horizontal stress σ_h; and σ_θ is the vertical stress σ_v.

Since it is a symmetric problem, only half of the tunnel is considered in the numerical analysis with the Block-Spring Model. Fig.3.17 shows an artificially discretized mesh for analysis with the proposed model. In order to compare with the theoretical solution, one step linear analysis was conducted.

In Eq.(3.46), $p=\gamma h$ is the vertical primary ground stress and $q=\frac{\mu}{1-\mu}\gamma h$ is the lateral primary ground stress. To comply with this condition, the lateral boundary on the right hand side of the rock medium is imposed with a linearly distributed stress ($q=\frac{\mu}{1-\mu}\gamma h$). As the left hand side boundary is a neutral section, it is constrained with rollers (Fig.3.17). The bottom boundary is also constrained with rollers.

The principal stress distribution around the tunnel obtained from the Block-Spring Model is shown in Fig.(3.18). It is obvious, in Fig.(3.18), that the ground stresses are disturbed by the opening. The tangential stresses around the tunnel surface are the major principal stresses. The radial stresses around the tunnel surface are the minor principal stresses.

The horizontal and vertical stresses on section I-I (Figs.3.16 and 3.17) calculated from Eq.(3.46) are plotted in Fig.3.19. (All the stresses are compressive. The minus sign for compression is omitted in Fig.3.19). Fig.3.19 also shows the results from the Block-Spring Model. It can be noted in Fig.3.19 that the results obtained from the proposed Block-Spring Model are very close to the analytical solutions.

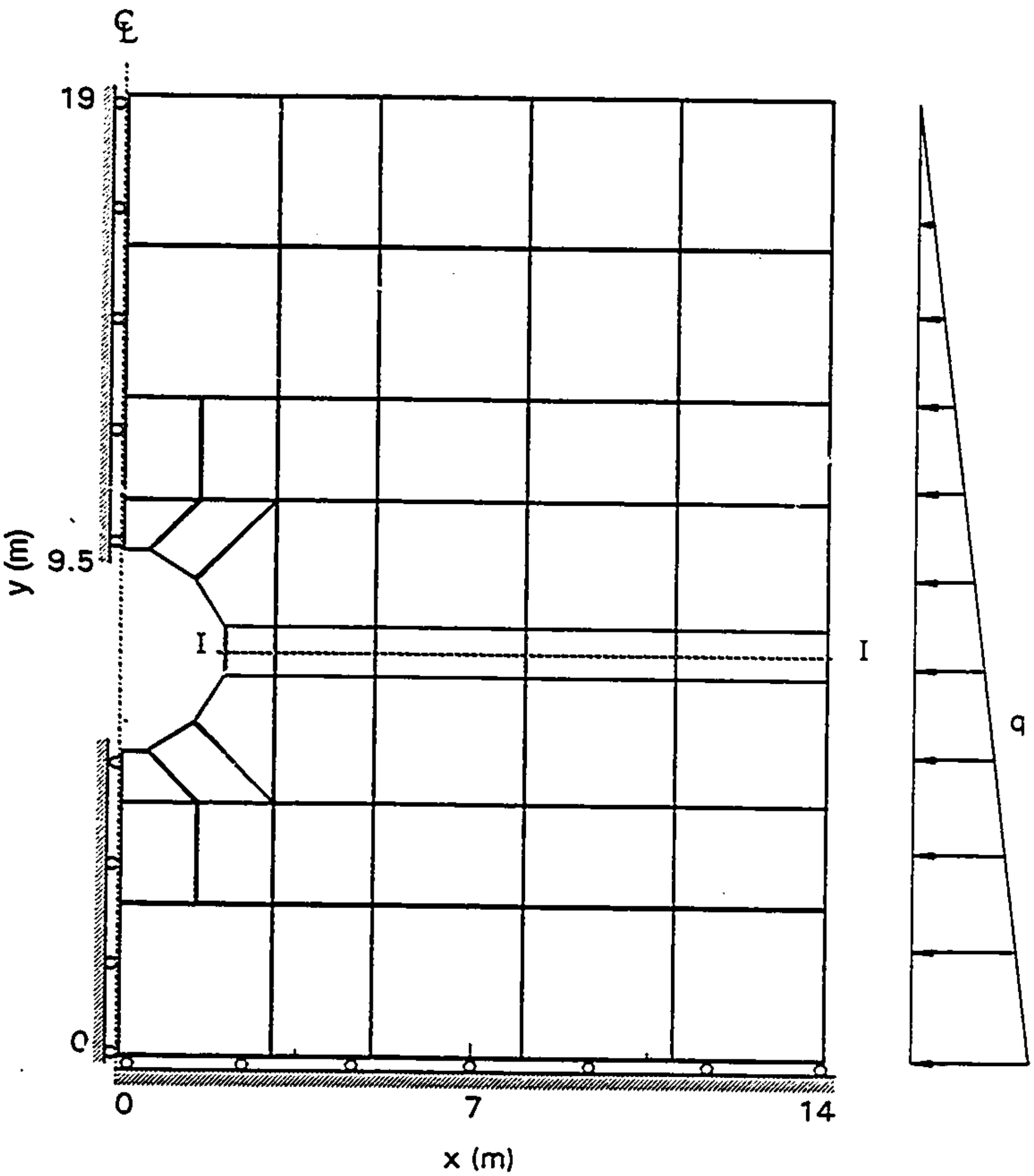

Fig.3.17 Example 1: Rock medium considered and discretized blocks

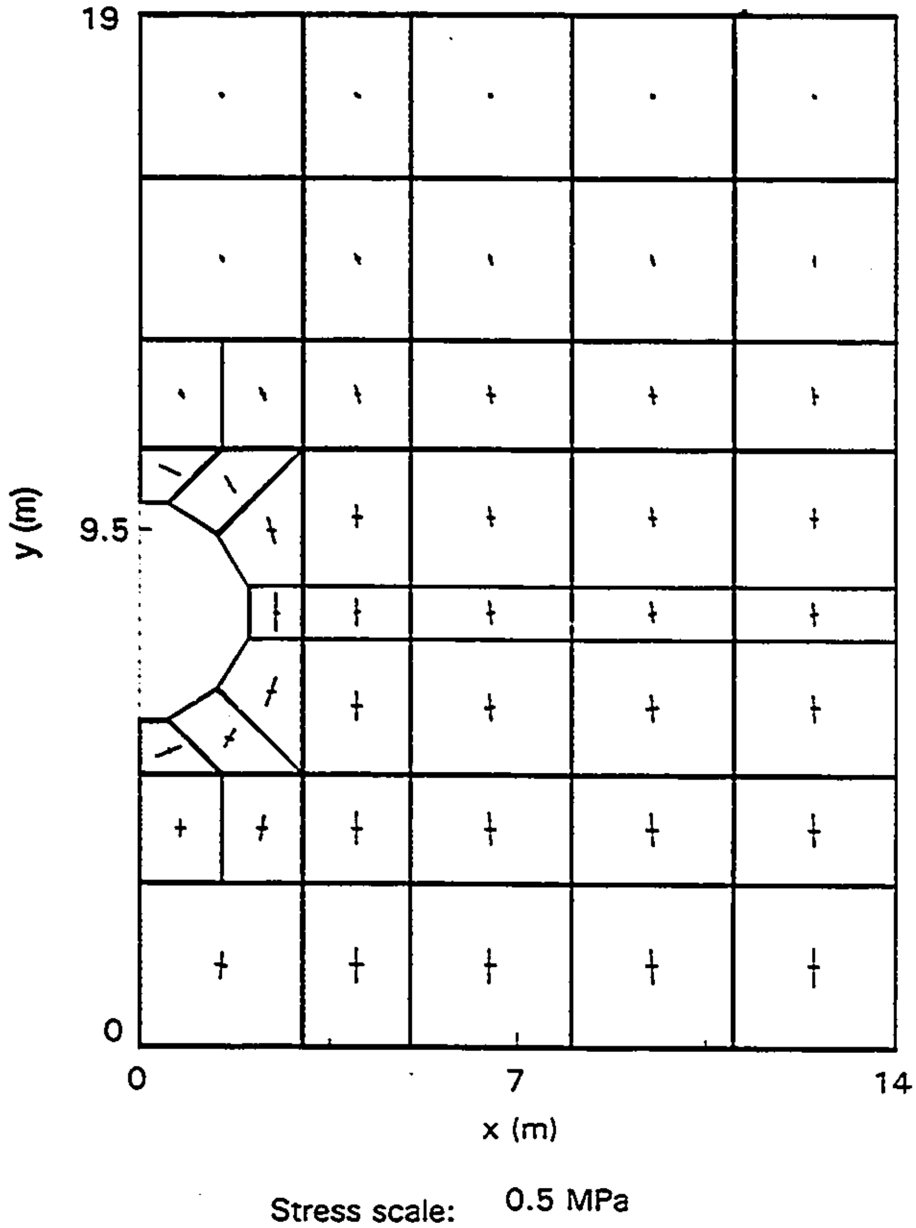

Fig.3.18 Example 1: Stress vectors obtained from the proposed model

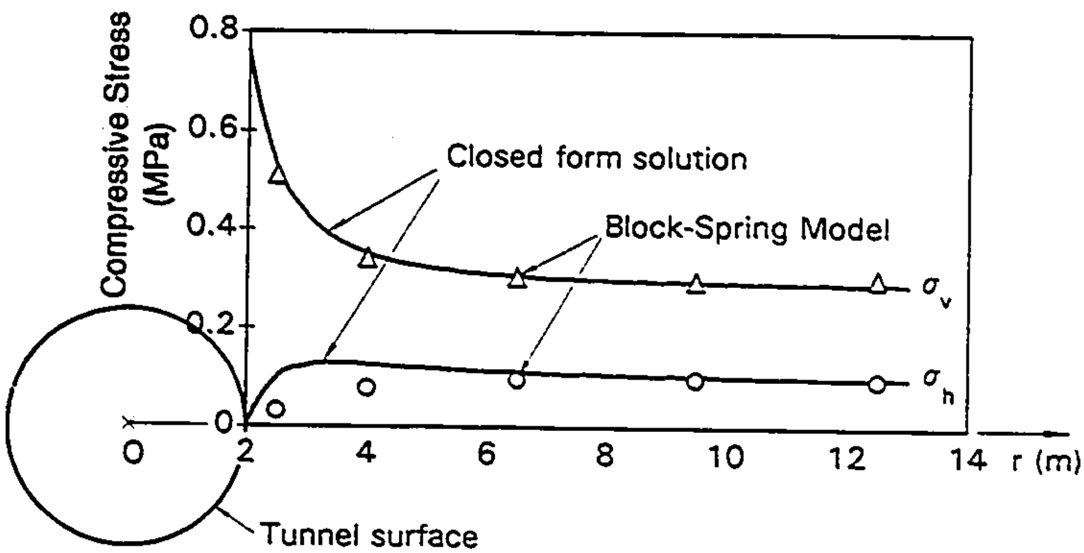

Fig.3.19 Example 1: Stress distribution on section I-I

CHAPTER 4

JOINT FAILURE BEHAVIOUR AND INCREMENTAL PROCEDURE

4.1 Introduction

The behaviour of the jointed rock mass is not a simple linear problem. The deformation of the rock joints are often irrecoverable particularly if failure takes place. The shear forces along the joints may exceed the shear strength of the joints and result in shear failure. Sliding may take place as a result of the shear failure. The blocks may be separated since the joints have no tensile capacity. An incremental procedure must be used if any numerical method is developed to simulate the large scale displacement.

Some joint failure models are reviewed in this chapter and a joint failure criterion used in the Block-Spring Model is discussed.

To model the failure behaviour of the joints and the large scale displacements of the blocks, an iteration procedure is developed based on the basic methodology of the Block-Spring Model described in Chapter 3. The computation scheme for simulation of the large displacements and determination of unstable blocks is presented in this chapter.

Rock excavation is an unloading procedure for the rock mass. The original equilibrium state of the ground stress is disturbed by removing certain volume of rocks. Different excavation procedures may result in different states of stresses and deformations. It is therefore necessary to make the Block-Spring Model capable of modelling the sequential excavation problems. A procedure for simulating the stress redistribution due to excavation is also discussed in this chapter.

4.2 Review of Some Representative Rock Joint Models

Deformation of the jointed rock masses can be greatly affected by not only the number and orientations of the joints, but also the strength of the joints. Failure behaviour of the rock joints may depend on several factors, such as, the joint surface irregularities, the normal stresses and the physical properties of the asperities on the joint walls. Various models developed for the rock joints can be found in the literature, e.g., Patton (1966), Ladanyi and Archambault (1970), Coulson (1970), Schneider (1976), Barton and Choubey (1977). The failure models were proposed based on the joint tests or physical modelling of the joints with either artificial asperities or natural roughnesses. It is widely recognized that sliding of rough joint surfaces may take place with riding up over the surface asperities and/or shearing off of the asperities depending upon the geometry of the asperities, the normal force and the strength of the intact rock.

4.2.1 Patton's joint model

Patton (1966) proposed a bi-linear model for the rock joints with non-planar surfaces as illustrated in Fig.4.1. Patton's model can be described as follows. Under low normal stresses, the irregular rock joints slide over asperities without cohesion. Joint sliding can be initiated if the shear stress exceeds the shear resistance defined by

$$S = F_n \tan(\phi + i) \tag{4.1}$$

where S denotes the shear resistance of the joint;
F_n denotes the normal force imposed on the joint;
ϕ denotes the angle of frictional sliding resistance along the contact surfaces of the asperities; and
i denotes the angle of inclination of the asperities.

On large displacements and with increase of the normal pressure, the mode of failure changes and the asperities are sheared off. The shear resistance can then be approximated by the Coulomb equation:

$$S = C + F_n \tan \phi_r \tag{4.2}$$

where C is the cohesion mobilized in shearing through the asperities;
ϕ_r is the residual friction angle of the joint surface after shearing.

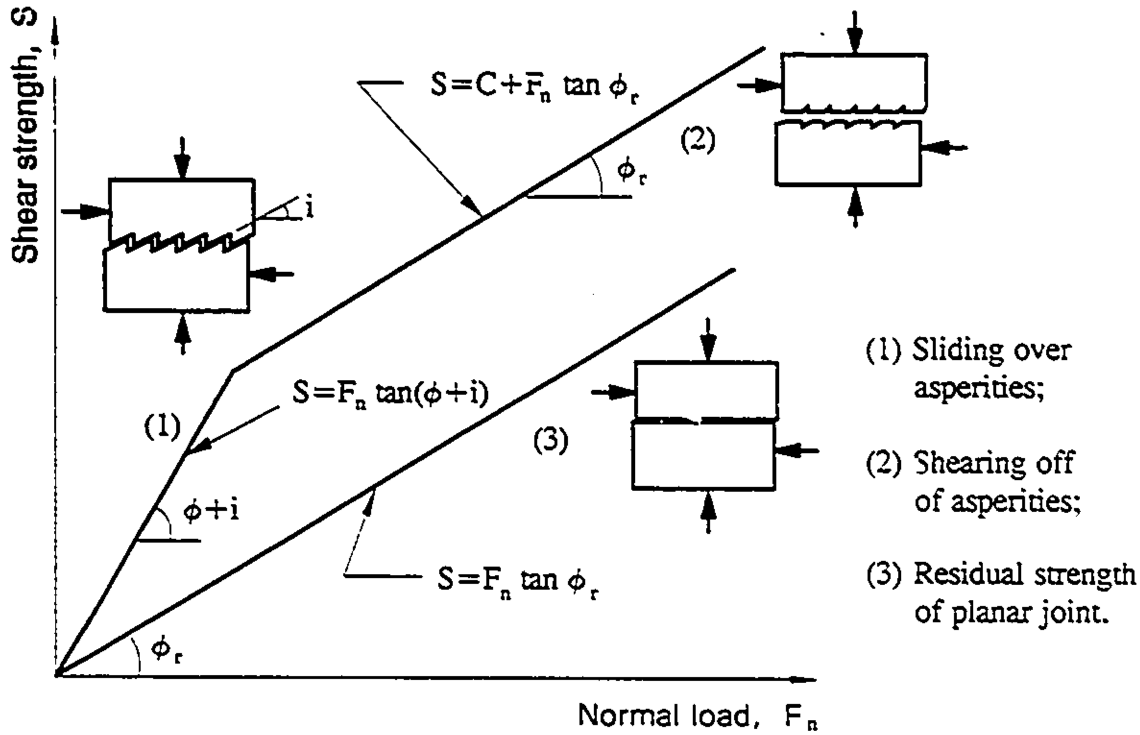

Fig.4.1 Shear strength envelopes for joints with irregular surface (after Patton, 1966)

Based on the joint tests on various plaster specimens, Patton (1966) reported that the value of ϕ_r in Eq.(4.2) was always quite close to the angle of residual sliding resistance obtained after large displacements occurred along macroscopically smooth surfaces.

It is obvious that the bi-linear model describes the joint failure behaviour in a very simple and straight forward manner. This model describes fairly well the shear strength for shearing along plane surfaces containing a number of regular and equal teeth. However, "failure envelopes for rocks would not reflect a simple change in the mode of failure but changes in the intensities of different modes of failure occurring simultaneously." (Patton, 1966).

4.2.2 Ladanyi and Archambault "LADAR" model

Ladanyi and Archambault (1970) developed a comprehensive model called "LADAR" model for joint behaviour, which can be written as follows:

$$\tau_p = \frac{\sigma_n (1-a_s)(D+\tan\phi) + a_s S_r}{1-(1-a_s) D \tan\phi} \tag{4.3}$$

where

τ_p is the peak shear strength of the rock joint;

σ_n is the normal stress across the joint;

a_s is the shear area ratio, the ratio of the sum of areas of failed asperities to the total sample area;

D is the rate of dilation at the instant of peak shear stress (joint normal displacement Δv/shear displacement Δu);

S_r is the shear strength of the intact rock (i.e., asperities).

At very low normal stresses, when $a_s \rightarrow 0$ and $D \rightarrow \tan(i)$, Eq.(4.3) reduces to

$$\tau_p = \sigma_n \tan(\phi + i) \tag{4.4}$$

At extremely high normal stresses, when $a_s \to 1$, Eq.(4.3) reduces to

$$\tau_p = S_r \tag{4.5}$$

The LADAR model combined the friction, dilatancy and interlock contributions to peak shear strength of the discontinuities. The model has been proved to be able to give a physically correct simulation of the shearing process. Comparing with Patton's bi-linear model, the LADAR model requires more sophisticated parameters such as the shear area ratio and the rate of dilation. The LADAR model may fit the joint strength curves more closely than the Patton's model does. However, due to the complexity of the rock joints, the joint parameters required by the LADAR model are difficult to determine for practical engineering applications.

4.2.3 Barton-Bandis joint model

Different from most of the other joint models, the Barton-Bandis joint model relates the strength and deformation behaviour of the rock joints to index properties (Barton and Choubey, 1977; Barton and Bakhtar, 1983 and Barton, 1973). This model describes the joint peak shear strength by the following equation:

$$\tau = \sigma_n \tan \phi' \tag{4.6}$$

where

$$\phi' = \mathrm{JRC} \log_{10}\left[\frac{\mathrm{JCS}}{\sigma_n}\right] + \phi_r \tag{4.7}$$

JRC is the Joint Roughness Coefficient;

JCS is the Joint wall Compression Strength;

ϕ_r is the residual friction angle of the joint, which can also be determined by index parameters according to Barton and Choubey (1977).

The parameters used in the model, i.e., JRC, JCS and the residual friction angle ϕ_r can be obtained from index tests performed on intact and jointed pieces of rock core. One of the reasons for relating the JRC to the joint strength and deformation behaviour in this model lies in that JRC is an equivalent measure of, or proportional to, the amplitude of roughness divided by the length of the profile.

Compared to other types of joint models, the Barton-Bandis joint model requires relatively less expensive joint data acquisition, and also reportedly provides realistic simulation of observed phenomena (Barton and Bakhtar, 1983).

Reference may be made to Barton and Bakhtar (1983) for a comprehensive review of the available rock joint models.

4.3 Modelling of Joint Strength in the Proposed Model

4.3.1 Joint shear failure criterion

In the proposed Block-Spring Model, Patton's bi-linear law is utilized for modelling the joint failure behaviour. Although any failure criterion can be incorporated in the Block-Spring Model without difficulty, Patton's law is used for its simplicity and wide availability of parameters. The shear angle of frictional resistance, ϕ, cohesion (or shear strength intercept), C, for the rock materials or the rock joints can easily be found in the literature. (Representative values of shear strength parameters for selected rocks and rock discontinuities are listed in Table A.3 in Appendix A). The bi-linear criterion is used also for its reasonable representation of the generally recognized curvature envelope of the joint shear strength (Fig.4.2) and for its ability to incorporate the residual shear strength.

In the proposed numerical model, it is assumed that the rock joint has its peak shear strength at the beginning determined by the following expression:

$$F_s \leq S_p = \min(S', S'') \tag{4.8}$$

where

$$S' = F_n \tan(\phi + i) \qquad \text{(Eq.4.1);}$$
$$S'' = C + F_n \tan \phi_r \qquad \text{(Eq.4.2);}$$

S_p is considered as the peak shear strength of the joint.

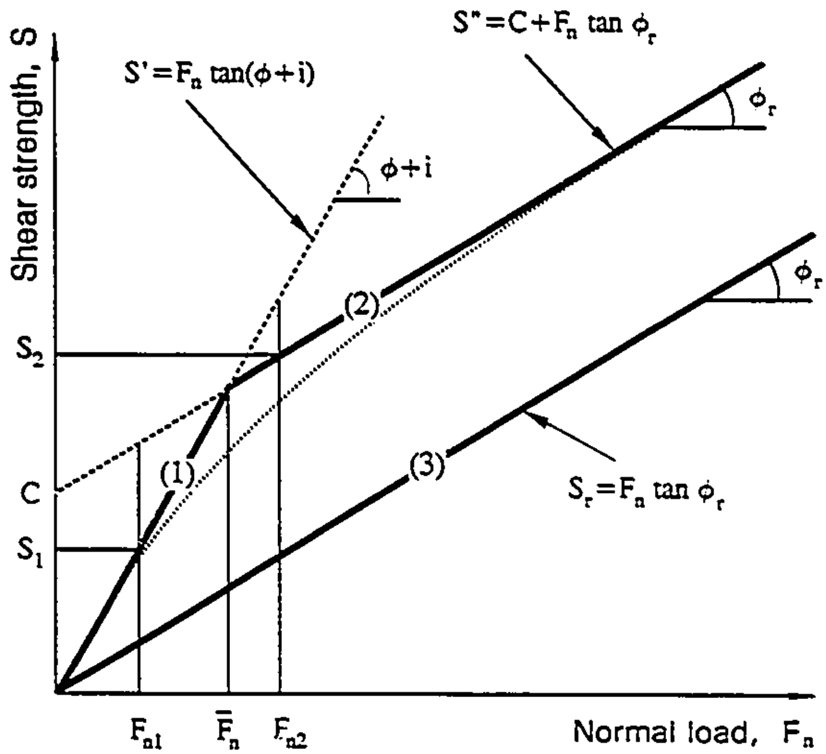

Fig.4.2 Determination of shear strength of rock joints

Eq.(4.8) implies that shear failure takes place if the shear force on the joint is greater than either S' or S". If the strength parameters, ϕ, i, C, and ϕ_r are known, whether the failure point falls on line 1 or 2 depends on whether the normal force is less or greater than $\overline{F}_n$. The force $\overline{F}_n$ determines a turning point of the shear strength envelope from line 1 to line 2 (Fig.4.2). If the normal force on a joint is $F_n=F_{n1}<\overline{F}_n$, for example, the joint shear strength is determined by $S=S'=F_{n1}\tan(\phi + i)$ ($<S"$). If $F_n=F_{n2}>\overline{F}_n$, the shear strength is determined by $S=S"=C+F_{n2}\tan\phi_r$ ($<S'$).

If shear failure occurs along the rock joint due to $F_s>S"$ (line 2 in Fig.4.2), it is assumed that the asperities along the joint surfaces are sheared off and the residual strength $S_r=F_n\tan\phi_r$ (line 3 in Fig.4.2) is then used for that joint in the next step of computation.

The contact shear failure behaviour between blocks may be simulated by incorporating a "slider" with the shear spring as shown in Fig.4.3. The slider is also connected with the normal spring, which implies that the shear strength of the joint is related to the normal pressure. The shear forces on the joint surfaces may be determined from the relative displacements of the joints by the procedure described in Chapter 3. The resulting shear forces may exceed the actual shear strengths of the joints. In such a case, sliding may take place between the two blocks and the actual shear force should be set to the value of the shear resistance $F_s=S$. In physical terms, the slider shown in Fig.4.3 ensures that the shear spring force F_s does not exceed the maximum available strength S. Simulation of further deformation of the joints and re-evaluation of the state of the contact forces are required if shear failure is detected. A procedure for modelling the joint failure behaviour is discussed in Section 4.4.

4.3.2 Joint non-tension criterion

As the rock joint has no tensile capacity in the normal direction, a non-tension criterion is used for the rock joints. If tension occurs between any two blocks, the two blocks are separated and the corresponding contact forces are set to zero. As the compressive force is defined negative, the non-tension criterion can be written as follows:

$$F_n \leq 0 \tag{4.9}$$

where F_n denotes the normal contact force between two blocks.

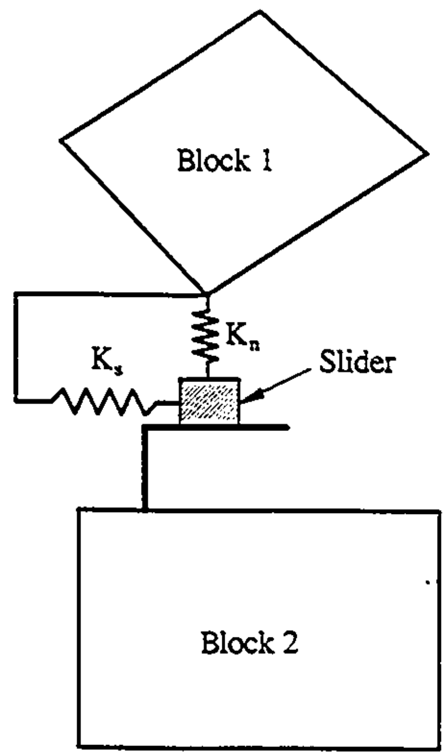

Fig.4.3 Simulation of contact failure behaviour

The slider in Fig.4.3 models not only the shear failure behaviour but also the non-tension behaviour of the joints. The normal spring imposes a normal pressure on the slider which increases the shear resistance of the contact. Also, the two blocks are separated if a tensile force from the normal spring is imposed on the slider. Both spring forces are released when the two blocks are separated.

4.4 An Iteration Procedure and Large Displacement Problems

4.4.1 Re-setting the contact forces upon failure

The contact forces evaluated by the procedure described in Chapter 3 satisfy the equilibrium conditions. These contact forces are obtained from multiplying the spring stiffnesses by the relative displacements between the blocks. As mentioned in section 4.3, tensile forces may develop in the normal springs and the forces in the shear springs may become greater than the joint shear resistance. The joint failure criteria should therefore be applied after the contact forces are evaluated.

As described in the previous section, when normal tensile forces are detected in the joints, the corresponding two blocks are separated and the contact forces are set to zero. When shear forces (shear spring forces) exceed the shear resistances of the joints, slidings initiate on the corresponding joints. Upon shear failure, the actual shear force should be the maximum shear resistance instead of the shear spring force as shown in Fig.4.4.

If either normal failure or shear failure occurs along a joint, the deformation-determined spring forces are replaced by the forces determined by the failure criteria. In this case, the equilibrium state of the previously determined force system is disturbed.

An example in Fig.4.4 illustrates the resetting of the contact forces due to shear failure. The contact forces, F_n and F_s, between blocks 1 and 2 can be determined by the procedure described in Chapter 3. The shear resistance S of the contact surface can be determined by Patton's criterion Eq.(4.8). If $|F_s| > S$, shear failure occurs between block 1 and block 2, and the two blocks slide against each other. In this case, the actual shear force between the two blocks is $F_s' = S$, rather than F_s, as shown in

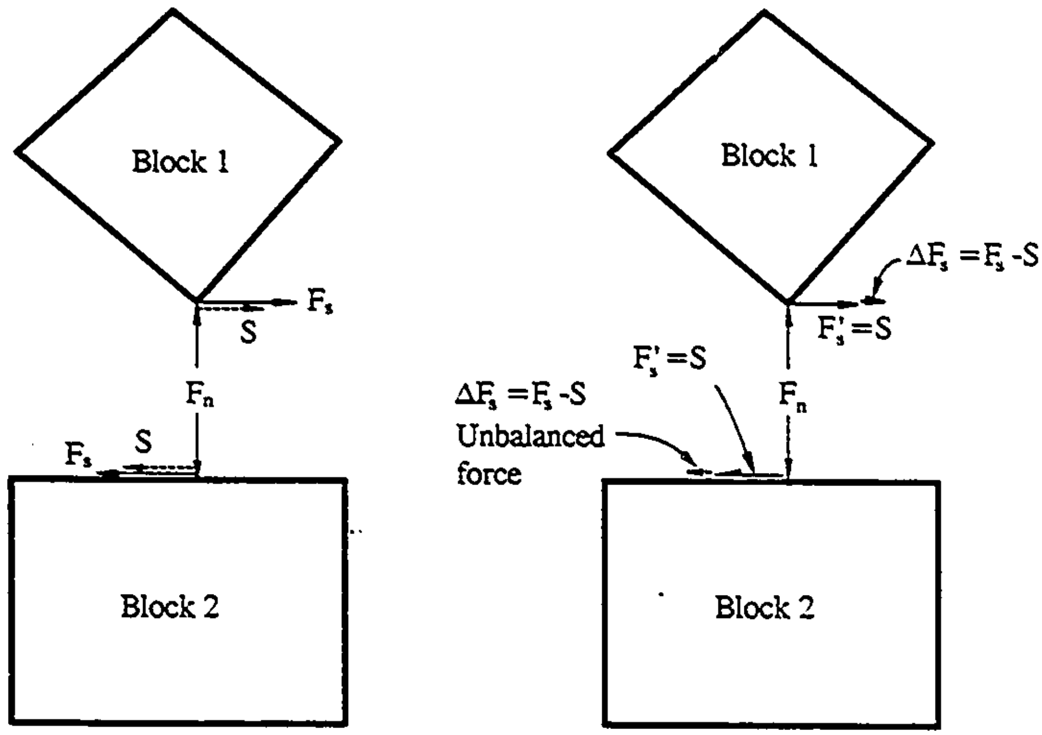

(a) Shear spring force is greater than shear resistance

(b) Shear resistance is taken as the actual shear force

Fig.4.4 Resetting contact forces after shear failure

Fig.4.4(b). However, F_s is necessary to keep the force system in an equilibrium state in the rock mass. If F_s is replaced by $F_s'=S$ ($<F_s$), the equilibrium is disturbed. The force difference $\Delta F_s=F_s-F_s'$ is unbalanced. Further computation is therefore required to determine the redistributed forces.

The same reason applies to the normal tensile failure of the contacts between blocks. If normal tension occurs, the contact forces are set to zero, $F_n'=0$ and $F_s'=0$. The originally evaluated F_n ($\neq 0$) and F_s ($\neq 0$) are unbalanced. Therefore, further computation is also required in the case of normal tensile failure to determine the redistributed forces.

4.4.2 An iteration procedure

In order to re-evaluate the state of the force system for a new equilibrium, the following steps are performed:

(1) Update the contact data (including coordinates of the contact points, the contact stiffnesses, and the contact forces);

(2) Assemble a global stiffness matrix;

(3) Re-apply the contact forces including the updated contact forces;

(4) Re-apply the boundary conditions;

(5) Solve the stiffness equations for the displacements of the blocks;

(6) Update the coordinates of the blocks;

(7) Evaluate the contact forces;

(8) Check the contact forces with failure criteria.

The above steps forms a cycle of computation which is repeated if joint failure is detected. For the *i*th cycle of computation, the displacements of the blocks can be obtained by solving the following stiffness equations, which is an incremental form of Eq.(3.40).

$$[\mathbf{K}_{i-1}]\ \{\Delta\mathbf{U}_i\} = \{\mathbf{P}_{i-1}\} \tag{4.10}$$

where $[\mathbf{K}_{i-1}]$ is a stiffness matrix assembled after the computation cycle $(i-1)$;

$\{\mathbf{P}_{i-1}\}$ is a column array consisting of the boundary conditions and the contact forces obtained from computation cycle $(i-1)$;

$\{\Delta\mathbf{U}_i\}$ is a column array consisting of the increments of the displacements of the blocks.

When $\{\Delta\mathbf{U}_i\}$ is determined, the coordinates of any point of the blocks can be updated from $\{\mathbf{x}_{i-1}\}$ to $\{\mathbf{x}_i\}$ as follows:

$$\{\mathbf{x}_i\} = \{\mathbf{x}_{i-1}\} + [\mathbf{B}_{i-1}]\ \{\Delta\mathbf{U}_i\} \tag{4.11}$$

where $\{\mathbf{x}_{i-1}\}$ and $\{\mathbf{x}_i\}$ denote the coordinates of the point obtained after iteration cycles $(i-1)$ and i, respectively;

$[\mathbf{B}_{i-1}]$ is a $[2\times3]$ matrix defined in Eq.(3.6).

The contact forces $\{\Delta\mathbf{F}_i\}$ which develop in the ith cycle can be evaluated from $\{\Delta\mathbf{U}_i\}$ using Eq.(3.15). When the increments of the displacements and the contact forces are determined, the total displacements and the total contact forces subsequent to the ith cycle can be obtained by adding the increments to the previous results as follows:

$$\{\mathbf{U}_i\} = \{\mathbf{U}_{i-1}\} + \{\Delta\mathbf{U}_i\} \tag{4.12}$$

$$\{\mathbf{F}_i\} = \{\mathbf{F}_{i-1}\} + \{\Delta\mathbf{F}_i\} \tag{4.13}$$

The new contact forces $\{\mathbf{F}_i\}$ must be checked to assess failure. If any normal force is detected positive (tension), the corresponding contact forces (in both the normal and shear directions) are set to zero, i.e., $F_i'=0$. If the normal force is negative (compression), the shear force is checked with the shear failure criterion (Eq.4.8). In the case of shear failure, the shear force is set to the value of the joint shear resistance as described earlier.

If either normal failure or shear failure is detected, another cycle of computation has to be conducted. In this case, the stiffness of the block system is re-evaluated and the updated contact forces are re-entered for the next cycle of computation.

As the coordinates of the blocks are always updated after each cycle of computation, accumulation of the incremental displacements of the blocks results in large scale displacements. Consequently, after each cycle of computation, the block-to-block contact must be checked for termination of the old contacts and creation of new contacts. Some blocks may cease to be in contact and some new contacts may also be created due to the large displacements.

The above procedure can be described as a tangent iteration approach as shown in Fig.4.5. The analysis starts from establishing an initial stiffness matrix K_0 based on the initial state of the contacts. Under an external load P, the block system undergoes some finite deformation U_I. A set of contact forces may now develop as a result of this deformation U_I to balance the load P. However, joint failure may take place which reduces the contact force to F_I. In other words, the rock discontinuity and the strength of the joints may determine that only F_I out of P can be balanced by the contact forces between the blocks. An extra external load $\Delta P_I = P - F_I$ remains unbalanced at this stage. Therefore, further deformation of the rock mass induced by ΔP_I should be expected. Since the rock mass has deformed by U_I, the coordinates of the blocks must be updated. The contacts between the blocks should also be updated, which leads to a new stiffness K_I of the block system. Upon application of the unbalanced force ΔP_I and with stiffness K_I, the block system further deforms to U_2. The block system can now carry a load F_2 at this stage. The load $\Delta P_2 = P - F_2$ therefore remains unbalanced. Another cycle of computation similar to the previous one has to be conducted. The computation cycle is repeated until the unbalanced force is close to zero, i.e., $\Delta P_n \rightarrow 0$. When ΔP_n is within the specified range, the iteration is terminated and a statically stable solution is obtained. Under certain circumstances, the block system may not converge to a stable condition. This problem is discussed in the next section.

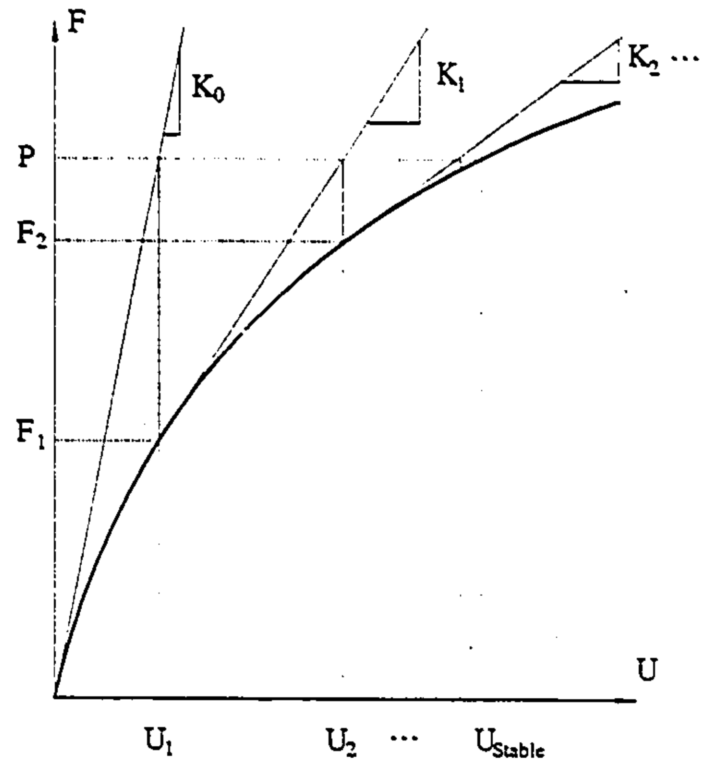

Fig.4.5 A tangent iteration procedure for stable block system

Fig.4.6 demonstrates a simple block system that becomes stable only after the large displacement takes place. Block B2 was originally on the top of the inclined surface of block B1. Shear failure occurred along the contact between blocks B1 and B2. Upon applying the iteration procedure, block B2 slid down incrementally. When the new contact was formed between blocks B2 and B3, the shear force between blocks B1 and B2 was reduced and the block system became stable.

4.4.3 Determination of unstable blocks

The block system may not always become stable after undergoing certain displacements. In the iteration procedure described in previous section, the blocks displace incrementally and some blocks may become unbalanced. Fig.4.7 demonstrates an unstable two block system. Similar to the blocks in Fig.4.6, block B2 in Fig.4.7 slid down along the inclined surface of block B1. When block B2 reached the lower end of the inclined surface, it tended to fall down. When there was only one corner to edge contact left between the two blocks, block B2 lost its balance. At this stage, block B2 became a "free" block and the equilibrium condition could no longer be applied. If the stiffness matrix is still assembled, zero diagonal element may appear during manipulation which will render the stiffness equations unsolvable. Therefore, further movements of such unstable blocks can not be modelled by solely using the stiffness matrix. Newton's second law of motion may be used, as in the Distinct Element Method, for modelling further movements of the "free" blocks. However, simulation of further movements of such blocks is usually unnecessary in practical excavation problems once they are detected to be unstable. In the iteration procedure, the computation is terminated when unstable blocks are detected and the unstable blocks are identified.

For the unstable block system, the iteration procedure can be described by Fig.4.8. After certain number of iteration cycles, some blocks may appear to be unstable. In Fig.4.8, K represents the stiffness of the block system. The iteration continues until $K_i \rightarrow 0$ which indicates that some blocks are becoming unstable and the diagonal elements corresponding to the unstable blocks in the stiffness matrix are zero. In this case, any unbalanced force may result in infinite displacement, i.e., $U_i \rightarrow \infty$.

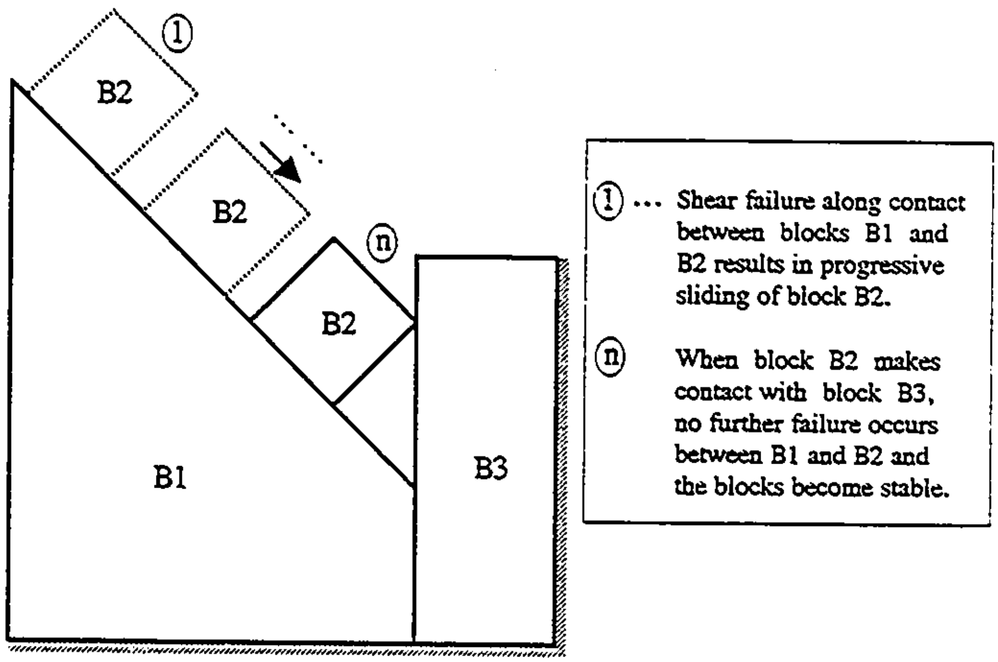

Fig.4.6 A stable block system after large displacement takes place

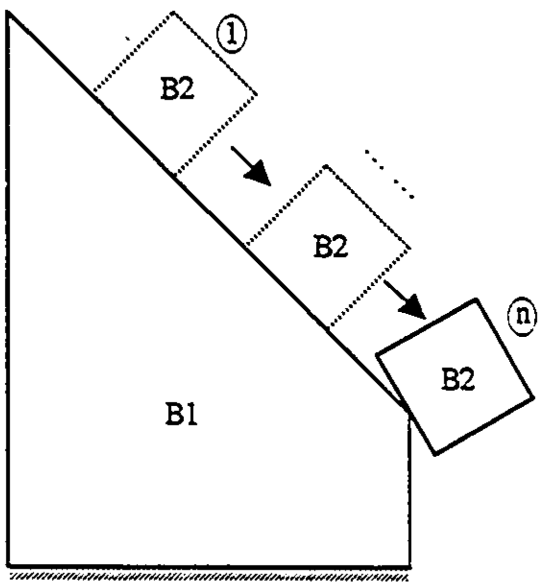

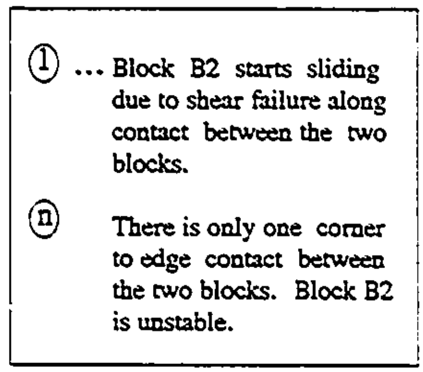

Fig.4.7 An unstable block system resulted after large displacement

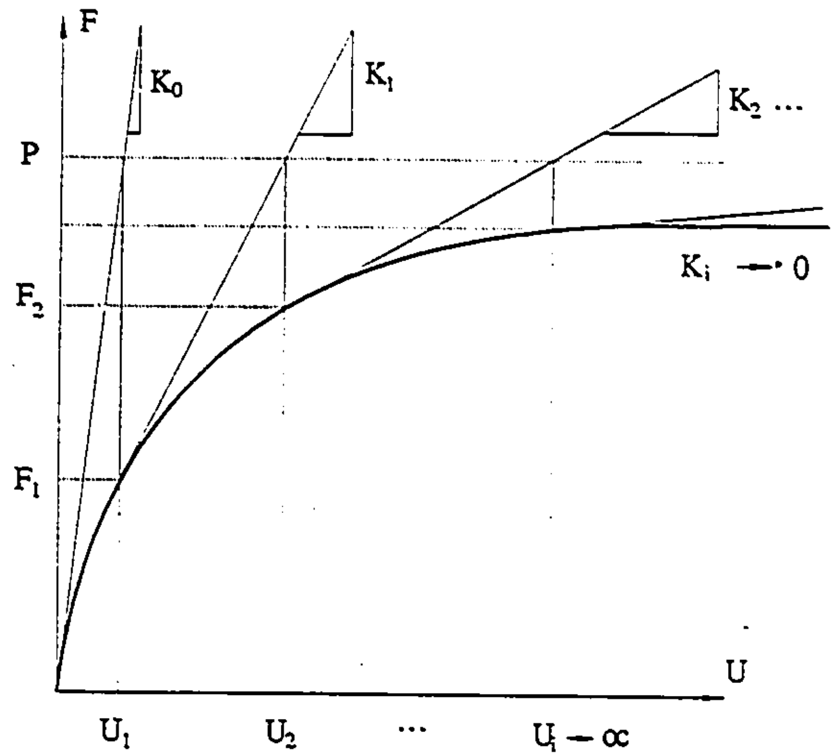

Fig.4.8 Iteration procedure for unstable block system

4.4.4 A flowchart of the iteration procedure

The iteration procedure discussed in the previous sections can be summarized in a flowchart shown in Fig.4.9. After the iteration is initiated, the same computation cycle as shown in the flowchart is repeated until two conditions are met: (1) no joint failure is detected; (2) unstable ('free') blocks are detected. If the program exits from the iteration cycle due to case (1), the average stresses within the blocks are calculated and a statically stable solution is determined. If the iteration is terminated due to case (2), the unstable blocks are identified.

4.5 Sequential Excavation Problem

The stresses in the rock masses prior to the excavations are often referred to as the initial stresses. Rock excavation disturbs the equilibrium state of the initial stresses and induces a new stress state. Different excavation procedures may result in different states of the induced stresses and different modes of deformation of the rocks. An optimized excavation procedure is often required for safety, economy, and productivity. Consequently, the capability of simulating the sequences of the excavations is a desirable feature in an analysis.

4.5.1 Initial ground stress field

The in-situ ground stresses prior to the excavations could be affected by various factors such as gravity, tectonic movement, denudation, topography, and thermal effects. The distribution of the ground stresses may vary from site to site. Generally, the vertical stresses on the horizontal planes are close to the overburden pressures. The horizontal stresses on the vertical planes may vary dramatically from site to site depending upon the geological histories. From compilations of appreciable number of in-situ stress measurements, Brown and Hoek (1978) as well as Herget (1986) showed that the vertical stresses were close to the gravitational stresses evaluated from the weight of the overlying rocks (Fig.4.10). The vertical stress, σ_v, may be calculated as follows:

$$\sigma_v = \gamma h \tag{4.14}$$

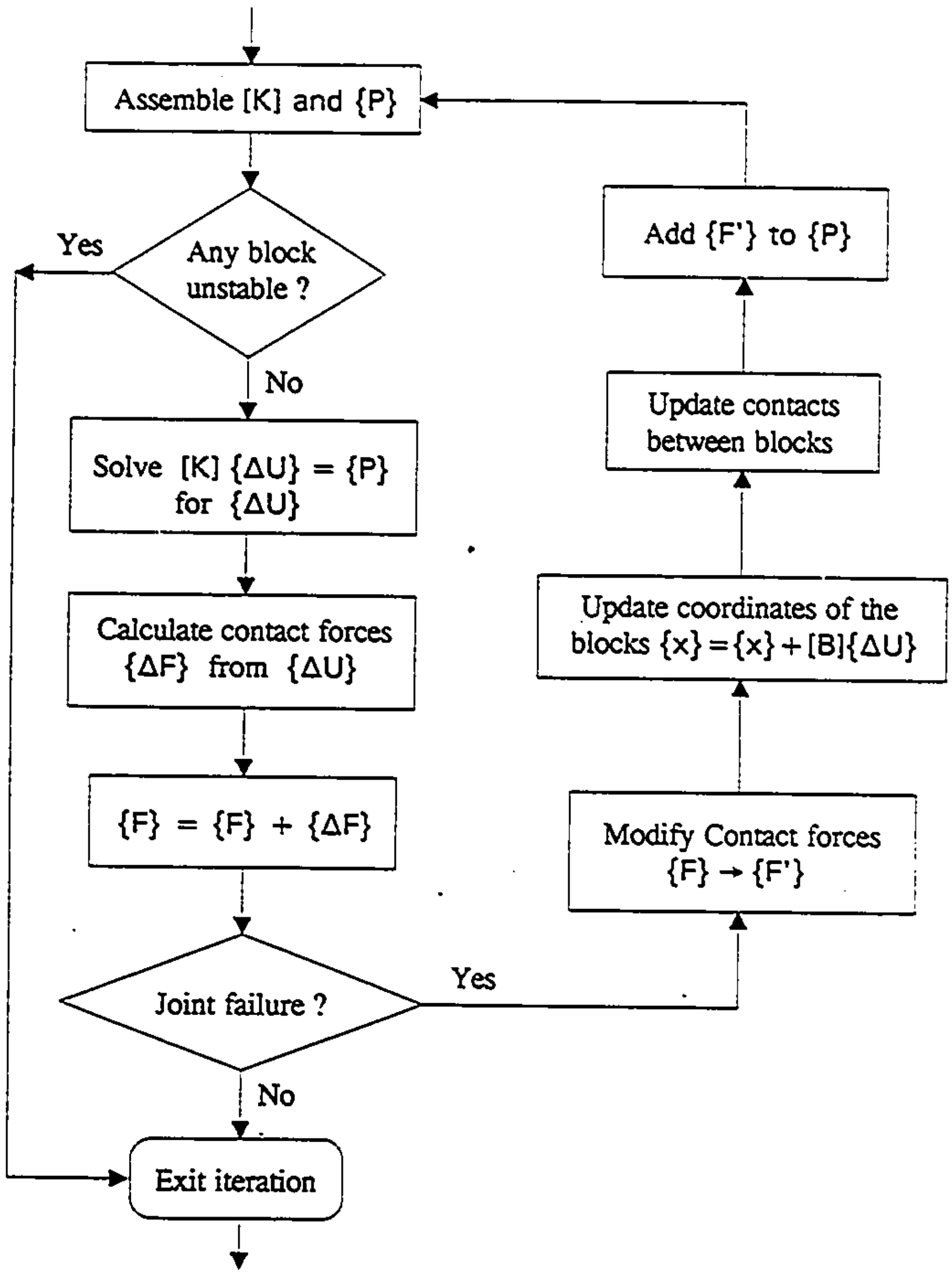

Fig.4.9 A flowchart of the iteration cycle performed upon joint failure

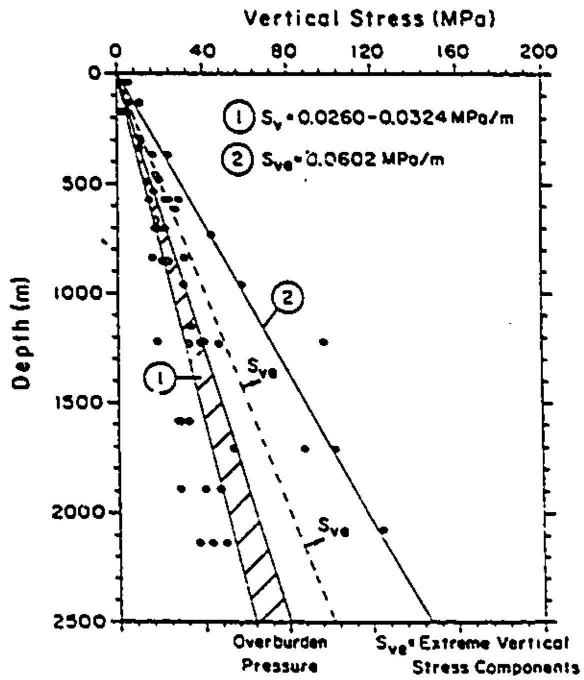

Fig.4.10 Vertical stress distribution (after Herget, 1986)

where γ is the unit weight of the rock; and h is the depth at which the stress is calculated.

Brown and Hoek (1978) and Herget (1986) also showed that the horizontal stresses near the ground surface, within 1 km of depth or so, were much higher than the gravitational stresses. Variations of the ratio of average horizontal stress to vertical stress, $K=\frac{\sigma_h}{\sigma_v}$, with depth were demonstrated to have the trend shown in Fig.4.11. Herget (1980, 1982, 1986, and 1987) showed from Canadian shield data that the average horizontal stresses are 1.5 times higher than the vertical stresses at depths of 1,000 to 2,500 m. At depths within 100 m the ratio $K=\frac{\sigma_h}{\sigma_v}$ approaches 5. Similar trend was also indicated by Brown and Hoek (1978) for the worldwide data.

In order to determine the initial stresses in the rock mass with the Block-Spring Model, boundary conditions of the rock mass can be assumed based on the in-situ data of the concerned site or those of comparable sites. The gravity forces can be applied as vertical loads. Appropriate loads must also be imposed on the lateral boundaries to simulate the horizontal stresses. The horizontal loads can be determined based on measurements of in-situ horizontal stresses. The least square regression method can be used for the best estimation of the initial ground stresses based on the in-situ data (e.g., Guo, et al., 1983; Wang and Ma, 1986). In practical designs, it is not unusual that the horizontal stresses are assumed uniformly distributed as shown in Fig.4.12 (e.g., Trow and Lo, 1989). Others have used a constant ratio, K, of horizontal stress to vertical stress (e.g., Benson, et al., 1970). In this case, a linearly distributed horizontal load (as shown in Fig.4.13) is determined by $K\sigma_v$, where σ_v is the overburden stress and K is estimated from in-situ data.

Based on compilation of in-situ data from Canadian shield, Herget (1986, 1987) proposed an empirical relation between the ratio of average horizontal stress to vertical stress (K) and the depth as follows:

$$K = \frac{\sigma_h}{\sigma_v} = \frac{267}{h} + 1.25 \tag{4.15}$$

where h is the depth in meter.

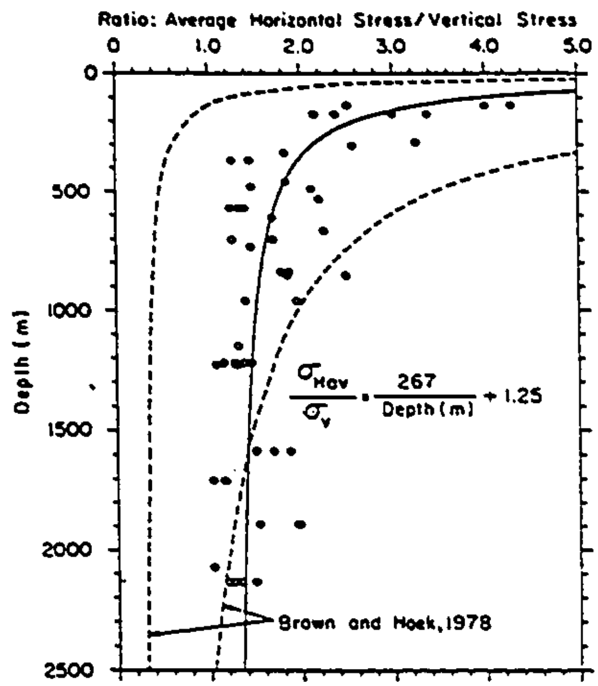

Fig.4.11 Variation of ratio, $K=\frac{\sigma_h}{\sigma_v}$, with depth (after Herget, 1986)

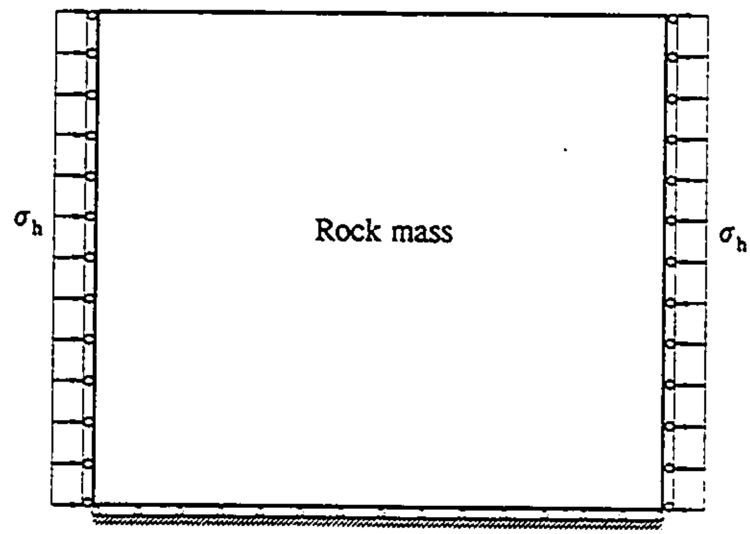

Fig.4.12 Uniformly distributed horizontal load

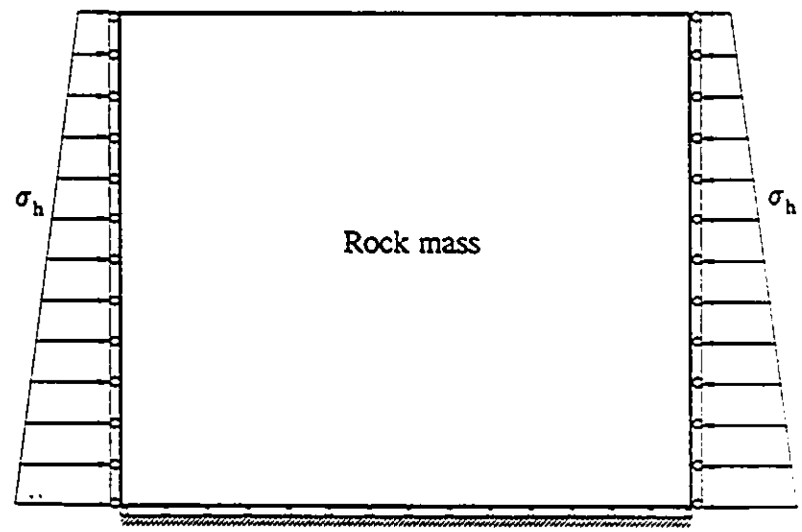

Fig.4.13 Horizontal load with a constant $K=\frac{\sigma_h}{\sigma_v}$

A similar relation of K to depth was proposed by Brown and Hoek (1978) for worldwide data:

Upper bound: $$K = \frac{1500}{h} + 0.5 \qquad (4.16)$$

Lower bound: $$K = \frac{100}{h} + 0.3 \qquad (4.17)$$

Eqs.(4.15), (4.16) and (4.17) provide the trends of variation of ratio K with depth. However, for important projects, in-situ stresses and the site K values may be measured.

Once the boundary loading conditions are determined, the corresponding initial stress distribution in the rock mass can be evaluated easily by the Block-Spring Model.

4.5.2 Excavation induced stresses

The excavation induced stress redistribution may be evaluated by removing the corresponding blocks. Analysis of a sequential excavation is illustrated in Fig.4.14. Fig.4.14(a) shows a rock mass prior to excavation with boundary conditions. The dashed line Γ is the surface of the opening to be excavated. The initial ground stress prior to excavation σ_0 can be determined with the Block-Spring Model. To simulate the excavation induced stress redistribution, the rock body within Γ can be removed step by step depending on the excavation sequences. If a part of the rock body is removed (Fig.4.14.b), the contact forces along the newly formed opening surface are set to zero. The other boundary conditions are still applied including the displacement and the force boundary conditions and the gravity forces. In addition, the initial contact forces between the remaining blocks are also applied. A new set of stiffness equations can now be established for the excavated rock mass. The increment of the deformation of the rock can be obtained by solving these equations. Subsequently, the new contact forces between blocks and the stresses within the blocks can be determined.

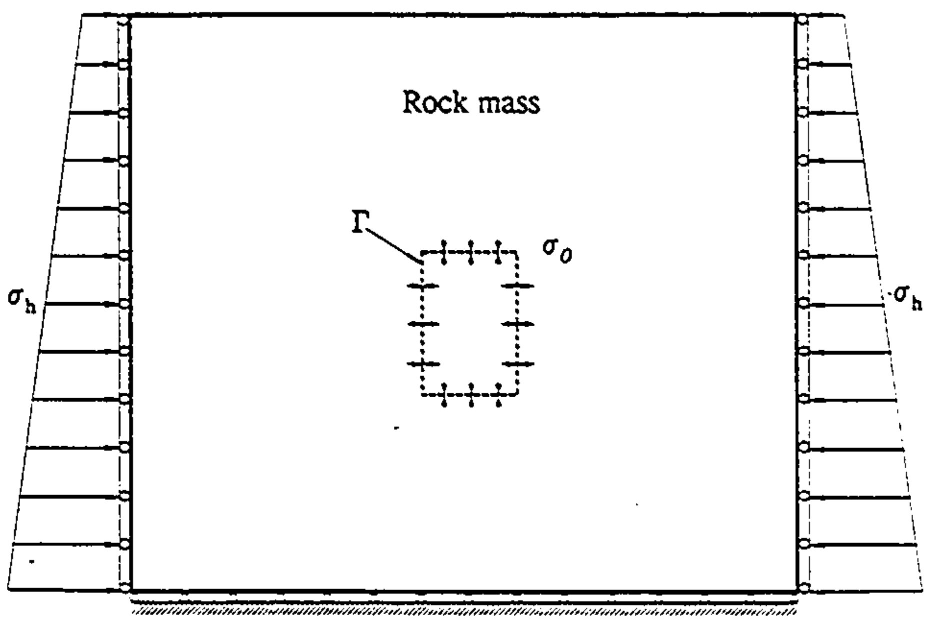

(a) Rock mass prior to excavation – initial stress σ_0

Fig.4.14 Simulation of sequential excavation

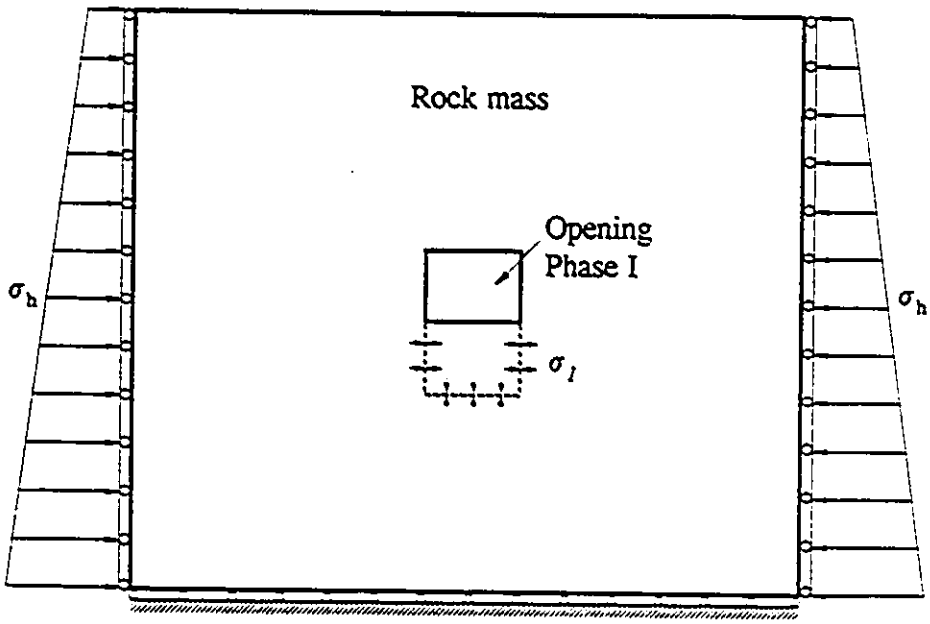

(b) First step of excavation – Original boundary conditions are still applied. Contact forces between remaining blocks are re-imposed. The stresses on the excavated surfaces are reduced from σ_0 to zero. New stress state is represented by σ_1

Fig.4.15 Simulation of sequential excavation (continued)

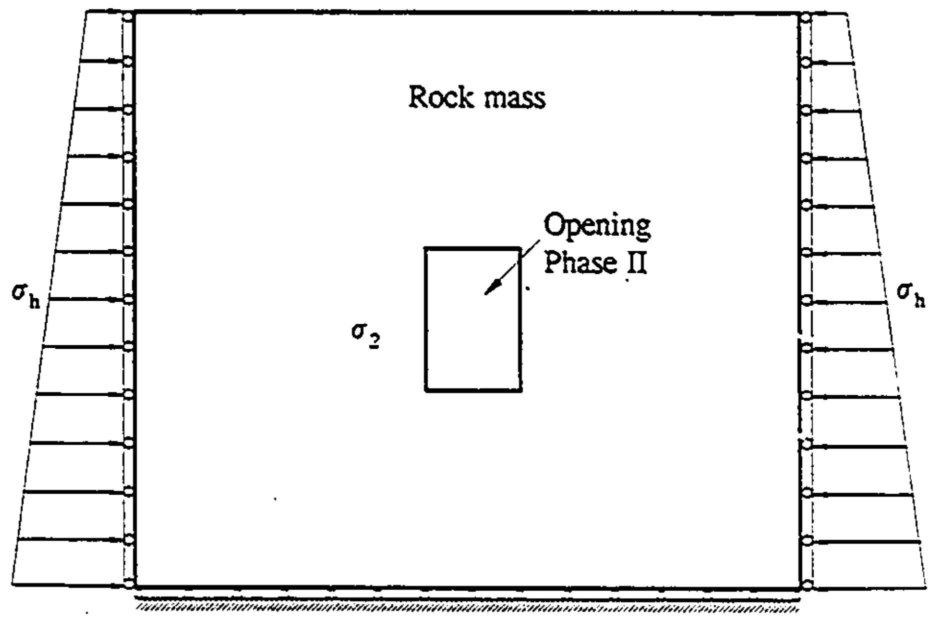

(c) Second step of excavation – Original boundary conditions are still applied. Contact forces between remaining blocks obtained from excavation phase I are re-imposed. The contact forces on the newly excavated surfaces are reduced from σ_1 to zero. New stress state is now represented by σ_2.

Fig.4.15 Simulation of sequential excavation (continued)

For simulating further excavations, the computation can be continued by removing the corresponding blocks and re-applying the boundary conditions. To model the second step of excavation, the contact forces obtained from the first step are re-imposed as the initial contact forces. Again, the stresses along the newly excavated surfaces are reduced from σ_I to 0, where, σ_I represents the stresses obtained at the first stage of excavation (Figs.4.14.b, c).

It should be mentioned that the selected region of the rock mass must be large enough so that the boundary conditions are not affected by the excavation.

4.6 Examples 2 and 3: Large Displacement Problems

The following examples demonstrate the capability of the Block-Spring Model in simulating large scale displacements and unstable blocks. Examples of the excavation induced stresses are given in Chapter 8.

Example 2: Stable and unstable blocks

Fig.4.16 shows a three block system. Blocks 1 and 3 are fixed. Block 2 on top of block 1 is 0.5m away from block 3. A horizontal force P is imposed on block 2 as shown in Fig.4.16. The final state of the blocks determined by the Block-Spring Model is shown in Fig.4.17, in which the dashed lines indicate the original position of block 2. It can be noted, in Fig.4.17, that block 2 displaced towards block 3. When a new contact was formed between blocks 2 and 3, the block system became stable and the computation was terminated.

Fig.4.18 shows another three block system similar to the previous one, but block 3 is separated from block 1. Again, a horizontal force P was imposed on block 2. Analysis with the Block-Spring Model indicates that block 2 displaced towards block 3. When block 2 reached the corner of block 1, the computation was terminated. Block 2 was identified as being unstable. Fig.4.19 shows the status of the blocks when the computation was terminated. The original location of block 2 is given by the dashed lines. The solid lines show the update locations of the blocks. The unstable block is shaded in the graphics output.

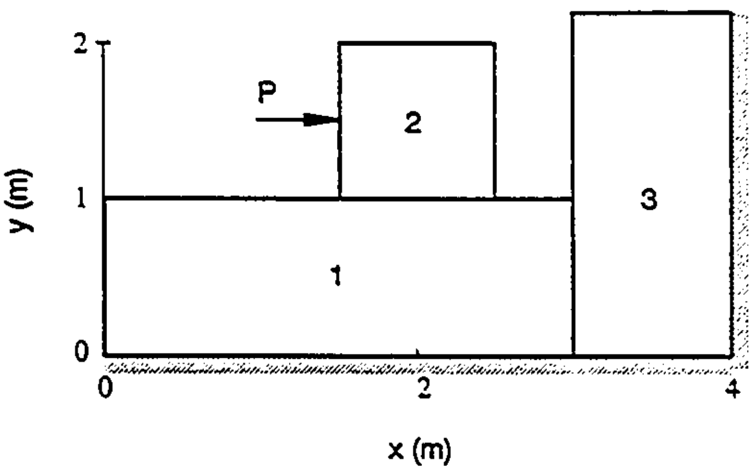

Fig.4.16 Example 2: A three block system

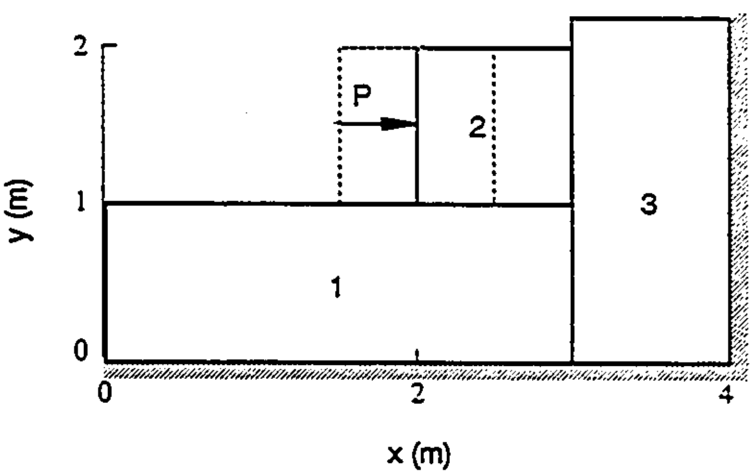

Fig.4.17 Example 2: Final state of the block system
from the proposed model

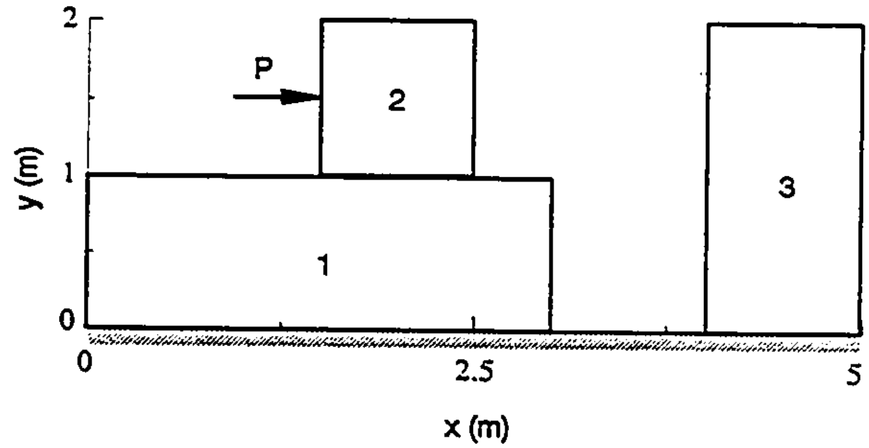

Fig.4.18 Example 2: A three block system with block 3 separated from the others

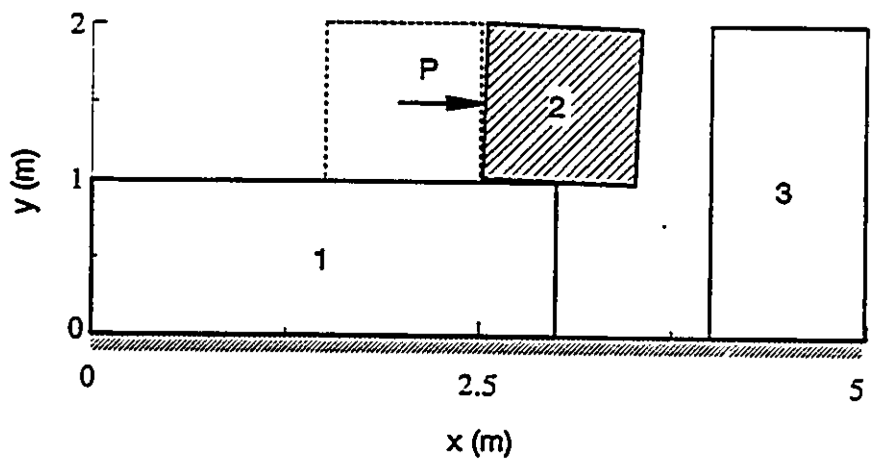

Fig.4.19 Example 2: Unstable block system determined by the Block-Spring Model

Example 3: Sliding of a slope

This is a simple example for demonstrating the capability of the proposed Block-Spring Model in modelling the slope sliding problem. Fig.4.20 shows a hypothetical slope with stratified rocks. There are two major sets of joints. Joint set 1 is parallel to the slope surface and joint set 2 is perpendicular to the slope surface. The assumed characteristics of the rock blocks and the joints are listed in Table 4.1.

Table 4.1 Example 3: Parameters of the rocks and the joints assumed for the simple slope

	Intact rock	Joint set 1	Joint set 2
Elastic Modulus: (MPa)	70,000	40,000	50,000
Poisson's ratio:	0.2	0.3	0.3
Unit weight: (kN/m^3)	26	–	–
Cohesion: (MPa)	30	1	1
Friction angle: (°)	45	25	30

The bottom of the mesh is fixed and the two lateral boundaries are constrained in horizontal direction (Fig.4.20). The rock mass is subjected to gravity forces.

Figs.(4.21) and (4.22) are the intermediate and the final states of the slope, respectively, obtained from the Block-Spring Model. Fig.4.21 shows that the upper two layers of rocks had slidden down and layer 2 (see Fig.4.20) had reached the bottom of the slope. When layer 1 reached the bottom of the slope, as shown in Fig.4.22, the sliding was stopped. It can also be noted in this example that the contacts between blocks were always re-arranged and the new contacts were created.

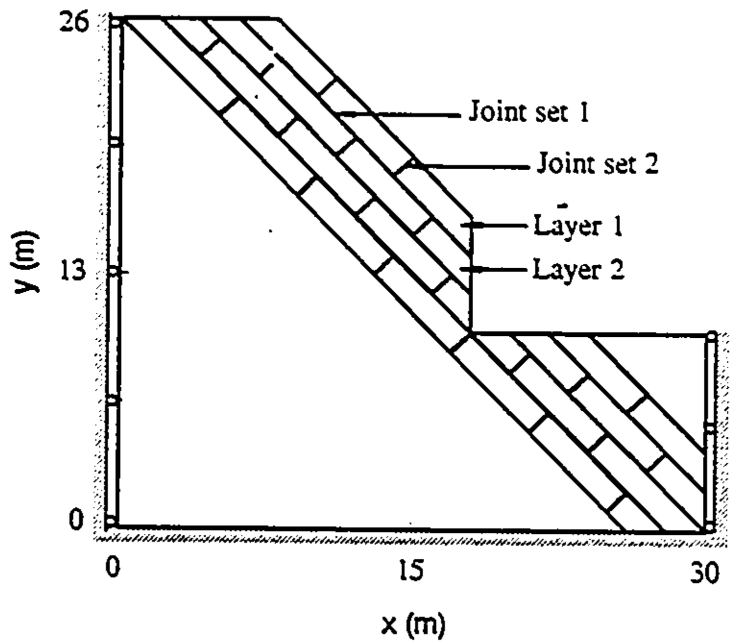

Fig.4.20 Example 3: A simple rock slope with stratified rocks

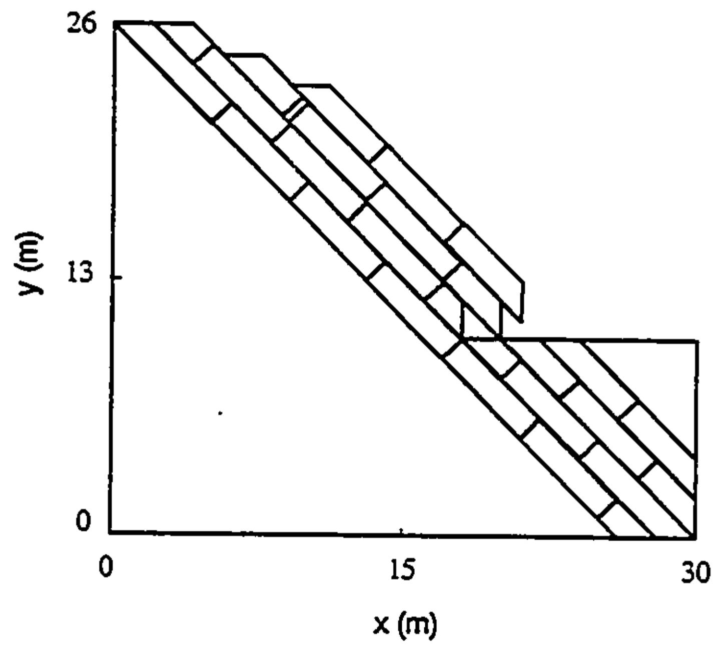

Layer 2 has reached the bottom and Layer 1 is sliding over layer 2.

Fig.4.21 Example 3: Intermediate result

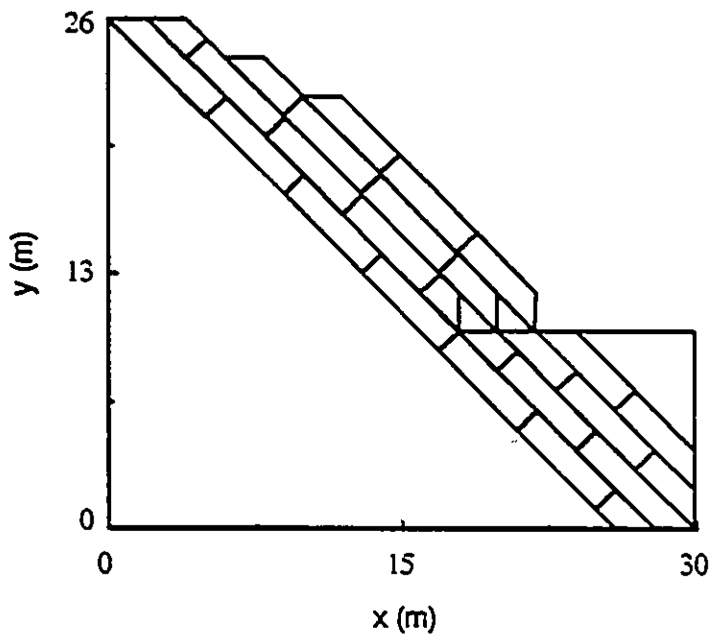

Layer 1 has reached the bottom of the slope

Fig.4.22 Example 3: Final result

CHAPTER 5
MODELLING OF ROCKBOLTS

5.1 Introduction

Rockbolting has become a very important measure for providing ground support for rock excavations, particularly in mining engineering. Consequently, it is important to be able to analyze the action of the rock bolts and reinforced rock masses for a rational design of rock excavations. A wide variety of bolt types and bolting techniques, perhaps hundreds (Hoek and Brown, 1980), have been used in the world. However, based on the type of anchoring condition, the rock bolts may be classified into two main categories, i.e., end anchored (or point-anchored) rockbolts and fully grouted rockbolts (or dowels). The end anchored rockbolts are usually anchored to the rocks either mechanically by expanding the ends of the bolts, e.g., slot and wedge anchors and expanding shell anchors, or by grouting with cement or resin at the tip of the reinforcing bar (Hoek and Brown, 1980; Sinha and Schoeman, 1983). A fully grouted rock bolt, in contrast, is usually bonded over its entire length to the adjacent rock in the drill hole by some grouting materials, typically cement or resin (e.g., Franklin and Dusseault, 1989; Hoek and Brown, 1980). Exceptions to the above two categories may be the tubular steel rock bolts, such as the split sets and "Swellex" bolts. These tubular rockbolts are anchored to the rocks over the full length by forcing the bolts to enlarge the diameters and to fit the drill hole surfaces. These tubular steel rock bolts, from a theoretical viewpoint, may be regarded as variations of fully grouted bolts since they all offer shear resistance to relative movements between bolts and the surfaces of drill holes (Gerrard, 1983).

Based on the stress conditions at the time of installation, the rock bolts, either end-anchored or fully grouted, can be further classified into pretensioned (or active) rockbolts and untensioned (or passive) rockbolts. The pretensioned rockbolts apply active loads (compressions) to the rock blocks as the bolts are tensioned at the time of installation. The untensioned rockbolts apply forces to the rocks only as response to the movement of the rock blocks.

In discussing the rockbolt behaviour, Gerrard (1983) classified the rockbolts into three main categories, i.e.,

(i) tensioned, ungrouted bolts;

(ii) untensioned, grouted bolts; and

(iii) tensioned grouted bolts.

The untensioned, ungrouted rockbolt was not mentioned by Gerrard (1983). As to whether the ungrouted rockbolt should be tensioned, Franklin and Dusseault (1989) noted that the end-anchored, ungrouted rockbolts must be tensioned and remain tensioned if they are to work at all. However, Bergman and Bjurstrom (1983) pointed out that the use of untensioned bolts — grouted and ungrouted — was propagating around the world.

A computer scheme has been incorporated in the Block-Spring Model for simulating the four types of rock bolts, i.e., the end-anchored and fully grouted rockbolts, either pretensioned or untensioned.

5.2 Modelling of End-Anchored Rockbolt

5.2.1 Numerical representation of the end-anchored rockbolt

The end-anchored rockbolt usually has two point-anchorages. The inner end of the bolt is anchored in solid rock and the outer end is tightened against the rock surface. The rockbolt can be represented by a one dimensional deformable element or a spring (Fig.5.1). The two ends of the spring are assumed fixed on the rock blocks. If the stiffness of the bolt is K_b, then the relative displacements between the two anchored blocks result in an axial force T in the bolt, which can be written as follows:

$$T = K_b \cdot \Delta L \tag{5.1}$$

where ΔL is the relative displacement between the two anchorage points, assumed as the elongation of the rockbolt.

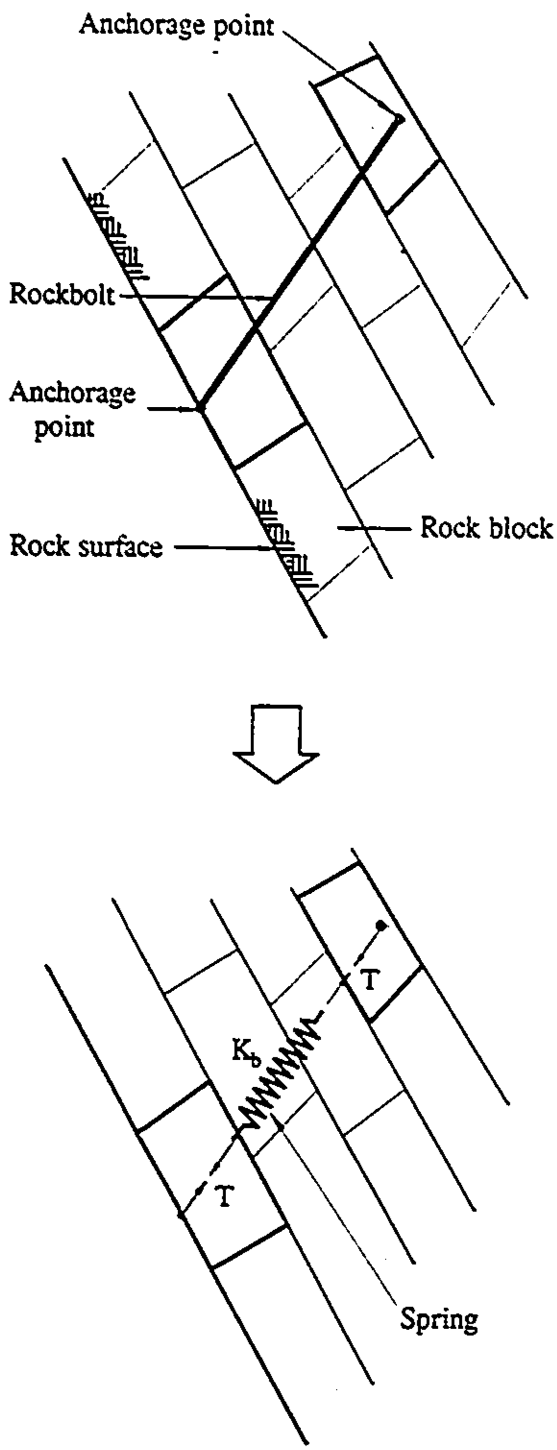

Fig.5.1 Simulation of end-anchored rockbolt

Here the effect of the movements of the other blocks through which the bolt passes is ignored.

The stiffness of the rockbolt can be determined from the elastic modulus and the dimension of the bolt as follows:

$$K_b = \frac{E_b \cdot A}{L} \tag{5.2}$$

where E_b is the elastic modulus of the rockbolt;

A is the area of the cross-section of the rockbolt; and

L is the length of the bolt.

5.2.2 Failure criteria

It is assumed that the rockbolt has no compressive capacity. If any compressive force develops in the rockbolt, the bolt force is set to zero.

The rockbolt may fail due to yielding of the bolt material. The yield strength of the bolt material is used to govern the tensile failure behaviour of the bolt. It is assumed that the failure behaviour of the bolt material is governed by an elastic-plastic rule as illustrated in Fig.5.2. In other words, the bolt may deform elastically with the axial force less than the yield strength T_{yield} of the material. The bolt continues to deform at the yield point without increase of the stress.

The rockbolt may also fail due to an insufficient capacity of the bolt/rock anchorage. A rigid-plastic criterion is adopted for describing the failure behaviour of the bolt/rock anchorage (Fig.5.3). It is assumed that there is no relative displacement between the bolt and the rock at the anchorage point until the tensile forces in the bolt becomes equal to or greater than T_{anch}, a maximum allowable load of the bolt/rock anchorage.

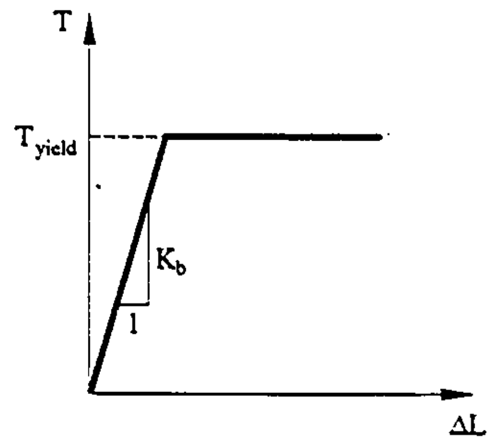

Fig.5.2 A yield failure criterion for bolt material

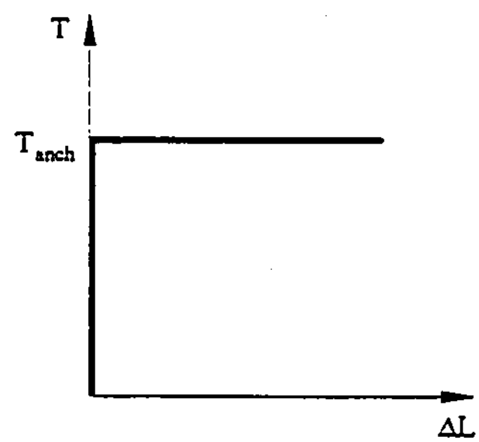

Fig.5.3 A rigid-plastic criterion for the bolt/rock anchorage

Considering the strengths of both the bolt material and the bolt/rock anchorage, a rockbolt failure criterion can be written as follows:

$$T \leq T_{max} = \min (T_{yield}, T_{anch}) \tag{5.3}$$

where T is the tension in the rock bolt;

T_{max} is the maximum allowable tension in the rockbolt;

T_{yield} is the yield strength of the bolt material (in the unit of force); and

T_{anch} is the capacity of the bolt/rock anchorage (in the unit of force).

If T evaluated from Eq.(5.1) exceeds the maximum allowable load T_{max} determined by Eq.(5.3), the bolt force is set to

$$T' = T_{max} \tag{5.4}$$

The bolt forces determined either by Eq.(5.1) or by Eq.(5.4) are imposed on the anchored blocks as shown in Fig.5.1. The end-anchored rockbolt may apply a compression to the blocks between the two anchored blocks thus increasing the normal pressures and the shear strength along the rock joints.

5.3 Modelling of Fully Grouted Rockbolt

5.3.1 Conventional fully grouted rockbolt model

Various techniques of modelling the fully grouted rockbolts with numerical methods can be found in literature (e.g., Lorig, 1988; Mitri and Rajaie, 1990). A typical model is shown in Fig.5.4, which simulates the fully grouted rockbolt by a series of 1-D deformable elements (or springs) joined end to end. Each joint or node has one degree of freedom. Shear springs attached at the nodes model the grouting materials as shown in Fig.5.4 (e.g., Lorig, 1988). The stiffnesses of the axial and shear springs represent

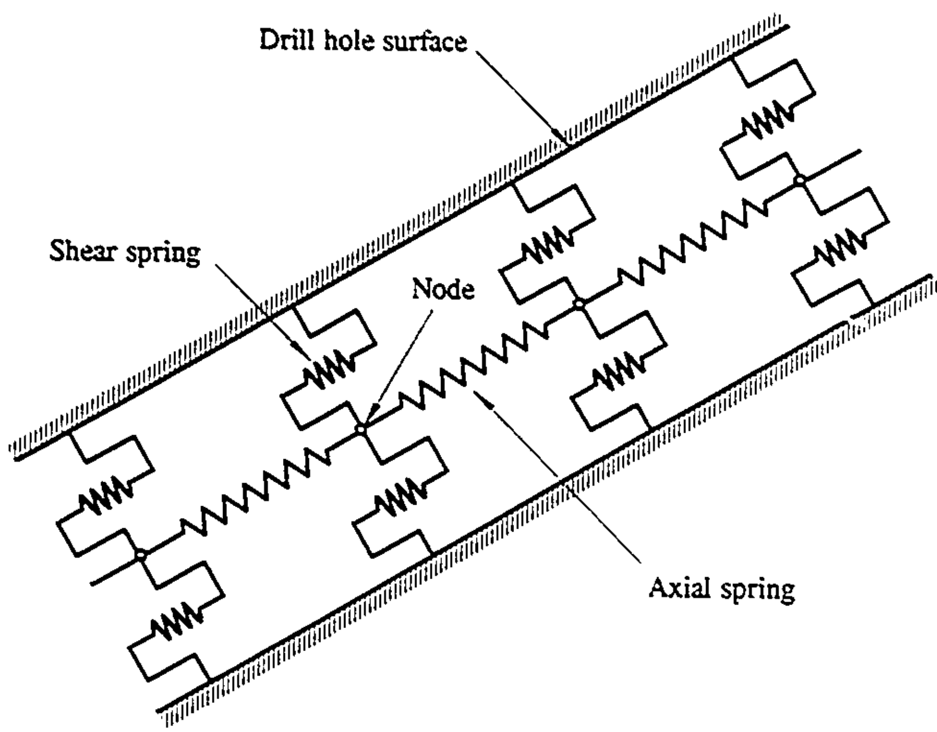

Fig.5.4 A typical model of the fully grouted rockbolt

the deformabilities of the steel bolt and the grout respectively. The relative displacements between the nodes and the rocks result in shear forces between the bolt and the drill hole surface. The relative displacements between two adjacent nodes result in axial forces along the bolt.

An advantage of the above rockbolt model is that deformations of both the rockbolt and the grouting materials are modelled. A disadvantage of this model is that the nodes along the rockbolt increase the number of the degrees of freedom. In the stiffness matrix based numerical method, the size of the matrix is increased if the above rockbolt model is adopted. As the rock blocks and the rockbolt elements are two different types of elements, significant increase of the band width of the stiffness matrix may be expected, though there is only one degree of freedom at each node.

5.3.2 Proposed fully grouted rockbolt model

In the Block-Spring Method developed in this thesis, an alternate fully grouted rockbolt model is proposed. The rockbolt is discretized into segments by the rock blocks through which the bolt passes (Fig.5.5). Each segment is considered as a one dimensional element. The bolt elements are connected at nodes as shown in Fig.5.5. Further, the bolt elements also interact with the rock blocks at the nodes. In other words, the bonding along the entire length is simplified as a series of equivalent point bondings (Figs.5.5 and 5.6).

The rigid-plastic rule shown in Fig.5.3 is also adopted for describing the behaviour of the "point bonding". It implies that the bolt elements are rigidly bonded to the drill hole surface at the nodes until bonding failure occurs. Bonding failure may occur as a result of inadequate bond capacity either along the steel bolt/grout interface or along the grout/rock interface. The determination of the shear force which may develop along these two interfaces between the node and the drill hole is discussed in Section 5.3.3.

Before failure occurs, the relative displacements between the nodes and the rock surface along the drill hole are zero (since rigid bonding is assumed). Therefore, the nodal displacements of the bolt elements can be determined by the displacements of the rock blocks. The nodes of the bolt elements slide along the drill hole when bonding failure occurs.

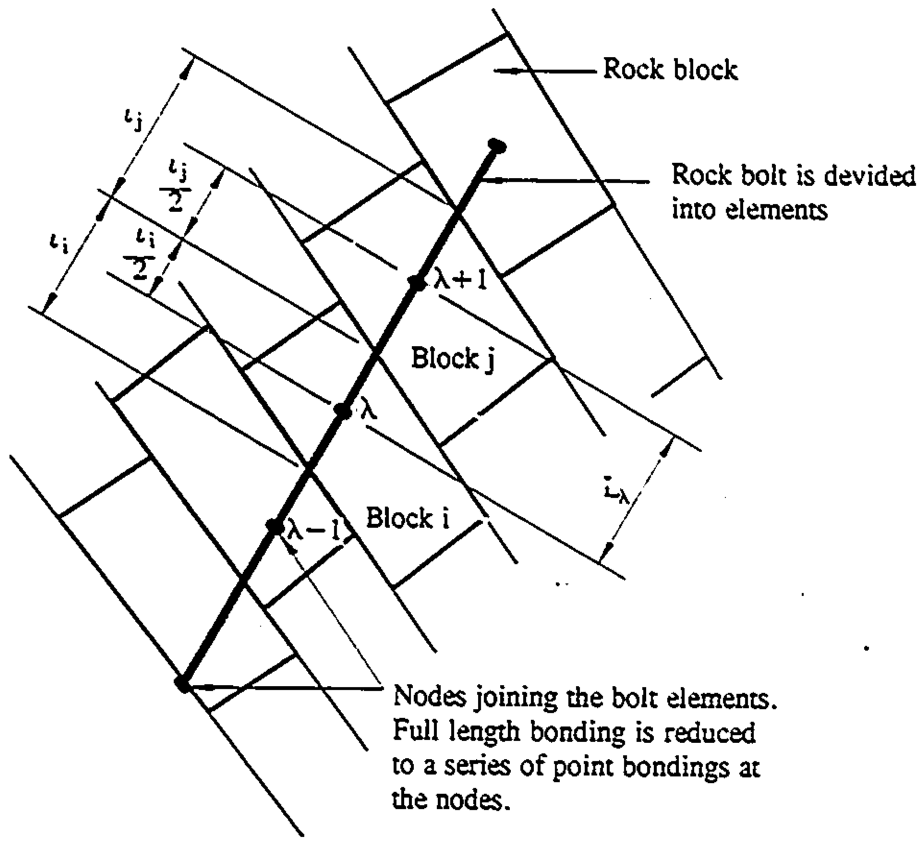

Fig.5.5 Representation of rockbolt with elements joined by nodes

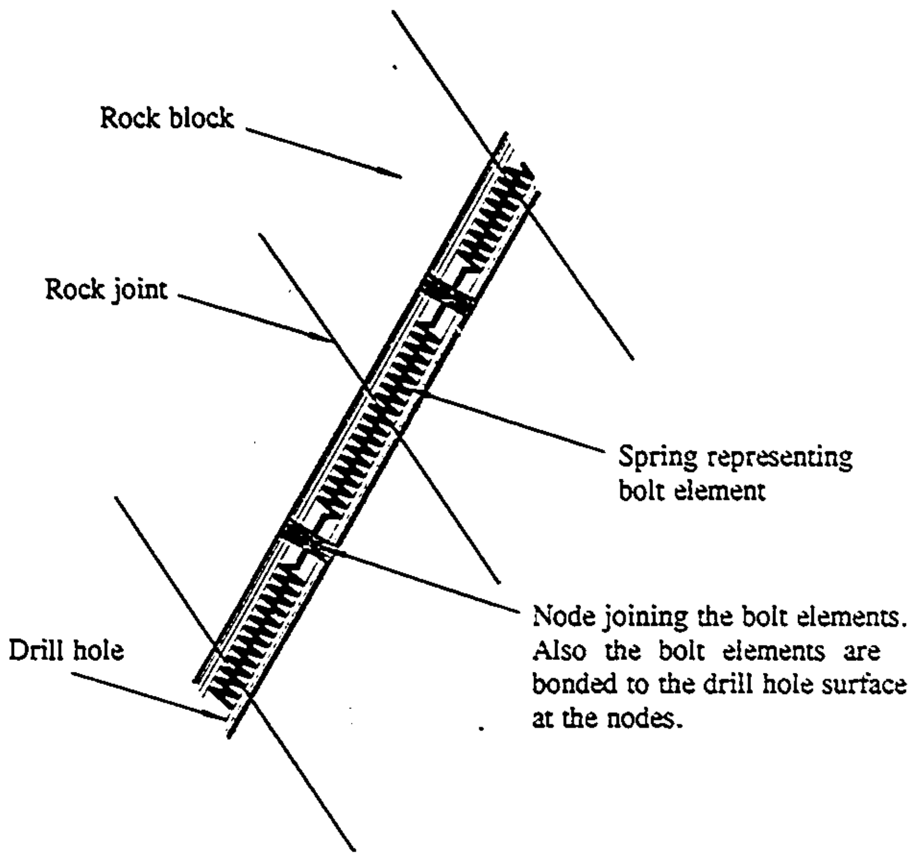

Fig.5.6 Rockbolt elements bonded to the rock at the nodes

The bolt element itself may also fail due to yielding of the bolt material. The elastic-plastic criterion shown in Fig.5.2 is used to describe the strength and deformation behaviour of the bolt element. Similar to the end anchored rockbolt, the fully grouted rockbolt element deforms elastically before yielding takes place. Yield flow may occur if the axial force in the bolt element exceeds the yield strength of the bolt material.

It can be noticed that an end-anchored rockbolt model discussed in Section 5.2 is a special case of the fully grouted rockbolt model. There is only one element with two bonding points for the end-anchored rockbolt.

An advantage of the proposed rockbolt model over the one shown in Fig.5.4 is that it does not increase the number of degrees of freedom. Hence, the band-width of the stiffness matrix of the Block-Spring Model is not affected by the rockbolts.

5.3.3 Determination of the bolt forces

The axial forces along the rockbolt can be determined based on the elongations of the bolt elements. The elongations of the bolt elements are the relative displacements of the nodes. As mentioned in Section 5.3.2, the relative displacements of the nodes may be determined by the relative displacements between the rock blocks. If the length of a bolt element λ is increased by ΔL_λ, then the force in the bolt element as a response to ΔL_λ can be calculated by the following equation:

$$T_\lambda = K_\lambda \cdot \Delta L_\lambda \tag{5.5}$$

where T_λ is the force in bolt element λ as a response to ΔL_λ (Fig.5.7);

K_λ is the stiffness of the bolt element λ.

The nodes of the bolt elements may be numbered starting from the outer end of the bolt. The bolt element next to the node λ is also numbered as λ as shown in Fig.5.7. However, numbering of the bolt elements and the nodes does not affect the stiffness matrix.

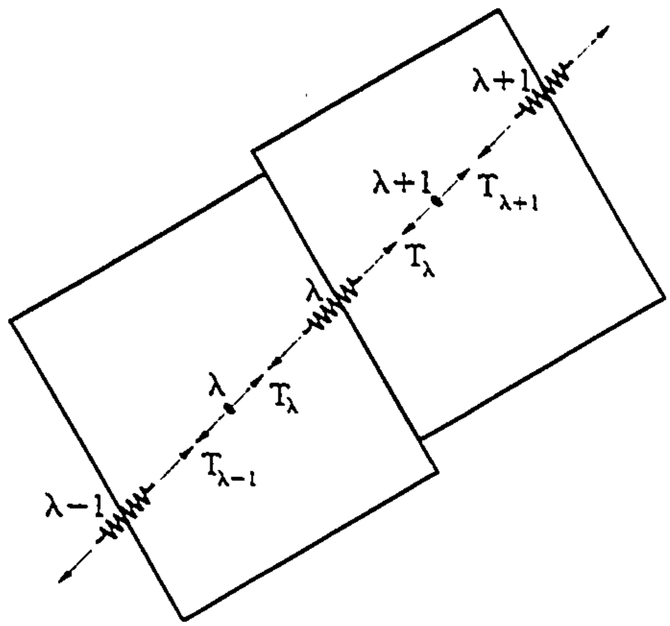

Fig.5.7 Bolt forces imposed on rock blocks

Similar to the end-anchored bolt model discussed in Section 5.2, if the axial force T_λ in the bolt element λ exceeds T_{yield}, the yield strength of the bolt material, then the bolt force is reset to $T'_\lambda = T_{yield}$.

The rockbolt elements impose forces on the rock blocks at the nodal points. These forces can be considered as the shear forces between the rockbolts and the rock blocks (or more precisely, the shear forces along the steel/grout or grout/rock interfaces). Therefore, each node is subjected to three forces, i.e., two forces from the adjacent bolt elements and one force from the rock block as shown in Fig.5.8. If the two bolt element forces are known, the shear force between the bolt and rock can be determined from the equilibrium condition of the node. In a general case, if a node λ is subjected to tensile forces $T_{\lambda-1}$ and T_λ from the two adjacent elements (Fig.5.8), the average shear force between the bolt and the rock at node λ may be determined by the following equation:

$$S_\lambda = T_\lambda - T_{\lambda-1} \tag{5.6}$$

where S_λ denotes the average shear force between the bolt elements and the rock block at node λ.

In order to determine the maximum shear stress which can develop and cause debonding failure, it should be noted that a fully grouted rockbolt may fail in any of the following four modes:

(i) breakage of the bolt due to insufficient tensile capacity of steel (very rare in practice);

(ii) failure due to insufficient bond strength at the steel/grout interface;

(iii) failure due to inadequate bond strength at the grout/rock interface;

(iv) failure in the rock close to the drill hole surface. This would occur only in the case of very weak rock, and can be prevented in practice by undertaking consolidation grouting.

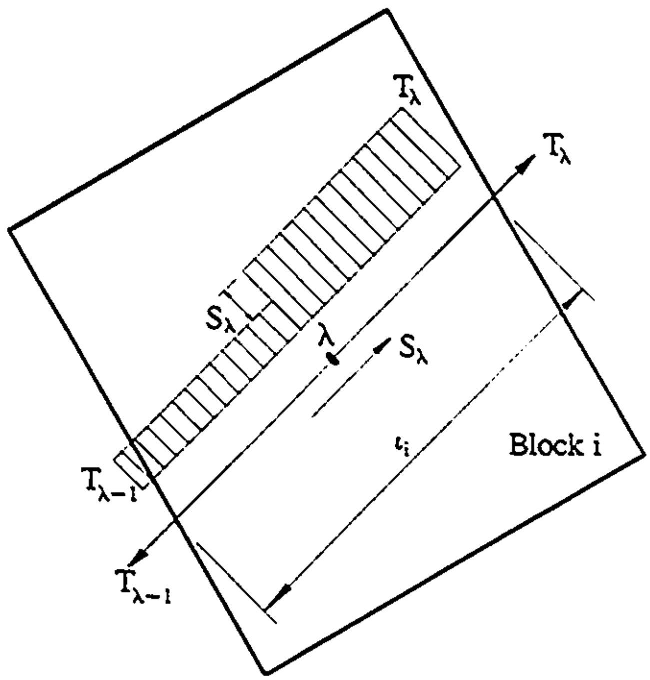

Fig.5.8 Determination of average shear force between rockbolt and rock block

Among these four failure modes, the second and third modes are more commonly encountered, and the shear strength at these two interfaces must be considered.

If the diameter of the steel bar is d_1 and the diameter of the drill hole is d_2 and the shear strengths per unit area at the steel/grout and grout/rock interfaces are $\tau_{1(max)}$ and $\tau_{2(max)}$ respectively, then the maximum shear force allowed on the system is given by:

$$S_{max} = \min\left(\pi\, d_1\, \ell_i\, \tau_{1(max)},\ \ \pi\, d_2\, \ell_i\, \tau_{2(max)} \right) \tag{5.7}$$

where ℓ_i is the length of the rockbolt portion passing through block i (Figs.5.5 and 5.8).

The minimum bond strength at the two interfaces has been referred to as the "bolt/rock" strength in subsequent text.

As the "point bonding" at node λ (Fig.5.5) represents the bonding along the whole length ℓ_i, the strength determined by Eq.(5.7) may be considered as the bonding strength at node λ.

5.3.4 Modification of forces in bolt elements due to bonding failure

If bonding failure occurs, the rockbolt may slide along the drill hole. In this case the bolt/rock shear force is adjusted to the value of the maximum bonding strength determined by Eq.(5.7). As the bolt/rock shear force, S_λ, and the bolt element forces, $T_{\lambda-1}$ and T_λ, make up an equilibrium force system at node λ (Fig.5.8), any change of S_λ may result in changes in $T_{\lambda-1}$ and T_λ. Therefore, if S_λ is modified due to bonding failure, $T_{\lambda-1}$ and T_λ should also be modified accordingly. If the bolt/rock shear force is reduced by ΔS_λ, the bolt element forces should be adjusted by $\Delta T_{\lambda-1}$ and ΔT_λ, respectively. The adjustments $\Delta T_{\lambda-1}$ and ΔT_λ can be determined from ΔS_λ based on the stiffnesses of the bolt elements by the following procedure.

Upon bolt/rock shear failure at node λ, the shear force S_λ should be reduced to $S'_\lambda=S_{max}$ (Eq.5.7), consequently, the following portion of the shear force remains unbalanced:

$$\Delta S_\lambda = S_\lambda - S'_\lambda \tag{5.8}$$

If this unbalanced shear force is transferred to the adjacent bolt elements $\lambda-1$ and λ, the bolt element forces are changed from $T_{\lambda-1}$ and T_λ to $T'_{\lambda-1}$ and T_λ, respectively, as follows:

$$\begin{aligned} T'_{\lambda-1} &= T_{\lambda-1} + \Delta T_{\lambda-1} \\ T'_\lambda &= T_\lambda + \Delta T_\lambda \end{aligned} \tag{5.9}$$

The adjustments $\Delta T_{\lambda-1}$ and ΔT_λ can be determined by considering a two spring system as shown in Fig.5.9. The effect of the unbalanced shear force ΔS_λ on the axial forces in the adjacent elements may be evaluated by applying a force ΔS_λ to node λ on the spring system in the direction opposite to S_λ. If the node displaces δ under the force ΔS_λ, the equivalent axial force $\Delta T_{\lambda-1}$ and ΔT_λ may be calculated by the following equations:

$$\begin{aligned} \Delta T_{\lambda-1} &= K_{\lambda-1} \cdot \delta \\ \Delta T_\lambda &= -K_\lambda \cdot \delta \end{aligned} \tag{5.10}$$

where $K_{\lambda-1}$ and K_λ are the stiffnesses of the two springs (the bolt elements) connecting at node λ.

From the equilibrium condition,

$$\Delta S_\lambda = \Delta T_{\lambda-1} - \Delta T_\lambda \tag{5.11}$$

From Eqs.(5.10) and (5.11), $\Delta T_{\lambda-1}$ and ΔT_λ can be determined from the unbalanced force ΔS_λ as follows:

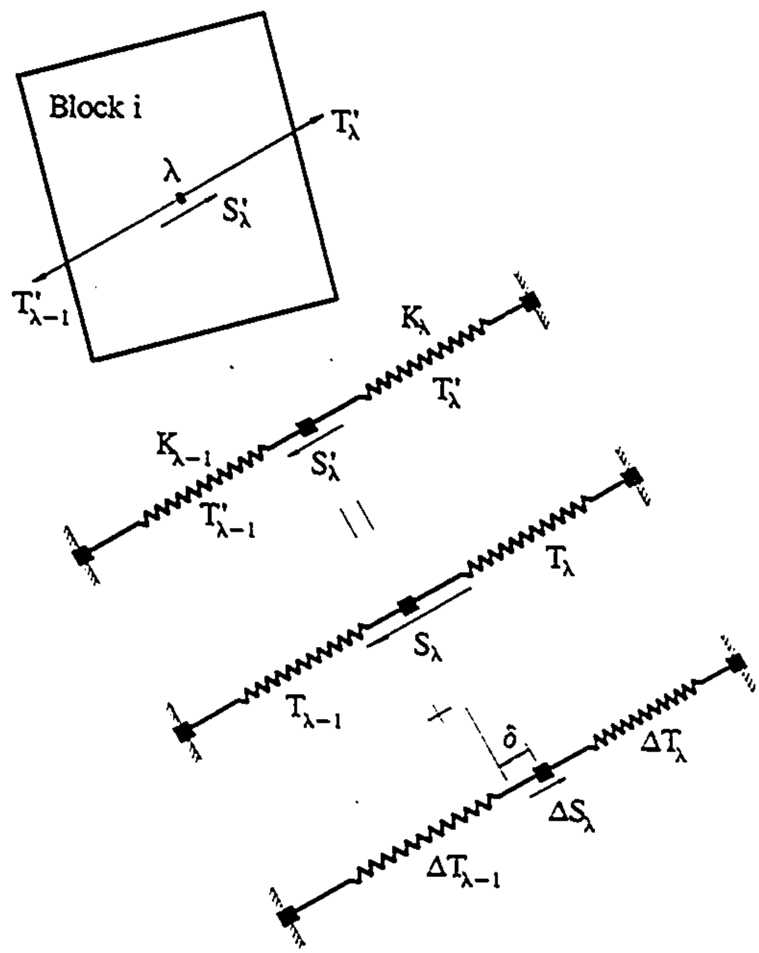

Fig.5.9 Updating the bolt/rock shear force by modifying the rockbolt forces

$$\Delta T_{\lambda-1} = \frac{K_{\lambda-1}}{K_{\lambda-1}+K_{\lambda}} \Delta S_{\lambda}$$

$$\Delta T_{\lambda} = -\frac{K_{\lambda}}{K_{\lambda-1}+K_{\lambda}} \Delta S_{\lambda} \tag{5.12}$$

Hence, by introducing Eq.(5.12) into Eq.(5.9), the bolt element forces can be updated as follows:

$$T'_{\lambda-1} = T_{\lambda-1} + \frac{K_{\lambda-1}}{K_{\lambda-1}+K_{\lambda}} \Delta S_{\lambda}$$

$$T'_{\lambda} = T_{\lambda} - \frac{K_{\lambda}}{K_{\lambda-1}+K_{\lambda}} \Delta S_{\lambda} \tag{5.13}$$

These adjusted bolt forces are now imposed on the two adjacent blocks.

5.4 Analysis of Rockbolts with the Block-Spring Model

5.4.1 Elongation of bolt elements and the block displacements

The effect of rockbolt on the deformation of the rock mass can be evaluated with the Block-Spring Model by introducing the bolt forces into the equilibrium equations. The bolt element forces may be determined by Eqs.(5.1) and (5.5). It should be noted that Eq.(5.1) is a special case of Eq.(5.5). As the elongation ΔL of the bolt element can be determined by the relative displacements of the blocks, the bolt forces may be expressed in terms of the displacements of the blocks.

In a general case, if a bolt element λ is bonded (or anchored) at blocks i and j as shown in Fig.5.10, the elongation of the element can be determined by the relative displacements between blocks i and j. From Eq.(3.5), the displacements of the nodes λ and $\lambda+1$ may be determined in terms of the displacements of the centroids of blocks i and j as follows:

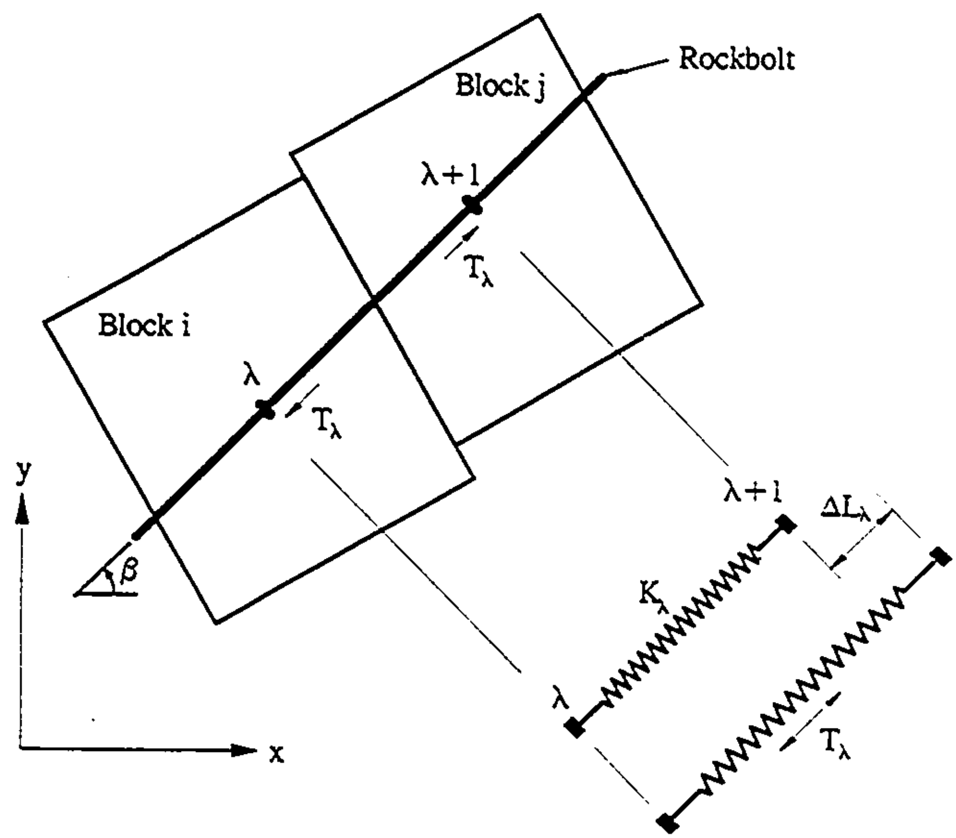

Fig.5.10 Determination of rockbolt elongation and axial force

$$\{u\}_\lambda = [B]_i \{U\}_i$$
$$\{u\}_{\lambda+1} = [B]_j \{U\}_j \qquad (5.14)$$

where $\{u\}_\lambda = \{u_\lambda, v_\lambda\}^T$ and $\{u\}_{\lambda+1} = \{u_{\lambda+1}, v_{\lambda+1}\}^T$ are the displacements of the nodes λ and $\lambda+1$, respectively;

$[B]_i$ and $[B]_j$ are defined in Eq.(3.6);

$\{U\}_i$ and $\{U\}_j$ are the displacements of the centroids of blocks i and j (Eq.3.7).

The elongation of the bolt element λ may be calculated by the following equation:

$$\Delta L_\lambda = \{c\}^T (\{u\}_{\lambda+1} - \{u\}_\lambda) \qquad (5.15)$$

where ΔL_λ is the elongation of the bolt element λ;

$\{c\} = \{\cos\beta, \sin\beta\}^T$;

β is an angle which the rockbolt makes from the x axis (Fig.5.10);

By introducing Eq.(5.14) to (5.15) and considering Eq.(3.10), the elongation of the bolt element λ can be written as follows:

$$\Delta L_\lambda = \{c\}^T [D]_{ij} \{U\}_{ij} \qquad (5.16)$$

where $[D]_{ij}$ is a $[2\times6]$ matrix defined in Eq.(3.10);

$\{U\}_{ij}$ is a column vector consisting of $\{U\}_i$ and $\{U\}_j$ as given by Eq.(3.9).

5.4.2 Determination of bolt forces in terms of block displacements

The bolt forces may be obtained from multiplying the elongations by the stiffnesses of the bolt elements as discussed in Sections 5.2 and 5.3. As the elongations of the bolt elements are determined by the relative displacements of the blocks, the bolt forces may therefore be determined by the displacements of the blocks.

By introducing Eq.(5.16) into Eq.(5.5), the following equation is obtained.

$$T_\lambda = K_\lambda \{c\}^T [D]_{ij} \{U\}_{ij} \tag{5.17}$$

where T_λ is the axial force in bolt element λ;

K_λ is the stiffness of the bolt element.

The axial bolt force T_λ can be expressed by its x and y components as follows:

$$\{f_b\}_x = \{c\} T_\lambda \tag{5.18}$$

or

$$\{f_b\}_x = K_\lambda \{c\} \{c\}^T [D]_{ij} \{U\}_{ij} \tag{5.19}$$

where $\{f_b\}_x = \begin{Bmatrix} F_{bx} \\ F_{by} \end{Bmatrix}$;

F_{bx} and F_{by} are the x and y components of the bolt force on block i (node λ).

The bolt force $\{f_b\}_x$ on block i can be transformed to the centroid of the block and a set of equivalent forces can be obtained as follows:

$$\{F_b\}_{ij} = [K_b]_{ij} \{U\}_{ij} \tag{5.20}$$

where $\{F_b\}_{ij} = \begin{Bmatrix} F_{bx} \\ F_{by} \\ M_{bc} \end{Bmatrix}$;

M_{bc} is the moment of $\{f_b\}_x$ on the centroid of block i;

$$[K_b]_{ij} = [\ K_{bi} \mid K_{bj}\ ] = K_\lambda\ [B]_i^T\ \{c\}\ \{c\}^T\ [D]_{ij} \tag{5.21}$$

$[B]_i$ is a $[2\times3]$ matrix defined in Eq.(3.6), which consists of the local coordinates of the node λ;

$[K_b]_{ij}$ is a $[3\times6]$ stiffness matrix;

K_{bi} and K_{bj} are $[3\times3]$ sub-matrices of $[K_b]_{ij}$.

5.4.3 Bolt forces in the equilibrium equations

The bolt forces affect the equilibrium condition of the rock blocks and therefore must be included in the analysis of the whole block system. The bolt force vector $\{F_b\}_{ij}$ in Eq.(5.20) can be introduced into the equilibrium equation (Eq.3.39) to evaluate the rockbolt effect. The stiffness matrix $[K_b]_{ij}$ in Eq.(5.20) or (5.21) can be added into the global stiffness matrix [K] in Eq.(3.40). If all the rockbolts are considered, a set of global stiffness equations $[K]\{U\}=\{P\}$ similar to Eq.(3.40) can be assembled. The displacements $\{U\}$ of all the blocks can be obtained by solving the global stiffness equations.

The contact forces between blocks and the boundary constraining forces can be calculated by the procedure described in Chapter 3. The rockbolt forces can be determined using Eq.(5.17) or Eq.(5.19). After the bolt forces are obtained, the failure criteria discussed in Sections 5.2 and 5.3 are applied. If any bolt element or any bonding (or anchoring) point fails, the corresponding bolt forces are updated. Eq.(5.18) may be used to transform the updated axial bolt forces to x and y components, which are required in the iteration procedure as explained in the following section.

5.5 Iteration Procedure, Tensioned and Untensioned Rockbolts

If the rockbolt forces are modified due to tensile failure of the bolt elements or shear failure of the bolt/rock bonding (or anchorages), or due to compression in the bolt, the equilibrium of the force system is disturbed. After modifying all the contact forces and the rockbolt forces, another cycle of computation should be performed for a new equilibrium state of the forces. The iteration procedure already described in Chapter 4 may be applied.

In addition to re-applying the contact forces in each step of iteration, the rockbolt forces are re-imposed on the blocks. For example, if $\{f_b\}_{i-1}$ is a bolt force vector obtained from iteration step $(i-1)$, it can be imposed on the corresponding blocks in step i as an external load. After the global stiffness equations are solved in the ith step, an increment of the bolt force $\{\Delta f_b\}_i$ can be evaluated. The bolt force vector can be updated by adding the increment to the previous results as follows:

$$\{f_b\}_i = \{f_b\}_{i-1} + \{\Delta f_b\}_i \tag{5.22}$$

Again, $\{f_b\}_i$ can be used as an initial force for the next step of iteration after proper modifications are made upon failure.

The bolt forces discussed above are the accumulations of the incremental forces. The initial state of the bolt forces prior to the deformation of the rock masses should therefore be known. The rockbolts may be tensioned or untensioned at the time of installation. The pre-tensioning or untensioning of the rockbolts may be considered as the initial stress condition.

For the untensioned rockbolts, no bolt forces are imposed on the blocks in the first step of iteration, since the bolt forces develop only after the relative displacements take place between blocks. Hence, the initial bolt force for the untensioned rockbolt is zero.

The tensile forces installed in the pre-tensioned rockbolts are considered as the initial forces of the bolts, $\{f_b\}_0$. Any increment of the bolt forces, $\{\Delta f_b\}_1$, as a response to the block movement may be added to $\{f_b\}_0$, to obtain a new set of bolt forces, i.e., $\{f_b\}_1=\{f_b\}_0+\{\Delta f_b\}_1$. Hence, the pre-stress condition can automatically be modelled with the iteration procedure by specifying the initial load installed in the rockbolt.

The tensile stress in the pre-tensioned rockbolt is same throughout its length at the time of installation. If a bolt is pre-tensioned with a force $\{f_b\}_0$, the force may be imposed on all the nodes in the first step of iteration. Actually, at this stage, $\{f_b\}_0$ is applied on the blocks only at the two ends of the rockbolt. At the nodes other than the two ends of the rockbolt, $\{f_b\}_0$ is not active since the forces from the bolt elements on both side are balanced. Any increase in the rockbolt forces results from the relative displacements between blocks, and can be determined after each step of iteration. The forces can be updated by adding the increments to the initially installed forces.

The iteration procedure modified for simulating the rockbolts is summarized in a flowchart shown in Fig.5.11. It is an expansion of the flowchart previously shown in Fig.4.9.

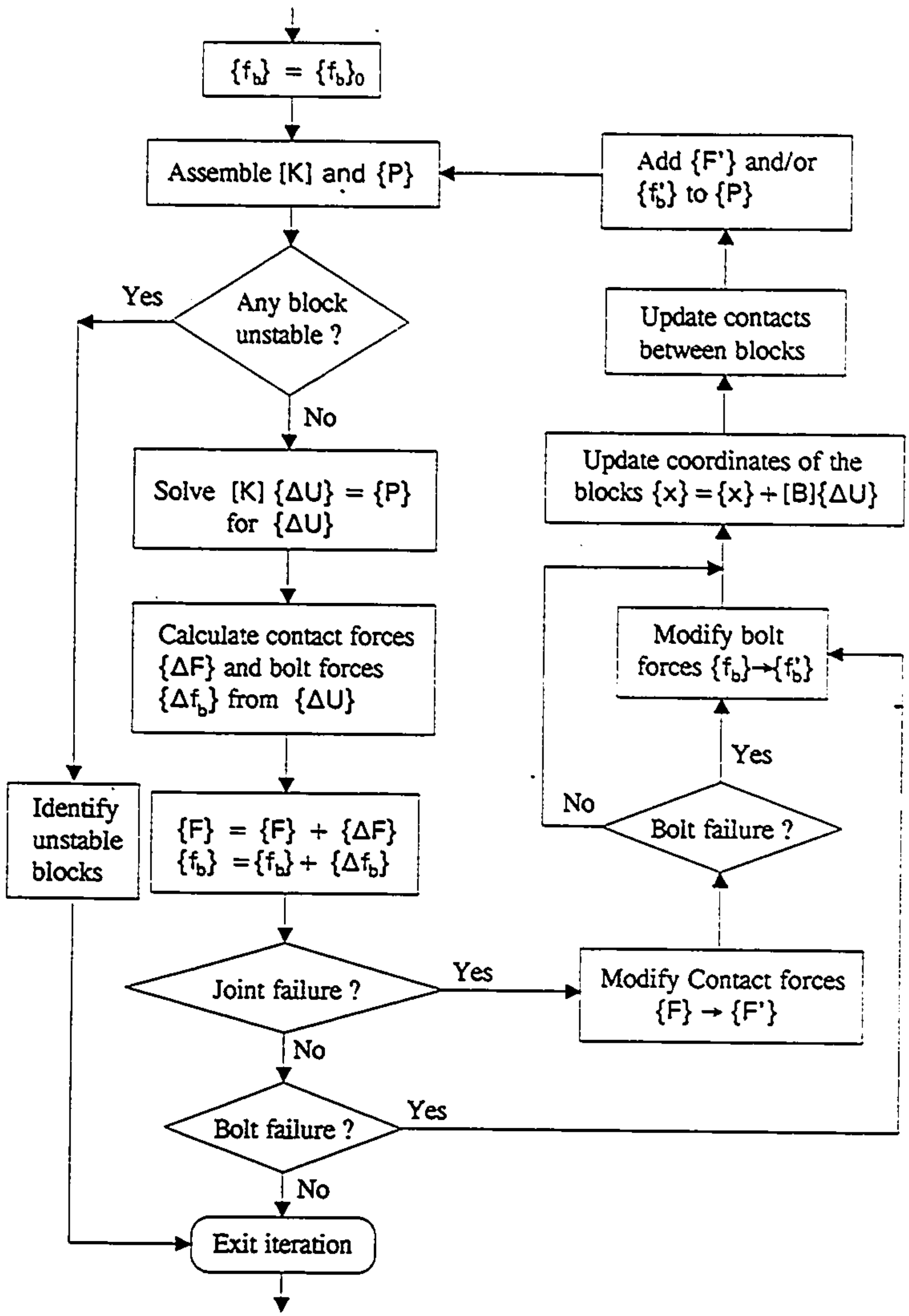

Fig.5.11 A flowchart of the iteration procedure for consideration of rockbolts

5.6 Example 4: Application to a Simple Rock Excavation

The following is an example of modelling the rockbolt effect on stability of the rock blocks with the proposed Block-Spring Model. For demonstration purposes, a hypothetical excavation is analyzed. More detailed rockbolt analysis and comparisons of results are provided in an application to a practical problem in Chapter 8.

Fig.5.12 shows an excavation in jointed rock. It is assumed that the rock is divided into blocks by the joints which are filled with thin layers of a soft material. The bottom boundary of the mesh is fixed. The lateral boundaries are constrained in horizontal direction by rollers. The top surface is subjected to a uniformly distributed surcharge of 1 MPa. There are 24 blocks in the mesh. The assumed properties of the rock material and the joint filling material are listed in Table 5.1.

Table 5.1 Characteristics of the rock and joint filling materials

	Intact rock	Joint filling
Elastic modulus: E (MPa)	40,000	0.1
Poisson's ratio: μ	0.25	0.30
Unit weight: γ (kN/m^3)	26	-
Cohesion: C (MPa)	-	0.01
Friction angle: ϕ (°)	-	35

The computer program was run only one cycle before it was terminated. The output indicates that a block on the roof of the excavation is unstable as shown in Fig.5.13.

Subsequently, a fully grouted untensioned rockbolt was applied to support the block on the roof as shown in Fig.5.14. A high capacity rockbolt was used in order that further simulation could be carried out. The roof of the excavation was now stabilized

(Fig.5.14), however, another block on the left sidewall was detected to be unstable. This block had been totally separated from adjacent two blocks and had displaced a large distance before it was determined unstable.

Another rockbolt was next used to support the block on the left sidewall as shown in Fig.5.15. No block was detected unstable after the two blocks were stabilized by the rockbolts. Fig.5.15 shows the stable state of the block system after the two unstable blocks were supported.

It may be noted from Fig.5.15 that a block at the lower left corner of the opening displaced towards the opening, nevertheless, it was still in a stable condition. To prevent this large displacement, a rockbolt was used to support this block and Fig.5.16 shows the corresponding solution.

It should further be noted that in practical engineering, rockbolts are seldom used for securing the hanging blocks directly as the one shown in Fig.5.13. They are usually used for supporting the rock mass indirectly by increasing the self-support capability of the blocks. However, the extreme cases assumed in this example demonstrate the capability of the Block-Spring Model in simulating the stabilizing effect of the rockbolts. Also simulation of large displacements of the blocks and prediction of unstable blocks are demonstrated in this example.

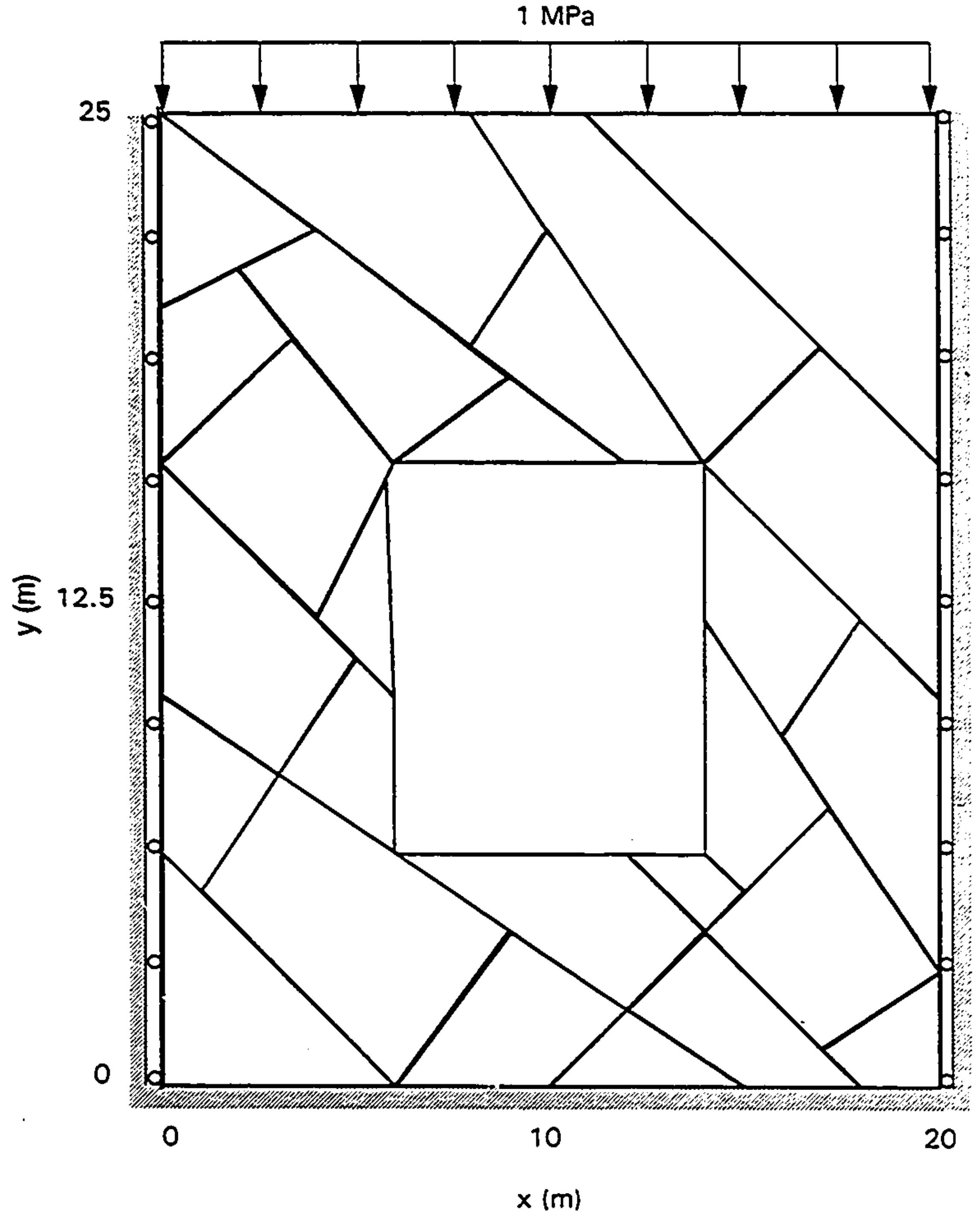

Fig.5.12 Example 4: An underground excavation in jointed rocks

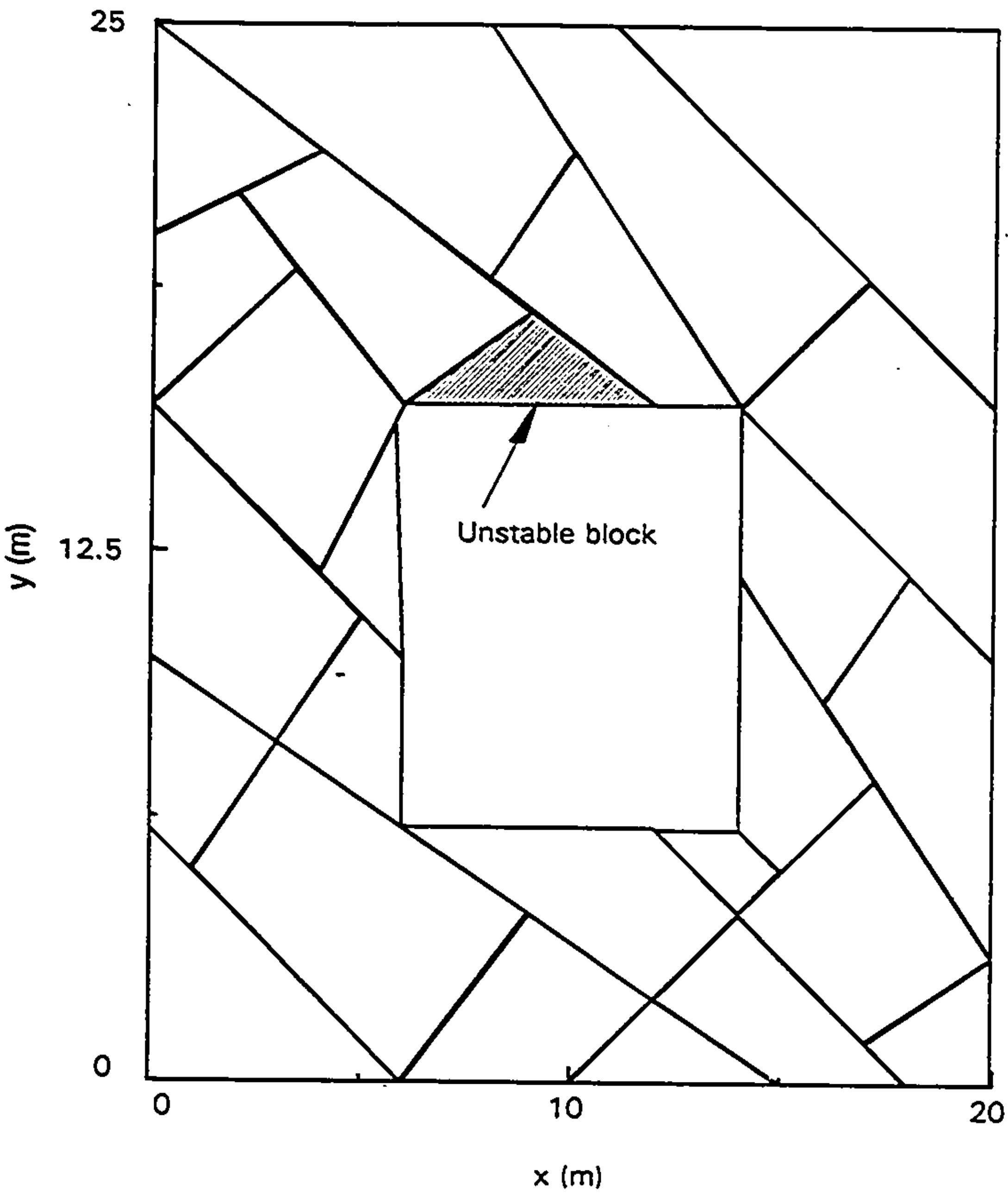

Fig.5.13 Example 4: Unstable block first detected

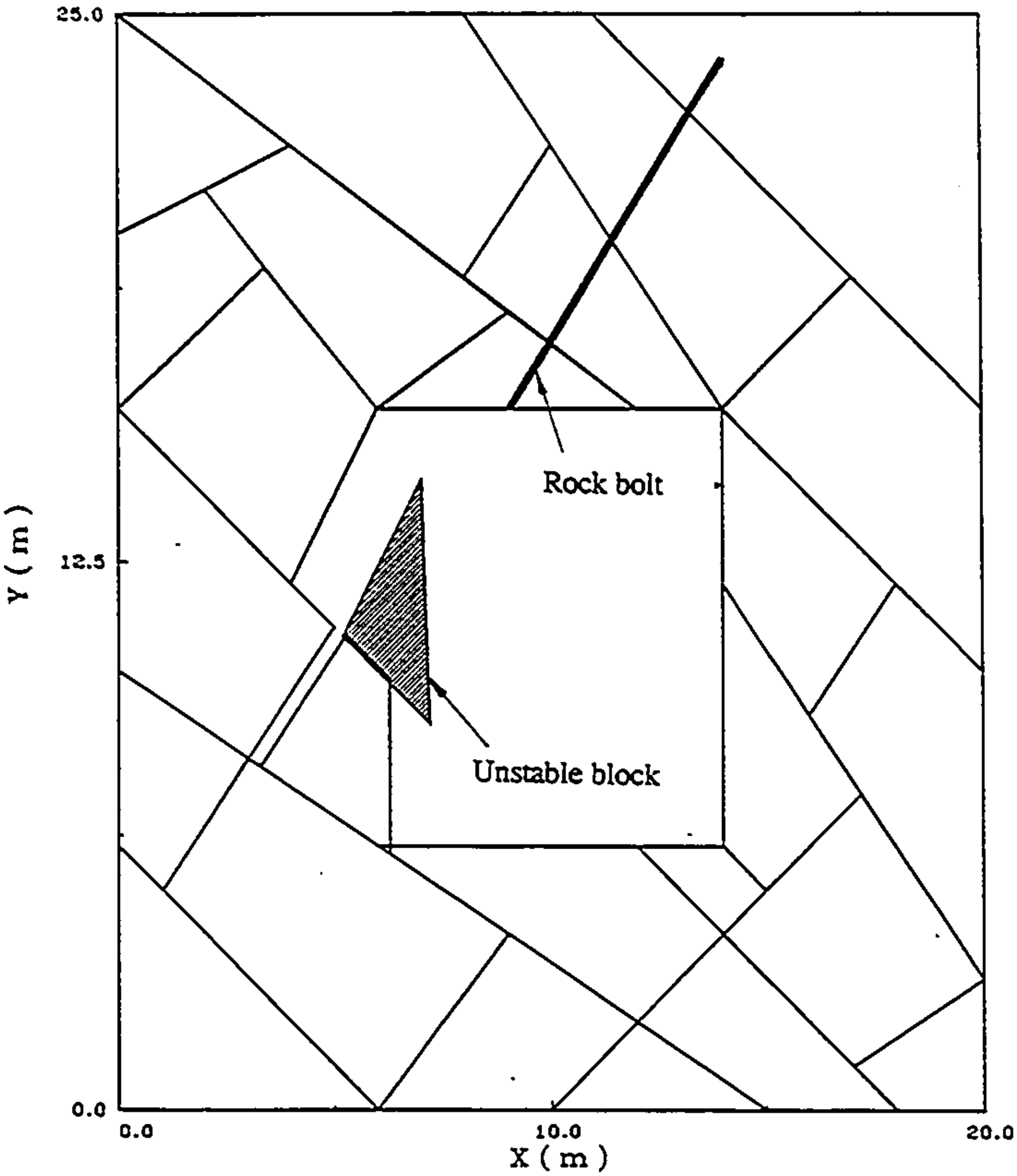

Fig.5.14 Example 4: Another block is detected unstable after the roof is stabilized

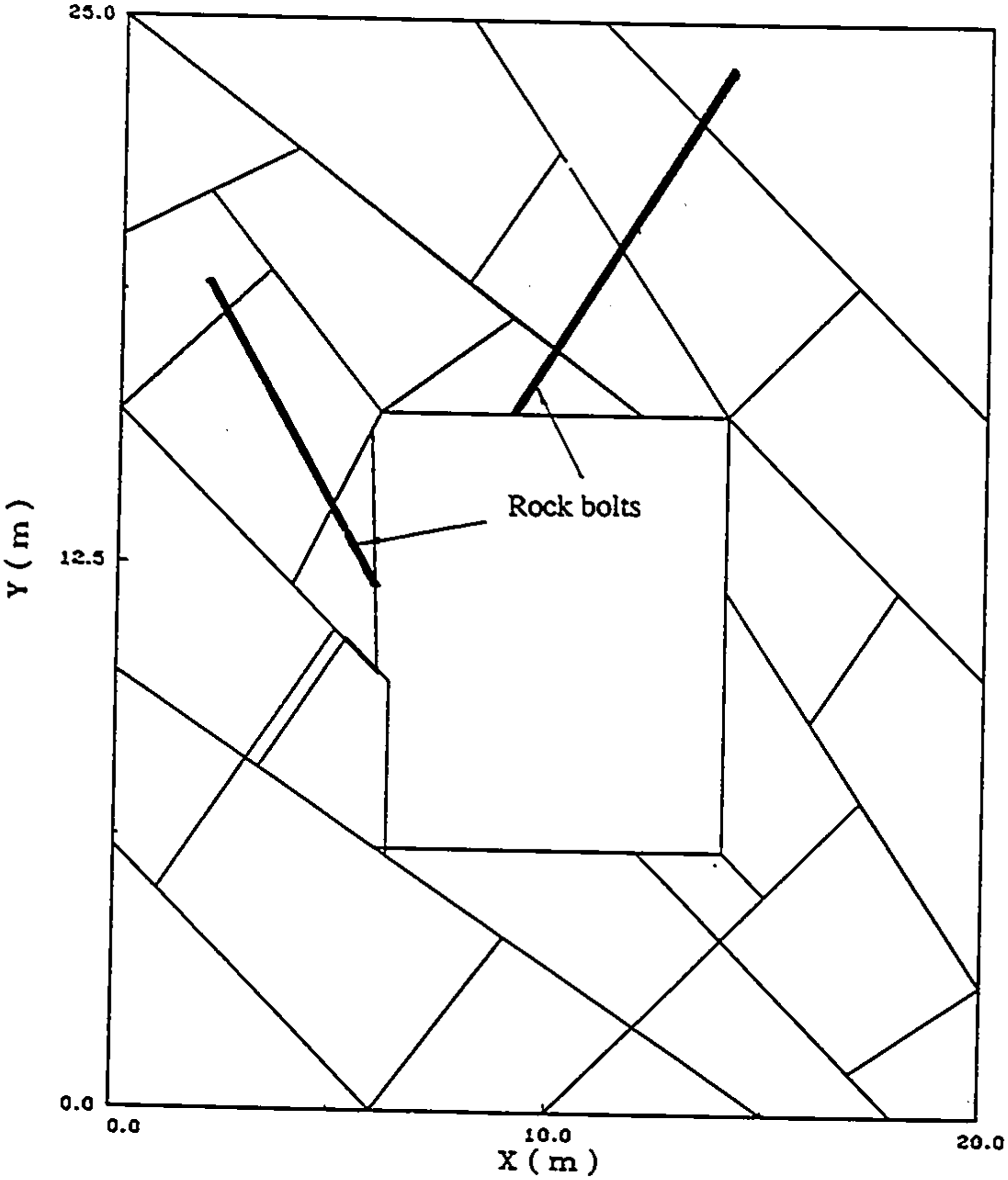

Fig.5.15 Example 4: All the blocks are stabilized

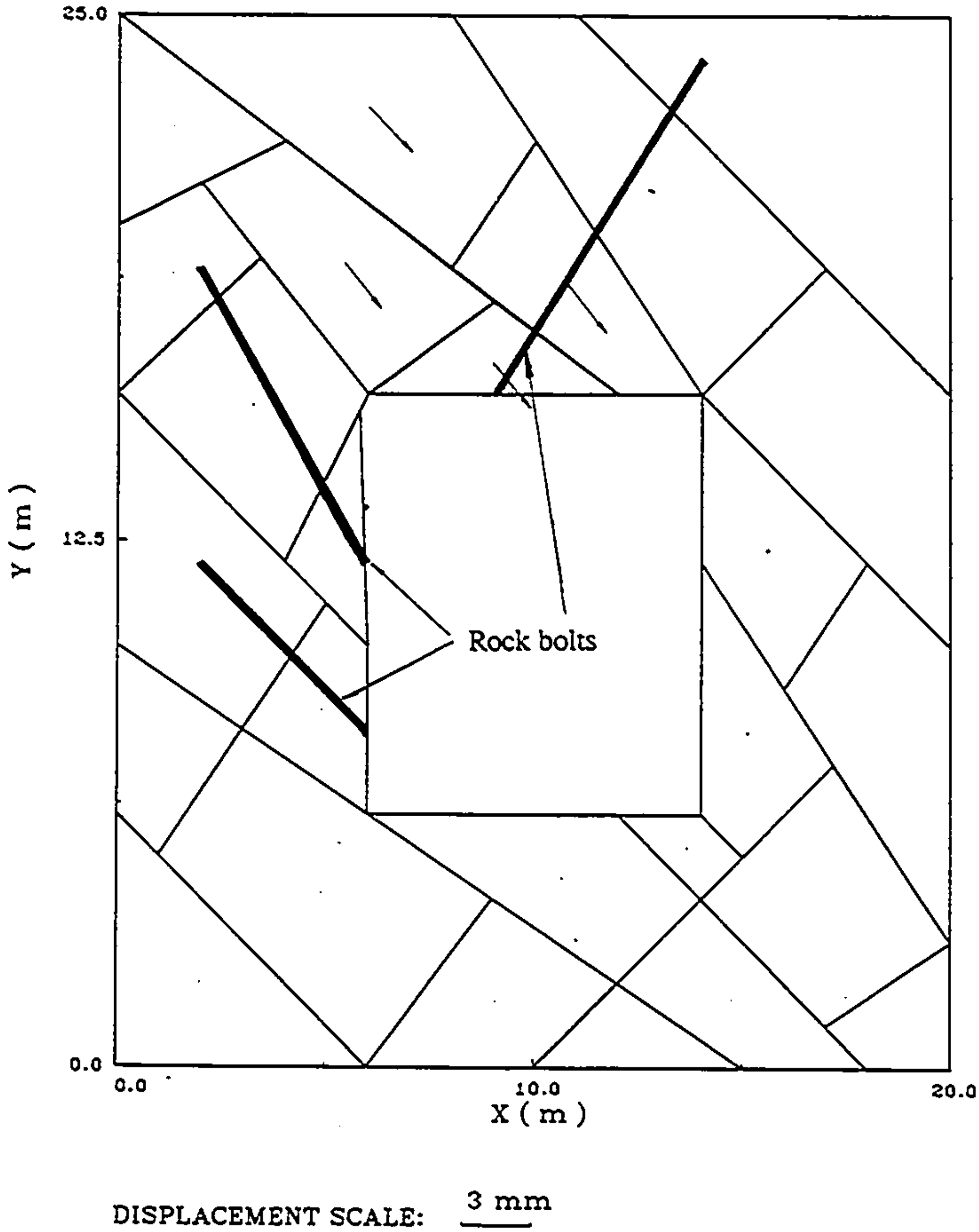

Fig.5.16 Example 4: Displacements of the blocks after three blocks are supported

CHAPTER 6

SIMULATION OF GROUNDWATER PRESSURES

6.1 Introduction

Groundwater affects stability of the jointed rocks in various ways; the most obvious is through the operation of the effective stress law (Brady and Brown, 1985). Water under pressure in the joints imposes a normal pressure on the rock surfaces which reduces the normal effective stress between the rock surfaces. The shear strengths of the joints, which are related to the effective normal forces, may therefore be reduced. The strengths of the joints may also be reduced as a result of softening of the infilled material. Groundwater may also have other effects on the rocks such as freezing and swelling, dissolving of minerals and weathering, etc. The modelling of the groundwater effect on the normal effective stress on the joints has been incorporated in the proposed Block-Spring Model.

6.2 Simplifications

A groundwater model is proposed to simulate the hydro-static pressure imposed on the rock joints. It is assumed that a single steady water table exists which is a locus of points where water pressure equals the atmospheric pressure (Fig.6.1). The rocks above the water table are free from water pressure. It is further assumed that the hydraulic head of any point below the water table is the depth (vertical distance) of the point from the water table. Hence the water pressure increases linearly with depth. The pressure is assumed to be linearly distributed along the joint as shown in Fig.6.2.

The seepage forces are determined by the boundary pressure method which can be demonstrated by an example shown in Fig.6.3. The difference of the water pressures, Δq_h, between the two vertical faces of a rock element may result in a downward force which may increase the instability of the rock slope.

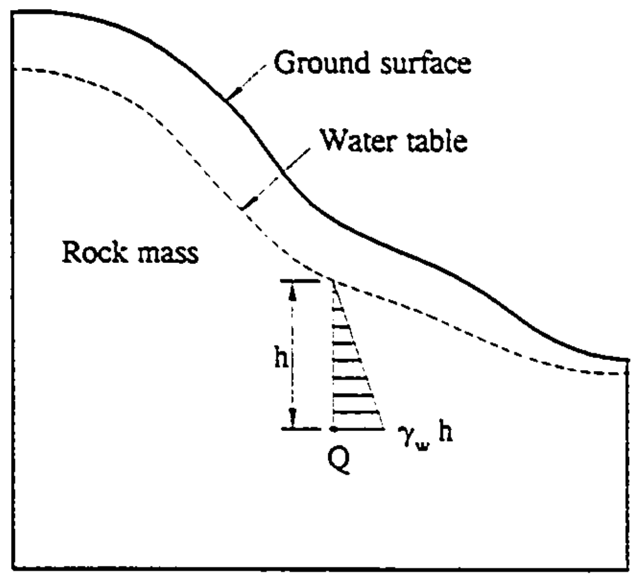

Fig.6.1 Simplification of groundwater problem in rock mass

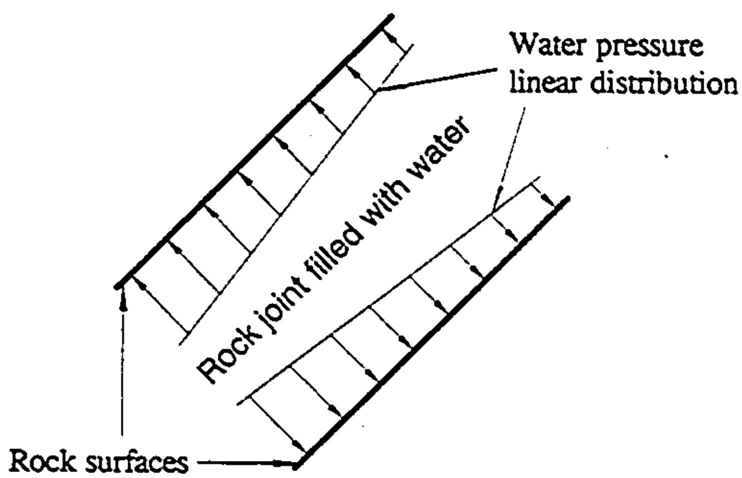

Fig.6.2 Water pressure in rock joint

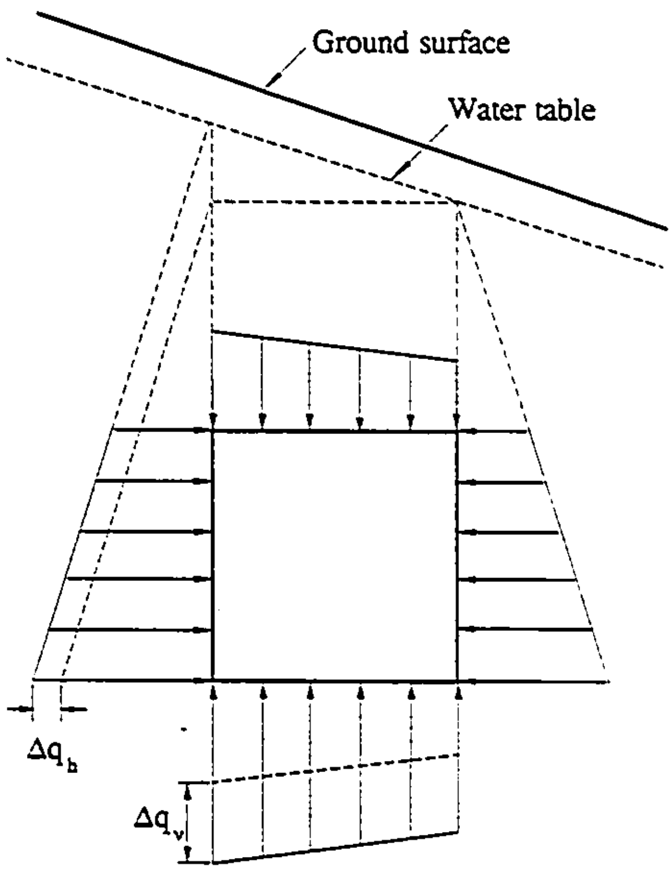

Fig.6.3 A rock element under different water pressures on different faces

6.3 Evaluation of the Groundwater Effect

In modelling the groundwater effect with the Block-Spring Model, the water table may be represented by straight line segments as shown in Fig.6.4. The water table can be specified by the coordinates of a few turning points. Water pressure on each face (or edge) of the block can be determined by the depths of the corners of the block from the water table. A face of a block may be above the water table, or partially or fully submerged (Fig.6.4).

For a fully submerged face (face 1-2 in Fig.6.5) of the block, the distribution of water pressure on the face can be determined by the depths of the two corners. If the depths of the two corners are h_1 and h_2 from the water table, the water pressures on the two points can be calculated as follows:

$$q_1 = \gamma_w \cdot h_1$$
$$q_2 = \gamma_w \cdot h_2 \tag{6.1}$$

where q_1 and q_2 are the water pressure intensities on corners 1 and 2, respectively;

γ_w is the unit weight of water.

The linearly distributed water pressure on the face can be transformed into two concentrated forces P_{w1} and P_{w2} acting on the two ends of the face 1-2. The equivalent forces can be calculated by the following expressions:

$$P_{w1} = \frac{1}{6} l \,(2q_1 + q_2)$$
$$P_{w2} = \frac{1}{6} l \,(2q_2 + q_1) \tag{6.2}$$

where l is the length of the face.

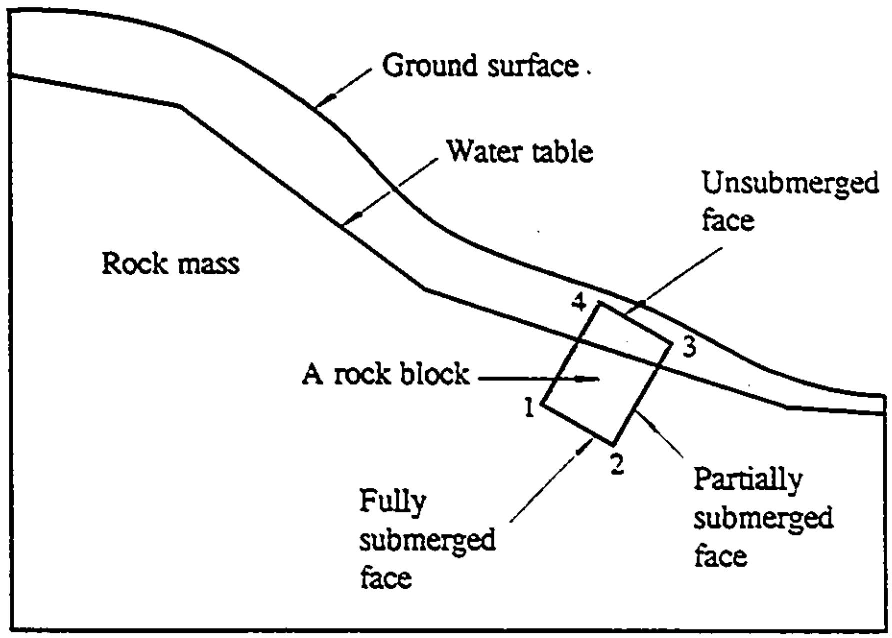

Fig.6.4 Straight line segments representing the groundwater table and a partially submerged block

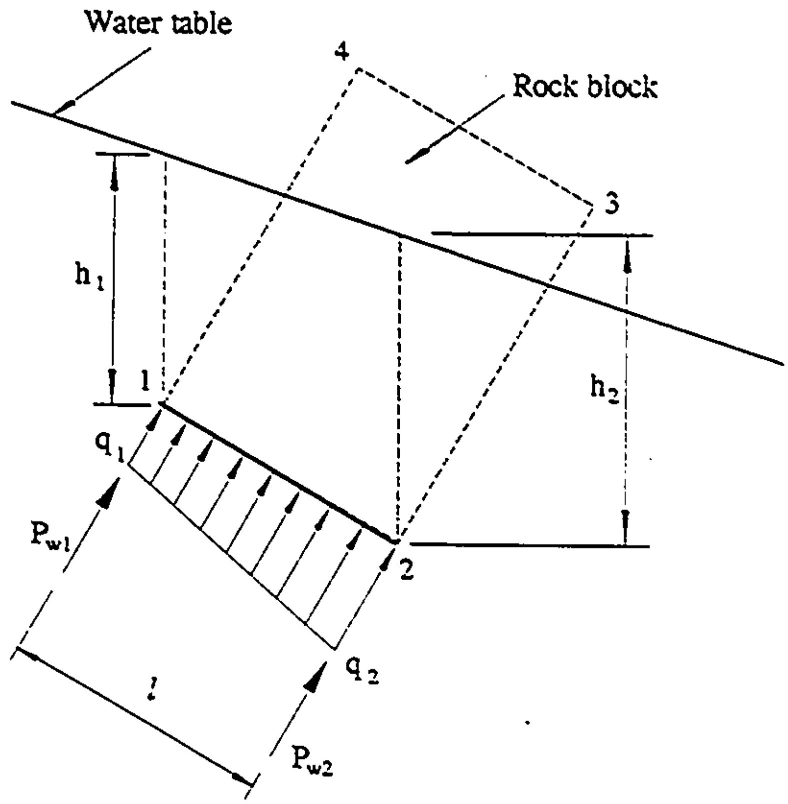

Fig.6.5 Water pressure on a fully submerged face of a blcck

For a face which is partially submerged (face 2-3 in Fig.6.6), the distributed water pressure may also be represented by two concentrated forces at the two corners. If corner 2 is under the water table and corner 3 is above the water table as shown in Fig.6.6, the resultant water pressure, R_w, may be determined by

$$R_w = \frac{1}{2} l' \, q_2 \tag{6.3}$$

where l' is the submerged length of the face;

q_2 is the water pressure intensity on corner 2 determined by Eq.(6.1).

The resultant water pressure R_w can be transformed to the equivalent forces at the two corners of the face. The following expressions of the equivalent forces on the two corners can be easily derived:

$$\begin{aligned} P_{w2} &= \left(1 - \frac{1}{3}\frac{l'}{l} \right) R_w \\ P_{w3} &= \frac{1}{3}\frac{l'}{l} R_w \end{aligned} \tag{6.4}$$

The submerged length l' of the face can be determined by

$$l' = \frac{|q_2|}{|q_2| + |q_3|} \, l \tag{6.5}$$

where q_3 is a hypothetical water pressure intensity on corner 3 (Fig.6.6).

It should be noted that the actual water pressure on corner 3 is zero since it is unsubmerged. In determining whether corner 3 is above or under water table, the hydraulic head at the corner is calculated. If the hydraulic head is negative, it implies that the actual water pressure on this corner is zero. However, this negative head may be used to determine the submerged length of the face as shown in Eq.(6.5), if the other end of that face is under the water table.

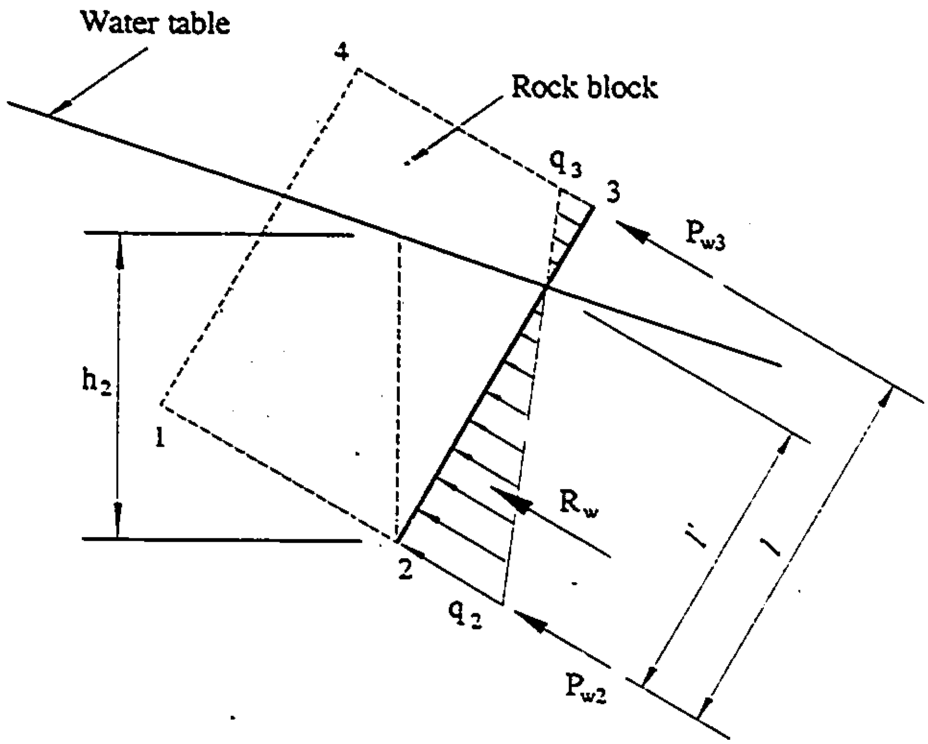

Fig.6.6 Determination of water pressure on a partially submerged face of a block

The equivalent water pressure P_w on each corner of the face may be expressed by the horizontal and vertical components as follows (Fig.6.7):

$$\{P_w\}_x = -\{c\}^T P_w \tag{6.6}$$

where $\{P_w\}_x = \begin{Bmatrix} P_{wx} \\ P_{wy} \end{Bmatrix}$;

P_{wx} and P_{wy} are the horizontal and vertical components of P_w on the corner;

$\{c\}^T = \{\cos\alpha, \sin\alpha\}$;

α is an angle of the outward normal of the rock surface from the horizontal axis of the coordinate system (Fig.6.7).

$\{P_w\}_x$ can be transformed to the centroid of the block and a set of equivalent forces may be determined as follows:

$$\{P_w\}_c = [B]^T \{P_w\}_x \tag{6.7}$$

where $\{P_w\}_c = \begin{Bmatrix} P_{wx} \\ P_{wy} \\ M_c \end{Bmatrix}$;

M_c is the moment of $\{P_w\}_x$ on the centroid of the block;

[B] is defined in Eq.3.6.

Eq.(6.7) can be added, in a proper manner, to the column vector {P} in the set of global stiffness equations [K]{U}={P} (Eq.3.40) to evaluate the effect of the groundwater pressures on the displacements of the blocks. After the displacements of the blocks are determined, the contact forces can be evaluated using the procedure discussed in Chapter 3. The contact forces obtained are the effective forces between the blocks.

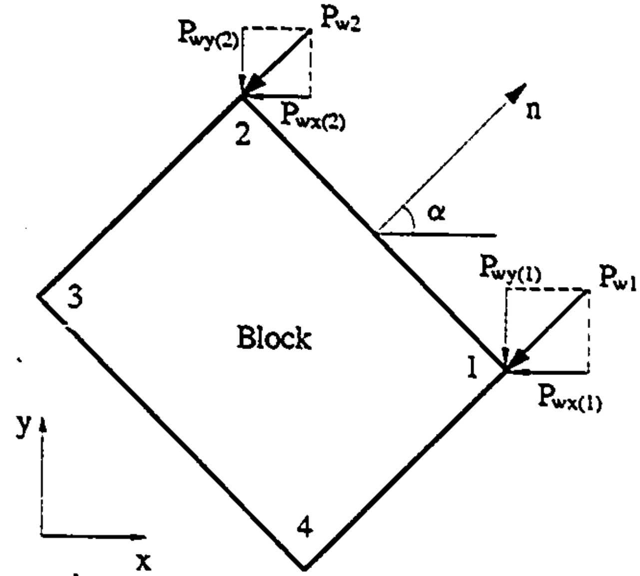

Fig.6.7 Horizontal and vertical components of the equivalent forces

6.4 Example 5: Modelling the Effect of Groundwater Pressure

A hypothetical dam foundation was analyzed with the Block-Spring Model. This example illustrates the capability of the Block-Spring Model in simulating the effect of water pressure on the displacements of the rock blocks. Application to a real groundwater problem is presented in Chapter 8.

Fig.6.8 shows a rock foundation of a concrete dam. The rock mass is divided into blocks as defined by the system of joints shown in this figure. The concrete dam has been considered as a rigid block. The water pressure profile is plotted as dashed lines in Fig.6.8. All the rock blocks are under the water table. The block system is subjected only to gravity forces and the water pressure. The bottom boundary of the rock mass is fixed and the lateral boundaries are constrained in horizontal directions by rollers.

Fig.6.9 shows a plot of the displacement vectors of the dam and the rock blocks obtained from the Block-Spring Model. Fig.6.10 is a plot of the exaggerated movement of the dam and the blocks (original position is shown by dotted lines). It can be seen in Fig.6.9 and Fig.6.10 that the dam is pushed downstream by the water pressure. The dam tends to be separated from the upstream rock block. The block at the downstream doe of the dam is pushed up, which may cause instability of the dam.

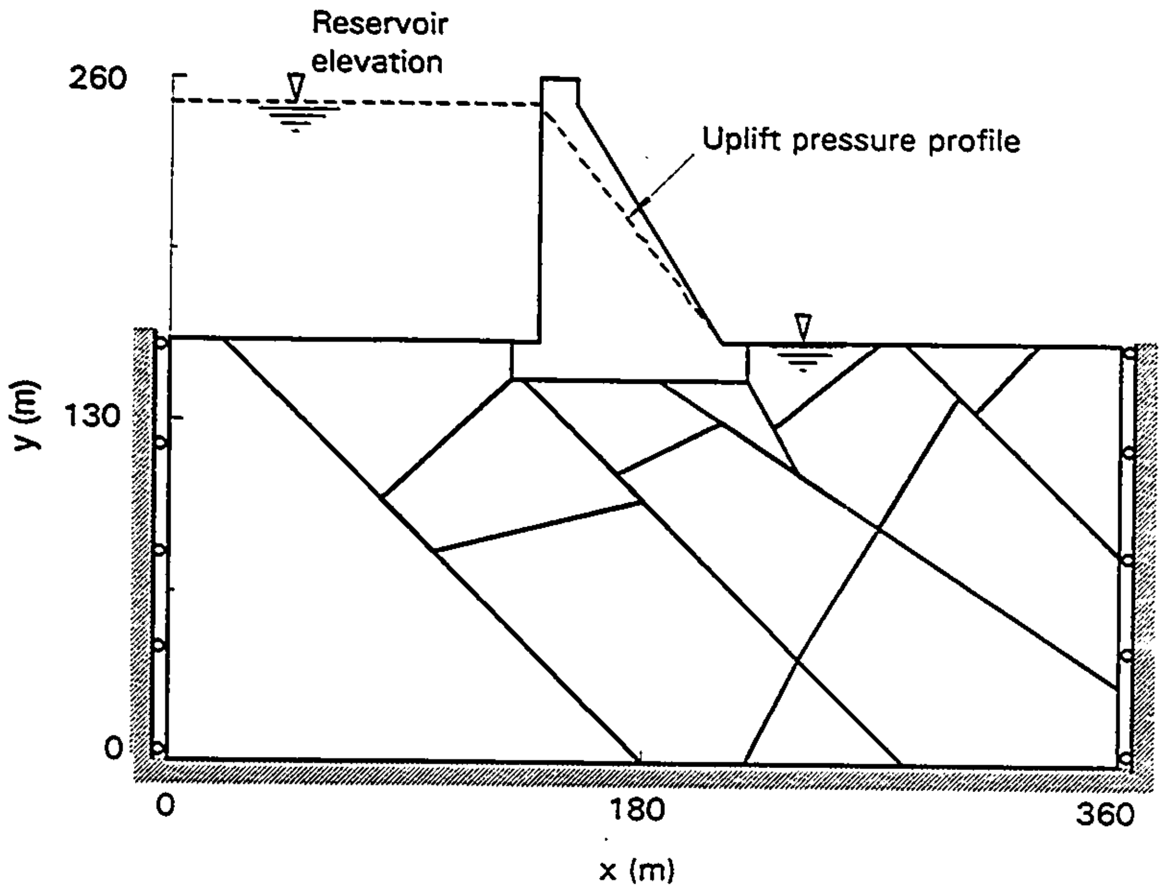

Fig.6.8 Example 5: A hypothetical rock foundation of a concrete dam

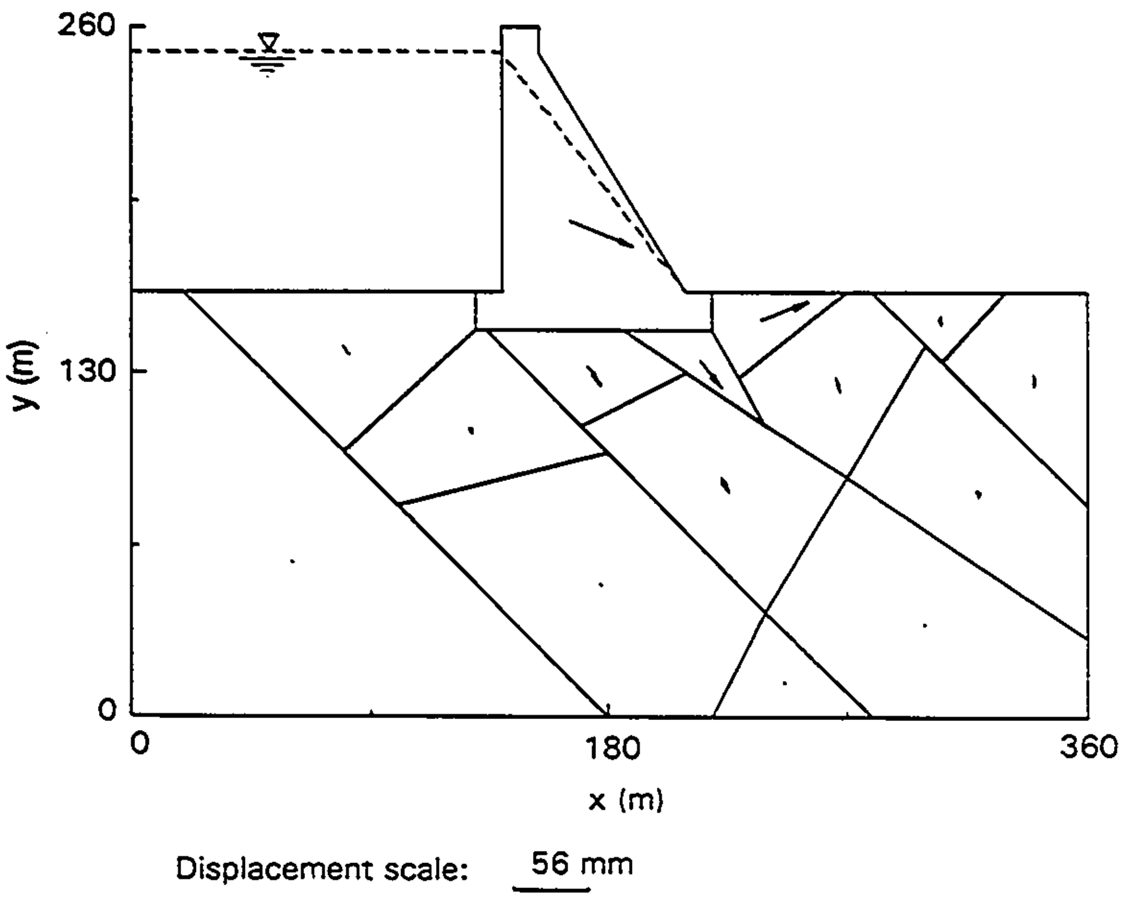

Fig.6.9 Example 5: Displacement vectors of the dam and the rock blocks

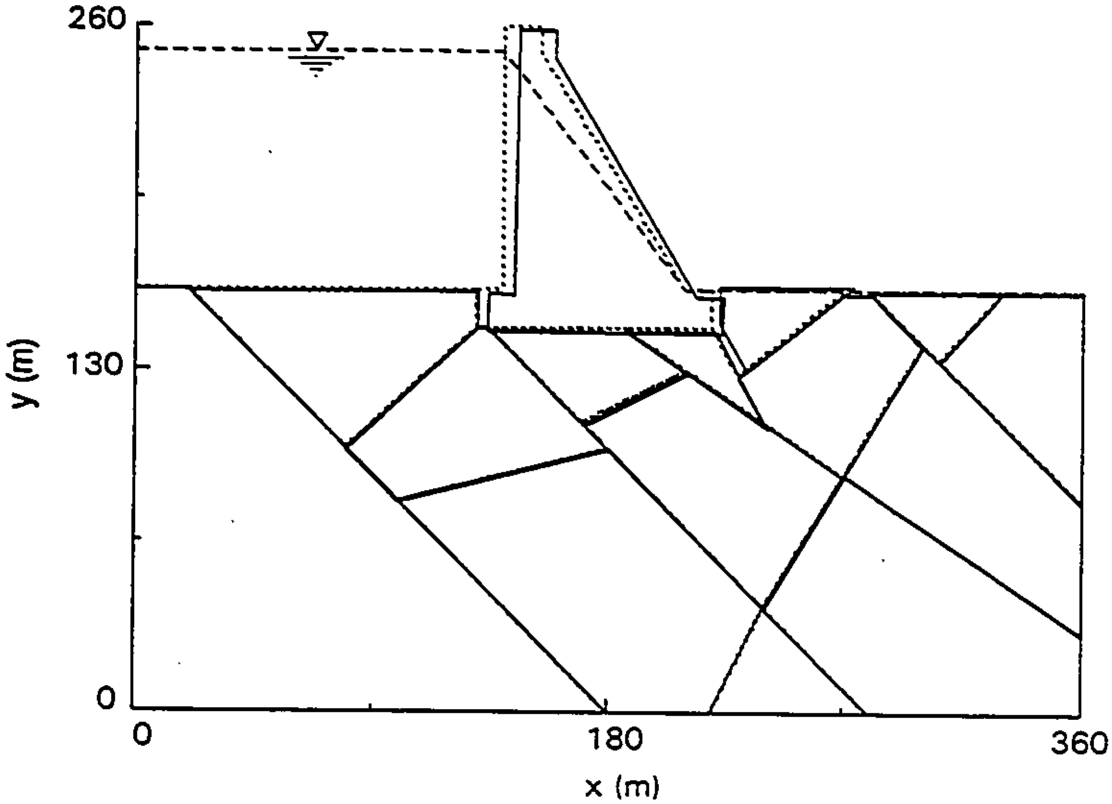

Fig.6.10 Example 5: Exaggerated movements of the dam and the rock blocks

CHAPTER 7

COMPUTER PROGRAM FOR THE BLOCK-SPRING MODEL

A computer program called BLOSMER (BLOck Spring Model for Excavation in Rocks) has been written in FORTRAN based on the principle of the Block-Spring Model. All features of the model described in the present thesis have been incorporated in the program. The data required for running the program include the following:

(i) Coordinates and material types of the blocks (auto-generation included; all the contact data are automatically generated);

(ii) Boundary conditions (auto-generation included);

(iii) Characteristics of the rock materials including the deformation and strength parameters such as the elastic modulus, the Poisson's ratio, the unit weight, the cohesion, and the angle of frictional resistance;

(iv) Characteristics of the rock joints including the thickness of the joints, the stiffness factors, the cohesion, the basic frictional angle, the residual frictional angle, the elastic modulus and the Poisson's ratio of the filling material;

(v) Coordinates and characteristics of the rock bolts (if applicable) including the coordinates of the two ends of the rock bolts, the type of the bolt (end-anchored or fully-grouted), the average stiffness of the bolt in a unit length, the yield strength of the steel and the shear strengths at the steel/grout interface and the grout/rock interface (or the anchorage capacity for the end-anchored rock bolt);

(vi) Coordinates of groundwater profile (if applicable);

(vii) Block numbers to be excavated (if applicable).

The following types of results can be produced by the program BLOSMER:

(i) Displacements of the blocks (with graphics output);

(ii) Average stresses in the blocks (with graphics output);

(iii) Contact forces between blocks;

(iv) Boundary constraining forces;

(v) Numbers of unstable blocks;

(vi) Rockbolt forces (if rockbolts are used);

(vii) Results after each step of excavation (if sequential excavation is analyzed).

A flowchart describing the major steps of the program BLOSMER is shown in Fig.7.1.

The program consists of approximately 4000 statements in 24 subroutines. The functions of the major subroutines are described in Table.7.1.

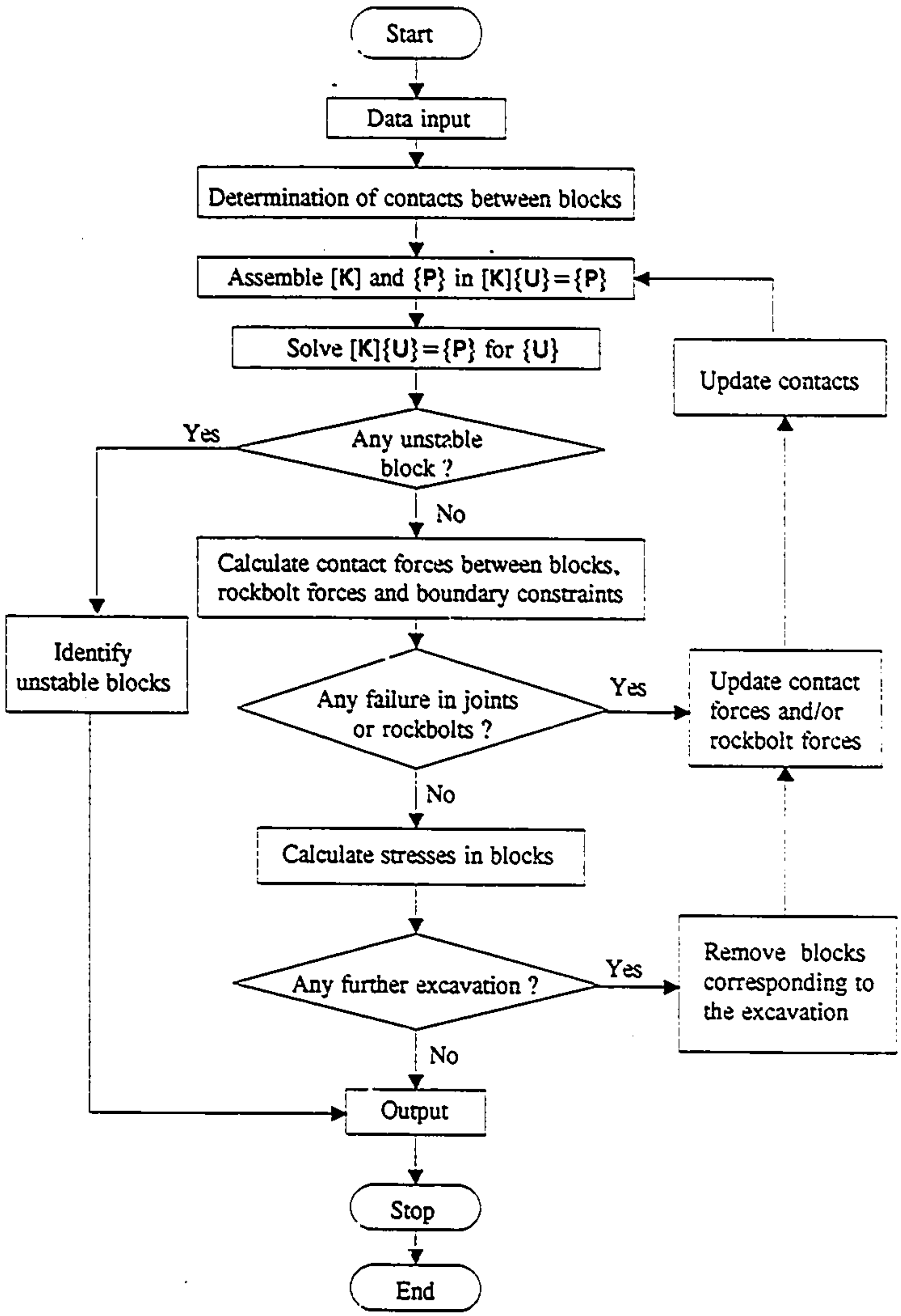

Fig.7.1 A flowchart of the program BLOSMER

Table 7.1 Descriptions of major subroutines in the program BLOSMER

Name of subroutine	Descriptions
INPUT	This subroutine is called to input all the data required to run the program BLOSMER.
BLOCK	Produces frequently used data of the blocks, such as the volumes and the weights of the blocks, the coordinates of the centroids of the blocks and the direction sines and cosines of the edges of the blocks.
CONTCT	Determines the contacts between the blocks and evaluates the contact stiffnesses.
BOLT	Produces rockbolt data. The coordinates of the two ends of each rockbolt, the properties and the initial stress conditions of the rockbolts are input by subroutine INPUT. BOLT determines which blocks the rockbolts pass through as well as the coordinates of the nodal points of the bolt elements for the fully grouted rockbolts. The stiffnesses of all the rockbolt elements are also determined by BOLT.
WATER	Evaluates water pressures on the block surfaces.
BAND	Determines the half-band-width of the stiffness matrix for assembling the matrix.
MATRIX	Assembles the global stiffness matrix and applies the boundary conditions, rockbolt forces and water pressures if applicable.

Table 7.1 (continued)

SOLVE	Solves the global stiffness equations for the displacements of all the blocks, using Gauss elimination method.
FORCE	Evaluates the contact forces between blocks and the rockbolt forces.
CRITRN	Applies the failure criteria to the contact forces and the rockbolt forces.
REACTN	Calculates the boundary constraining forces where the boundary displacements are applied.
UPDATE	Updates the coordinates of the blocks and the contacts between blocks.
EXCAV	Removes the blocks to be excavated next step. Renumbers the remaining blocks and zeroes the contact forces along the newly excavated surfaces.
STRESS	Calculates the average stresses within the blocks.
(Output)	Numerical output is produced in the above subroutines immediately after the results are generated. The major results include the displacements of the blocks, contact forces between blocks, boundary constraining forces, rockbolt forces, average stresses within blocks, and the numbers of the unstable blocks if applicable.

CHAPTER 8
APPLICATION OF BLOSMER TO CASE HISTORIES

8.1 Introduction

The features of the proposed Block-Spring Model have been demonstrated in a simplified form in the various examples in previous chapters. It is useful to compare the results of BSM analysis with observations from case histories. Regrettably, complete case histories with results of instrumentation and complete characterization of rock joint system are scarce. A few such case histories, selected from literature, have been used to compare the BSM results with the field observations and also with the numerical results from other methods.

8.2 Application to the Dupont Circle Station Case History

8.2.1 Background

An underground opening in Dupont Circle Station in Washington D.C. is one of the case histories analyzed with the Block-Spring Model. The field measurements of the rock movements in the Dupont Circle Station and the analytical results of the Finite Element Method with Goodman's slip line elements were reported by Rodriguez Perez (1980) in a study carried out at University of Illinois at Urbana-Champaign. This application also demonstrates the capability of the Block-Spring Model in analyzing the behaviour of the jointed rocks with and without rockbolt support. The feature of analyzing the excavation induced stresses is also shown in this application.

According to Rodriguez Perez (1980), the crown of the complete Dupont Circle Station excavation is located approximately 65 ft (20 m) below the ground surface with an average rock cover of 30 ft (9 m) and 35 ft (11 m) of soil (Fig.8.1). The station is 724 ft (220 m) long, 76 ft (23 m) wide and 44 ft (13 m) high.

The opening was driven in foliated metamorphic rock whose primary feature consisted of joints, shears and shear zones. The rock encountered was essentially unweathered to

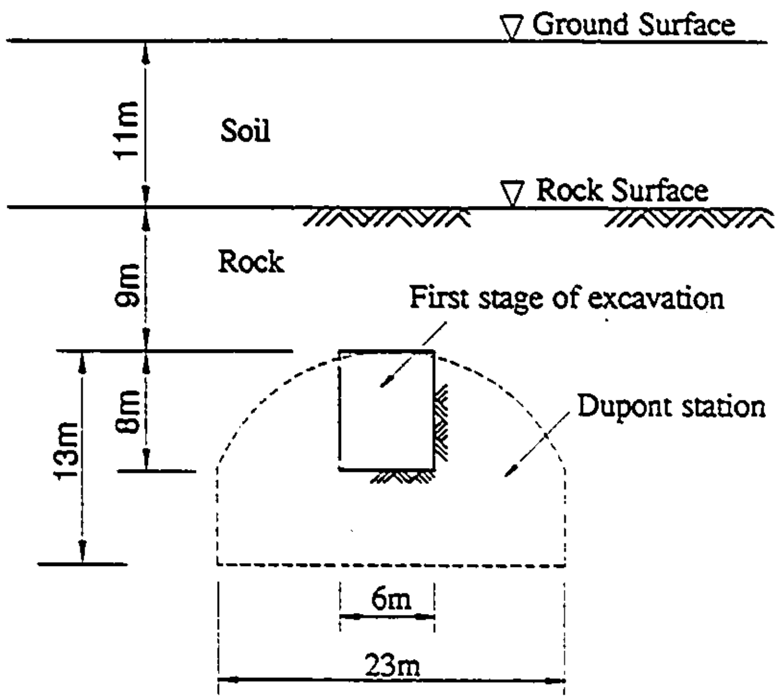

Fig.8.1 A cross-section of Dupont Circle Station
(After Rodriguez Perez, 1980)

slightly weathered schist and gneiss. The joints were highly continuous, smooth and planar, usually tight but occasionally open and weathered near the surface. In many cases, they could be traced for distances in excess of 100 ft (30m). Sometimes a thin filling of clay of approximately 1/16 to 1/8 in. (1/6 to 1/3 cm) thick was found in the joints. Slickensided joints (shears) containing gouge filling of clay and chlorite were also found. They were commonly spaced 4 to 10 ft (1 to 3 m) apart, except in the shear zones where they were more closely spaced. The major shear zones were generally 1 to 10 ft (1/3 to 3 m) wide and spaced 10 to 50 ft (3 to 15 m) apart. They consisted of zones of fractured rock containing several parallel shears and one or more gouge zones with thickness ranging from 1/4 to 12 in. (1/2 to 30 cm). The major shear zones were continuous and could be traced over distances of 250 ft (75m) along the station axis. The joint sets and shear zones present in the ground combined to form a blocky condition of the rock mass.

A typical geological cross-section is shown in Fig.8.2. It can be seen that the essential features of this geologic environment are the rock joints and the shear zones.

Rodriguez Perez (1980) also mentioned that "most of the fallouts and rock movements that occurred in the opening were related to wedges bounded by slickensided joints often coated with a thin layer of gouge." "The discontinuities striking within 25° of the tunnel axis (parallel or subparallel to the tunnel axis) and intersected by another set of joints led to the formation of long wedges in the sidewalls and crown of the opening that usually produced the most difficult tunnelling conditions."

The opening was excavated in five stages. Detailed analyses of each phase of the excavation were performed by Rodriguez Perez (1980) using the Finite Element Method. The first stage of the excavation in the crown area (Fig.8.1), which was the most difficult part, has been analyzed with the Block-Spring Model.

The first stage of excavation was approximately 20 ft (6m) wide and 26 ft (8m) high. The excavation was supported in the crown by 24-ft-long (7.3m) rock bolts installed at 5 ft (1.5m) longitudinal spacing. The sidewalls were supported by 12-ft-long (3.6m) rock bolts installed at 5-ft longitudinal spacing. The average support pressure developed on the sidewalls was estimated at between 7 and 12 psi (48 - 83 kPa).

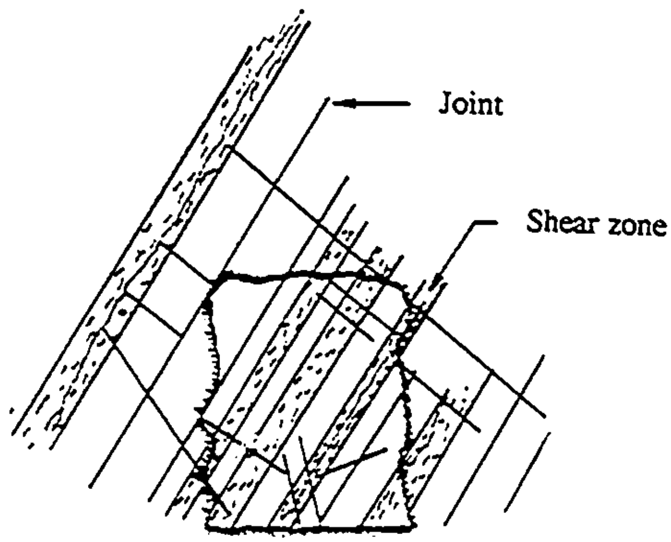

Fig.8.2 Dupont Station: A typical geologic cross-section
(after Rodriguez Perez, 1980)

The first stage of excavation was simulated by Rodriguez Perez (1980) using the finite element mesh shown in Fig.8.3, in which the rock joints were modelled by Goodman slip elements. The shear zones and the "intact" rock were modelled by quadrilateral elements. The initial state of the ground stress was modelled using the mesh shown in Fig.8.3(a). The bottom boundary of the mesh was fixed. The top boundary was the surface of the rocks which was free and subjected to a surcharge pressure from the soil on the top. The lateral extent of the mesh was approximately four times the opening width. The lateral boundaries were allowed only vertical displacements.

Fig.8.3(b) shows the finite element mesh used for simulating the first stage of excavation. An internal pressure P_i was imposed on the excavation walls to simulate the average pressures that rock bolts imposed on the walls.

8.2.2 Analyses of the Dupont Station with BLOSMER

The results reported herein include the analyses of the first stage excavation using the BLOSMER based on data provided in Rodriguez Perez (1980). For modelling the rockbolt pressures imposed on the opening walls, an average internal pressure $P_i = 10$ psi (69 kPa) was used similar to that in the Finite Element analysis. Also, since BLOSMER is capable of modelling the rockbolts, a supplemental analysis was performed with the rockbolts installed in the walls, rather than using a uniform internal pressure.

In order to compare the results from BLOSMER with those from the Finite Element analysis, the assumptions used in the Finite Element model were adopted herein. The Finite Element meshes and the boundary conditions shown in Fig.8.3 were used in the BLOSMER analyses. The finite elements in the mesh were considered as rigid blocks. The joints were automatically modelled as the interfaces between the blocks. The properties of the rock materials including the shear zones and the joints obtained from Rodriguez Perez (1980) are listed in Table 8.1.

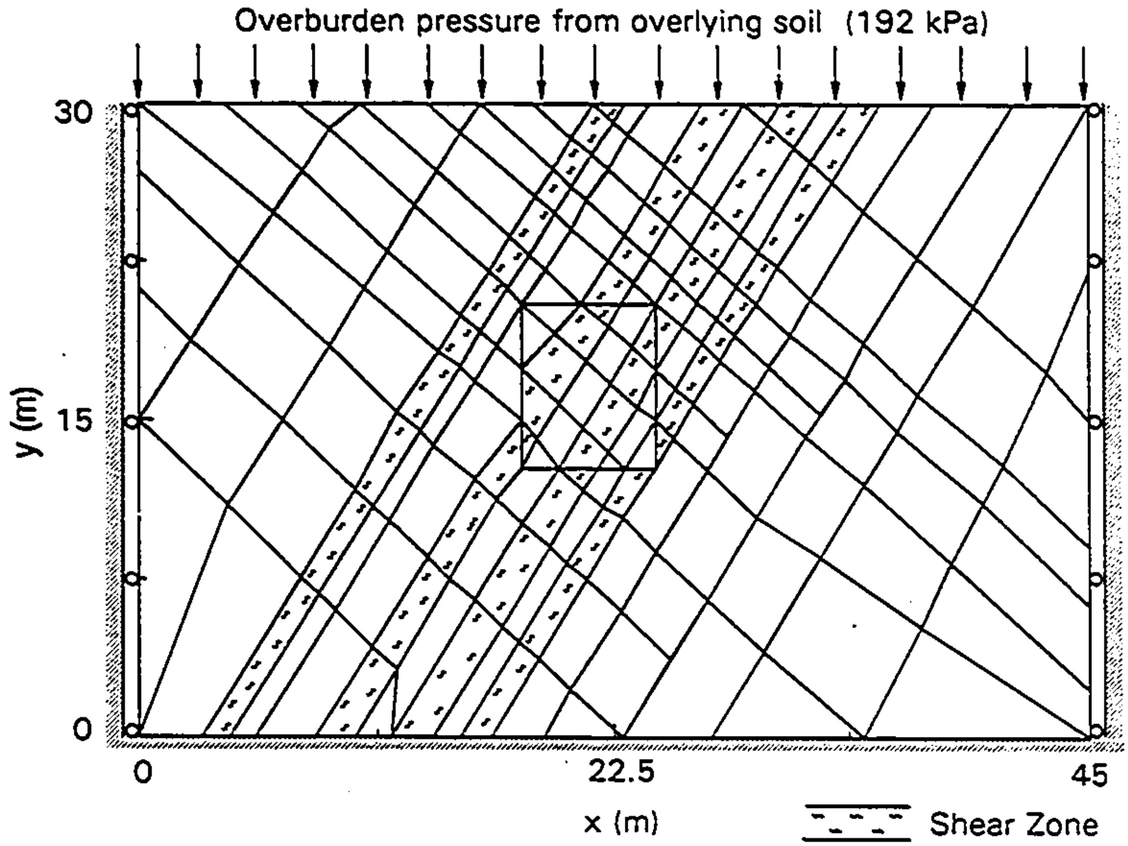

(a) Before excavation

Fig.8.3 Dupont Station: A Finite Element Mesh
and boundary conditions used by Rodriguez Perez (1980)
(Also used for BLOSMER analysis)

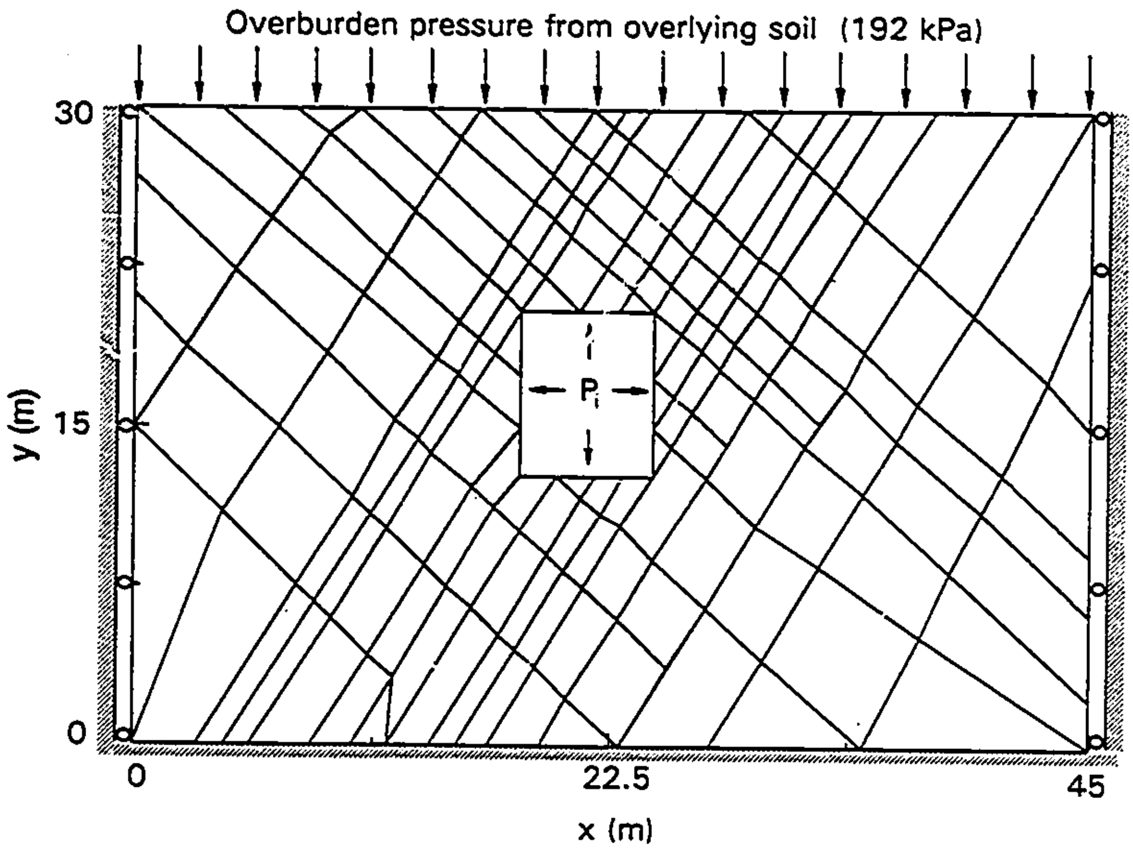

(b) After Stage 1 excavation

Fig.8.3 (Continued)

Table 8.1 Dupont Station: Basic material properties

	Rock between joints	Shear zones	Joints
Elastic Modulus (kPa)	6.89×10^6	3.45×10^6	-
Poisson's Ratio	0.15	0.30	-
Cohesion (kPa)	3.45×10^4	0	0
Friction Angle (°)	45	35	15
Shear Stiffness (kN/m³)	-	-	1.36×10^5
Unit Weight (kN/m³)	25.93	25.93	-

The initial stress condition was estimated using the mesh shown in Fig.8.3(a). By removing the blocks in the area of the first stage excavation, the mesh was reduced to that shown in Fig.8.3(b).

As mentioned earlier, rockbolt pressures imposed on the excavation walls were simulated in two different ways. Case 1 was similar to the Finite Element model, i.e., an average uniform internal pressure $P_i = 10$ psi (69 kPa) was applied on the walls as shown in Fig.8.3(b). In Case 2, the rockbolts were directly used in the mesh as shown in Fig.8.4, where the rockbolt pressures on the walls were automatically generated as response of the bolts to the block movements. According to Rodriguez Perez (1980), the magnitudes of the rockbolt pressure P_i (used in the Finite Element model) "were related to the inward rock movements developed at the opening walls." Therefore, passive rockbolts were used in the BLOSMER analysis. The assumed parameters of the rock bolts are listed in Table 8.2.

The results of the BLOSMER analysis and comparison with both the Finite Element results and the in-situ instrument data are summarized below.

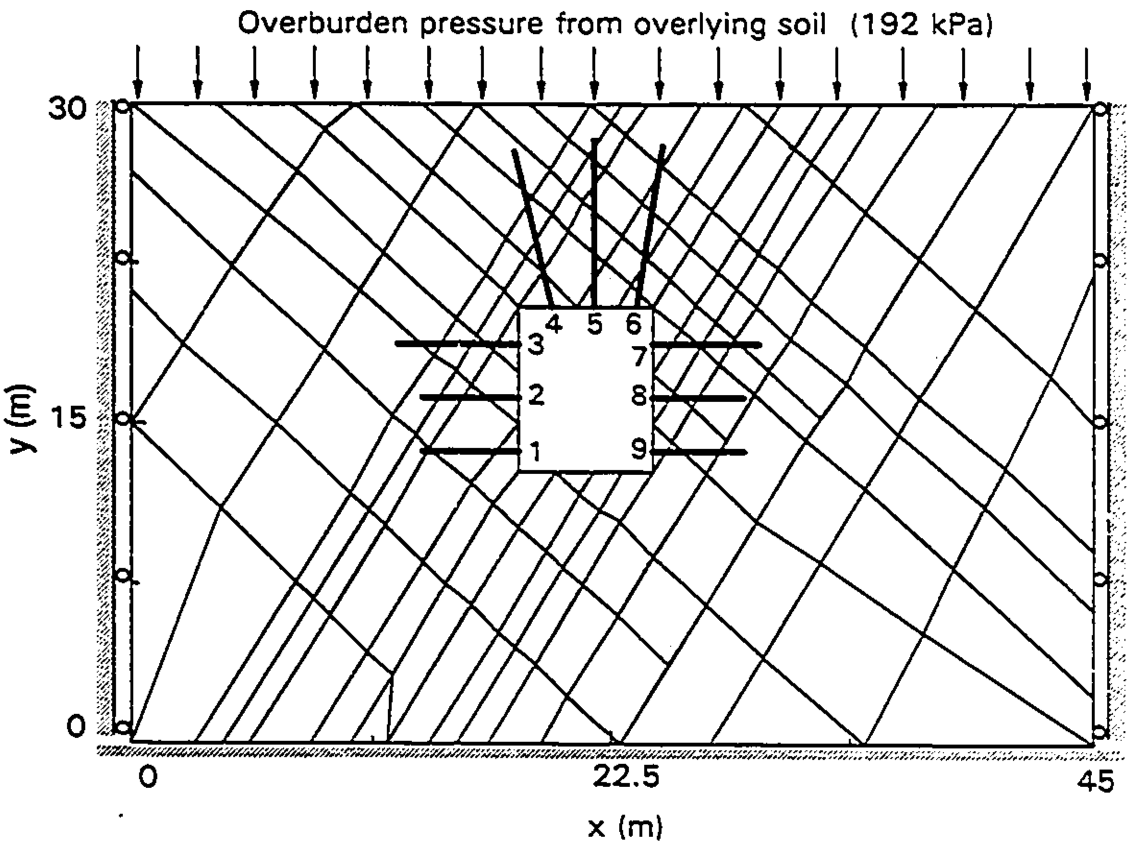

Fig.8.4 Dupont Station: A mesh with rockbolts for BLOSMER

Table 8.2 Dupont Station: Rock bolt properties used in BLOSMER analysis

Elastic modulus	210 GPa
Yield strength	360 MPa
Diameter of bolt	5 cm

Case 1: Rock bolt support modelled by applying an average pressure P_i

Fig.8.5 illustrates the displacement vectors of the rocks obtained from using the BLOSMER program with the pressure $P_i = 10$ psi (69 kPa) applied. It is observed in Fig.8.5 that the rock movements after the excavation are greatly influenced by the geologic features (joints and shear zones).

According to Rodriguez Perez (1980), most of the rock movements were concentrated around the opening crown and right wall and are largely controlled by the geology of the site. "The rock movements observed in the field were produced by the blocky rock presented in the opening and not by the compressibility or width of the shear zones themselves." Fig.8.6 shows the movements of the rocks around the excavation obtained from the BLOSMER program. A similar figure from Rodriguez Perez (1980) is shown in Fig.8.7 which illustrates the rock movements obtained from the Finite Element analysis. From Figs.8.5, 8.6 and 8.7, it can be observed that the pattern of deformation of the rocks from the BLOSMER program is similar to that from the FEM analysis. The results from both methods indicate that the patterns of deformation of the rocks come from the blocky condition of the rock mass. The sliding along the shear zones is a dominant feature of the rock movements.

Fig.8.8 illustrates the exaggerated deformations of the rocks obtained from BLOSMER. The settlements at the top of rock are evidently concentrated on the right side of the excavation centerline, though the uneven settlement trough extend to both sides of the centerline. Fig.8.9 shows the corresponding FEM results of the rock settlements. The maximum settlements of the rock surface occur at a distance of approximately 8 m to the right of the centerline which can be observed in both analyses (Figs.8.8 and 8.9). The maximum settlement from BLOSMER is 1 cm and the FEM result is 0.14 in. (0.4 cm). Although there is no field measurement available on the settlement, Rodriguez Perez (1980) mentioned that the measured rock movements were "higher in magnitude in some cases." The results obtained from both BLOSMER and FEM (Figs.8.8 and 8.9) indicate that "the concentration of movements at the opening crown and right wall has a great repercussion on the trough shape" It can be observed that most of the movements occurring at the opening crown and the right wall are largely transmitted through the joints to the rock surface at the right of the centerline. The influence of the discontinuities on the displacement pattern of the rock mass is clearly evident.

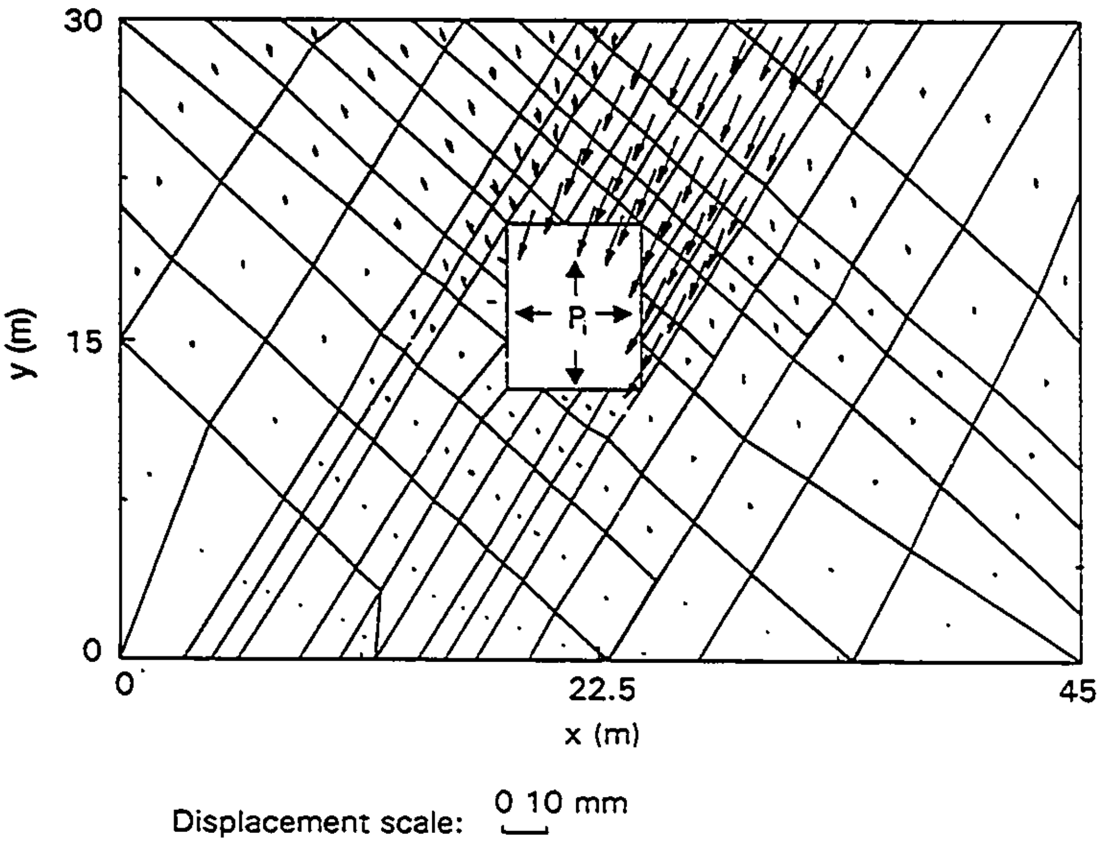

Fig.8.5 Dupont Station (Case 1):
Displacement vectors of the rock blocks from BLOSMER

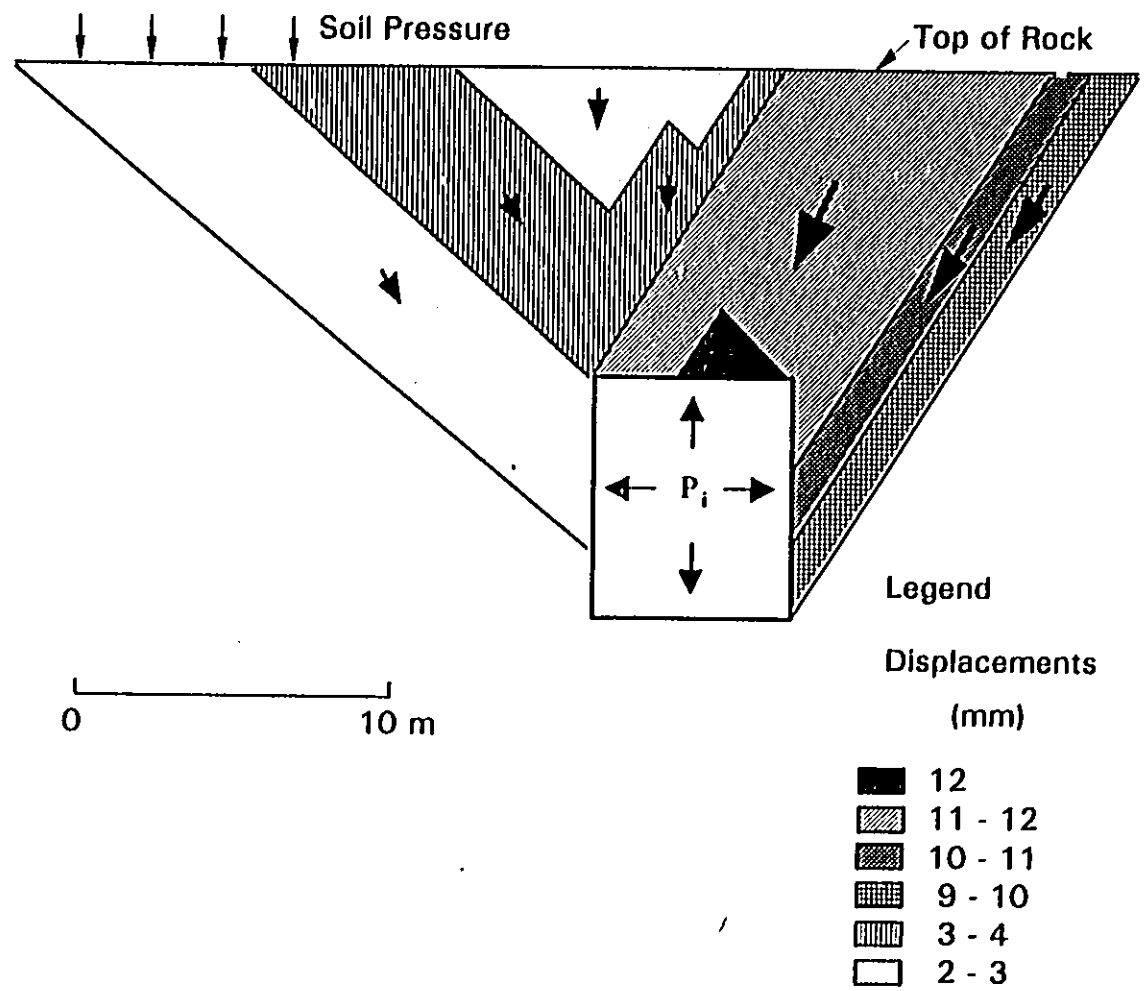

Fig.8.6 Dupont Station (Case 1)
Movements of the rock obtained from BLOSMER analysis

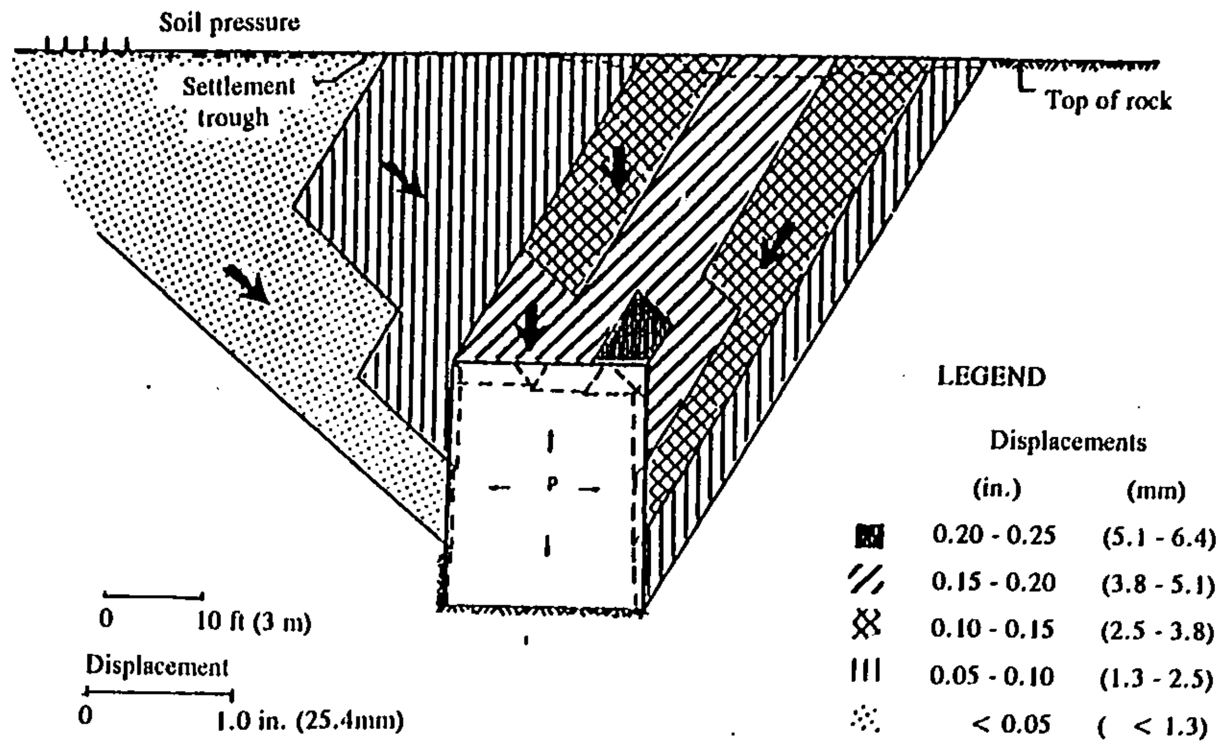

Fig.8.7 Dupont Station: Movements of the rocks obtained from FEM

(After Rodriguez Perez, 1980)

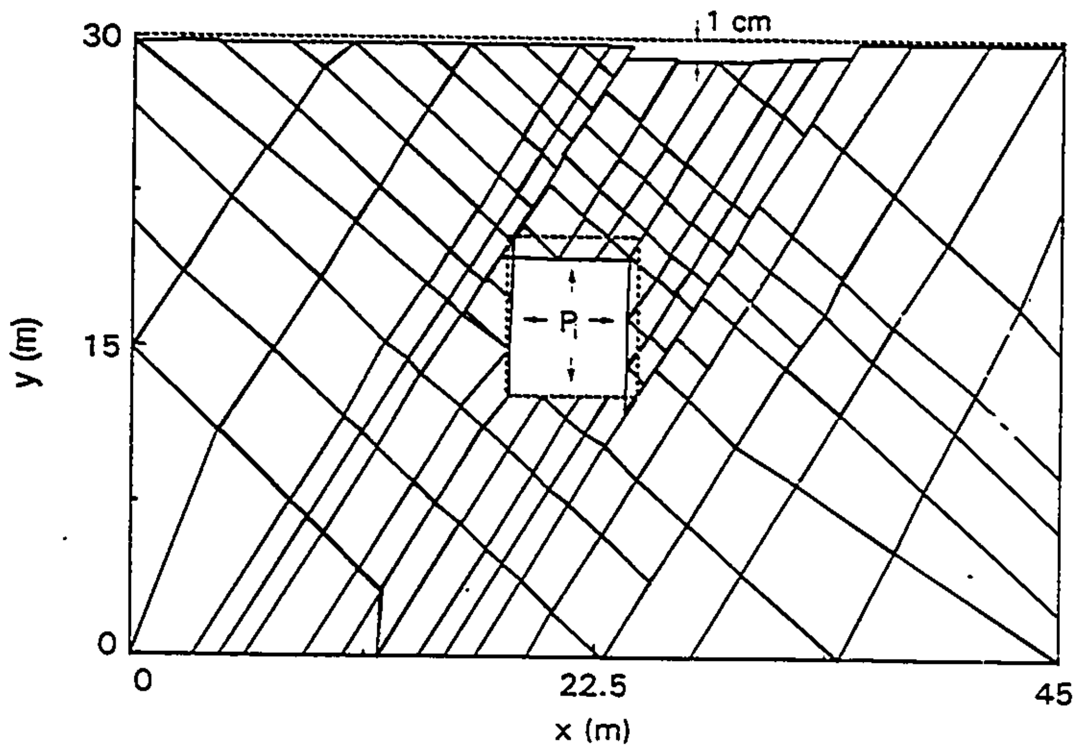

Fig.8.8 Dupont Station: Settlements at the top of the rock from BLOSMER

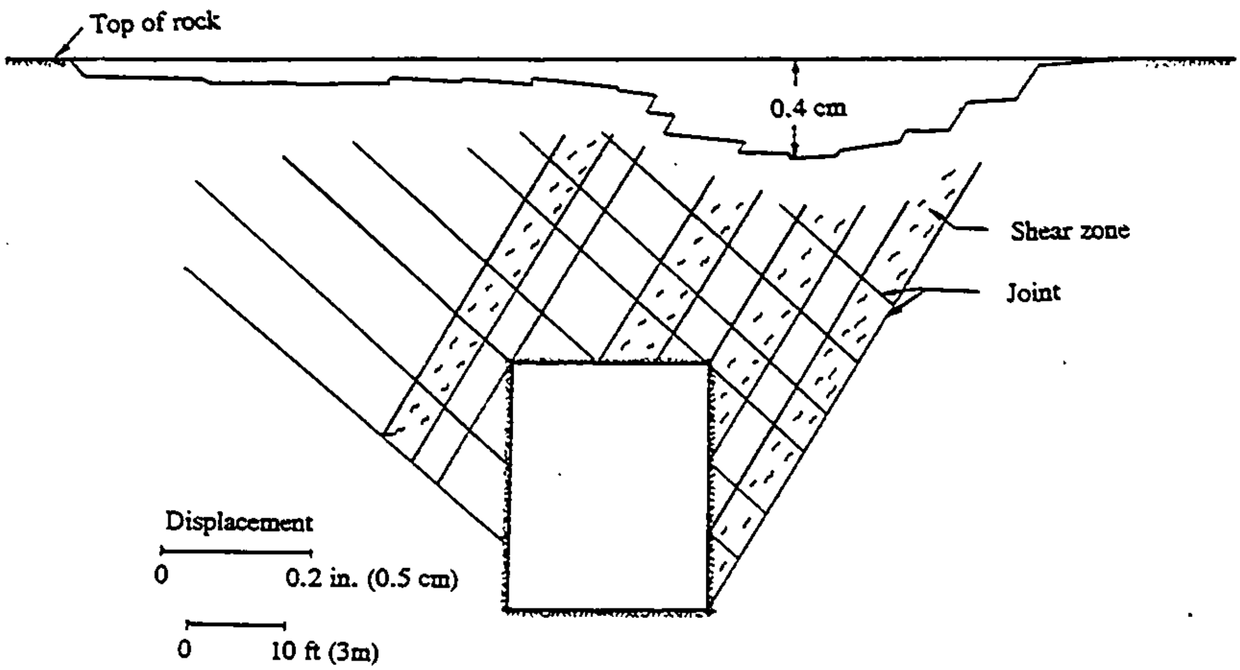

Fig.8.9 Dupont Station: Settlement trough at top of rock
(After Rodriguez Perez, 1980)

The results of extensometer measurements in the vicinity of the excavation are available for three different sections. These extensometers permitted the measurement of deformations at the walls as well as at various distance away from the excavation. At an equivalent rockbolt support pressure P_i=10psi (69 kPa), the measured lateral movements at the walls varied from 0.05 to 0.1 in. (0.13 to 0.25 cm) whereas the crown movements ranged from 0.2 to 0.4 in. (0.5 to 1 cm). The results from BLOSMER analysis (Figs.8.5 and 8.6), when compared with the field data as well as the Finite Element results (Fig.8.7), show a similar pattern of deformation range of magnitudes.

The extensometer results at the three cross-sections and the FEM results are shown in Figs.8.10(a, b, and c). The corresponding displacements of the rocks obtained from BLOSMER analysis are also plotted in Figs.8.10. In all cases, good agreement exists between the results from BLOSMER and those from the FEM, and the field measurement.

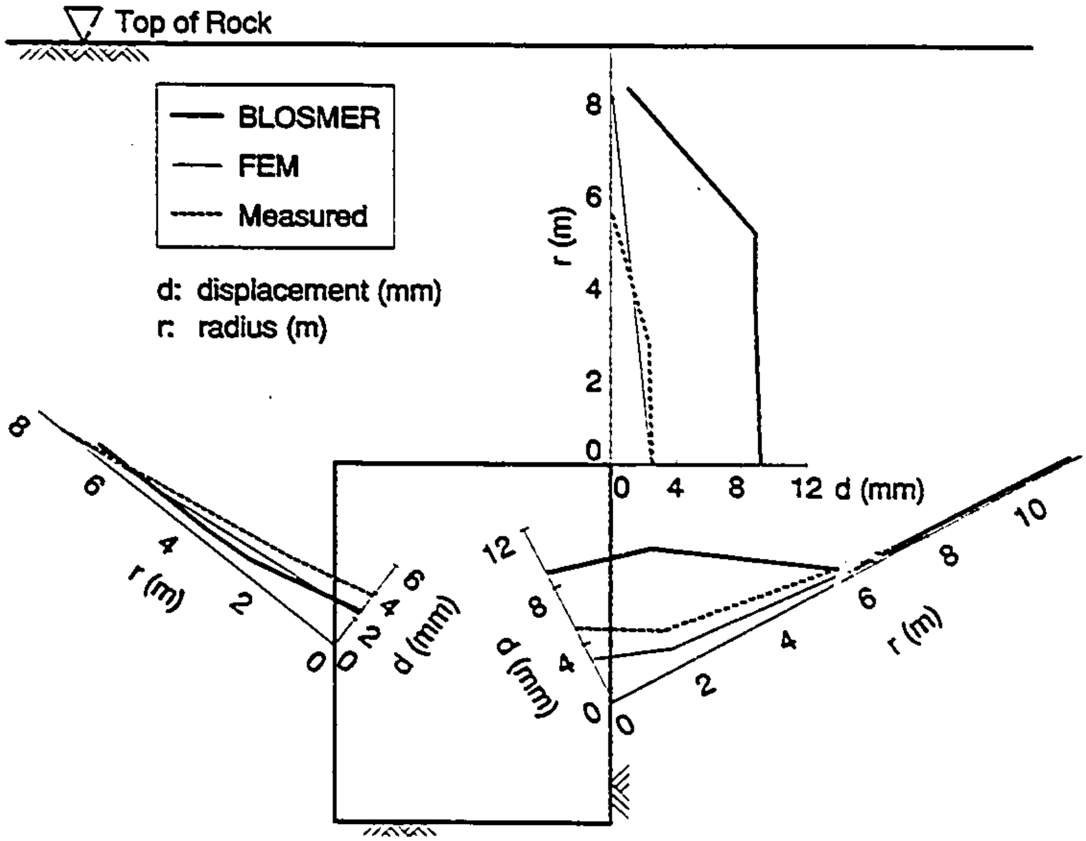

(a) Test section I

Fig.8.10 Dupont Station (Case 1 - uniform rockbolt pressure): Comparison of the displacements obtained from the different methods.

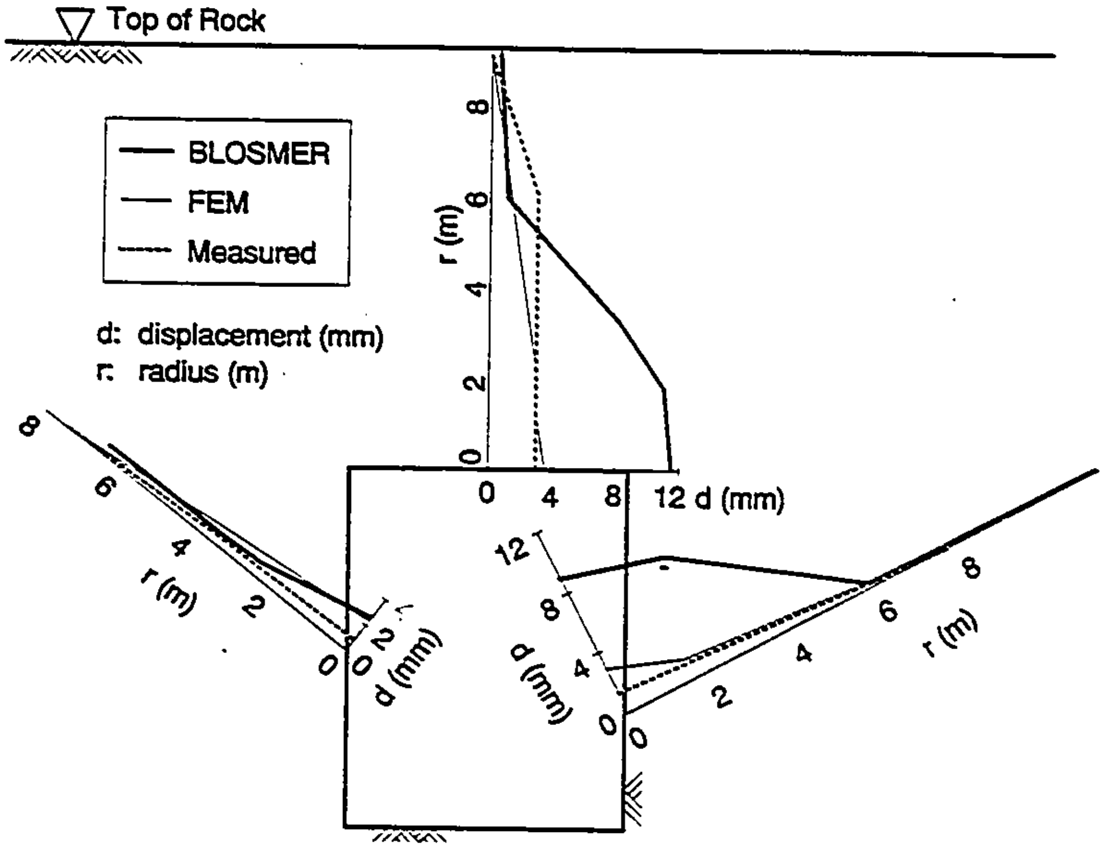

(b) Test section II

Fig.8.10 (Continued)

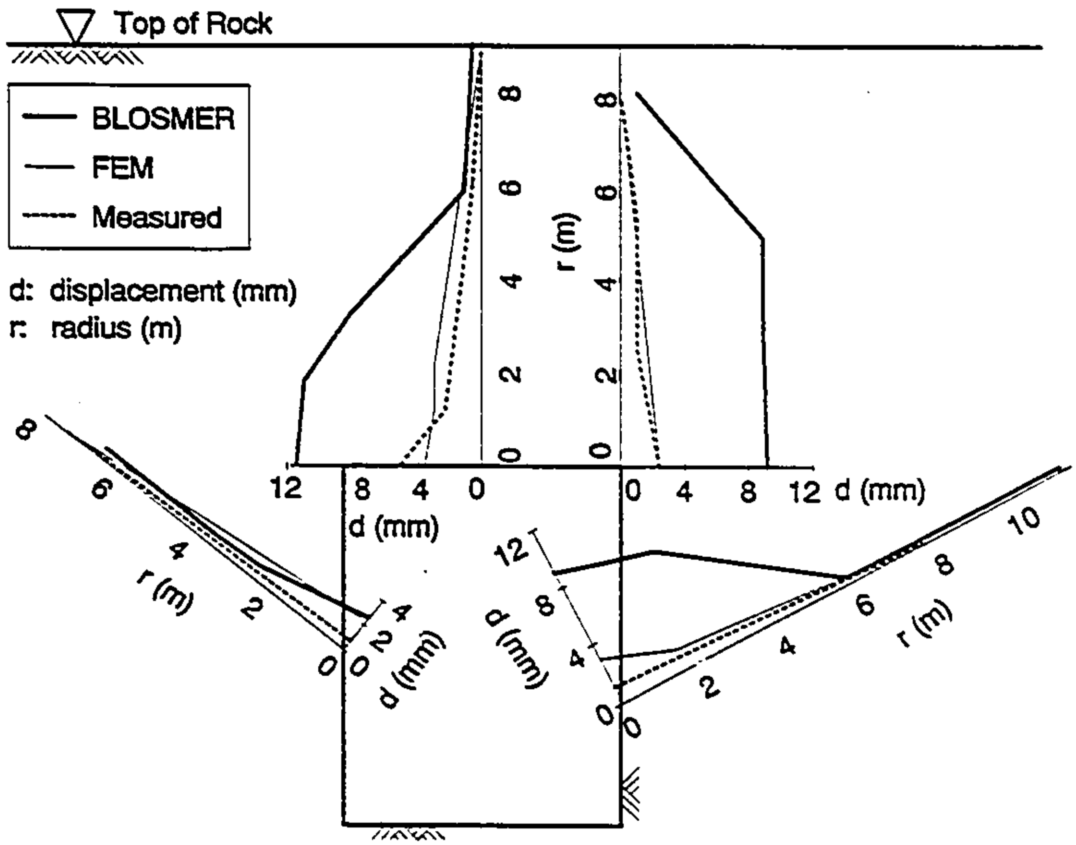

(c) Test section III

Fig.8.10 (Continued)

Case 2: Analysis using rock bolts

Instead of applying an equivalent average rockbolt pressure P_i on the excavation walls, fully grouted passive rock bolts (Fig.8.4) were used in this case. The initial state of the ground stresses prior to the excavation was evaluated using the mesh shown in Fig.8.3(a). The computation was continuously performed by the program for evaluating the excavation induced stresses. The iteration for the excavation induced stresses was initiated after removing the corresponding blocks from the original mesh and applying the rockbolts (Fig.8.4). The characteristics of the rockbolts are shown in Table 8.2.

Fig.8.11 illustrates the movements of the rocks obtained from BLOSMER analysis. The pattern of the rock movements shown in Fig.8.11 is similar to that of the FEM result (Fig.8.7) and the field observations as discussed previously.

The displacements along the extensometers are plotted in Fig.8.12, in which the FEM and extensometer data are reproduced. It is interesting to note that the displacements obtained from BLOSMER with rock bolts applied are very similar to the in-situ measurements as well as with the FEM results which were obtained by imposing an average pressure P_i on the excavation walls.

Fig.8.13 illustrates the distribution of forces along the rock bolts, which are obtained from running the BLOSMER program. The internal pressure $P_i=10$ psi (69 kPa) used in the FEM analyses is transformed into the equivalent forces on the points where the rock bolts are applied (P_i multiplied by the areas represented by the bolts). These equivalent forces are also plotted in Fig.8.13. It should be mentioned that P_i is the pressure applied on the opening surface to model the pressures imposed by the rockbolts. In the FEM analysis using the mesh shown in Fig.8.3(b), P_i remains constant both before and after the displacements of the rocks take place. In contrast, the rockbolt forces obtained herein from the BLOSMER are developed as response to the rock movements. This is an important distinction, and the two types of forces therefore cannot be compared directly. However, it can be noted in Fig.8.13 that the magnitudes of the rockbolt forces determined by BLOSMER are of the same order as the estimated rockbolt pressure applied on the surface of the opening.

The practical significance of the capability of the BLOSMER analysis to evaluate rockbolt forces is illustrated in Fig.8.14 which shows the average bolt pressures imposed on the excavation walls. These are compared to the estimated average pressures Pi=10 psi (69 kPa) used by Rodriguez Perez (1980). The BLOSMER results clearly indicate that the right wall and the crown of the opening require more support than the left wall does. The highest pressure develops at the upper right corner of the opening. These results are consistent with the deformation patterns observed in the rock.

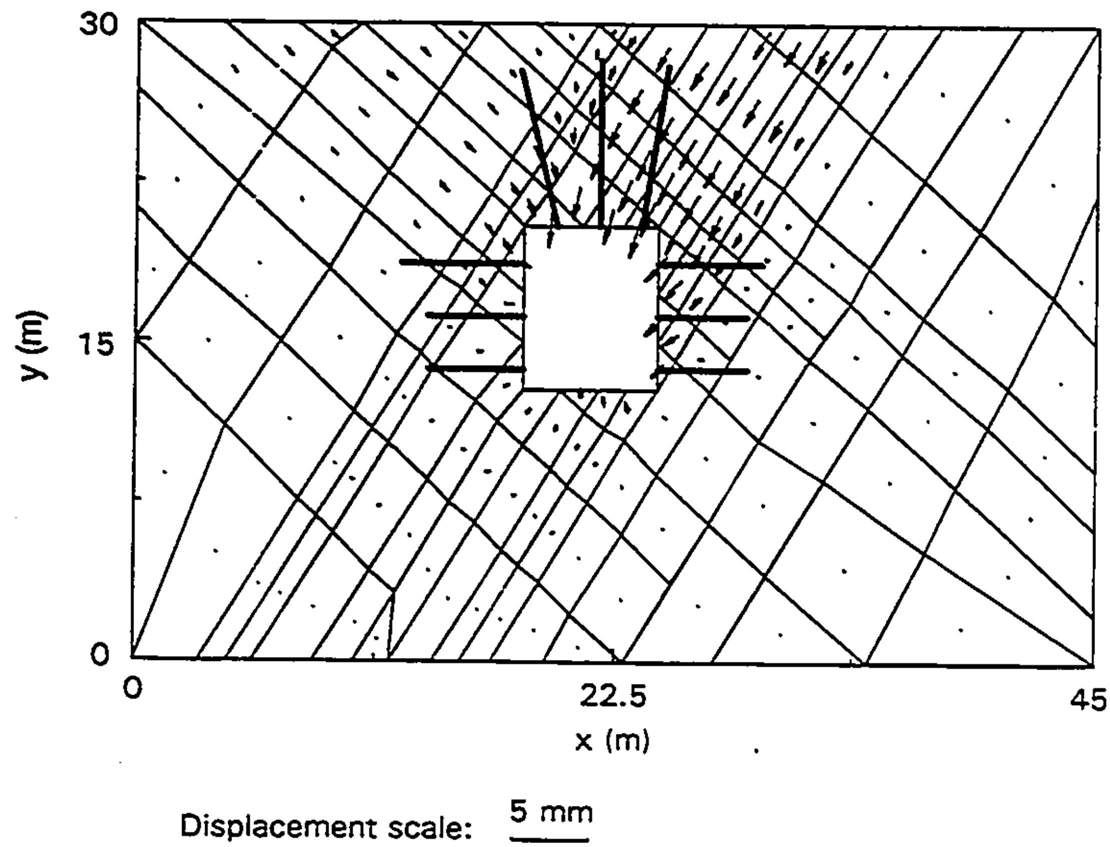

Fig.8.11 Dupont Station (Case 2): Rock displacement vector plot from BLOSMER

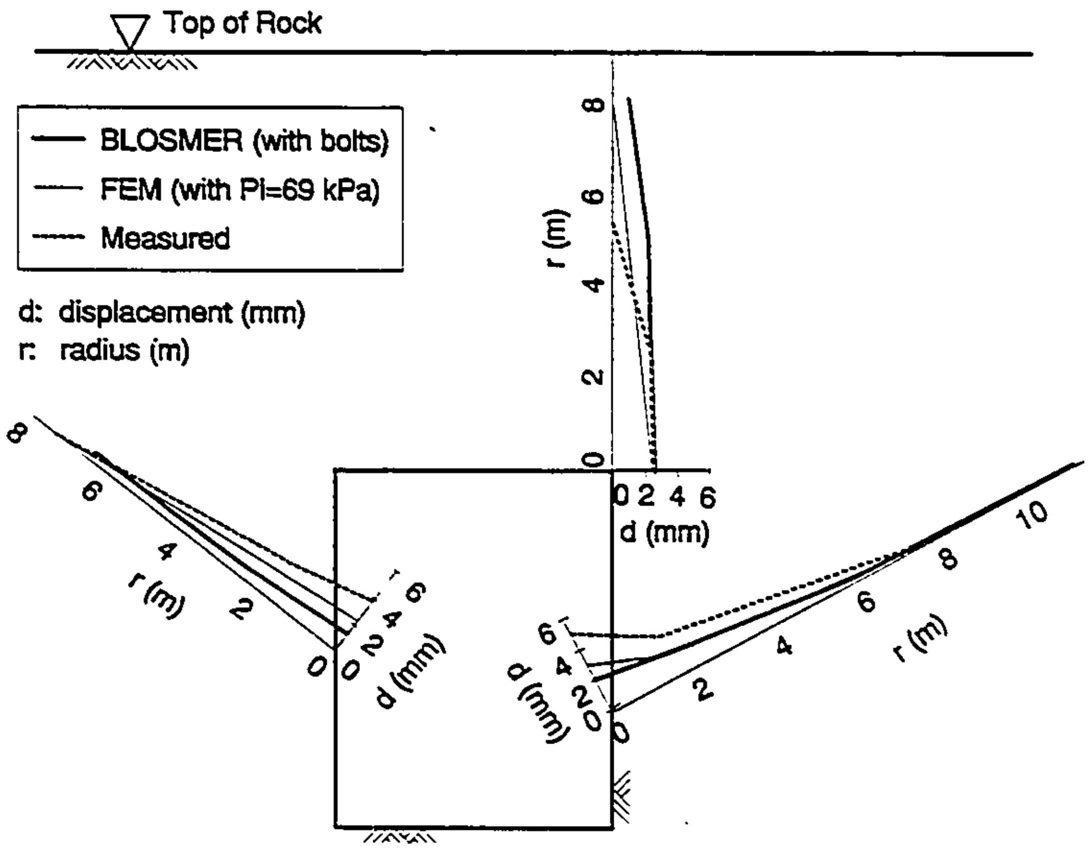

(a) Test section I

Fig.8.12 Dupont Station (Case 2 - rockbolts applied in BLOSMER): Comparison of the displacements from different methods

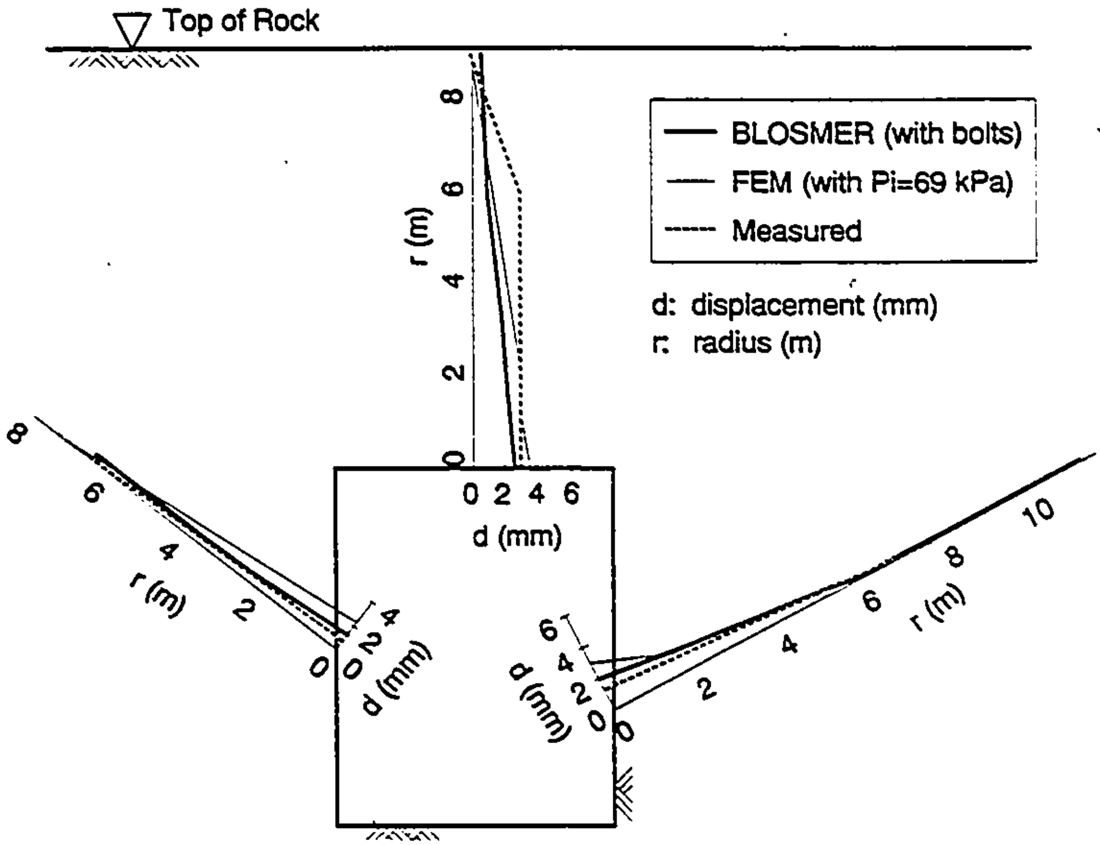

(b) Test section II

Fig.8.12 (Continued)

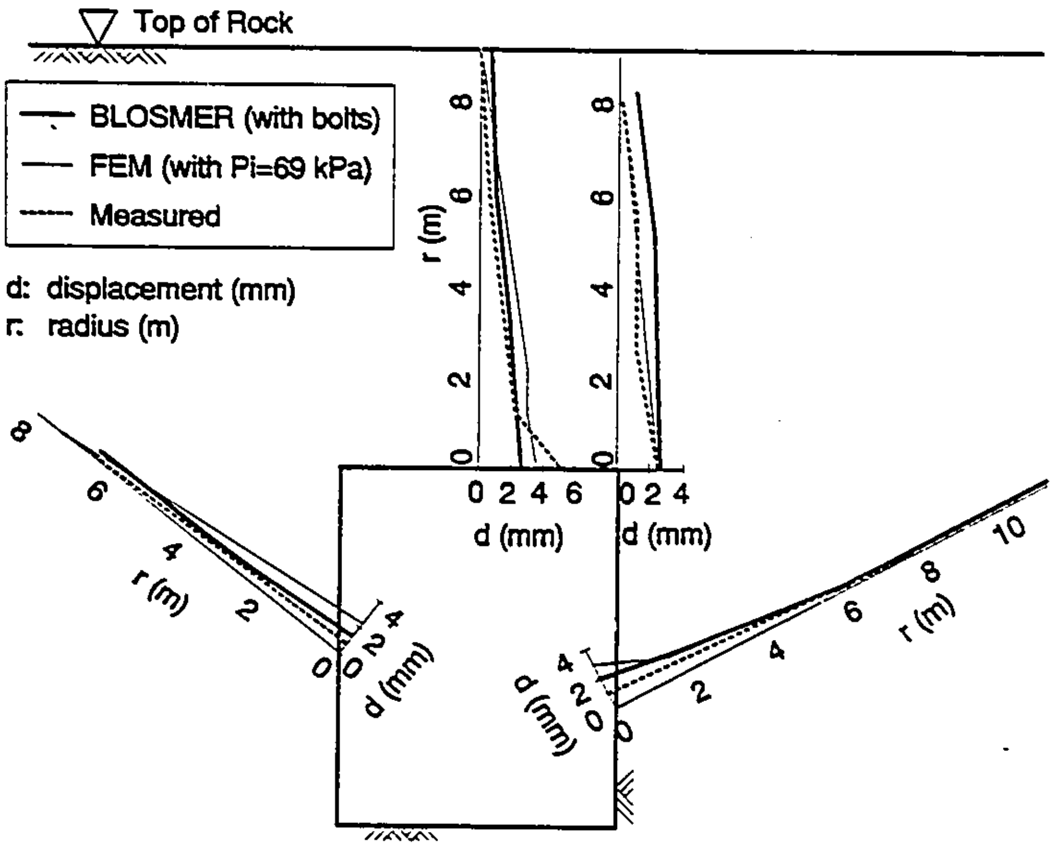

(c) Test section III

Fig.8.12 (Continued)

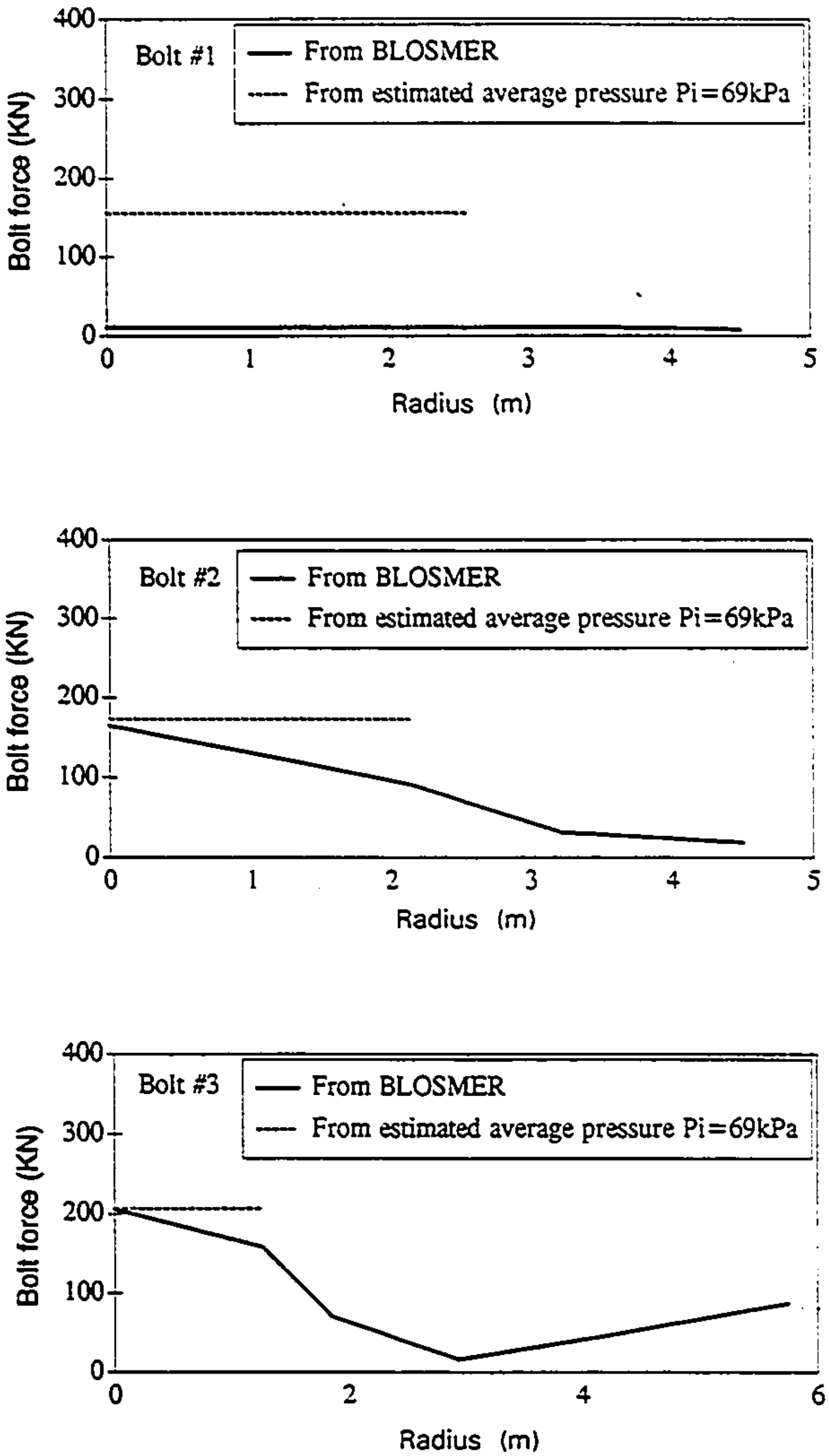

Fig.8.13 Dupont Station: Forces along the rock bolts from BLOSMER

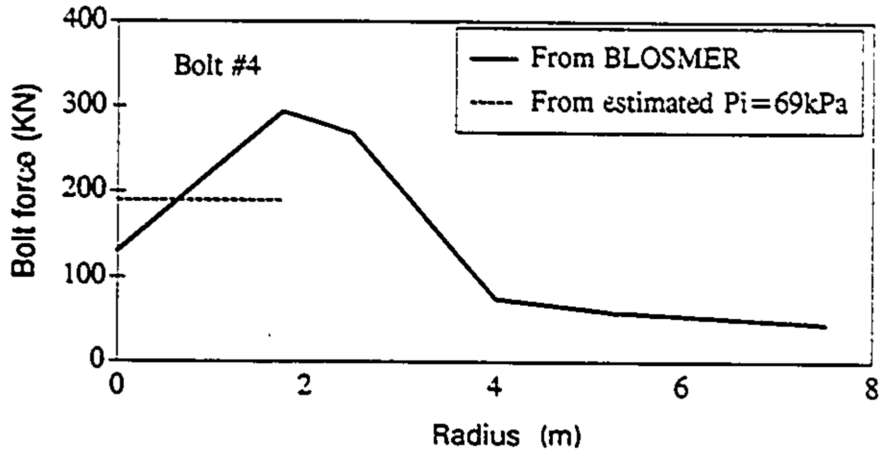

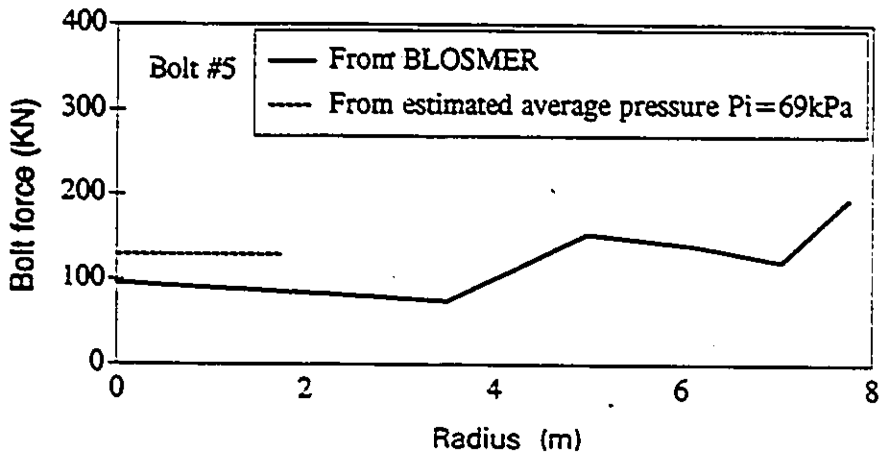

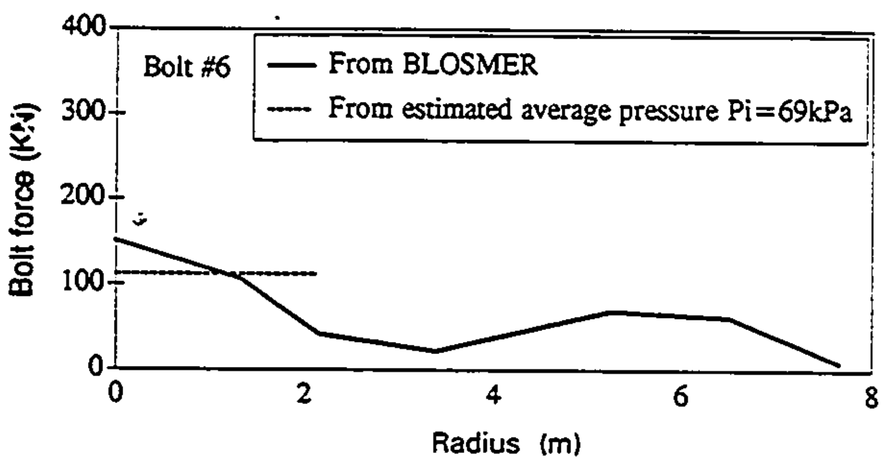

Fig.8.13 (Continued)

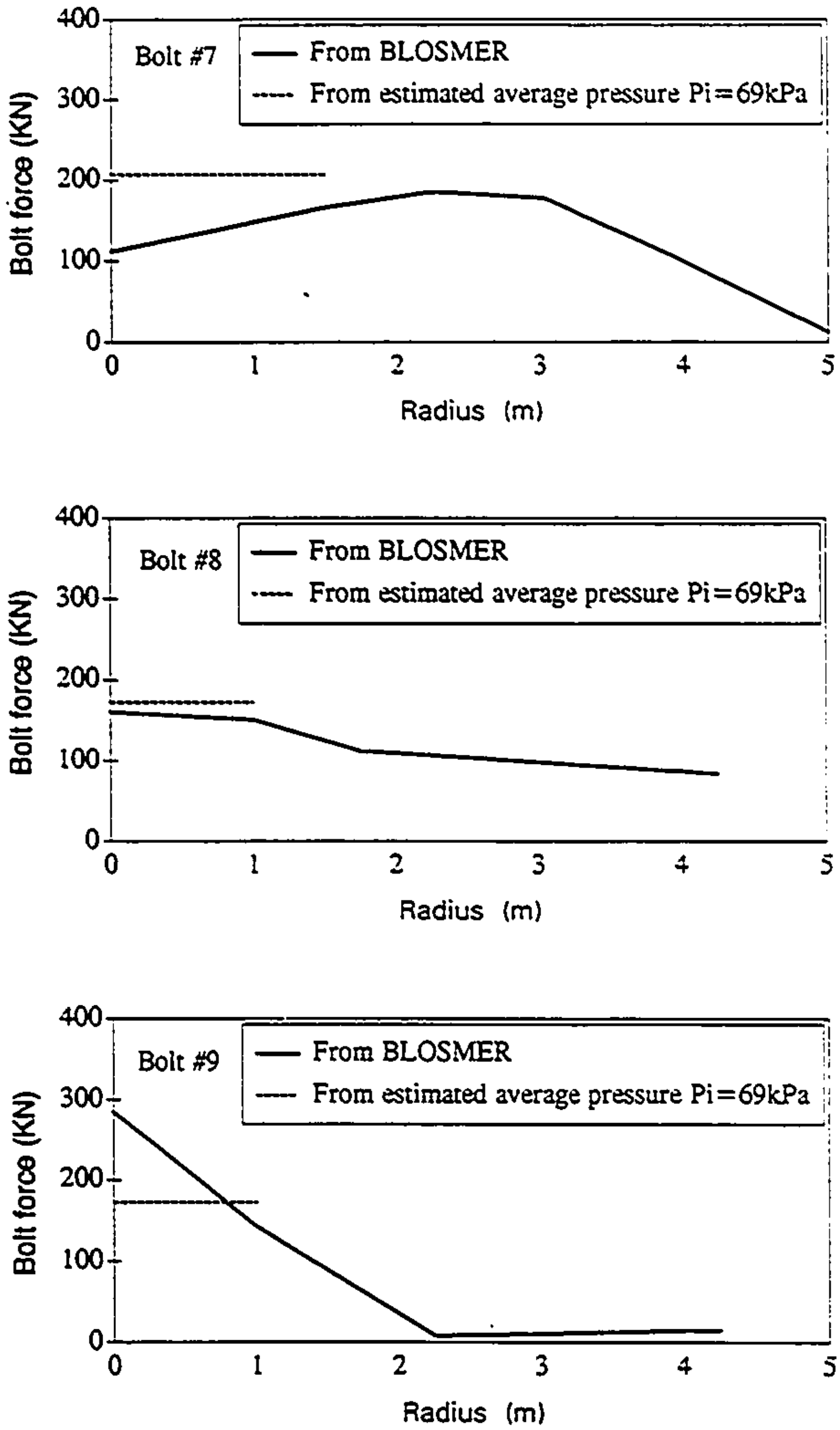

Fig.8.13 (Continued)

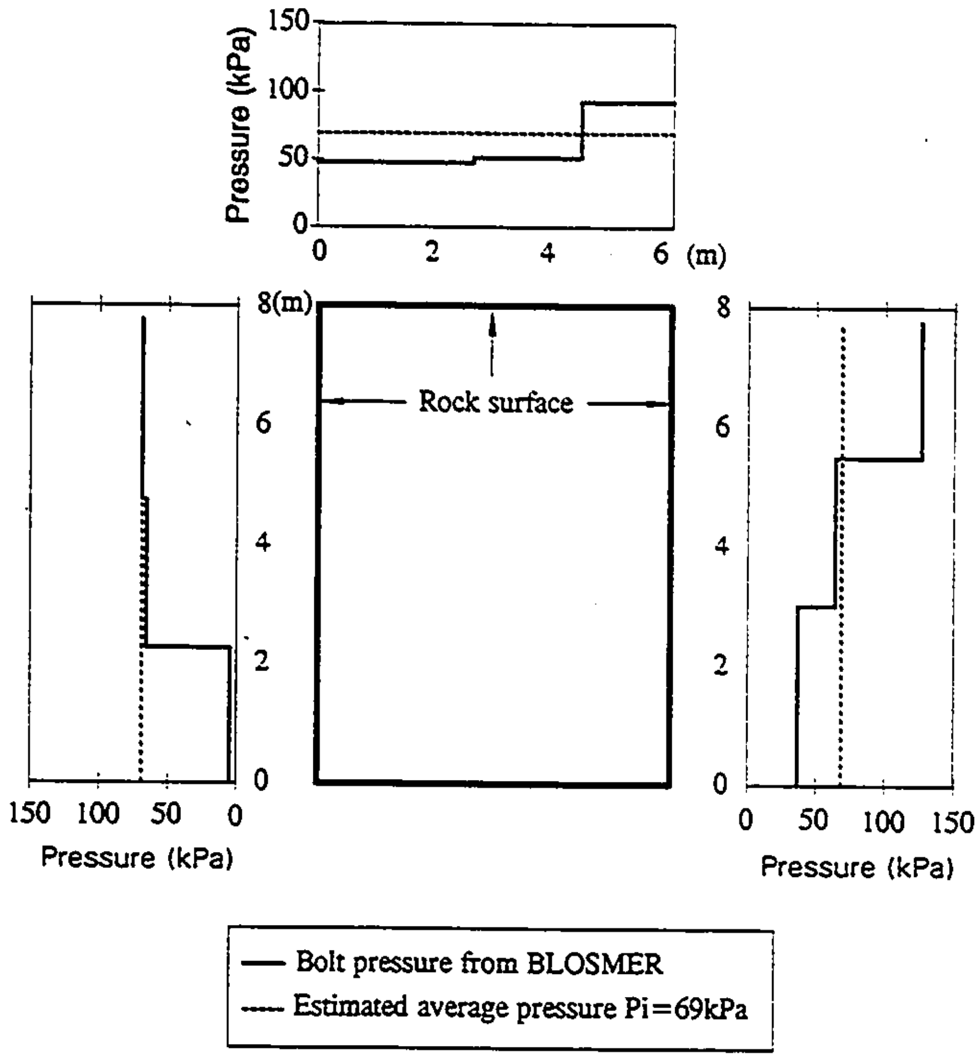

Fig.8.14 Dupont Station: Rockbolt pressures imposed on the excavation walls

8.3 Application to the Cassiar Mine Open Pit Slope

8.3.1 Background

The Block-Spring Model has also been applied to the Cassiar Mine Open Pit Slope. The Cassiar mine is located in steep mountainous terrain in northern British Columbia approximately 1,200 km north of Vancouver. Data used here are from a CANMET report prepared by Cassiar Mining Corporation and Piteau Associates Engineering Ltd. (1990) subsequently referred to as the 'CANMET report' for briefness.

The geological features around the Cassiar mine are very complex. The rock mass contains several major faults and shear zones, which exert a major influence on the slope stability. According to the CANMET report, instability developed in the approximately 330m hanging wall slope during development of the final phase of the open pit. In order to investigate the failure mechanism of the slope, extensive studies of the slope were reported in the CANMET report, including numerical analyses with UDEC (a Universal Distinct Element Code, e.g., Lemos, et al., 1985). A representative section through the slope failure used for the UDEC modelling is shown in Fig.8.15. Two major types of rocks, namely argillite and serpentinite, and several discontinuities present in this section. The discontinuities shown in this section include a serpentinite dyke, two faults, a contact between the argillite and the serpentinite zones, and five joints indicated as B, C, D, E and F. Seven points numbered 1 to 7, at which the displacements of the slope were monitored, are also shown.

The deformation of the slope was back analyzed with the UDEC program using various joint parameters under different groundwater conditions. The analyses presented in the CANMET report indicated that "three major discontinuities namely the Serpentinite Dyke, the North Fault and Fault A1 (Fig.8.15) had played a contributory role in the failure." "The failure was extremely sensitive to changes in the friction angle and was exacerbated by high groundwater pressures."

The present analysis of the Cassiar Slope is not aimed at repeating all the investigations with the Block-Spring Model. Instead, one of the cases analyzed with the UDEC in the CANMET report (as described in the following section) is selected and analyzed with the program BLOSMER. This application is presented for comparing the results from the BLOSMER with those of the UDEC. Also, the BLOSMER results are compared with the field observations of the initial failure movements of the slope.

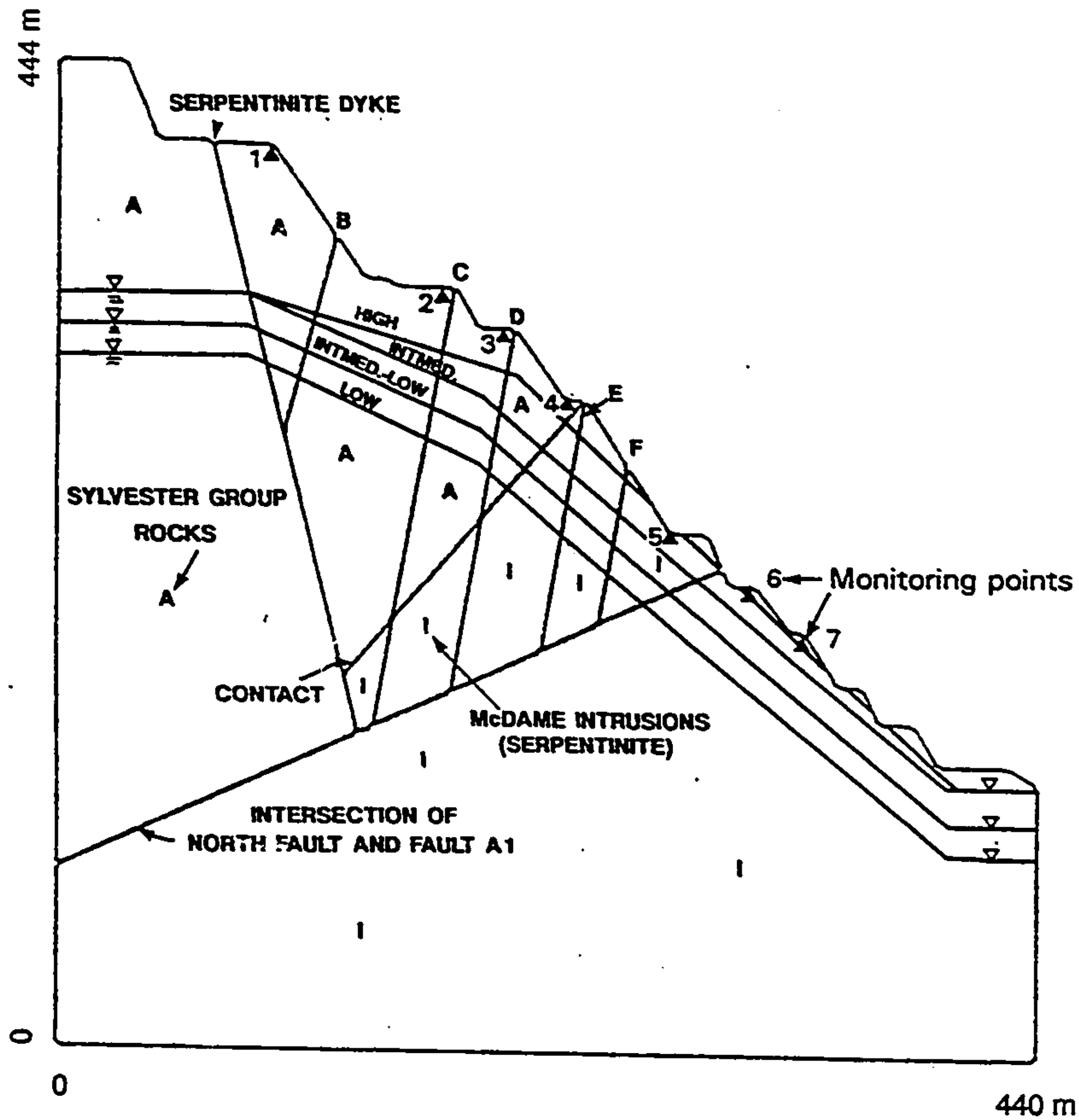

Fig.8.15 A section of Cassiar Open Pit Slope
(after Cassiar Mining Co. & Piteau Associates Engineering Ltd., 1990)

8.3.2 Analysis with BLOSMER

The cross-section of the Cassiar Slope shown in Fig.8.15 has been analyzed with the BLOSMER. A set of rock and joint properties used in the UDEC analysis as listed in Table 8.3 were also used in BLOSMER analysis.

A mesh of the slope used in the BLOSMER analysis is shown in Fig.8.16. Four groundwater levels shown in Fig.8.15 have been considered in the analysis.

Fig.8.17 shows the displacement vector plot (with high groundwater condition) obtained from the BLOSMER program. An obvious large displacement zone formed by the wedge located above the fault and to the right of the serpentinite dyke can be observed (Fig.8.17). The maximum displacement of approximately 0.73 m occurs at the top of this wedge. It can be noted in Fig.8.17 that the major discontinuities, i.e., the serpentinite dyke and the fault, had an important influence on the pattern of the slope movement, which corroborates the conclusions in the CANMET report.

Fig.8.18 shows a velocity vector plot obtained from the UDEC analysis under high groundwater condition. Regrettably no displacement vector plot is available in the CANMET report. However, the velocity plot in Fig.8.18 shows clearly the pattern of the slope movement. By comparing Fig.8.17 with Fig.8.18, it can be noted that the pattern of the slope movements obtained from the BLOSMER is similar to that obtained from the UDEC.

The BLOSMER analysis was also undertaken for the other groundwater conditions, i.e., with the intermediate, the intermediate-low and low groundwater tables (Fig.8.15), and for the condition of no groundwater. The displacements of the seven monitoring points on the slope corresponding to the different groundwater conditions are plotted in Fig.8.19. The displacements of the seven points obtained from the UDEC analysis are also shown in Fig.8.19. The initial failure movements observed at the monitoring points were used in the CANMET report to compare with the predicted movements. These observed data are also plotted in Fig.8.19. Under the high groundwater condition, the maximum displacements along the slope are of the order of 0.47m from the UDEC analysis and 0.73m from the BLOSMER. The observed initial failure movement is in the order of 0.74m. The maximum displacements took place on

Table 8.3 Cassiar Slope: Material properties used for numerical modelling

	Argillite (mass)	Argillite (Discontinuity)	Serpentinite (mass)	Serpentinite (Discontinuity)
Density (kN/m^3)	28.2		25.3	
Elastic Modulus (Pa)	2.1×10^{10}		9.65×10^{9}	
Poisson's Ratio	0.24		0.3	
Cohesion (Pa)	7.0×10^{5}	5.36×10^{5}	2.00×10^{5}	5.40×10^{4}
Friction Angle(°)	32	30	26	24
K_n (Pa/m)		4.40×10^{7}		4.30×10^{7}
K_s (Pa/m)		6.8×10^{6} $(1\times10^{8})^*$		2.7×10^{6} $(1\times10^{8})^*$

* Used in UDEC analyses as well as in the present modelling.

the top of the slope. The displacements of the seven monitoring points obtained from the numerical methods under the high groundwater condition and the observed data are also compared in Table 8.4.

As expected, the displacements at the slope increase with the increase of the groundwater elevation. The displacement of the bottom of the wedge (monitoring point 5) was especially sensitive to the groundwater level. According to the CANMET report, the groundwater levels have significant effect on the movement of the slope. When the groundwater table is lowered the movement of the slope decreases. This sensitivity is also observed in the BLOSMER results shown in Fig.8.19.

From Figs.8.17, 8.18 and 8.19 and Table 8.4, a good agreement can be noted between the BLOSMER results and the UDEC results both in magnitudes and in the patterns of the slope movements. The results from the Cassiar Mine Open Pit analysis again demonstrate the capability of the proposed method.

The computer time required to run the BLOSMER program is much less than that to run the UDEC. The number of cycles used in the UDEC analysis was as high as 12,500 cycles (CPU time for UDEC was not reported). The proposed BLOSMER required less than 3 minutes of CPU using an AMDHAL 5880 machine. The BLOSMER program ran for 51 cycles for the high groundwater table condition. The corresponding saving in computing time is obvious.

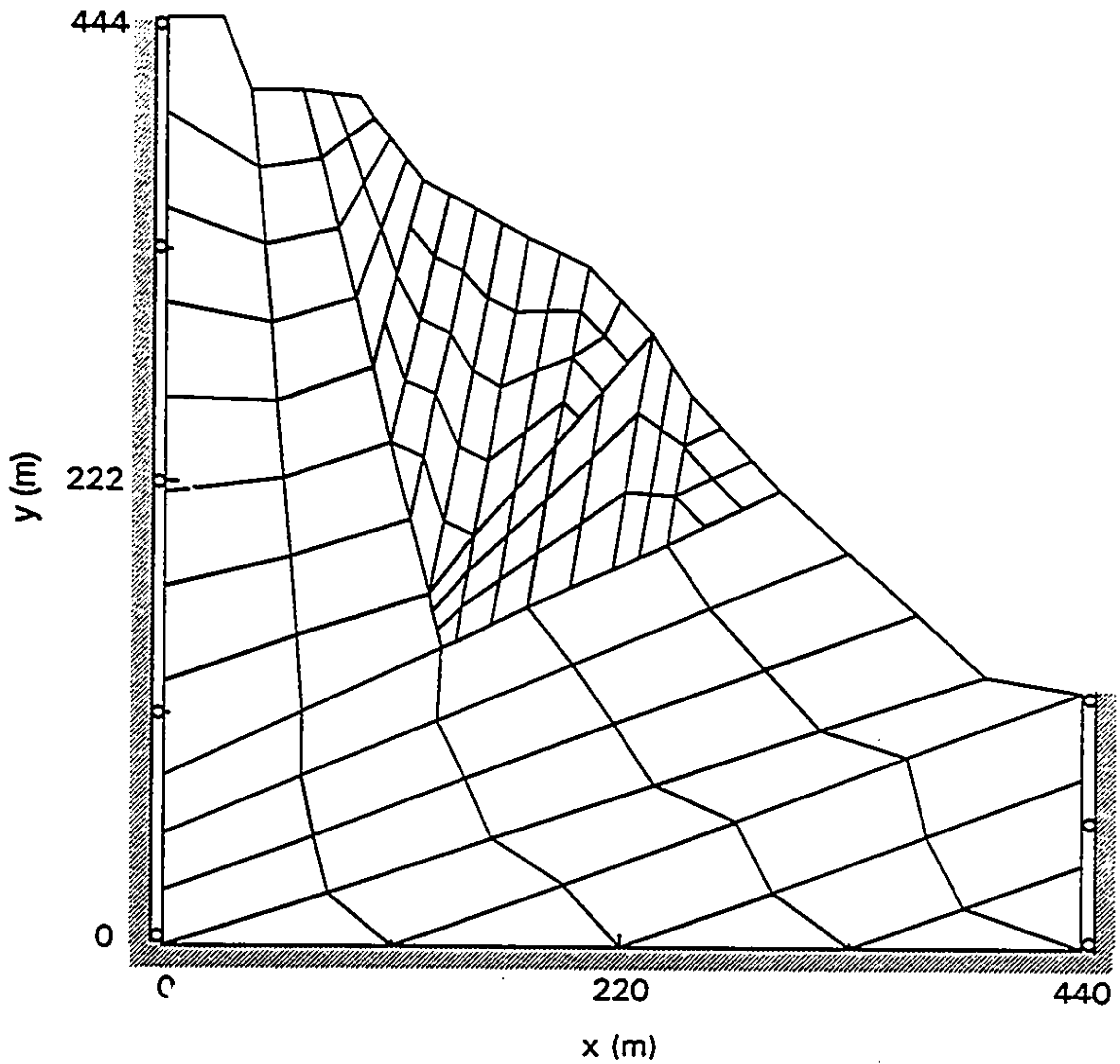

Fig.8.16 Cassiar Slope: A mesh of the Block-Spring Model

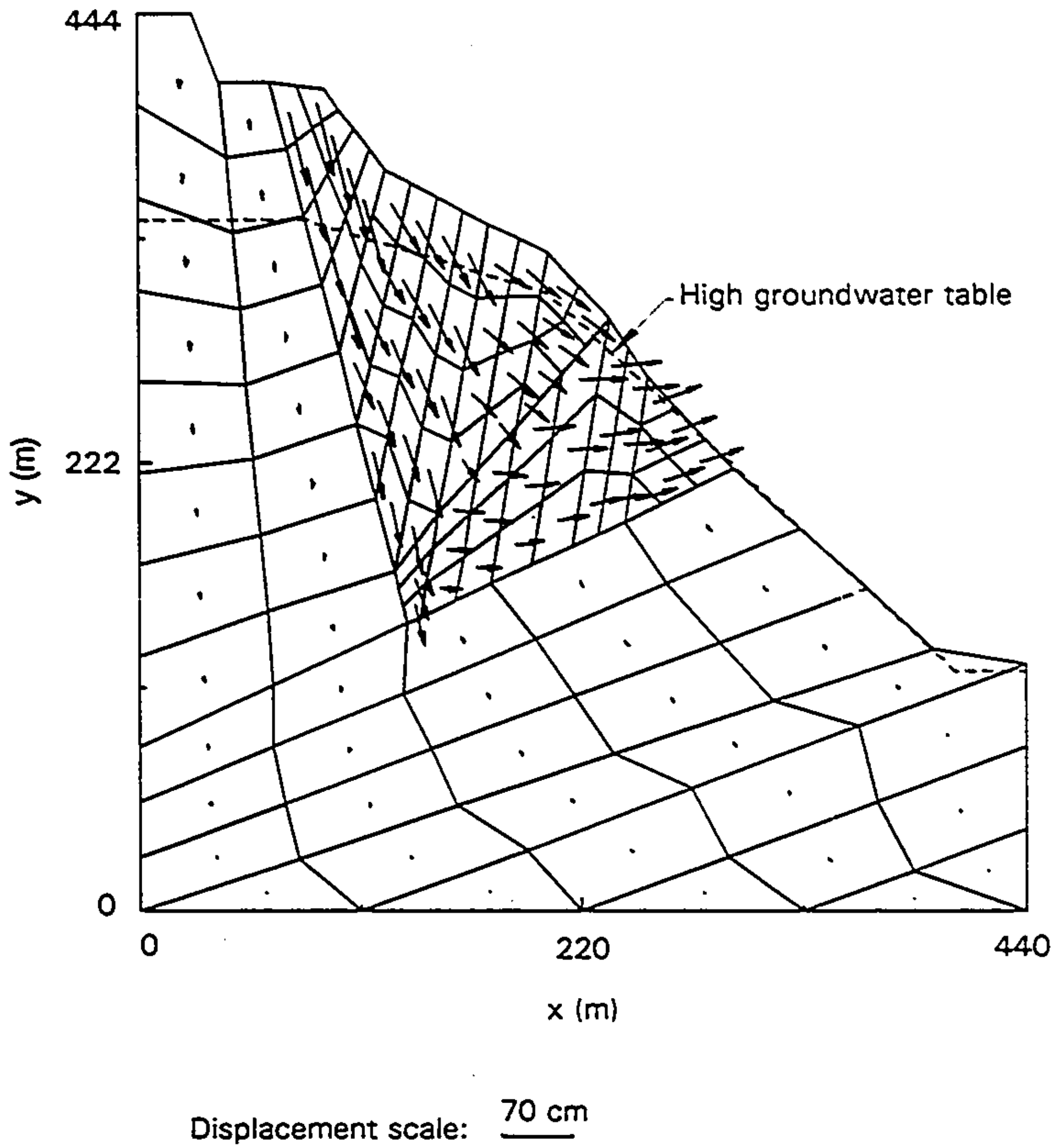

Fig.8.17 Cassiar Slope: Displacement vectors from BLOSMER analysis

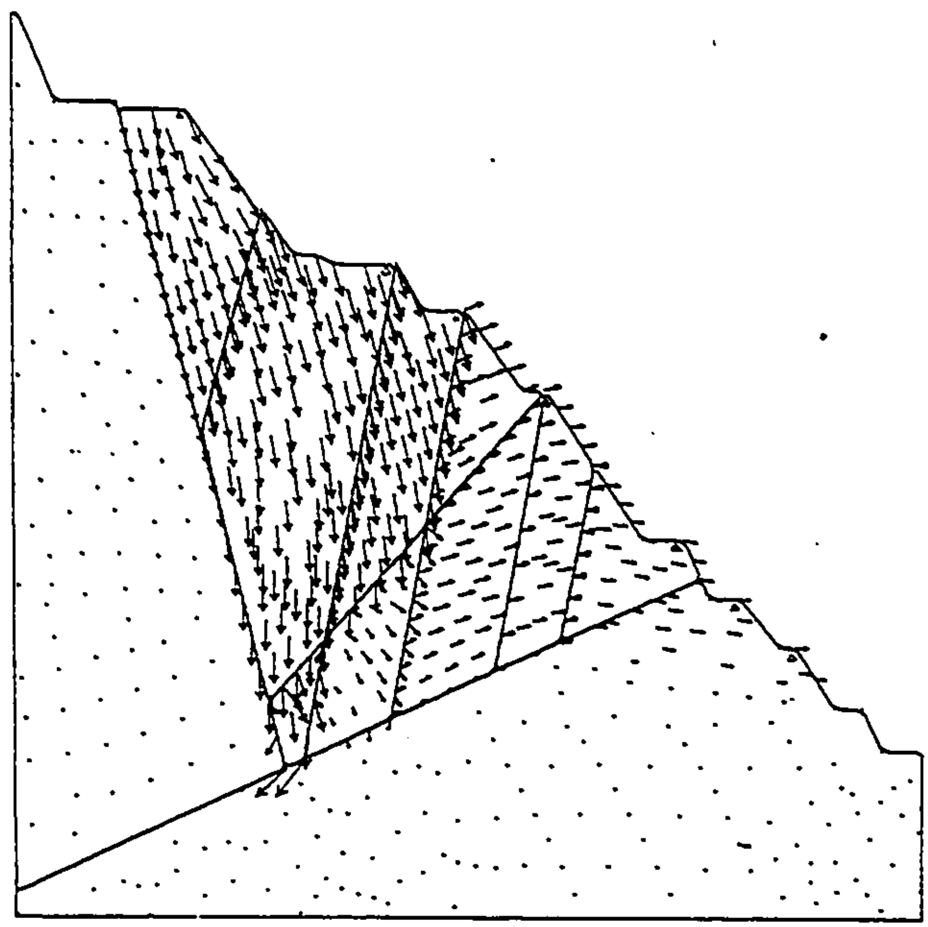

Fig.8.18 Cassiar Slope: Velocity vector plot from UDEC analysis

(after Cassiar Mining Co. & Piteau Associates Engineering Ltd., 1990)

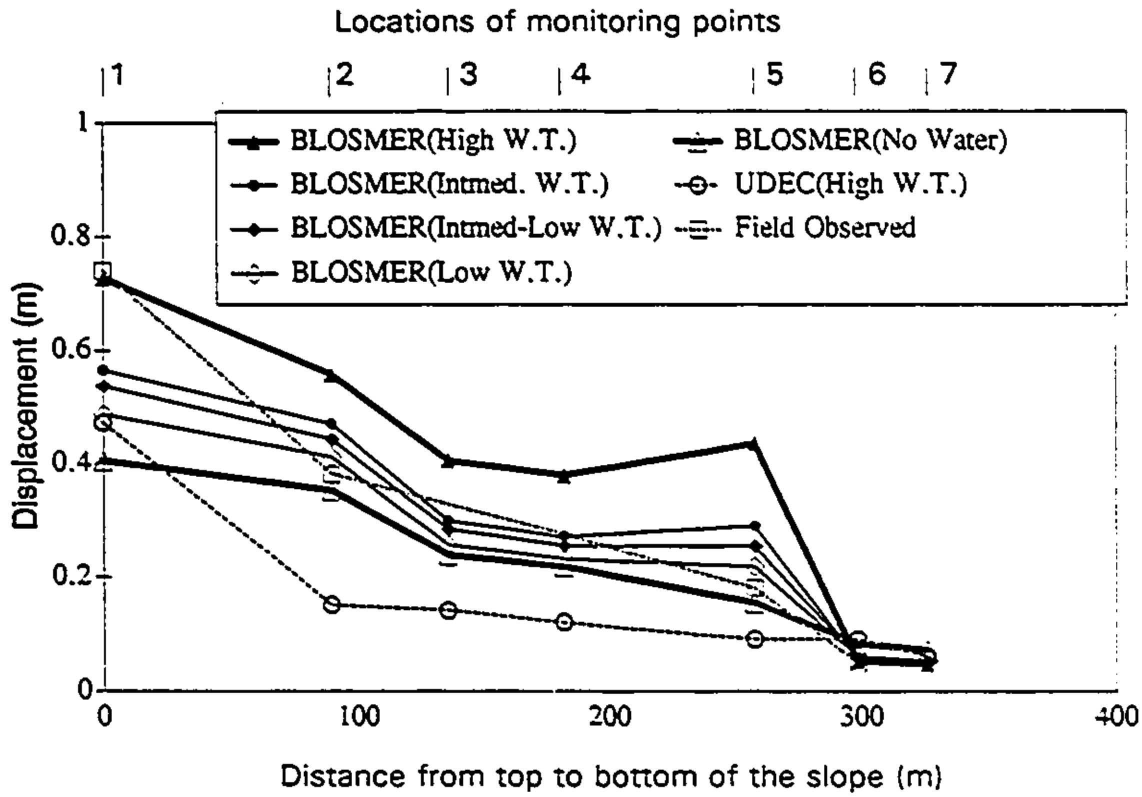

Fig.8.19 Cassiar Slope: Comparison of displacements along the slope

Table 8.4 Cassiar Slope: Displacements of the slope obtained from different methods

(unit: m)

Monitoring point	UDEC (High water table)	BLOSMER (High water table)	Observed
1	0.47	0.73	0.74
2	0.15	0.55	0.38
3	0.14	0.40	-
4	0.12	0.37	-
5	0.09	0.43	0.18
6	0.09	0.05	0.05
7	0.06	0.04	-

CHAPTER 9

CONCLUSIONS AND RECOMMENDATIONS

A numerical model called the Block-Spring Model has been developed for analysis of jointed rocks. The jointed rock masses are simulated by rigid blocks. The model can be used to analyze the rock deformation and the state of stresses around the openings near ground surface. The capability of simulating large displacements or sliding of the rock blocks makes the proposed method attractive for use in practice. The method is also able to determine whether the rock blocks are stable or unstable based on the capability of modelling large displacements. It can therefore provide useful data for rational design of the rock excavations.

By directly dealing with forces, the model can easily simulate rockbolt effects. Two rockbolt models were proposed and incorporated in the Block-Spring Model. One is the end-anchored rockbolt model and the other is the fully grouted rockbolt model. Both pre-tensioned rockbolt and untensioned rockbolt can be easily modelled by an iteration approach adopted in the Block-Spring Model. The proposed model can therefore be used for ground support design.

Another feature investigated in the Block-Spring Model is simulation of groundwater pressure in the rock joints. The groundwater has been considered reducing the effective normal stress in the joints by imposing normal pressure on the joint surfaces. The shear strength of the joints which is related to the normal stress may therefore be reduced.

The Block-Spring Model has also been made capable of simulating the sequential excavation problem. It can be used to investigate the effects of different sequences of excavations. The model can therefore help optimizing the excavation sequence of an underground opening.

In comparison to the Distinct Element Model, the proposed Block-Spring Model is more convenient for modelling stable rock masses in static conditions. As the proposed model is a static approach, it does not require any damping procedure to make the rock blocks converge to a stable state as the dynamic procedure requires. By using the static procedure, the proposed model avoids the problems associated with the dynamic approach such as the damping effect. Although the proposed model dose not simulate the "free dropping" blocks as the dynamic model dose, it is capable of predicting the unstable blocks. The unstable block is identified when "free dropping" is initiated.

A major advantage of the proposed model over the other static block models is its capability of simulating large displacements. While other static models concentrate on studying the discontinuities of the rock masses, the proposed model is developed to simulate large sliding of the blocks. Re-arrangement of the rock blocks after displacement is allowed for in the proposed model. This feature determines that the model can predict the unstable blocks more realistically. Also, the methodology and formulation of the proposed model are simpler and more direct than those of the other static models.

The approaches and formulation of the Block-Spring Model are suitable for densely jointed rock masses in which the discontinuities play a major role in the stability of the rock masses. In most excavations at shallow depth, such as open pits and shallow underground mines, the stabilities of the surrounding rocks are often controlled by the joints rather than the deformation of the intact rock blocks. The rigid block assumption is suitable in these cases where the ground stresses are relatively low and the deformation of the intact rocks can be ignored compared to the deformation of the joints. However, for deep mines where the rocks are relatively intact and the stress levels are high enough to result in significant deformation of the intact rocks, the rigid block assumption may not be suitable. It is therefore recommended that a deformable block model be developed in future for analyzing very deep excavations.

Modelling of groundwater effect has been based on applying static pressures on the surfaces of the rock joints. The effective stress law has been applied in the proposed model. This assumption is suitable perhaps in the cases where groundwater is relatively steady and a free water table exists. However, further development is required for extensive modelling of the groundwater effects, e.g. confined flow.

The deformation behaviour of the block to block contact has been governed by the non-tension criterion in the computation scheme. A linear normal force—normal displacement relation between the blocks has been assumed in the Block-Spring Model. Local compressive failure or crushing of the block surface was not taken into account.

The present model assumes that in a highly jointed rock mass under low stress condition, the deformation of the rock mass is mainly due to the shearing along the discontinuities. The closure of the discontinuity does not play a significant role in the deformation of the rock mass. However, as the joint normal stiffness may increase dramatically with the joint closure, it is recommended that a scheme for the nonlinear normal force−normal displacement relation be investigated in future.

The computation scheme of the proposed model has been developed for two dimensional analysis. If the dominant sets of discontinuities in a rock mass have similar strike direction, the 2-D model may well represent the structural conditions of the rock mass. In the case of the rock masses with complex geological features, the structural conditions in the third direction may not be represented by a 2-D model. It is therefore recommended that a computation scheme for three dimensional analysis be developed.

REFERENCES

Bandis, S., Lumsden, A. C. and Barton, N., (1981). Experimental studies of scale effects on the shear behaviour of rock joints. Int. J. Rock Mech. Sci. and Geomech. Abstr., Vol.18, No.1, pp.1-21.

Bandis, S., Lumsden, A. C. and Barton, N., (1983). Fundamentals of rock joint deformation. Int. J. Rock Mech. Min. Sci. and Geomech. Abstr., Vol.20, No.6, pp.249-268.

Bardet, J.-P. and Scott, R. F.,(1985). Seismic stability of fractured rock masses with the distinct element method. Research & Engineering Applications in Rock Masses, 26th US Symposium on Rock Mechanics, Rapid City, SD, pp.139-149.

Barton, N., (1972). A model study of rock joint deformation. Int. J. Rock Mech. Min. Sci., 9, pp.579-602.

Barton, N., (1973). Review of a new shear strength criterion for rock joints. Engineering Geology, Vol.7, No.4, pp.287-332.

Barton, N. and Bakhtar, K., (1983). Rock joint description and modelling for the hydrothermomechanical design of nuclear waste repositories. Report to CANMET, Mining Research Laboratories, Canada.

Barton, N. and Choubey, V., (1977). The shear strength of rock joints in theory and practice. Rock Mechanics, Vol.10, pp.1-54.

Belytschko, T., Plesha, M. and Dowding, C. H., (1984). A computer method for stability analysis of caverns in jointed rock. International Journal for Numerical and Analytical Methods in Geomechanics, Vol.8, pp.473-492.

Benson, R. P., Kierans, T. W., and Sigvaldason, O. T., (1970). In-situ and induced stresses at the Churchill Falls Underground Powerhouse, Labrador. Proceedings of the Second Congress of the International Society for Rock Mechanics, Beograd, Vol.II, pp.821-832.

Bergman, S. G. A. and Bjurstrom, S., (1983). Swedish experience of rock bolting: A keynote lecture. Proceedings of the International Symposium on Rock Bolting, Abisko, Sweden, O. Stephansson (Ed.), pp.243-255.

Best, B. S., (1970). An Investigation into the Use of Finite Element Methods for Analyzing Stress Distributions in Block Jointed Masses. Dissertation (Ph.D.), James Cook University of North Queensland.

Bétournay, M. C., (1986). A design philosophy for surface crown pillars of hard rock mines. 88th C.I.M. Annual General Meeting, Montreal, paper 146.

Bétournay, M. C., (1989). State of the art address. Surface Crown Pillar Evaluation for Active and Abandoned Metal Mines, International Conference Proceedings, Timmins, Ontario, Canada, M. C. Bétournay (Ed.), pp.17-33.

Bieniawski, Z. T., (1984). Tunnelling in coal mines — designing development entries for stability. Proc. 2nd Int. Conf. Stability in Underground Mining (Lexington, Ky.), Szwilski, A.B. and C.O. Brawner Eds.; Am. Inst. Min. Eng., New York, pp.3-22.

Brady, B. H. G., (1987). Boundary element and linked methods for underground excavation design. Chapter 5 in Analytical and Computational Methods in Engineering Rock Mechanics, E. T. Brown (Ed.), pp.164-204.

Brady, B. H. G. and Brown, E. T., (1985). Rock Mechanics for Underground Mining, George Allen & Unwin (Publishers) Ltd., 527.p.

Brown, E. T. and Hoek, E., (1978). Trends in relationships between measured in-situ stresses and depth. Int. J. Rock Mech. Min. Sci. & Geomech. Abstr., Vol.15, No.4, pp.211-215.

Burman, B. C., (1971). A numerical approach to the mechanics of discontinua. Ph.D Thesis, James Cook University of North Queensland, Townsville, Australia.

Burman, B. C., (1974). Development of a numerical model for discontinua. Australian Geomechanics Journal, Vol. G4, No.1, pp.13-22.

Cassiar Mining Corporation and Piteau Associates Engineering Ltd., (1990). Engineering Geology and Rock Mechanics Assessments of Slope Deformation and Slope Instability in the Cassiar Open Pit. A report to Supply and Services Canada, Energy Mines and Resources Canada, CANMET. Contract No.23440-9-9227/01-SQ.

Celestino, T. B., (1981). Deformation modes of filled joints in rock. Ph.D. thesis, University of California, Berkeley, 111p.

Christian, J. T., (1987). Numerical Methods and Computing in Ground Engineering. Ground Engineer's Reference Book. F. G. Bell (Ed.), Butterworths, pp.57/(1-18).

Coulson, J. H., (1970). The effects of surface roughness on the shear strength of joints in rock. Technical Report, U.S. Army Corps of Engineers, 283p.

Crotty, J. M. and Wardle, L. J., (1985). Boundary Integral Analysis of Piecewise Homogeneous Media with Structural Discontinuities. Int. J. Rock Mech. Min. Sci. & Geomech. Abstr. Vol.22, No.6, pp.419-427.

Crouch, S. L., Starfield, A. M., (1983). Boundary Element Methods in Solid Mechanics: with Applications in Rock Mechanics and Geological Engineering, London.

Cundall, P. A., (1971). A Computer Model for Simulating Progressive, Large-scale Movements in Blocky Rock Systems, Proceedings of the Symposium of the International Society of Rock Mechanics, Nancy, France, Vol. 1, Paper No. II-8.

Cundall, P., (1976). Computer interactive graphics and the distinct element method. Rock Engineering for Foundations and Slopes, Proceedings of a Specialty Conference (Sponsored by the Geotechnical Engineering Division of ASCE through its Committees), Vol. II, PP.193-199.

Cundall, P. A., (1987). Distinct Element Models of rock and soil structure, Chapter 4 in Analytical and Computational Methods in Engineering Rock Mechanics, E. T. Brown (Ed.), pp.129-163.

Cundall, P. A., (1988). Formulation of a three-dimensional Distinct Element Model - Part I: A scheme to detect and represent contacts in a system composed of many polyhedral blocks. Int. J. Rock Mech. Min. Sci. & Geomech. Abstr. Vol.25, No.3, pp.107-116.

Cundall, P. A. and Strack, O. D. L., (1979). The development of constitutive laws for soil using the Distinct Element Method. Third International Conference on Numerical Methods in Geomechanics, Aachen, pp.289-298.

Cundall, P. A. and Strack, O. D. L., (1979). A Discrete Numerical Model for granular assemblies. Geotechnique, Vol.29, No.1, pp.47-65.

Drescher, A. and De Josselin de Jong, G., (1972). Photoelastic verification of a mechanical model for the flow of a granular material. Journal of the Mechanics and Physics of Solids, V.20, pp.337-351.

Fairhurst, C., (1988). Foreword. Int. J. Rock Mech. Min. Sci. & Geomech. Abstr. Vol.25, No.3, pp.vv-viii.

Farahmand, D. and Li, G. Y., (1986). An application of Boundary Element Method for underground excavations in jointed rock. Rock Mechanics: Key to Energy Production, Proceedings of the 27th U.S. Symposium on Rock Mechanics, pp.299-303.

Franklin, J. A. and Dusseault, M. B., (1989). Rock Engineering. McGraw-Hill Publishing Company, 600p.

Gencer, M., (1985). Progressive failure in stratified and jointed rock mass. Rock Mechanics and Rock Engineering, Vol.18, No.1, pp.267-292.

Gerrard, C., (1983). Rock bolting in theory: A keynote lecture. Proceedings of the International Symposium on Rock Bolting, Abisko, Sweden, pp.3-32.

Ghaboussi, J., Wilson, E. L. and Isenberg, J., (1973). Finite element for rock joints and interfaces. Journal of the Soil Mechanics and Foundations Division, ASCE, Vol.99, No. SM10, pp.833-848.

Goodman, R. E., (1976). Methods of Geological Engineering in Discontinuous Rock. West Publishing Co., St. Paul, Minn.

Goodman, R. E., and Shi, G., (1985). Block Theory and Its Application to Rocks Engineering, Prentice-Hall, Inc..

Goodman, R. E. and Shi G., (1983). Geology and rock slope stability -- Application of the keyblock concept for rock slopes. Proc. 3rd Int. Conf. on Stability in Surface Mining, New York, pp.347-373.

Goodman, R. D., Taylor, R. L. and Brekke, T. L., (1968). A model for the mechanics of jointed rock. Journal of the Soil Mechanics and Foundations Division, ASCE, Vol.14, No. SM3, pp.637-659.

Guo, H., Ma, Q., Xue, X., and Wang, D., (1983), An analytical method of the initial stress field for rock masses. Journal of Geotechnical Engineering (in Chinese), Vol.5, No.3, pp.64-75.

Hamajima, R., Kawai, T., Yamashita, K., and Kusabuka, M., (1985). Numerical analysis of cracked and jointed rock mass. Fifth International Conference on Numerical Methods in Geomechanics, Nagoya, pp.207-214.

Hart, R., Cundall, P. A. and Lemos, J., (1988). Formulation of a three-dimensional Distinct Element Model - Part II: Mechanical calculations for motion and interaction of a system composed of many polyhedral blocks. Int. J. Rock Mech. Min. Sci. & Geomech. Abstr. Vol.25, No.3, pp.117-125.

Herget, G., (1980), Regional stresses in Canadian shield. 13th Canadian Rock Mechanics Symp., Toronto, CIM Spec. Vol.22, pp.9-16.

Herget, G., (1982). High stress occurrences in the Canadian shield. 23rd U.S. Symposium on Rock Mechanics (Edited by Goodman, R.E. and Heuze, F.E.), AIME, New York, pp.203-210.

Herget, G., (1986). Changes of ground stresses with depth in the Canadian shield. Proceedings of Int. Symposium on Rock Stress and Rock Stress Measurements, Stockholm, Sweden, pp.61-68.

Herget, G., (1987). Stress assumptions for underground excavations in the Canadian shield. Int. J. Rock Mech. Min. Sci. & Geomech. Abstr., Vol.24, No.1, pp.95-97.

Heuze, F. E. and Barbour, T. G., (1982). New models for rock joints and interfaces. Journal of the Geotechnical Engineering Division, ASCE, 108 (GT5), pp.757-776.

Hoek, E. and Brown, E. T., (1980, a). Empirical strength criterion for rock masses. Journal of the Geotechnical Engineering Division, ASCE, Vol.106, No. GT9, pp.1013-1035.

Hoek, E. and Brown, E. T., (1980, b). Underground Excavations in Rock. The Institution of Mining and Metallurgy, London, 527p.

Jumikis, A. R., (1983). Rock Mechanics (2nd Ed.). Trans Tech Publications, pp.320-326.

Kawai, T., (1977, a). A new discrete model for analysis of solid mechanics problems. "Seisan'Kenkyu" Journal of Institute of Industrial Science, University of Tokyo, Vol.29, No.4, pp.208-210.

Kawai, T., (1977, b). A new discrete analysis of non-linear solid mechanics problems involving stability, plasticity and crack. Proceedings of the Symposium on Applications of Computer Methods in Engineering, Los Angeles, California, pp.1029-1038.

Kawai, T., Kawabata, Y., Kondou, K. and Kumagai, K., (1978). A new discrete model for analysis of solid mechanics problems. Proceedings of the First International Conference on Numerical Methods in Fracture Mechanics, Swansea, Luxmoore, A. R. and Owen, D. R. J. (Editors), pp.26-37.

Kawai, T., Takeuchi, N. and Kumeta, T., (1981). New discrete models and their application to rock mechanics. Proceedings of the International Symposium on Weak Rock, Tokyo, pp.725-730.

Kobayashi, S., Nishimura, N. and Yoshida, K., (1979). Applications of boundary integral equation method to changing boundary shape problems. Third International Conference on Numerical Methods in Geomechanics, Aachen, pp.39-46.

Kulatilake, P. H. S. W., (1984). Estimating elastic constants and strength of discontinuous rock. Journal of Geotechnical Engineering, Vol.111, No.7, pp.847-864.

Ladanyi, B., and Archambault, G., (1969). Simulation of shear behaviour of a jointed rock mass. Rock Mechanics—Theory and Practice, W. H. Somerton (ed.), Proc. 11th U.S. Symposium on Rock Mechanics, Berkeley, Calif., pp.105-125.

Lemos, J. V., Hart, R. D. and Cundall, P. A., (1985). A generalized distinct element program for modelling jointed rock mass — A keynote lecture. Proceedings of the International Symposium on Fundamentals of Rock Joints, Bjorkliden, pp.335-343.

Lorig, L. J., (1984). A hybrid computational model for excavation and support design in jointed media. A Ph.D. thesis, University of Minnesota.

Lorig, L. J., (1988). Rock reinforcement: mechanical representations and use in finite difference schemes. International Symposium on Underground Engineering, New Delhi, pp.223-232.

Lorig, L. J., Brady, B. H. G., and Cundall, P. A., (1986). Hybrid distinct element-boundary element analysis of jointed rock. Int. J. Rock Mech. Min. Sci. & Geomech. Abstr. Vol.23, No.4, pp.303-312.

Maini, T., Cundall, P., Marti, J., Beresford, P., Last, N., and Asgian, M., (1978). Computer modelling of jointed rock masses. Technical Report N-78-4, U.S. Army Engineer Waterways Experiment Station, Vicksburg, Mississippi, 396p.

Mitri, H. S. and Rajaie, H., (1990). Stress analysis of rock mass with cable support — A finite element approach. Proceedings of Speciality Conference: Stresses in Underground Structures, Ottawa, Canada, pp.110-119.

Niwa, K., Kawai, T., Ikeda, M. and Takeda, T., (1984). Application of a new discrete method to fracture analysis of brittle materials. Proceedings of the Third International Conference on Numerical Methods in Fracture Mechanics, Swansea. U.K., pp.13-27.

Patton, F. D., (1966, a). Multiple modes of shear failure in rock and related materials. Ph.D. Thesis, University of Illinois, 282p.

Patton, F. D., (1966, b). Multiple modes of shear failure in rock. Proc. 1st Cong. Int. Soc. Rock Mech., Lisbon, Vol.1, pp.509-513.

Plesha, M.E., (1983). Numerical Methods for Jointed Media and Structures. Ph.D. Thesis, Northwestern University, Illinois.

Rodriguez Perez, C. E., (1980). Analysis of an underground opening in jointed rock. A Ph.D. thesis, University of Illinois at Urbana-Champaign, 214p.

Rosso, R., (1976). A comparison of joint stiffness measurements in direct shear, triaxial compression and in-situ. Int. J. Rock Mech. Min. Sci. and Geomech., Vol.13, No.6, pp.167-172.

Schneider, H. J., (1976). The friction and deformation behaviour of rock joints. Rock Mechanics, Vol.8, pp.169-184.

Shi, G. and Goodman, R.E., (1988). Discontinuous deformation analysis - A new method for computing stress, strain and sliding of block systems. Key Questions in Rock Mechanics, 29th U.S. Symp. on Rock Mech., Minnesota, pp.381-393.

Singh, B., (1973). Continuum characterization of jointed rock masses, Part II: Significance of low shear modulus. Int. J. of Rock Mech. and Mining Science, Pergmon Press, Oxford, England, Vol.10, pp.337-349.

Sinha, R. S. and Schoeman, K. D., (1983). Rock tunnels and rock reinforcement. Proceedings of the International Symposium on Rock Bolting, Abisko, Sweden, pp.333-344.

Stewart, I. J., (1981). Numerical and Physical Modelling of Underground Excavations in Discontinuous Rock. A Ph.D. thesis, University of London (Imperial College of Science and Technology), 483p.

Stewart, I. J. and Brown, E. T., (1984). A static relaxation method for the analysis of excavations in discontinuous rock. Design and Performance of Underground Excavations, ISRM Symposium - Cambridge, U.K., E. T. Brown and J. A. Hudson (eds.), pp.149-155.

Suzuki, K., Sugimoto, K, Kakurai, M, Uamashita, K., Ueda, M. and Kawai, T., (1985). Elasto-plastic, dynamic response analysis based on the rigid-body-spring-model for earth structure. Fifth International Conference on Numerical Methods in Geomechanics, Nagoya, pp.215-220.

Tao, Z. Y., and Chen, J. X., (1983). Behaviour of rock bolting as tunnelling support. Proceedings of the International Symposium on Rock Bolting, Abisko, Sweden, pp.87-92.

Trow, W. A. and Lo, K. Y., (1989). Horizontal displacements induced by rock excavation: Scotia Plaza, Toronto, Ontario. Canadian Geotechnical Journal, Vol.26, No.1, pp.114-121.

Wang, B. and Ma, Q., (1986). Boundary element analysis methods for ground stress field of rock masses. Computers and Geotechnics, Vol.2, No.5, pp.261-274.

Warburton, P. M., (1981). Vector stability analysis of an arbitrary polyhedral rock block with any number of free faces. Int. J. Rock Mech. Min. Sci. & Geomech. Abstr. 18, pp.415-427.

Zienkiewicz, O. C., Valliappan, S. and King, I. P., (1968). Stress analysis of rock as a 'no-tension' material. Geotechnique, Vol.18, No.1, pp.56-66.

APPENDIX A

REPRESENTATIVE VALUES OF DEFORMATION AND STRENGTH PARAMETER FOR SELECTED ROCKS AND ROCK JOINTS

Table A.1 Typical values of elastic parameters for various rock types

Rock type	Location	Elastic modulus E (GPa)	Poisson's ratio μ	Unit weight γ (kN/m^3)	Reference
Argillites	Cassiar Mine, B.C.	174.4	0.23	26.7	1
Volcanics	Cassiar Mine, B.C.	259.9	0.24	29.9	1
Sylvester group rocks	Cassiar Mine, B.C.	211.0	0.24	28.1	1
Jointed serpentinite	Cassiar Mine, B.C.	96.5	0.30	25.3	1
Serpentinite rock shear	Cassiar Mine, B.C.	17.9	0.33	-	1
Crystalline limestones	-	60 (17-100)*	0.25 (0.06-0.50)*	-	2
Porous limestones	-	45 (10-100)	0.24 (0.15-0.29)	-	2
Chalk	-	2 (0.1-12)	0.10 (0.05-0.15)	-	2
Salt	-	26 (5-44)	0.26 (0.06-0.73)	-	2
Sandstones	-	18 (1-100)	0.15 (0.02-0.51)	-	2
Quartzite	-	62 (11-119)	0.18 (0.10-0.40)	-	2
Slates and high-durability shales	-	40 (12-96)	0.22 (0.02-0.38)	-	2
Low-durability shales	-	5 (2-30)	-	-	2
Coal	-	3 (1-30)	0.42 (0.17-0.49)	-	2
Coarse-grained igneous rocks	-	56 (8-125)	0.20 (0.05-0.39)	-	2
Fine-grained igneous rocks	-	62 (7-117)	0.22 (0.07-0.38)	-	2
Schists	-	40 (5-98)	0.15 (0.01-0.40)	-	2

* Typical values are given together with ranges of reported values in parentheses.

1. Cassiar Mining Corporation and Piteau Associates Engineering Ltd., (1990). (see REFERENCES)

2. Franklin, J. A., and Dusseault, M. B., (1989). (see REFERENCES)

Table A.2 Stiffness factors for the rock joints reported in the literature

Specimen description	Location	Test description	Discontinuity thickness (mm)	Initial normal stress (MPa)	Shear stiffness K_s (GPa/m)	Normal stiffness K_n (GPa/m)	Source (*)
Serpentinite shear zones, cores, large specimens	Cassiar Mine, B.C.	Laboratory direct shear	-	-	0.27	2.03	1
Serpentinite joints, cores, large specim.	Cassiar Mine, B.C.	Laboratory direct shear	-	1.72	0.86	9.52	1
Argillite joints, cores, large specimens	Cassiar Mine, B.C.	Laboratory direct shear	-	-	0.667	43.2	1
Boise sandstone, dry, rough sawn joint	QP2-U.C. Berkeley	Laboratory direct shear	-	2.43	1.29	35.1	(2)
Marly sand filled joint	Vouglans Dam	Field direct shear	1-2	0.98	2.34	1.96	(3)
Closely jointed shale zone in limestone	SLL Khajuri Dam	Field direct shear	2-5	0.02	0.02	0.24	(3)
Shale interbed, wet	SLL Khajuri Dam	Field direct shear	2-5	0.02-0.03	0.02	0.26	(3)
Sierra white granite	-	-	-	-	1.7	100	(4)
NX cores of shale intersected by natural joints	-	Laboratory direct shear	-	3.5	43.6	8.6	(5)
		Laboratory direct shear	-	7.1	49.7	81.1	
		Laboratory direct shear	-	10.6	77.0	102	
		Jointed triaxial	-	1-2.7	22.3	38.5	
		Jointed triaxial	-	3.5-8.6	33.4	96.3	
		Jointed triaxial	-	7.1-18	96.3	96.3	

* References in parentheses are from Belytschko, T., Plesh, M. and Dowding C. H., (1984).

1. Cassiar Mining Corporation and Piteau Associates Engineering Ltd., (1990). (see REFERENCES)
2. Mahtab, M. A., (1969). Three-dimension Finite Element Analysis of Joint and Rock Slope. Ph.D. Thesis, University of California, Berkeley.
3. Goodman, R. E., (1968). Report MRD-TR-5, U.S. Army Corps of Engineers, Mo. River Division, Omaha, NE.
4. Goodman, R. E., Heuze, F. E. and Ohnishi, Y., (1972). Research on Strength-deformability-water Pressure Relationship for Faults in Direct Shear. Final Report on ARPA contract H0210020, University of California, Berkeley.
5. Rosso, R., (1976). A Comparison of Joint Stiffness Measurements in Direct Shear, Triaxial Compression and in-situ. Int. J. Rock Mech. Min. Sci. and Geomech. 13, pp.167-172.

Table A.3 Representative values of shear strength parameters for selected rocks and rock joints

Description	Location	Cohesion C (MPa)	Friction angle ϕ(°)	Confining pressure or normal stress (MPa)	Reference (*)
Serpentinite shear zones	Cassiar Mine, B.C.	0.14	26.5-27	-	1
Serpentinite joints	Cassiar Mine, B.C.	0	26-30	1.7	1
Asbestos fiber vein	Cassiar Mine, B.C.	-	21-26	-	1
Argillite joints	Cassiar Mine, B.C.	0	27.3-33	-	1
Argillite	Cassiar Mine, B.C.	0.69	32	-	1
Barren (waste) serpentinite	Cassiar Mine, B.C.	0.35	26	-	1
Ore bearing serpentinite	Cassiar Mine, B.C.	0.21	26	-	1
Berea sandstone	-	27.2	27.8	0-200	(5)
Bartlesville sandstone	-	8.0	37.2	0-203	(4)
Pottsville sandstone	-	14.9	45.2	0-68.9	(9)
Repetto siltstone	-	34.7	32.1	0-200	(5)
Muddy shale	-	38.4	14.4	0-200	(5)
Stockton shale	-	0.34	22.0	0.8-4.1	(3)
Edmonton bentonitic shale (water content30%)	-	0.3	7.5	0.1-3.1	(10)
Sioux quartzite	-	70.6	48.0	0-203	(4)
Texas slate; loaded					
30° to cleavage	-	26.2	21.0	34.5-276	(7)
90° to cleavage		70.3	26.9	34.5-276	
Georgia marble	-	21.2	25.3	5.6-68.9	(9)
Wolf Camp limestone	-	23.6	34.8	0-203	(4)
Indiana limestone	-	6.72	42.0	0-9.6	(9)
Hasmark dolomite	-	22.8	35.5	0.8-5.9	(5)
Chalk	-	0	31.5	10-90	(2)
Blaine anhydrite	-	43.4	29.4	0-203	(4)
Inada biotite granite	-	55.2	47.7	0.1-98	(8)
Stone Mountain granite	-	55.1	51.0	0-68.9	(9)
Nevada Test Site basalt	-	66.2	31.0	3.4-34.5	(11)
Schistose gneiss					
90° to schistocity	-	46.9	28.0	0-69	(4)
30° to schistocity		14.8	27.6	0-69	

* References in parentheses are from Goodman, R. E., (1989). Introduction to Rock Mechanics, 2nd Ed., John Wiley & Sons, 562p.

1. Cassiar Mining Corporation and Piteau Associates Engineering Ltd., (1990). (see REFERENCES)
2. Dayre, M., Dessene, J. L., and Wack, B. (1970). Proc. 2nd Congress of ISRM, Belgrade, Vol.1, pp.373-381.
3. DeKlotz, E., Heck, W. J., and Neff, T. L., (1964). First Interim Report, MRD Lab Report, 64/493, U.S. Army Corps of Engineers, Missouri River Division.
4. Handin, J. and Hager, R. V., (1957). Bull. A.A.P.G., 41: 1-50.
5. Handin, J., Hager, R. V., Friendman, M., and Feather, J. N., (1963) Bull. A.A.P.G., 47: 717-755.
6. Kulhawy, F. (1975). Eng. Geol., 9: 327-350.
7. McLamore, R. T. (1966). Strength-deformation characteristics of anisotropic sedimentary rocks, Ph.D. Thesis, University of Texas, Austin.
8. Mogi, K., (1964). Bull. Earthquake Res. Inst., Tokyo, Vol.42, Part 3, pp.491-514.
9. Schwartz, A. E., (1964). Proc. 6th Symp. on Rock Mech., Rolla, Missouri, pp.109-151.

10. Sinclair, S. R. and Brooker, E. W., (1967). Proc. Geotech. Conf. on Shear Strength Properties of Natural Soils and Rocks, Oslo, Vol.1, pp.295-299.
11. Stowe, R. L., (1969). U.S. Army Corps of Engineers Waterways Experiment Station. Vicksburg, Misc. Paper C-69-1.

APPENDIX B

DERIVATION OF THE AVERAGE STRESS EQUATIONS

The average stress, $\overline{\sigma_{ij}}$, in volume A, in which the stress states σ_{ij} presents and is in equilibrium, can be defined by the following expression:

$$\overline{\sigma_{ij}} = \frac{1}{A} \int_A \sigma_{ij} \, dA \tag{B.1}$$

The integral on the volume A in Eq.(B.1) can be transformed into an integral along the boundary S of the volume A. The equilibrium equation and Green's theorem may be used in the transformation.

The general equilibrium equation commonly used in the elastic theory may be written as follows:

$$\sigma_{kj,k} + b_j = 0 \tag{B.2}$$

where

b_j denotes the j component of the body force on a unit volume ($j=1, 2$ in 2-D problem);

$$\sigma_{kj,k} = \frac{\partial \sigma_{1j}}{\partial x_1} + \frac{\partial \sigma_{2j}}{\partial x_2},$$

x_k ($k=1, 2$) denotes k-coordinates.

The Green's theorem is re-called as follows:

Let A be a closed bounded region whose boundary is a piecewise smooth orientable surface S. Let A_{jk} be a vector function which is continuous and has continuous first partial derivatives in some domain containing A. Then

$$\int_A A_{jk,i}\, dA = \int_S A_{jk}\, n_i\, ds \tag{B.3}$$

where n_i is the i-directional cosine of the outer normal vector of S.

It is noticed that

$$\sigma_{ij} = \delta_{ik}\, \sigma_{kj} = x_{i,k}\, \sigma_{kj} \tag{B.4}$$

where $\delta_{ik} = \begin{cases} 1 & \text{if } i=j \\ 0 & \text{if } i \neq j \end{cases}$ is the Kroneker delta;

Because σ_{ij} satisfies the equilibrium condition, from Eqs.(B.2) and (B.4), the stress tensor can be written as follows.

$$\sigma_{ij} = x_{i,k}\, \sigma_{kj} + x_i\, (\sigma_{kj,k} + b_j)$$

or

$$\sigma_{ij} = (x_i\, \sigma_{kj}\,)_{,k} + x_i\, b_j \tag{B.5}$$

By substituting Eq.(B.5) into Eq.(B.1), the following expression can be obtained.

$$\overline{\sigma_{ij}} = \frac{1}{A} \int_A (x_i\, \sigma_{kj})_{,k}\, dA + \frac{1}{A} \int_A x_i\, b_j\, dA \tag{B.6}$$

or

$$\overline{\sigma_{ij}} = I_1 + I_2 \tag{B.7}$$

where

$$I_1 = \frac{1}{A} \int_A (x_i\, \sigma_{kj})_{,k}\, dA \tag{B.8}$$

$$I_2 = \frac{1}{A} \int_A x_i\, b_j\, dA \tag{B.9}$$

The integral I_2 is the contribution of the body force b_j to the average stress $\overline{\sigma_{ij}}$. Because the body force b_j (here the unit weight) is a constant, Eq.(B.9) can be written as follows:

$$I_2 = b_j \frac{1}{A} \int_A x_i \, dA \tag{B.10}$$

or

$$I_2 = b_j \, x_{ci} \tag{B.11}$$

where

$$x_{ci} = \frac{1}{A} \int_A x_i \, dA \tag{B.12}$$

x_{ci} is the i-coordinate of the centroid of the region A.

If the local coordinate system is used, i.e., the origin of the coordinate system is located at the centroid of the block, then, $x_{ci}=0$. Therefore,

$$I_2 = 0 \tag{B.13}$$

By applying Eq.(B.3) to Eq.(B.8), the following equation is obtained.

$$I_1 = \frac{1}{A} \int_S x_i \, \sigma_{kj} \, n_k \, ds \tag{B.14}$$

From the equilibrium condition, following equation can be easily derived.

$$\sigma_{kj} \, n_k = f_j \tag{B.15}$$

where f_j is the j-component of the traction on the surface S.

From Eqs.(B.7), (B.13), (B.14) and (B.15), the average stress within the block can be determined by

$$\overline{\sigma_{ij}} = \frac{1}{A} \int_S x_i f_j \, ds \tag{B.16}$$

If the boundary S is divided into a finite number of small segments with the length of $\Delta s^{(n)}$ for segment n (Fig.B.1), the integral along S in Eq.(B.16) can be approximated by

$$\overline{\sigma_{ij}} = \frac{1}{A} \sum_{n=1}^{m} x_i^{(n)} f_j^{(n)} \Delta s^{(n)} \tag{B.17}$$

where m is the number of the small segments divided alone S;

$x_i^{(n)}$ denotes the i local coordinate of the middle point of segment n; and

$f_j^{(n)}$ denotes the j component of the average traction on segment n.

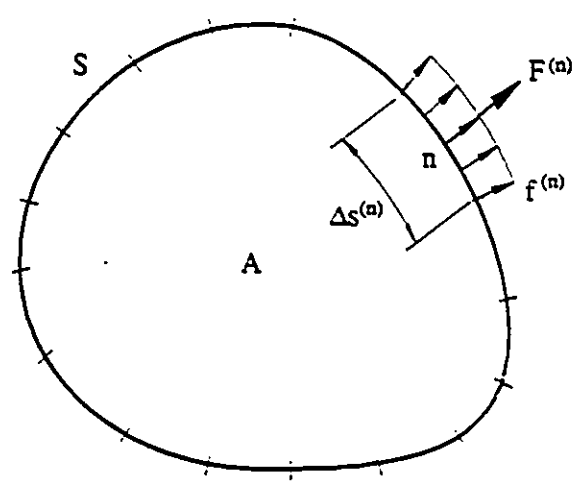

Fig.B.1 Discretization of boundary S of region A

Eq.(B.17) may be further simplified as

$$\overline{\sigma_{ij}} = \frac{1}{A} \sum_{n=1}^{m} x_i^{(n)} F_j^{(n)} \tag{B.18}$$

where $F_j^{(n)} = f_j^{(n)} \Delta s^{(n)}$ is the j-component of the resultant force on segment n.

The discrete forces on the surface S of region A can be used to evaluate the average stress in the region using Eq.(B.18).